

Naval Ocean Systems Center

San Diego, CA
92152-5000

Technical Document 1869
July 1990



1

AD-A226 192

DTIC
ELECTE
SEP 06 1990
S D

Second ONR Workshop
on Magnetohydrodynamic
Submarine Propulsion

San Diego, California
16-17 November 1989

90 09 05 018

NAVAL OCEAN SYSTEMS CENTER

San Diego, California 92152-5000

J. D. FONTANA, CAPT, USN
Commander

R. M. HILLYER
Technical Director

ADMINISTRATIVE INFORMATION

These proceedings were compiled for the Office of Naval Research, 800 N. Quincy St., Arlington, VA 22217-5000, on behalf of the Defense Advanced Research Projects Agency, 1515 Wilson Blvd., Suite 705, Arlington, VA 22209, and provides the presentations, summaries of results, and recommendations made by the three working groups of participants of the Second ONR Workshop on Magnetohydrodynamic Submarine Propulsion held on 16-17 November 1989 in San Diego, CA. Although this workshop was hosted by NOSC and these proceedings published by NOSC, much of the work represented by these papers was performed by private individuals and corporations without government support.

Released by
L. A. Parnell, Head
Propulsion and
Hydrodynamics Branch

Under authority of
R. H. Moore, Head
ASW Technology
Division

Second ONR Workshop on Magneto hydrodynamic Submarine Propulsion

San Diego, California
 November 16-17, 1989

Sponsored by

Dr. Gabriel D. Roy
 Mechanics Division, Propulsion & Energetics
 Office of Naval Research

On behalf of the
 Defense Advanced Research Projects Agency,
 LCDR Richard Martin, Program Manager for
 Mechanical Systems, Naval Technology Office



Accession For	
NTIS	CRA&I <input checked="" type="checkbox"/>
DTIC	TAB <input type="checkbox"/>
Unannounced <input type="checkbox"/>	
Justification	
By	
Distribution /	
Availability Codes	
Dist	Avail and / or Special
A-1	

FOREWORD

Magnetohydrodynamics (MHD) is a fascinating technology that offers challenge both to the experimentalist and the analyst. This interdisciplinary science that dates back to the pioneering experiments of Michael Faraday in the early eighteenth century, is still new with a lot of scientific issues left to explore. In the past decade, research has been focused on MHD electric power generation, with particular emphasis on fossil fuel-based combustion plasmas. Though Stewart Way, in 1966, demonstrated the possibility of MHD propulsion of underwater vehicles, it is only in the past couple of years this aspect of MHD has received some attention.

Recognizing the potential of MHD for underwater propulsion of Naval vessels, the Office of Naval Research organized a workshop in October 1988 in Washington, D.C. Experts from all over the country were invited for the two-day brainstorming sessions to explore the underlying issues of MHD propulsion. Research programs on MHD propulsion were initiated by ONR and DARPA to gain understanding of the fundamental mechanisms involved, and to demonstrate its feasibility. Some important issues were identified, solutions of which are of great significance for a successful MHD underwater thruster development. To address these issues and to seek solutions, the present workshop was organized. Substantial progress has resulted during the last year as evidenced by the numerous presentations which are included in these proceedings.

I would like to thank LCDR Martin of DARPA for his support and participation in this workshop. I very much appreciate the excellent organization of this meeting by Dr. Lynn Parnell and the Naval Ocean Systems Center. My thanks go to all participants for their contributions to a very scientifically stimulating workshop. I am looking forward to the third ONR workshop on underwater MHD propulsion some time near the end of 1990.

Dr. Gabriel D. Roy
Mechanics Division
Office of Naval Research

TABLE OF CONTENTS

SECOND ONR WORKSHOP ON MAGNETOHYDRODYNAMIC SUBMARINE PROPULSION

San Diego, California
November 16-17, 1989

Foreword	i
Participants	iv
Agenda	v
Introduction	1

WORKSHOP PRESENTATIONS

G. Roy - Overview of Issues	5
M. Petrick	17
J. Meng	73
D. Swallom	105
E. Doss	163
T. Lin	183
D. Bagley	199

R. Martin - DARPA Requirements	221
K. Tempelmeyer	225
C. Young	285
Y. Wu	321
M. Brouillette	351
K. Koester	369

SUMMARIES OF WORKING GROUP FINDINGS

Magnet Design - B. Wang, Chair	391
Electrolysis/Electrodes - K. Tempelmeyer, Chair	403
Conductivity Enhancement - C. Young, Chair	419

PARTICIPANTS

Dr. Tom Ankerman
KOCH Process Systems
20 Walkup Drive
Westboro, MA 01581
(508) 898-0279

Dr. David Bagley
David Taylor Research Center
Code 271
Annapolis, MD 21402
(301)267-3523

Mr. Greg Berry
Argonne National Laboratory
9700 South Cass Ave.
Argonne, IL 60439
(708) 972-6160

Mr. David Brady
Advanced Technology, Inc.
1515 Wilson Blvd, Suite 705
Rosslyn, VA 22209

Mr. Martin Brouillette
STD Research Corporation
P.O. Box C
Arcadia, CA 91006
(818) 357-2311

CDR James Carroll
Naval Ocean Systems Center
Code 605
San Diego, CA 92152-5000
(619) 553-6063

Dr. James Chapman
University of Tennessee Space Institute
Tullahoma, TN 37388
(615) 455-0631

Dr. Donald Cott
MSE Inc./INEL
P.O. Box 3767
Butte, MT 59702
(406) 454-7296

Dr. Steven Deutsch
Garfield Water Tunnel
ARL/PSU
P.O. Box 30
State College, PA 16804

Dr. E. Doss
Argonne National Laboratory
Engineering Physics Division
9700 South Cass Ave.
Argonne, IL 60439
(708) 972-5967

Ms. Tricia Dressler
DARPA/Advanced Technology
1515 Wilson Blvd, Suite 705
Arlington, VA 22209
(703) 276-1552

Mr. John Grant
Naval Underwater Systems Center
Newport Laboratory
Newport, RI 08241
(401) 841-3545

Dr. Sam Gurol
General Dynamics-Space Division
MZ-92-8260, P.O. Box 85990
San Diego, CA 92138
(619) 542-9015

Dr. Eric Hendricks
Naval Ocean Systems Center
Code 634
Newport, RI 02841
(401) 841-4013

Dr. Peter Hendricks
Naval Underwater Systems Center
Newport Laboratory
Code 804
Newport, RI 02841
(401) 841-4013

Dr. Stephen Herring
Idaho National Engineering Laboratory
MS 3523 Laboratory, P.O. Box 1625
Idaho Falls, ID 83415-3523
(208) 526-9497

Dr. Peter Huang
Intermagnetics/IGC
Charles Industrial Park
P.O. Box 586
Guilderland, NY 12084
(518) 456-5456

Dr. John Joynes
David Taylor Research Center
Code 271
Annapolis, MD 21402
(301) 267-2467

Dr Kent Koester
MHD Instruments
788 Stern Avenue
Palo Alto, CA 94303
(415) 856-2586

Dr. Arik Le'Boher
Ben Gurion University of the Negev
P.O. Box 653
Beer-Sheva, Israel 84105
(972) 573-4451

Mr. Luis Lema
Naval Underwater Systems Center
Newport Laboratory
Newport, RI 08241
(401) 841-3048

Prof. Tom Lin
Pennsylvania State University
Dept. of Nuclear Engineering
P.O. Box 30
State College, PA 16804
(814) 238-4657

Dr. John Lineberry
University of Tennessee Space Institute
Tullahoma, TN 37388
(615) 455-0631 ext 362

Prof. Sam Marshall
Michigan Technological University
Department of Physics
Houghton, MI 49931
(906) 487-2906 or 2900

LCDR Rich Martin
DARPA/Advanced Technology
1515 Wilson Blvd, Suite 705
STP 133
Rosslyn, VA 22209
(703) 276-1552
Fax (703) 525-4035

Mr. Craig Maxwell
STD Research Corporation
P.O. Box C
Arcadia, CA 91006
(818) 357-2311

Dr. James Meng
Naval Underwater Systems Center
Coe 8093
Newport Laboratory
Newport, RI 02841
(401) 841-3560

Mr. Arnold Musolf
Naval Ocean Systems Center
Code 631
San Diego, CA 92152-5000
(619) 553-1615

Dr. Takashi Nakamura
Astron Research and Engineering
130 Kifer Ct.
Sunnyvale, CA 94086
(408) 245-3200

Dr. Lynn Parnell
Naval Ocean Systems Center
Code 634
San Diego, CA 92152-5000
(619) 553-1588

Dr. Alexander Patrick
AVCO Research Laboratory
2385 Revere Beach Parkway
Everett, MA 02149
(617) 381-4993

Dr. Michael Petrick
Argonne National Laboratory
9700 South Cass Ave.
Argonne, IL 60439
(708) 972-5960

Dr. Basil Picologlou
Argonne National Laboratory
Bldg. 207, Rm. CA 133
9700 South Cass Avenue
Argonne, IL 60439

Mr. Michael Putnam
Naval Ocean Systems Center
Code 634
San Diego, CA 92152-5000
(619) 553-2926

Dr. Gabriel Roy
Office of Naval Research
Code 1132P
800 North Quincy Street
Arlington, VA 22217-5000
(202) 696-4403

Dr. Isaac Sadovnik
AVCO Research Corp.
2385 Revere Beach Parkway
Everett, MA 02149
(617) 381-4320

Dr. Sharad Singh
Westinghouse R&D Center
1310 Beulah Road
Pittsburgh, PA 15235
(412) 256-2137

Dr. Daniel Swallow
AVCO Research Laboratory
2345 Revere Beach Parkway
Everett, MA 02149
(617) 381-4384

Dr. Kenneth Templemeyer
Dept. of Mechanical Engineering
Southern Illinois University
Carbondale, IL 26901
(618) 453-7158

Mr. Steve Trimble
Allied-Signal Aerospace Co.
Fluid Systems Division
MS 1207-4P
1300 W. Warner Road
Tempe, AZ 85282
(602) 893-7199

Dr. B. Wang
Wang NMR Inc.
550 North Canyon Parkway
Livermore, CA 94450
(415) 443-0212

Dr. Y.C.L. Wu
Engineering Research & Consulting
P.O. Box 417
UTSI Research Park
Tullahoma, TN 37388
(615) 455-9915

Dr. Chris Young
Spectra Technology
2755 Northup Way
Bellevue, WA 98004
(206) 827-0460
Fax (206) 827-3517

SECOND ONR WORKSHOP ON MHD SUBMARINE PROPULSION

AGENDA - DAY 1 16 NOV 89

0830 - 0840 Welcome/Introduction - L. Parnell, NOSC
0840 - 0900 Overview of Issues - G. Roy, ONR

CURRENT PROGRAMS

0900 - 0930 M. Petrick - ANL
0930 - 1000 J. Meng - NUSC
1000 - 1030 D. Swallom - AVCO

1030 - 1045 COFFEE BREAK

1045 - 1115 E. Doss - ANL
1115 - 1145 T. Lin - ARL
1145 - 1200 D. Bagley - DTRC

1200 - 1300 LUNCH

1300 - 1315 LCDR R. Martin, DARPA
1315 - 1345 B. Wang, Wang NMR Inc.

ELECTROLYSIS/ELECTRODES: Chairman - K. Tempelmeyer

1345 - 1430 K. Tempelmeyer, US Naval Academy

CONDUCTIVITY ENHANCEMENT: Chairman - C. Young

1430 - 1500 C. Young, Spectra Technology

1500 - 1515 COFFEE BREAK

1515 - 1545 Y. C. L. Wu, Engineering Research and Consultants
1545 - 1615 C. Maxwell, STD Research Corporation
1615 - 1645 K. Koester, MHD Instruments
1645 - 1730 Other Speakers

1830 - 1930 SOCIAL HOUR
1930 - 2130 Dinner
Dinner Speaker - LCDR Martin, DARPA

AGENDA - DAY 2

17 NOV 89

0830 - 0840	Announcements — L. Parnell
	Form three groups for discussion
0845 - 1015	Group Discussion
1015 - 1030	COFFEE BREAK
1030 - 1200	Group Discussion
1200 - 1300	LUNCH
1300 - 1320	B. Wang - Summary
1320 - 1340	K. Tempelmeyer - Summary
1340 - 1400	C. Young - Summary
1400 - 1600	Group Discussion
1600 - 1630	Administrative Announcements/Wrap-Up — G. Roy

INTRODUCTION

On 16 and 17 November 1989, the ONR/DARPA Workshop on Magnetohydrodynamic Submarine Propulsion was held in San Diego, California, at the Travelodge-Harbor Island Hotel. The workshop was sponsored by Dr. Gabriel Roy of the Mechanics Division, Propulsion and Energetics, Office of Naval Research (ONR), on behalf of the Defense Advanced Research Projects Agency (DARPA), LCDR Richard Martin, Program Manager for Mechanical Systems, Naval Technology Office. The Naval Ocean Systems Center served as host. Fifteen presentations were made, including summaries of results and recommendations made by three working groups formed from the participants. This report documents these presentations, as well as the summaries and recommendations of the working groups.

The purpose of the meeting was to find solutions to three scientific and engineering issues which have been identified as pivotal to the technology development. These three issues are as follows: (1) development of low rate/volume, high performance superconducting magnet and minimization of magnetic signature; (2) conductivity enhancement; and (3) gasless electrode. Specific emphasis was placed on formulating the answers, insofar as the gathered community of expertise could provide at the workshop, to the scientific issues that must be addressed, including setting down the theoretical development required and experimental data which are needed to advance this technology.

The first day was spent reiterating the issues, solutions offered by the invited speakers, and presentations on current programs. On the second day the three working groups on the above mentioned subject areas convened in an open forum with sharing, and elaborating on ideas that will lead to the solution of the issues addressed. This was then followed by presentation the working group recommendations to the entire attendance of the workshop by the session chairmen, in which the whole group discussed the ideas presented.

This report is being distributed to all workshop participants and others interested. The list of participants and the agenda are included herein. Additional copies of this report can be obtained by contacting the undersigned at (619) 553-1588.

Lynn A. Parnell
Head, Propulsion Research & Hydrodynamics Branch
Naval Ocean Systems Center, Code 634
Science Advisor, ONR Propulsion Program

WORKSHOP PRESENTATIONS

OVERVIEW OF ISSUES

Presented by

Gabriel D. Roy

Sea Water MHD Propulsion Major Issues



Gabriel D. Roy
Office of Naval Research
Mechanics Division (Code 1132)

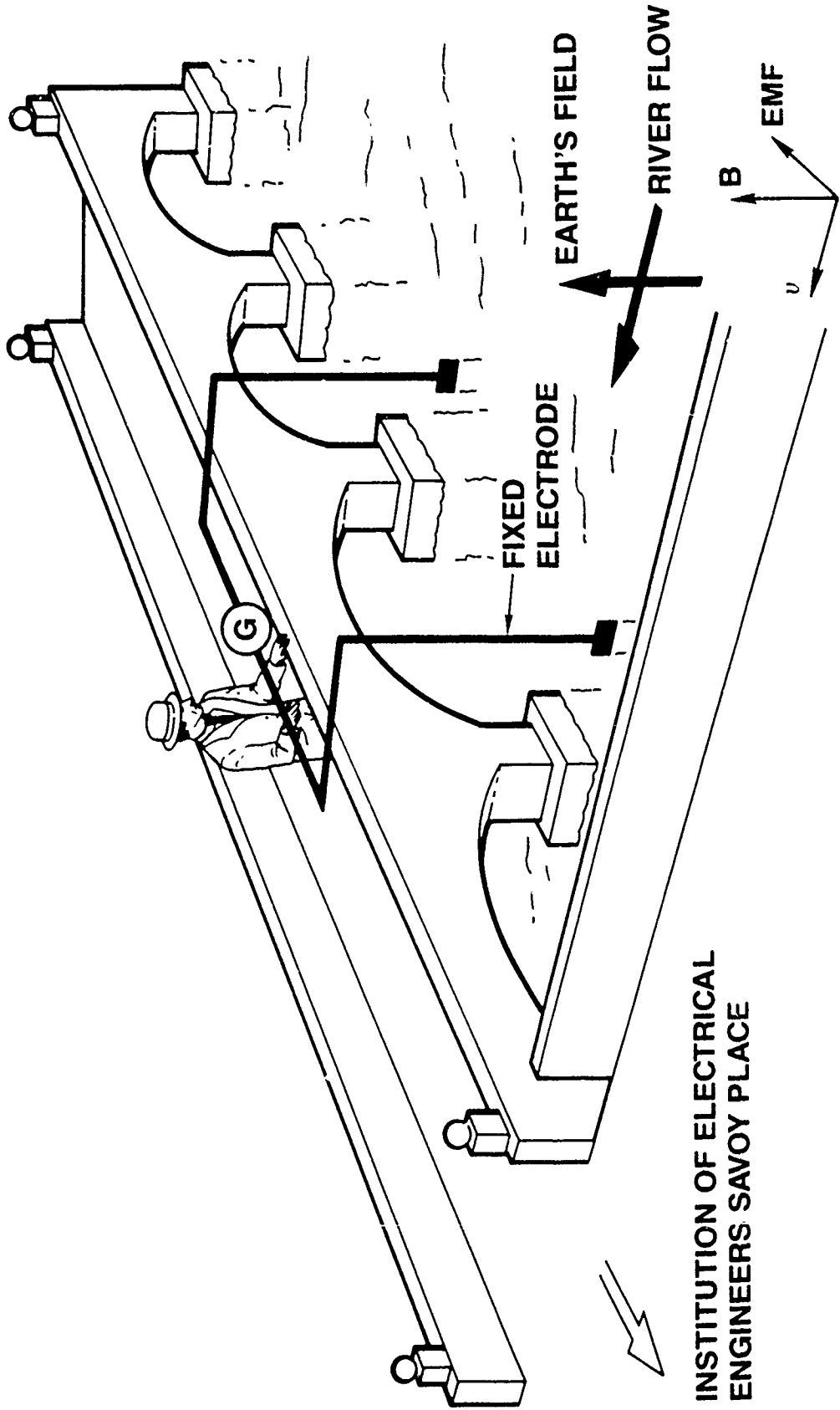
DARPA/ONR Workshop
MHD Submarine Propulsion

San Diego, California

16-17 November 1989



Faraday's Experiment on Waterloo Bridge, London, January





Faradays Words . . .

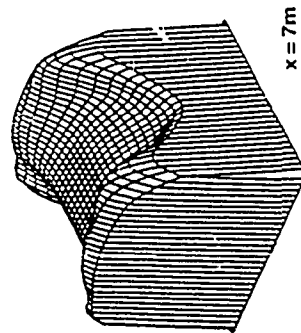
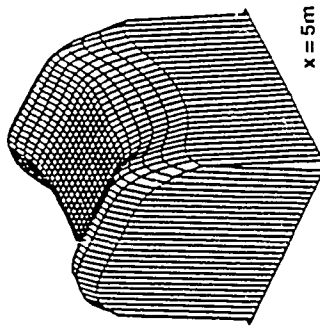
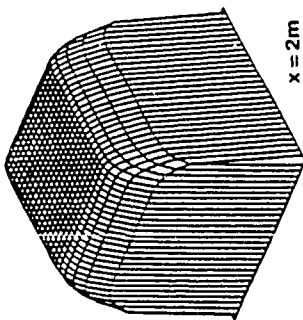
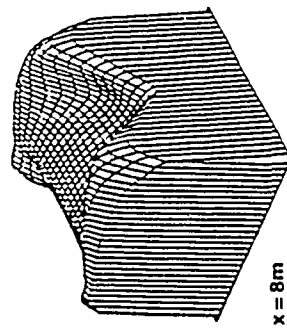
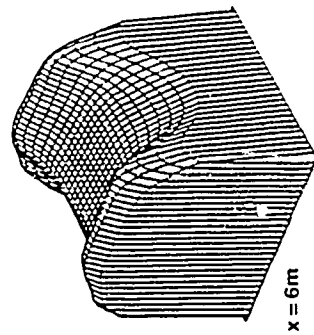
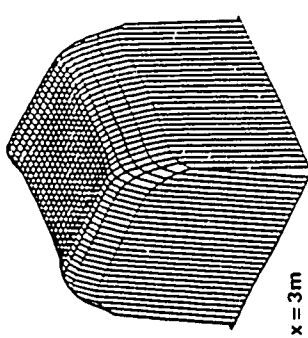
“ . . . It was not difficult to perceive that the earth would produce the same (electromagnetic induction) effect as a magnet and to an extent that it would, perhaps, render it available in the construction of new machines.”

“ . . . although the electricity obtained by magnetoelectric induction in a few feet of wire is but small intensity and has not yet been observed except in metals and carbon in particular state, still it has the power to pass through brine; and as the increased length of the substance acted upon produces increased intensity, I hope to obtain effects from extensive moving masses of water, though quiescent water gave none.”

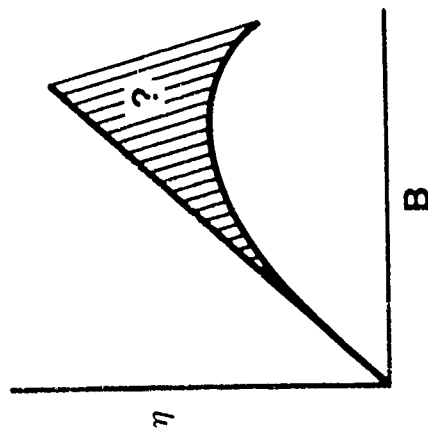
Michael Faraday
Bakerian Lecture Series, 1832



Interaction Of MHD Forces With The Fluid Flow

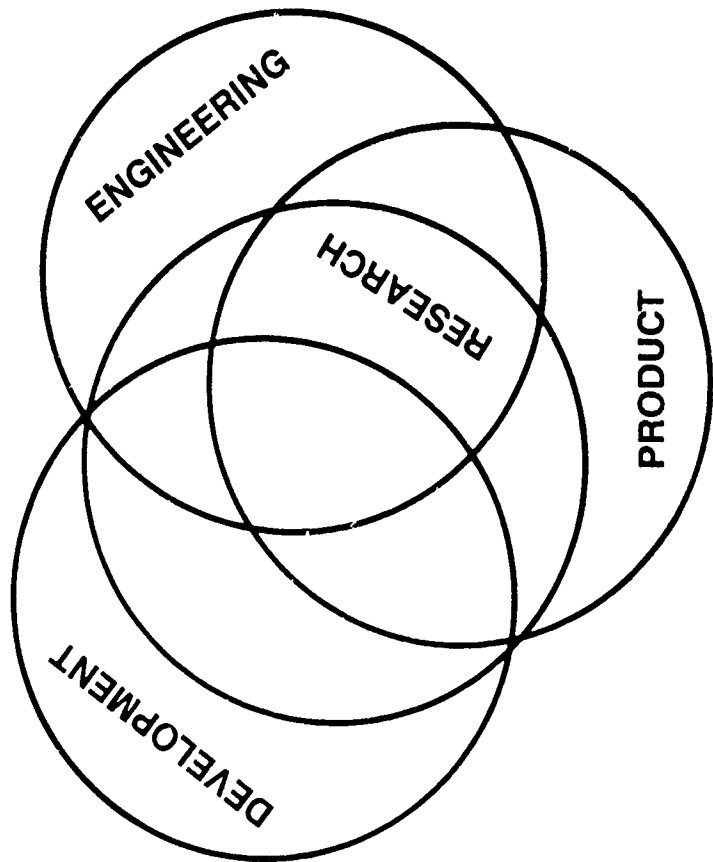
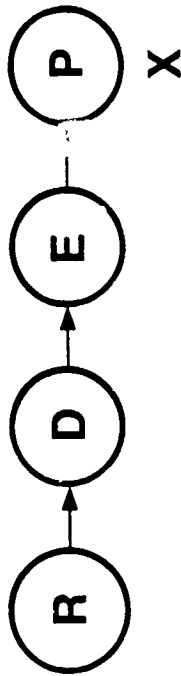


Velocity Overshoots in the Sidewall Boundary Layers
(AEDC channel, subsonic flow at 6.0T)





Integrated Research Approach



MHD Submarine Propulsion Major Issues

Three Issues are Specifically Addressed

1. Superconducting Magnet

- **Weight and volume reduction**
- **Magnetic signature reduction**

2. Electrodes

- **Ideally gasless**
- **Life**

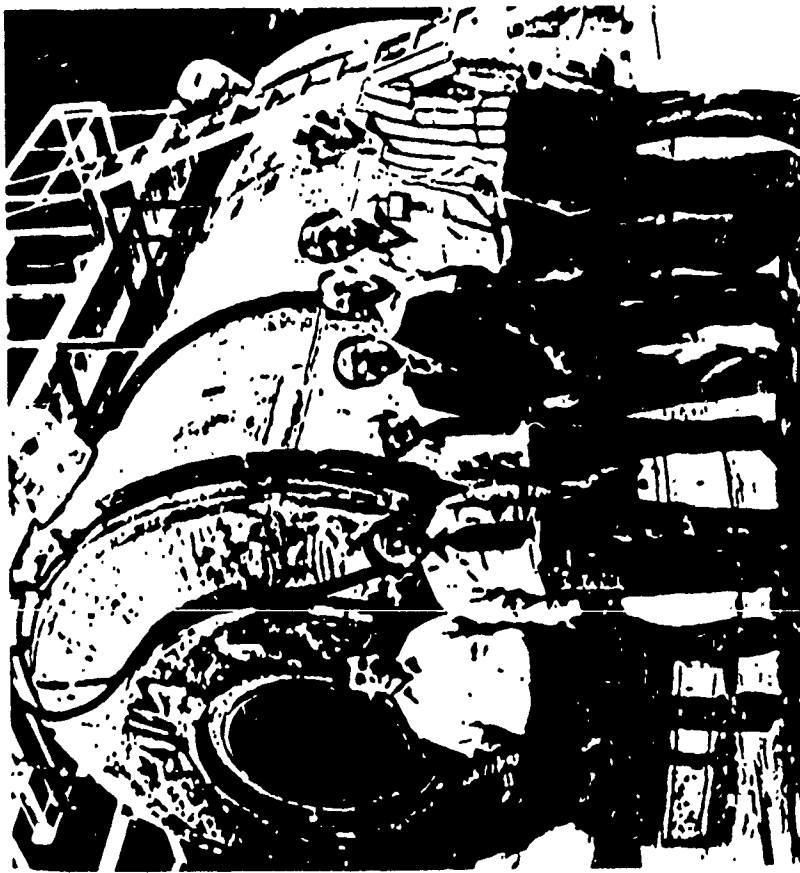
3. Sea Water Conductivity

- **Enhancement**
- **Control**

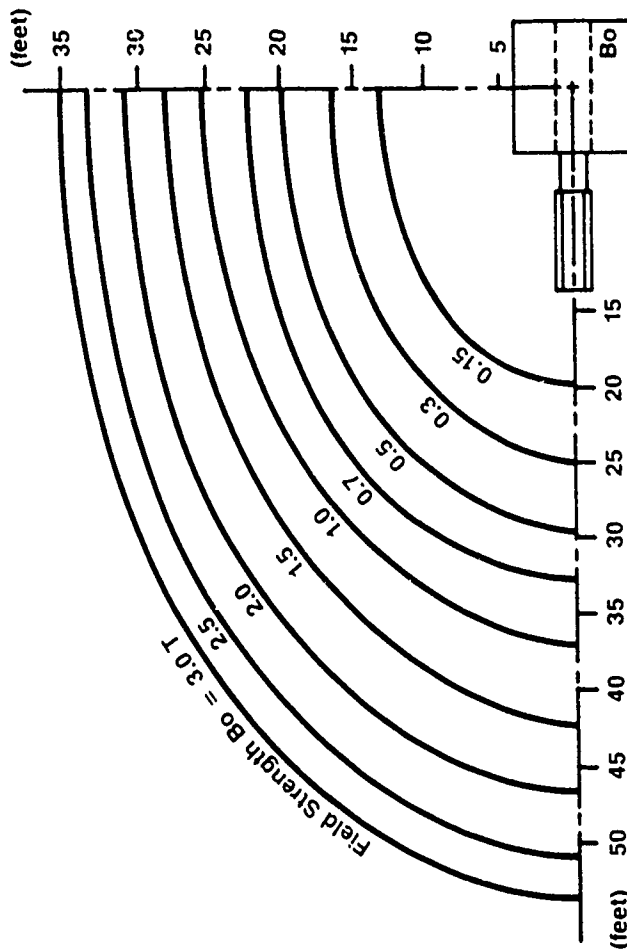


The Magnetic Signature Issue

Pictured after the successful test of the largest, most powerful superconducting dipole magnet ever built are many who helped make the project a success — left to right, Eugene Kraft (ENG), Project Manager Sou-Tien Wang (ARF), Raymond Wittkamp (PD), James Kolora (PD), Edward Johanson (EL), Anthony Lang (CS) and Richard Voogd (EL.)



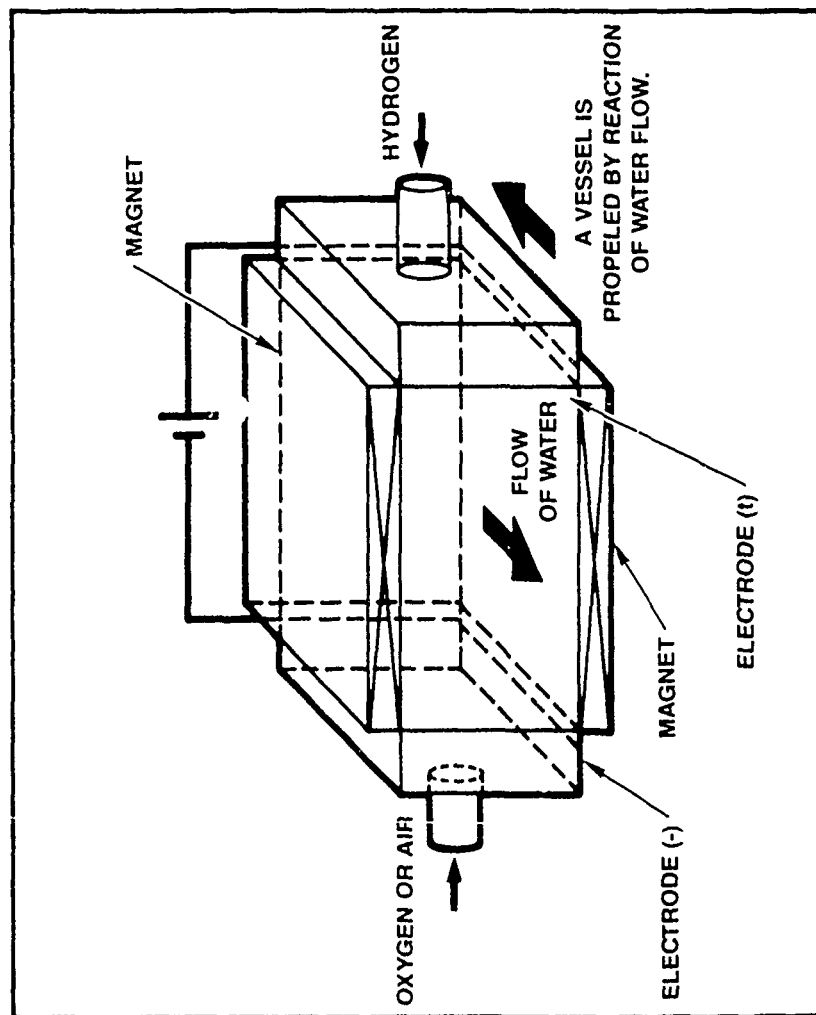
Argonne News October 1981



Five-Gauss field line without field shields for various field strengths



Gas Diffusion Electrode for MHD Thruster

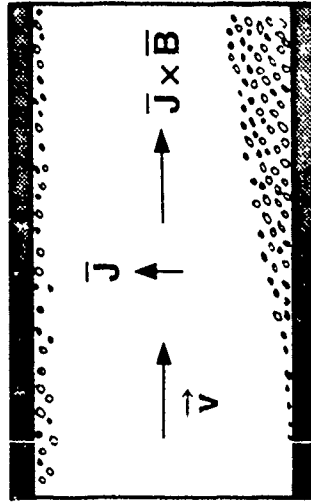


150 T displacement
22 m long
800 N thrust
Ti plates coated with
platinum
New Electrode
Carbon-fluorine resin
Prof. Furuya
Yamanashi University.

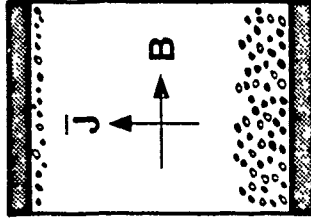
Electrode Configuration

Possible Bubble Accumulation

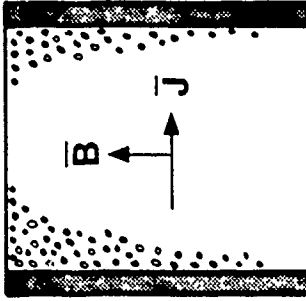
Which configuration is desirable?
Horizontal or vertical?



Horizontal Electrodes

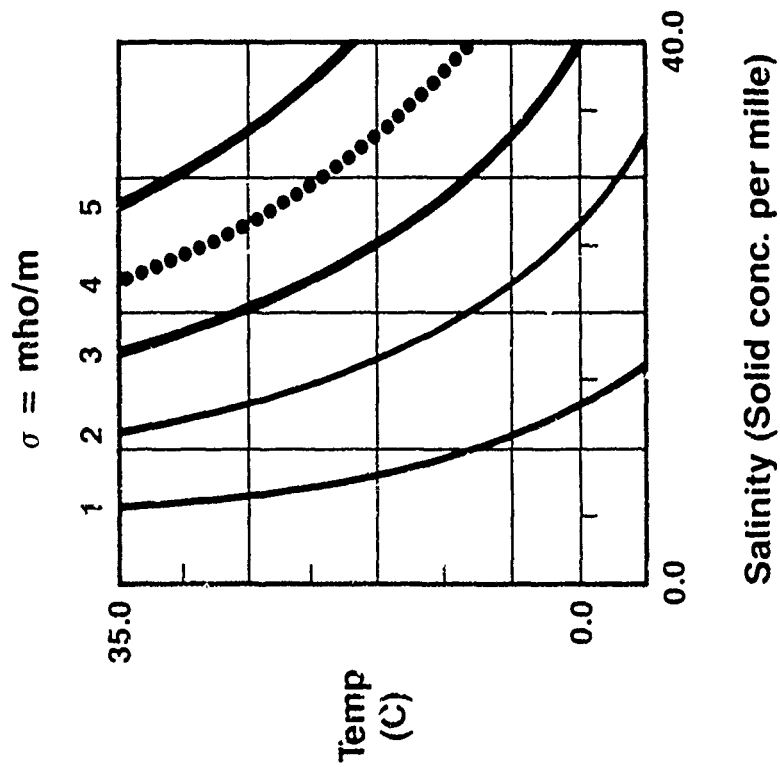


Vertical Electrodes





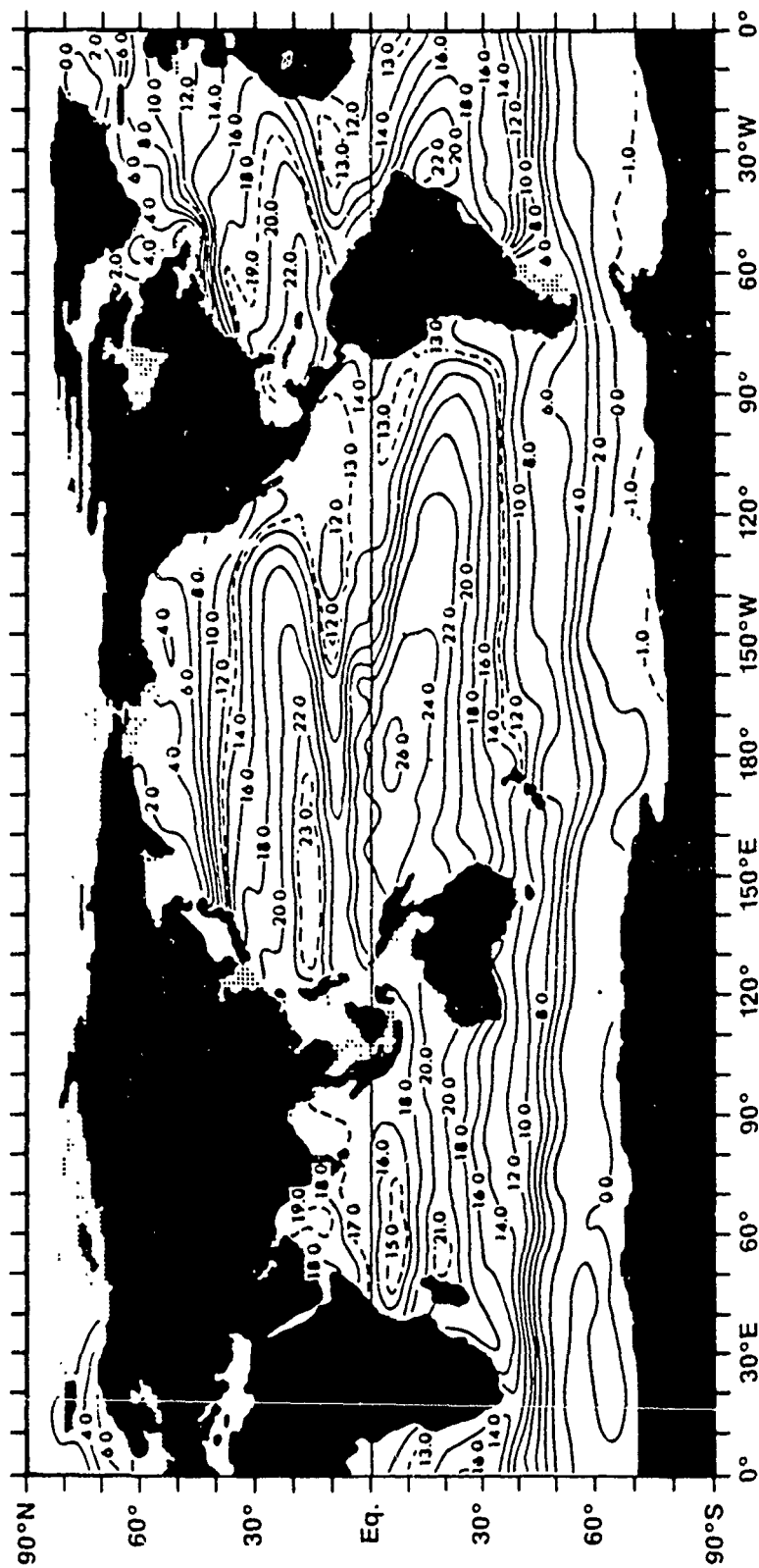
Seawater Electrical Conductivity



Use heat rejected
from the power unit
to heat water?



Average Mean Ocean Temperature



Annual mean potential temperature (°C) at 150 m depth.

**THE MHD PROPULSION PROGRAM
AT ARGONNE NATIONAL LABORATORY**

Presented by

M. Petrick

The feasibility, and perhaps more correctly, the practicality of MHD thrusters will depend on a number of performance, stealth, and engineering issues.

VIEWGRAPH 1

The desired MHD performance must be achieved at relatively high efficiency so as not to adversely impact other major submarine systems,(e.g. reactor, energy conversion, power conditioning, and condensor), from a wgt./vol-displacement perspective.

Equally important is the need for the thruster to operate effectively during transient and off design conditions. It seems clear that in regard to the latter, the MHD thruster, if designed for maximum efficiency at high velocities, should be much more efficient at lower velocities since the power requirements, and hence, ohmic losses will be substantially reduced, providing of course that other substantive loss mechanisms do not come into play.

There are a number of engineering issues in regard to the magnet and cryogenic system which impacts the practicality of the thruster.

The ANL program has been structured to address the performance issues and to develop preliminary data on the acoustic signature. The engineering issues are being addressed through System and Platform Integration Studies such as are being pursued by AVCO and NUSC.

VIEWGRAPH 1

PRACTICALITY OF MHD THRUSTES DEPENDS ON

- EFFICIENT MHD PERFORMANCE
 - STEADY STATE
 - TRANSIENT
 - OFF DESIGN

- STEALTH ISSUES (SIGNATURES)
 - ACOUSTIC
 - MAGNETIC
 - CHEMICAL

- ENGINEERING ISSUES
 - MAGNET
 - * WGT/VOL (2 TONS/M³)
 - * LOW HEAT LEAK
 - * SHOCK SUSCEPTABILITY
 - * CRYOSTABILITY

 - CRYOGENIC SYSTEM
 - * SIZE
 - * RELIABILITY
 - * SUPERFLUID HE (?)

•

There are a number of technical issues that could impact thruster performance, noise and scale up.

VIEWGRAPH 2

All these effects can, and will likely, impact performance, and hence, analyses to determine optimal thruster and magnet configurations. Thus, we need to be able to quantify their magnitude as a function of scale and key operating parameters

VIEWGRAPH 2

TECHNICAL ISSUES

- END EFFECTS
 - MAGNETIC FIELD PROFILE
 - * CHANNEL AND MAGNET GEOMETRIES
 - LOAD FACTOR
 - VELOCITY PROFILE CHANGES DUE TO ENDS
- VISCOUS EFFECTS
 - CURRENTS IN SIDE-WALL BOUNDARY LAYERS
 - * VELOCITY PROFILE EFFECTS
 - B WALL AND ELECTRODE WALL
 - * ENTRY LENGTH
 - * EFFICIENCY EFFECTS
 - MHD TURBULENCE DAMPING
 - CHANNEL AND MAGNET GEOMETRIES
- GAS PRODUCTION
 - GENERATION
 - * ELECTRODE DESIGN
 - IMPACT ON PERFORMANCE
 - IMPACT ON NOISE
- NOISE GENERATION
 - VARIOUS MECHANISMS

Considering these technical issues, we have proceeded to structure a program whose specific objectives are:

VIEWGRAPH 3

First, to investigate the performance of thrusters over a wide a parameter range as possible and in doing so identify and quantify the major loss mechanism as a function of the operating parameters.

Secondly, use the data obtained to develop and validate scaling relationships and models so that at the conclusion of the program a capability would exist to evaluate and/or predict the performance of large scale systems of any configuration.

Finally, attempt to develop data on the origin and levels of noise that could be tied to the thruster. The data, hopefully, will demonstrate that the projected low noise levels are likely to be achieved and provide the basis for designing more indepth hydro-acoustic experiments.

VIEWGRAPH 3

PROGRAM OBJECTIVES

- INVESTIGATE THE PERFORMANCE OF MHD THRUSTERS OVER WIDE PARAMETER RANGES AND IDENTIFY AND QUANTIFY MAJOR LOSS MECHANISMS
- DEVELOP VALIDATED MODELS AND/OR SCALING RELATIONSHIPS FOR PREDICTING PERFORMANCE OF FULL SCALE THRUSTER GEOMETRIES IN OPERATIONAL PARAMETER RANGES OF INTEREST
- OBTAIN PRELIMINARY DATA ON THE ORIGIN AND LEVEL OF ACOUSTIC NOISE THAT COULD BE ATTRIBUTED TO THE MHD THRUSTER

To achieve these objectives outlined and to live within cost constraints, we have adopted the following technical approach.

VIEWGRAPH 4

VIEWGRAPH 4

TECHNICAL APPROACH ADOPTED

- FOCUS ON GENERIC TECHNICAL ISSUES IMPACTING MAGNETOHYDRODYNAMIC PERFORMANCE
- TEST FACILITY DESIGN
 - NO MECHANICAL PUMP; FLOW GENERATED BY MHD THRUSTER
 - LARGE EXTERNAL PIPING TO MINIMIZE NOISE LEVELS
 - INTERMITTENT HEAT REMOVAL
 - NO EXTRAORDINARY MEASURES TO QUIET FACILITY
 - MINIMUM COST
- TEST SEVERAL THRUSTERS OF VARYING SIZE AND/OR CONFIGURATION
- EMPLOY 3-D MODELING/DIMENSIONAL ANALYSES TO DEVELOP FUNDAMENTAL UNDERSTANDING OF TECHNICAL ISSUES AND PROJECTION OF PERFORMANCE TO FULL SCALE
- UTILIZE EXISTING ELECTRODE SYSTEMS AVAILABLE FROM INDUSTRY
- ACQUIRE THE PRELIMINARY HYDROACOUSTIC DATA IN CONJUNCTION WITH ACQUISITION OF MAGNETOHYDRODYNAMIC DATA

At this time I would like to discuss several technical issues further to underscore their potential importance in operational ranges that are compatible with achieving acceptable efficiencies, (e.g. low K), and thus to establish the rationale for the program we are pursuing.

First, let me address the end loss mechanism, which is depicted in

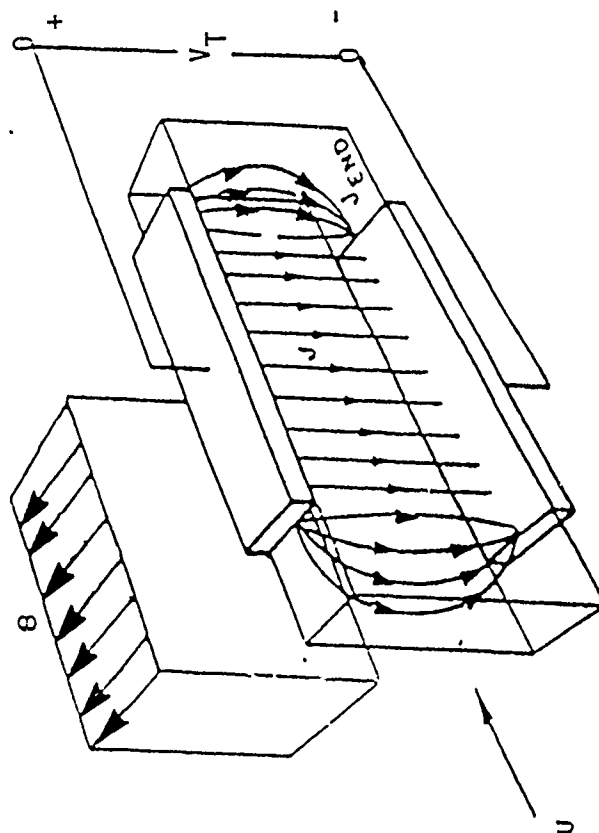
VIEWGRAPH 5

When a voltage is applied across the thruster electrodes, current flows directly between the electrode and also in the end region. The relative flow of current between the region internal and external to the electrodes will depend upon the aspect ratio L/A , the load parameter K , (e.g. $\frac{V_T}{U_a B}$) and the magnetic field distribution

internal and external to the electrodes.

VIEWGRAPH 5

ELECTRICAL END LOSS



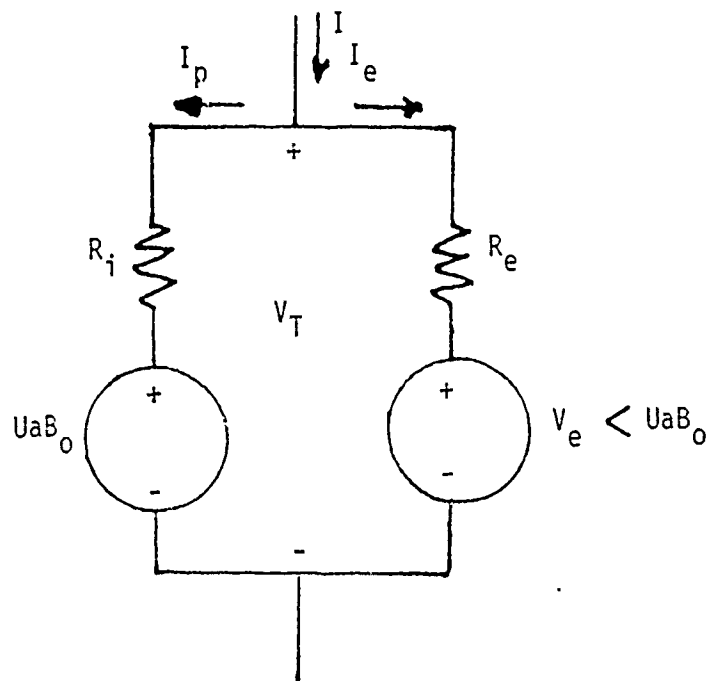
Electrode spacing = a
 Electrode length = L
 Aspect ratio = L/a
 Generated voltage = uaB_0

This fact is perhaps better illustrated on the next

VIEWGRAPH 6

by an equivalent thruster circuit. The thruster here is represented through parallel circuits, each having an effective resistance R_I and R_E . A back EMF is generated in between the electrode whose magnitude is UaB where U is the average velocity and B the magnetic field; in the end region the field tapers off and, therefore, the back EMF is considerably lower than that which exists between the electrodes. The key parameter is the load factor which determines the relative flow of the current to the ends, vis a vis between the electrodes. The uniformity of the field impacts the local load parameters and, hence, current distribution.

VIEWGRAPH 6



$$\text{LOAD FACTOR} = K = V_T / (uaB_o)$$

EQUIVALENT THRUSTER CIRCUIT

On the next

VIEWGRAPH 7

is a table which presents preliminary estimates of the magnitude of the potential losses due to end currents and the non-uniformity of the magnetic field for the large channel we are planing to test, whose aspect ratio $AR=6$.

The first column represents the ideal conditions, no end currents, and constant B field. The second column represents the ideal channel with the existing magnetic field. The third column is the calculated effect of the end current on efficiency. As is apparent, the effects are greatest at the low load parameter.

VIEWGRAPH 7

CALCULATED LOSS IN EFFICIENCY DUE TO NONUNIFORM FIELD AND END LOSS

<u>LOAD FACTOR</u>	<u>IDEAL EFFICIENCY</u>	<u>ACTUAL B EFFICIENCY</u>	
		<u>NO ENDS</u>	<u>WITH ENDS</u>
1.1 .	.90	.86	.78
1.3	.76	.73	.70
1.5	.66 .	.63	.61
2.0 .	.49	.48	.46
3.0	.33	.32	.31
4.0 .	.24	.24	.23

ELECTRODE LENGTH = 3.0 M

ELECTRODE SPACING = 0.5 M

ASPECT RATIO = 6.0

SUPERCONDUCTING FIELD PROFILE

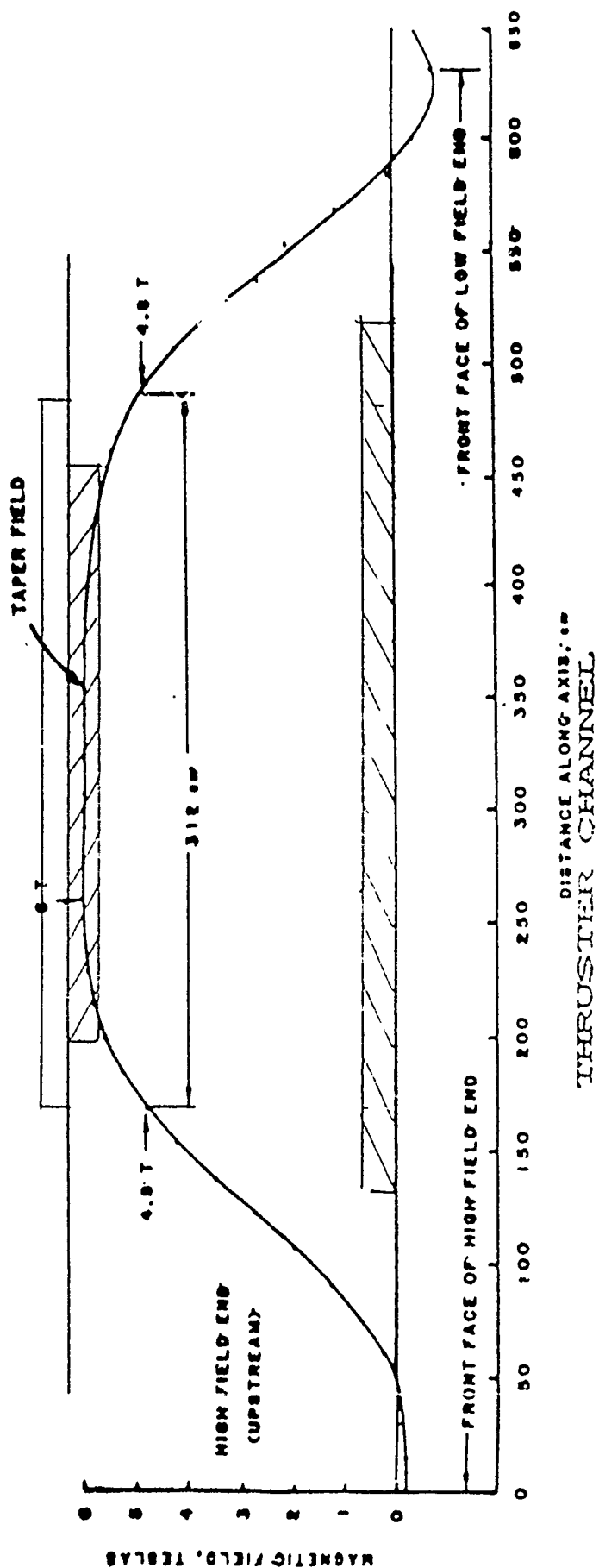
The previous data was for a specified electrode length of 3 meters.

An important issue is the effect on end loss and on efficiency of varying the electrode length within a given magnetic field distribution. Electrodes of various lengths can be positioned within the magnetic field as illustrated on the next

VIEWGRAPH 8

The magnetic field distribution shown is that of the 6T magnet we will use in our test program.

VIEWGRAPH 8



FIELD MEASURED ALONG MAGNET CENTRAL AXIS

Some very preliminary analysis indicates that the impact of electrode length can be significant and there is likely an optimal length. as shown on the next

VIEWGRAPH 9

As is indicated, as the electrode length is increased, the efficiency drops off rapidly; conversely, as the electrode length is reduced to zero, the efficiency approaches the ideal. Under such conditions, however, there is no thrust. Similarly, the ΔP generated increases, and peaks at the length corresponding to the total length of active field. The results suggest that from an overall system optimization viewpoint, there is likely an optimum. We have defined a figure of merit as the $\eta \times \Delta P$ which is plotted and which shows an optimum at about 4 meters.

The issue is to utilize as much of the field as you effectively can to maximize the overall power train performance. For example, as one goes from 3 meters to 4 meters the efficiency drops by

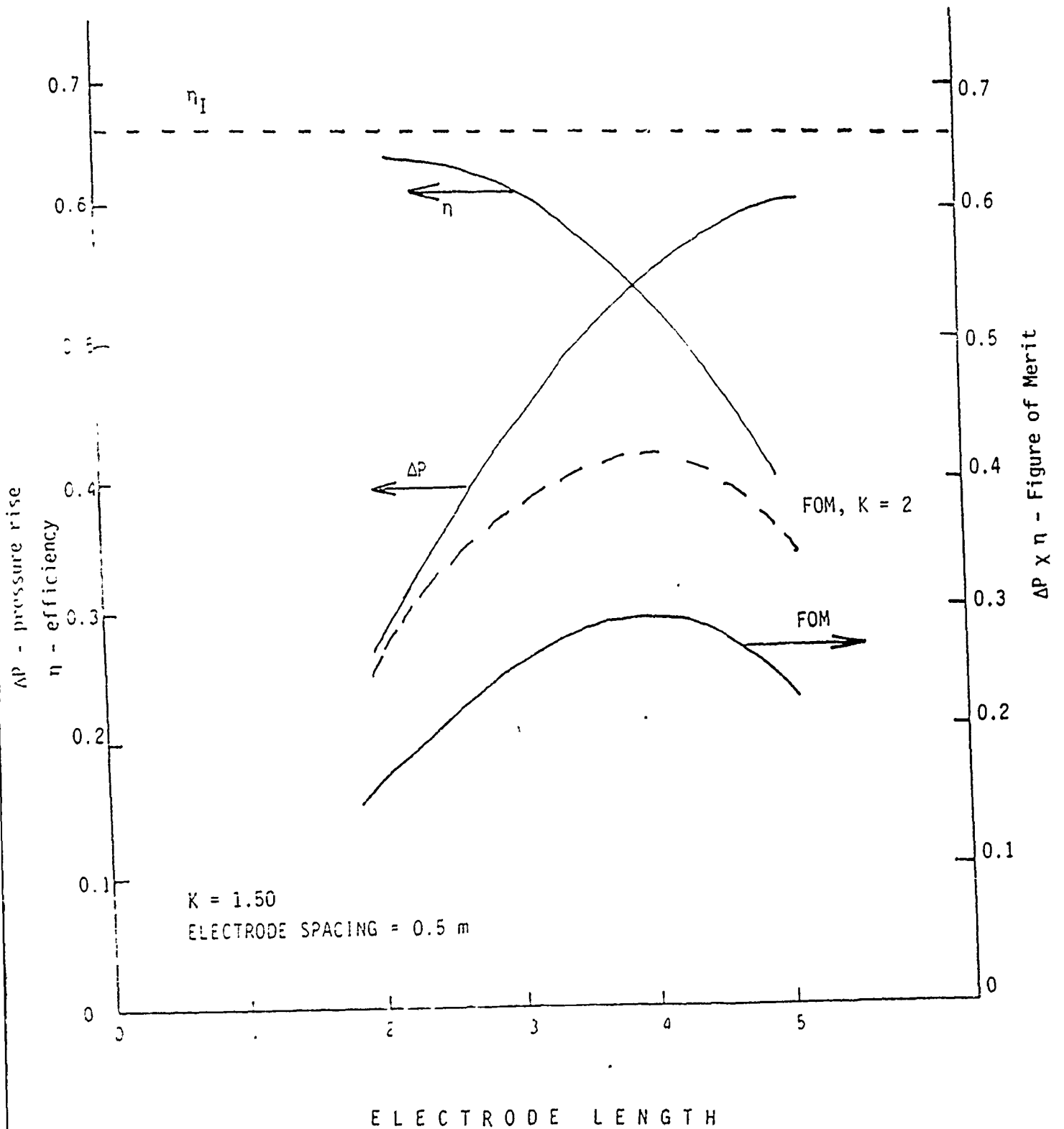
$$\frac{.6162 - .5323}{.6162} = 12\%$$

But the pressure rise increases by

$$\frac{.146 - .414}{.414} = 32\%$$

The relative importance of this phenomenon will depend upon the magnet design (field distribution).

VIEWGRAPH 9



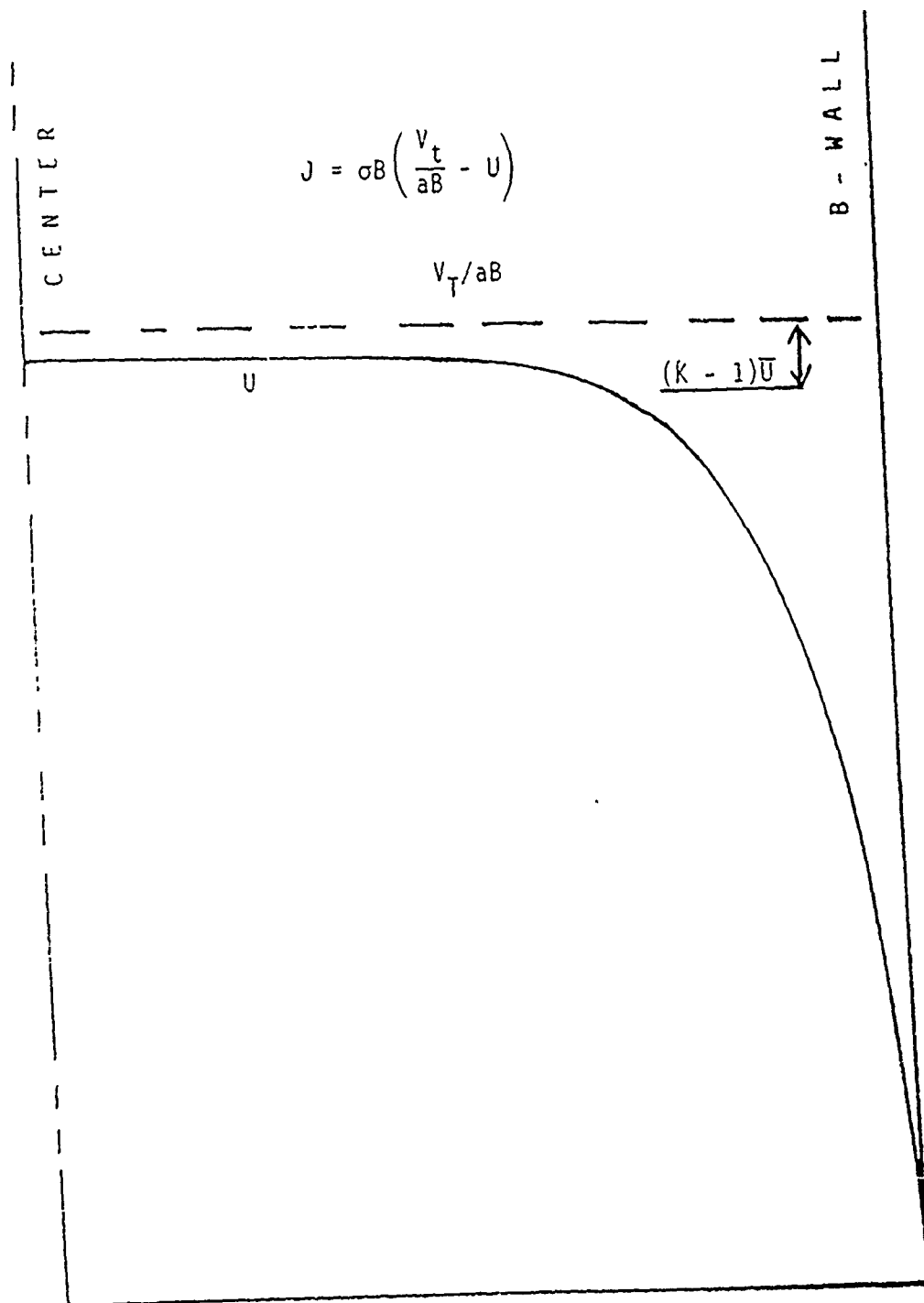
The magnetic field distribution load can also effect the velocity profiles and thus possibly impact the wall shear on both the B wall and the electrode wall and, hence, thruster viscous losses.

That this can happen can be seen from the schematic representation of the flow profile relative to the B wall as illustrated on the next

VIEWGRAPH 10

The current that will pass through the flow locally is given by the relationship indicated where V_T is the applied voltage, B the field, and U is the local velocity. Because of the velocity profile in the flow, the driving force or voltage gradient increases with decreasing distance to the B wall. Therefore, as the wall is approached, the current flow will be increased and the flow accelerated. The net effect is to flatten the velocity profile and increase the velocity gradient near the wall: this in turn will increase the viscous loss.

VIEWGRAPH 10



SIDE-WALL BOUNDARY-LAYER CURRENTS

The effect should be a strong function of the load factor K as schematically illustrated on the next

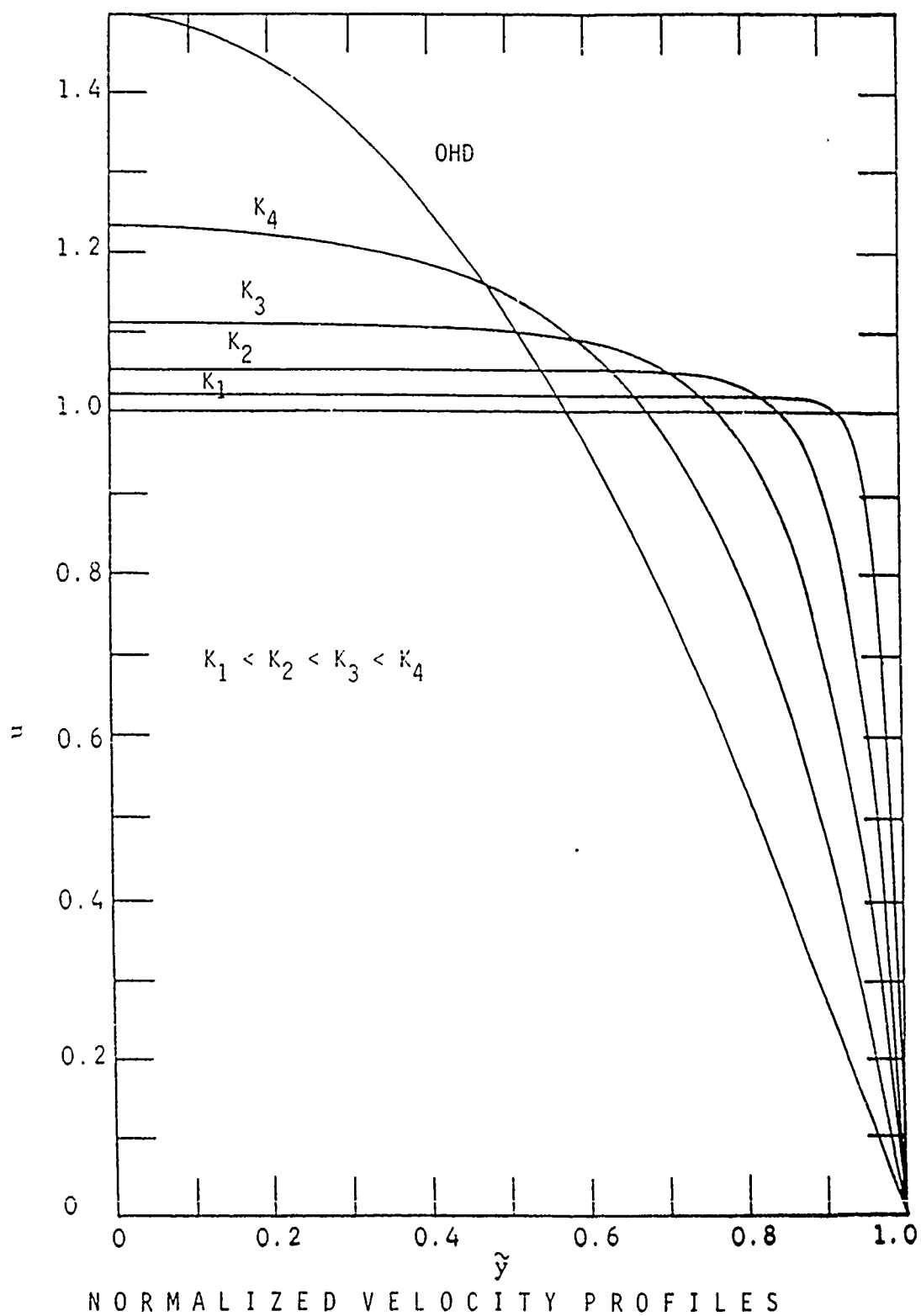
VIEWGRAPH 11

For very large load factors, the effect is expected to be very small and the profiles will be little changed from OHD flows. However, for the low load factors approaching 1, the effect would be significant as indicated. How fast the changes in flow profile will occur in a specific length thruster will be determined by the Interaction Parameter

$$N = \frac{\sigma B^2 L}{\rho U}$$

This effect is currently being evaluated with our 3-D codes.

VIEWGRAPH 11



The velocity profile on the electrode walls can be impacted by interaction of the currents and field distribution in the entrance region.

For example, in the entrance region as illustrated in

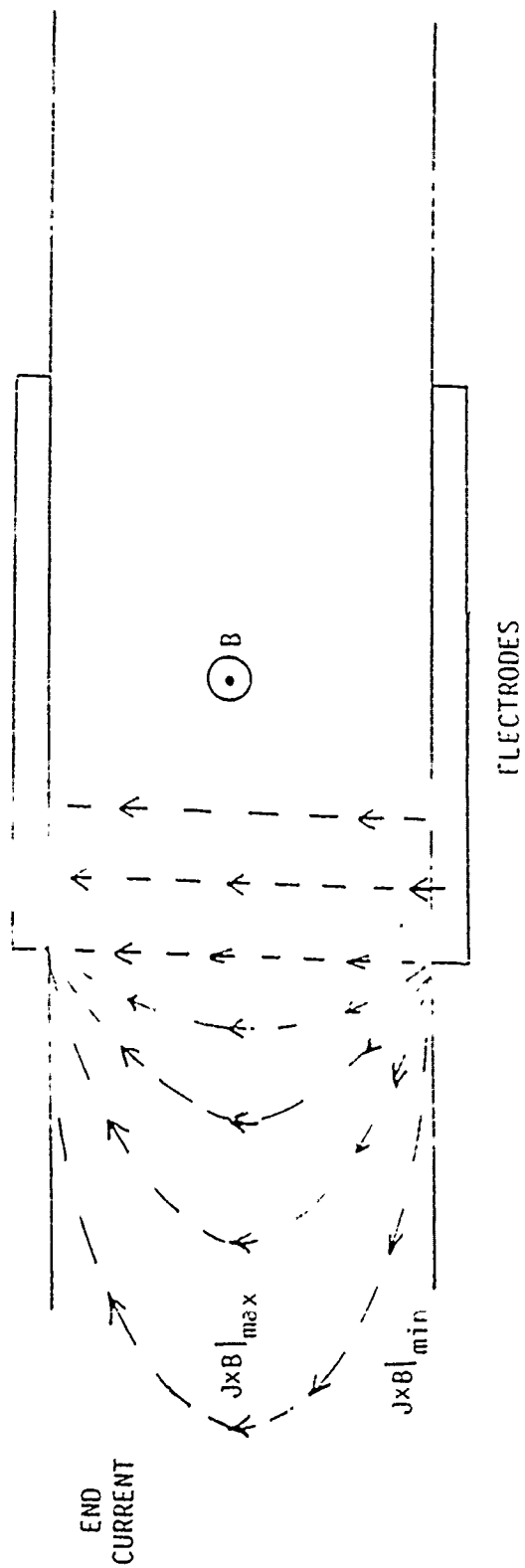
VIEWGRAPH 12

current flows in a pattern similar to that indicated. In the center of the duct the current is orthogonal to the field and flow, whereas as you get near the electrode wall it tends to become much less so. Therefore, the pumping action, the $J \times B$ is much stronger in the center, as compared to near the wall. Thus, one can expect that the velocity gradient will change near the wall thus impacting shear and viscous loss.

Once the flow enters the region in the thruster where the currents are eventually perpendicular to the flows, the $J \times B$ becomes a constant and thus there should be little effect on the velocity profile on the electrode wall. The same phenomena occurs in the exit region.

We have not, as yet, generated any numbers to quantify this affect since we have not completed modification of our 3-D code to account for the end currents. We hope to have this completed within a few months.

VIEWGRAPH 12



THRUSTER CHANNEL

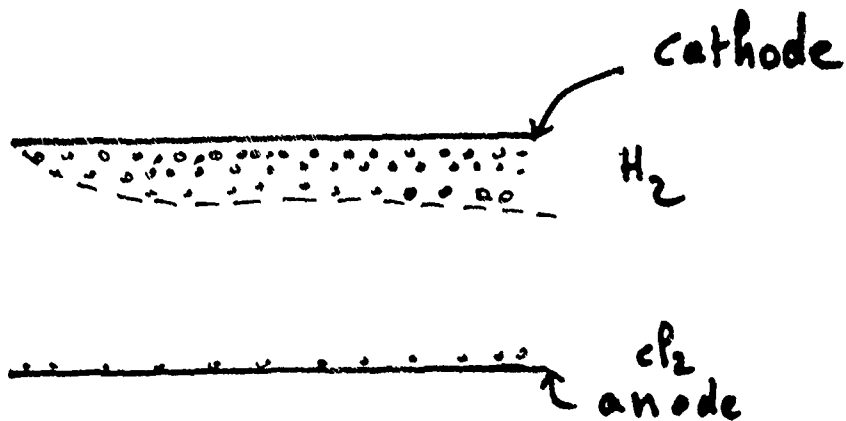
Another important issue that needs to be addressed is the impact of the gaseous bubble generated at the electrode due to electrolysis of the sea water as schematically illustrated on the next

VIEWGRAPH 13

As is indicated there are a number of potential impacts that need to be studied and quantified.

VIEWGRAPH 13

IMPACT OF PRESENCE OF BUBBLE UPON THRUSTER PERFORMANCE



- o DECREASE EFFECTIVE CONDUCTIVITY
- o INCREASE VOLTAGE DROP IN NEIGHBORHOOD OF ELECTRODES
- o DECREASE TOTAL EFFECTIVE VOLTAGE AND CURRENT
- o ALTER CURRENT DISTRIBUTION IN NEIGHBORHOOD OF ELECTRODES
- o DECREASE GLOBAL THRUST
- o INCREASE NOISE SIGNATURE
- o INCREASE ELECTRODE CORROSION AND REDUCE ELECTRODE OPERATING TIME

I would now like to turn to an important task in our program that we are focusing on at present - to develop a Research Plan and to design a Test Facility that will allow us to achieve our technical objectives. Before discussing the Test Plan definition activity, it is worthwhile to summarize the technical issues that we believe need to be investigated. They are as listed on

VIEWGRAPH 14

I tried to touch on most of these; time limitation clearly precludes a detailed discussion of all.

VIEWGRAPH 14

TECHNICAL ISSUES

END EFFECTS

- MAGNETIC FIELD PROFILE

 - CHANNEL AND MAGNET GEOMETRIES

- LOAD FACTOR

- VELOCITY PROFILE CHANGES DUE TO ENDS

VISCOUS EFFECTS

- CURRENTS IN SIDE-WALL BOUNDARY LAYERS

 - VELOCITY PROFILE EFFECTS

 - HARTMANN & TURBULENT PROFILES

 - ENTRY LENGTH

 - EFFICIENCY EFFECTS

- MHD TURBULENCE DAMPING

GAS PRODUCTION

- GENERATION

 - ELECTRODE DESIGN

- IMPACT ON PERFORMANCE

- IMPACT ON NOISE

NOISE GENERATION

SCALE-UP

- DIMENSIONLESS PARAMETERS

- RANGE FOR EXPERIMENTS

- RANGE FOR APPLICATIONS

We have adopted several specific objectives as we proceed to develop the Research Plan and the actual Test Program. They are given on the next

VIEWGRAPH 15

VIEWGRAPH 15

OBJECTIVE OF TEST PROGRAM

- ACQUIRE DATA OF SUFFICIENT BREADTH, RESOLUTION, AND ACCURACY FOR PROPER VALIDATION OF THRUSTER PERFORMANCE
 - CONFIRMATION OF KEY ASSUMPTIONS (E.G., VALIDITY OF TURBULENCE MODELS, TREATMENT OF END LOSSES)
 - RESOLUTION OF CRITICAL ISSUES (E.G., EFFECT OF H_2 BUBBLES ON THRUSTER PERFORMANCE)
 - PERFORMANCE PREDICTION AT DESIGN AND OFF DESIGN OPERATION
- ACQUIRED DATA ON ACOUSTIC NOISE (DTRC), IDENTIFY NOISE SOURCES, AND CORRELATE ACOUSTIC SIGNATURES WITH OPERATIONAL PARAMETERS OF THRUSTER
- CONFIRM ABSENCE OF UNANTICIPATED EFFECTS THAT CAN ADVERSELY AFFECT PERFORMANCE

The principal features of the Experimental Program we are developing are given in

VIEWGRAPH 16

VIEWGRAPH 16

FEATURES OF EXPERIMENTAL PROGRAM

- THRUSTERS OF DIFFERENT SIZES (AND POSSIBLY CONFIGURATIONS)
 - STUDY EFFECT OF SURFACE TO VOLUME RATIO
 - OBTAIN DATA TO CONFIRM SCALING RELATIONSHIPS
 - COMPARE PERFORMANCE OF DIFFERENT THRUSTER DESIGNS
- STEADY STATE, START-UP, AND COAST DOWN TESTING
 - STUDY ABILITY OF DESIGN CODES TO PREDICT TRANSIENT BEHAVIOR
 - DETERMINE TRANSIENT OPERATIONAL CHARACTERISTICS
- PERFORMANCE MEASUREMENTS UNDER A WIDE RANGE OF MAGNETIC FIELDS, LOAD FACTORS, AND EXTERNAL LOADS
 - OBTAIN PERFORMANCE CURVES OF THRUSTER
- GLOBAL AND LOCAL MEASUREMENTS
- VARIABLE AMBIENT PRESSURE TO STUDY EFFECTS OF GAS PHASE SOLUBILITY ON BUBBLE GENERATOR, EVOLUTION, AND CONTRIBUTION TO NOISE

The specific measurements we are planning to make are given on

VIEWGRAPH 17

VIEWGRAPH 17

GLOBAL MEASUREMENTS

- OVERALL PRESSURE RISE
- FLOW RATE
- APPLIED VOLTAGE
- ELECTRIC POWER INPUT
- MAGNETIC FIELD
- RAPID DATA ACQUISITION RATE ALLOWS STUDY OF TRANSIENT BEHAVIOR AND EXTENSIVE TEST PARAMETER RANGE

LOCAL MEASUREMENTS

- AXIAL PRESSURE DISTRIBUTIONS
- VELOCITY PROFILES (MEAN AND RMS)
- VOLTAGE DISTRIBUTIONS
- GAS PHASE DISTRIBUTIONS
- TAKEN AT SELECTED LOCATIONS AND OPERATING PARAMETERS TO PROVIDE IN DEPTH VALIDATION OF CODE MODELS AND HELP RESOLVE DISCREPANCIES BETWEEN PREDICTED AND MEASURED PERFORMANCE

The diagnostics we are considering to obtain the data desired are

VIEWGRAPH 18

VIEWGRAPH 18

INSTRUMENTATION

PRESSURE: HIGH QUALITY DIFFERENTIAL PRESSURE
TRANSDUCERS OUTSIDE MAGNETIC FIELD CONNECTED
THROUGH MANIFOLDS AND VALVES TO SEVERAL
PRESSURE MEASUREMENT LOCATIONS

VELOCITY: HOT FILM ANEMOMETRY
LDV (IF RESOURCES PERMIT)
SELECTED LOCATIONS INSIDE THE MAGNET
VELOCITY PROFILES AT NOZZLE AND DIFFUSER.
COMPUTER CONTROLLED TRAVERSING MECHANISMS
USING ANEMOMETERS

VOLTAGE: VOLTAGE PROBES

VOID FRACTION: CONDUCTIVITY PROBES. OPTICAL TECHNIQUES.

COMPUTER BASED DAS

The Hydroacoustics experiments that we plan to pursue on the thruster, while preliminary in nature, are very important. Therefore, it is appropriate that I expand a little on what is being planned in this area. It should be noted that the hydroacoustics research is being planned and will be implemented by Dr. Ted Farabee of David Taylor Research Center.

A listing of the potential noise mechanisms for an MHD propulsor is given in

VIEWGRAPH 19

The ANL program will be dealing with only the first three.

UNCLASSIFIED

POTENTIAL NOISE MECHANISMS FOR A MHD PROPULSOR

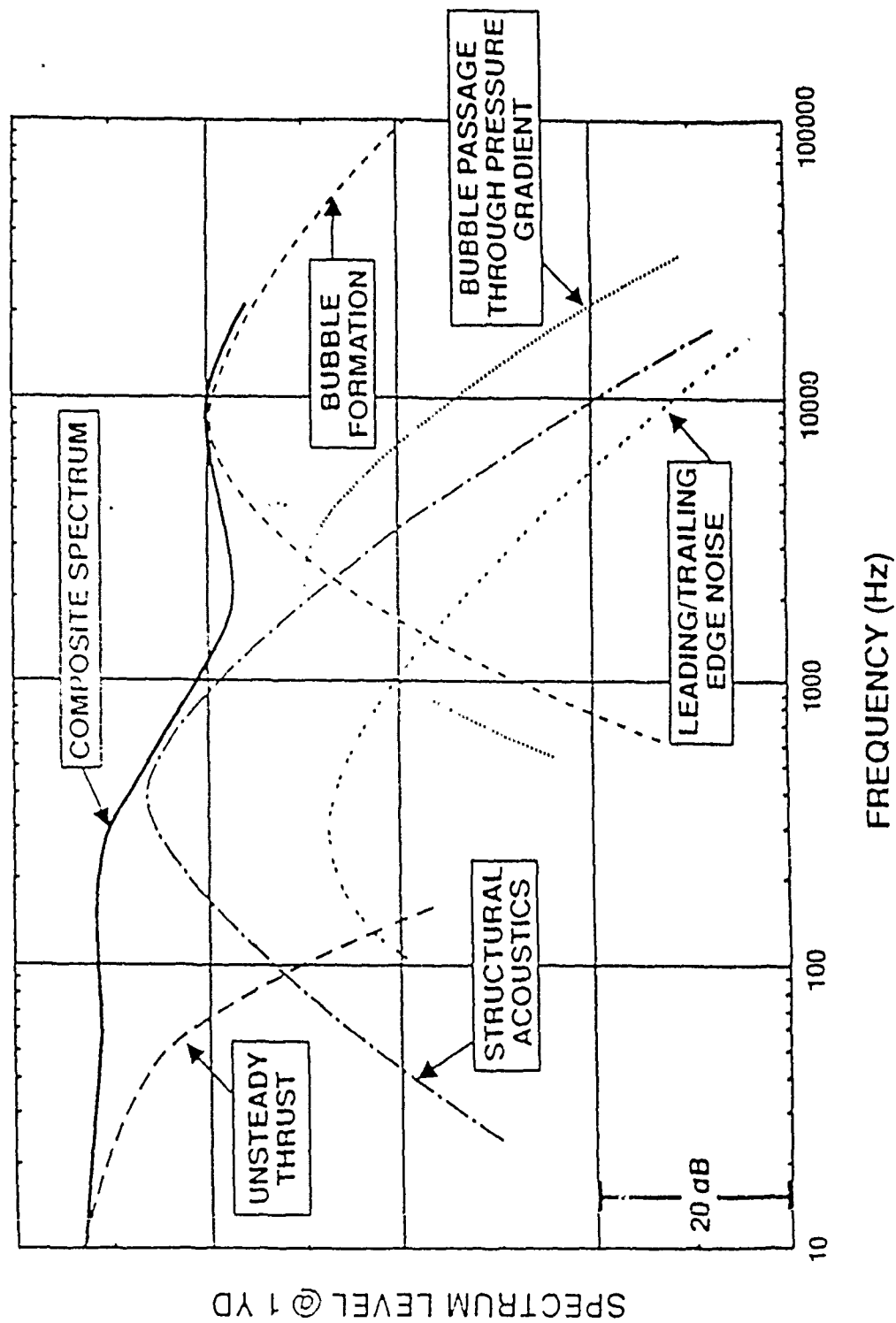
- BUBBLE FORMATION NOISE
- PASSAGE OF BUBBLES THROUGH PRESSURE GRADIENTS
- UNSTEADY THRUST
- LEADING AND TRAILING EDGE NOISE
- STRUCTURAL ACOUSTIC

A conceptual signature of the MHD thruster is given in

VIEWGRAPH 20

to illustrate potential frequency ranges associated with
each mechanism

CONCEPTUAL SIGNATURE OF MHD THRUSTER



The Hydroacoustic Program Objectives, it's associated Facility Design requirements, and the experimental approach is given in the next 4 viewgraphs.

VIEWGRAPHS 21, 22, 23, & 24

PROGRAM OBJECTIVES (ACOUSTIC ISSUES)

- DEVELOP PRELIMINARY DATA ON ACOUSTIC PERFORMANCE OF MHD THRUSTERS
- CONDUCT TESTS WITH A THRUSTER OF NEARLY PROTOTYPICAL SIZE
- ACQUIRE ACOUSTIC DATA OVER A WIDE RANGE OF PARAMETERS (ELECTRIC FIELD, MAGNETIC FIELD, AMBIENT PRESSURE, ETC.)
- PROVIDE GUIDANCE TO FUTURE ACOUSTIC EVALUATIONS OF MHD THRUSTER SYSTEMS

FACILITY DESIGN APPROACH (ACOUSTIC ISSUES)

- POTENTIAL NOISE SOURCES EVALUATED DURING CONCEPTUAL DESIGN PHASE AND DESIGN TRADE OFFS CONSIDERED
- CANDIDATE FLOW LOOP CONTAINS NO PUMP; FLUID DRIVE BY MHD THRUST ALONE
- LARGE DIAMETER PIPING REDUCES FLOW VELOCITIES; REDUCES NOISE (NOISE $\sim U^{**6}$)
- PROVIDE FOR STATIC PRESSURE VARIATIONS (15-50 PSI)
- TESTING OF VARIOUS SIZED THRUSTERS WITH ONE AT NEARLY PROTOTYPICAL SIZE
- PAY PARTICULAR ATTENTION TO FACILITY ACOUSTIC ISSUES BUT DO NOT ALLOW ACOUSTIC CONSIDERATIONS TO DRIVE FACILITY DESIGN (\$)

EXPERIMENTAL APPROACH (ACOUSTIC ISSUES) con't

TEST CONDITIONS

- ACQUIRE DATA OVER A RANGE OF PARAMETERS (ELECTRIC FIELD, MAGNETIC FIELD, STATIC PRESSURE, ETC.)
- CONDUCT EVALUATIONS FOR DIFFERENT THRUSTER GEOMETRIES
- ACQUIRE DATA FOR "COASTDOWN" RUNS TO HELP SEPARATE FACILITY NOISE FROM THRUSTER DATA
- EVALUATE FEASIBILITY OF ACQUIRING MEANINGFUL HYDROACOUSTIC DATA DURING FACILITY CHARACTERIZATION PHASE (FIRST PHASE)

EXPERIMENTAL APPROACH (ACOUSTIC ISSUES)

HYDROPHONE MEASUREMENTS

- ACQUIRE ACOUSTIC DATA USING GROUPS (3 ELEMENT ARRAY) OF FLUSH MOUNTED PRESSURE SENSORS
- LOCATE SENSOR GROUPS UPSTREAM AND DOWNSTREAM OF THRUSTER AND WITHIN THRUSTER DUCT
- USE CROSS SPECTRUM DATA BETWEEN PAIRS WITHIN GROUPS AND BETWEEN DIFFERENT GROUPS TO HELP SEPARATE THRUSTER NOISE FROM FACILITY NOISE
- MOUNT PRESSURE SENSORS BENEATH ELASTOMER BLANKET TO PROVIDE ATTENUATION TO TURBULENCE PRESSURES

ACCELEROMETER MEASUREMENTS

- UTILIZE WALL MOUNTED ACCELEROMETERS TO MONITOR DUCT VIBRATIONS (POSSIBLE ACOUSTIC CONTAMINATION)
- MEASURE ELECTRODE VIBRATIONS WITH ACCELEROMETERS

To facilitate implementation of the Experimental Program, a large Volumetric Flow Test Facility that can take full advantage of the capabilities of the large 6T magnet is being designed and built. This task has just been initiated and therefore what is presented must be construed as very preliminary; changes are assured.

The Facility design objectives, its main design features, and a schematic of the initial configuration being considered for the flow loop are given in

VIEWGRAPHS 25, 26, and 27

DESIGN OBJECTIVES

LOW HYDRAULIC LOSSES

MANAGEMENT OF ELECTROLYTIC PRODUCTS AND MAINTENANCE OF
WATER CHEMISTRY

ACCESSIBILITY FOR CLEANING AND REPAIRS

NOISE CONTROL

COST

MAIN DESIGN FEATURES OF FLOW TEST LOOP

LARGE DIAMETER POLYETHYLENE PIPE

- Low Frictional Losses Due to Smoothness and Low Velocity
- Low Cost
- Good Sound Damping Characteristics

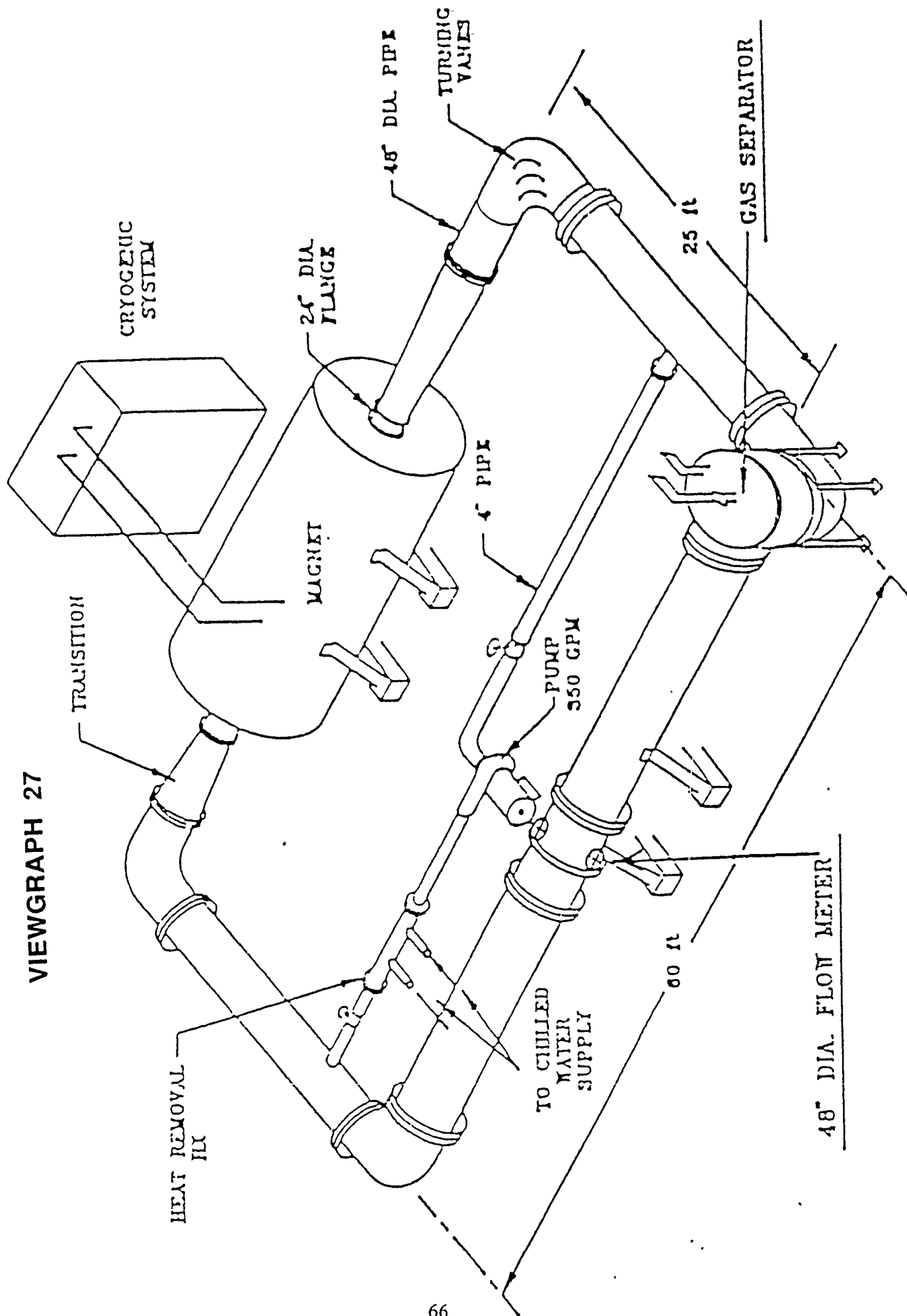
DIFFUSERS FOR ENTERING AND EXITING THE THRUSTER SECTION FLOW STRAIGHTENERS AT CORNERS

- Reduce Flow Losses

TANK INTEGRATED IN THE LOOP

- Provides a Free Surface for Hydrogen to Separate
- Convenient Place to Pressurize the System and Safely Vent Hydrogen

VIEWGRAPH 27



Last, but not least, I would like to describe briefly the analysis and modelling activity which is considered to be crucial to quantifying and developing a fundamental understanding of the loss mechanisms of interest; also for generating a validated capability for predicting full scale thruster performance.

The objectives, this approach and the specific tasks being pursued are summarized in

VIEWGRAPHS 28, 29, 30, and 31

VIEWGRAPH 28

ANALYSIS AND MODELING

OBJECTIVES

- 0 PREDICT AND ESTABLISH ELECTRICAL AND HYDRODYNAMIC CHARACTERISTICS OF THE SEA WATER THRUSTER
 - 0 ESTABLISH A THREE-DIMENSIONAL ELECTRICAL SOLUTION FOR THE THRUSTER CORE AND THRUSTER ENDS (PREDICTION OF END POWER LOSSES) FOR DIFFERENT OPERATING CONDITIONS
 - 0 ESTABLISH THE IMPACT OF BUBBLES PRODUCED BY ELECTROLYSIS UPON THRUSTER PERFORMANCE
 - 0 SELECT DIMENSIONAL ANALYSIS VARIABLES; CHECK DIMENSIONAL ANALYSIS CONCEPT BY PERFORMING THREE-DIMENSIONAL SIMULATIONS

VIEWGRAPH 29

APPROACH

0 MODIFY AND USE THE THREE-DIMENSIONAL SINGLE PHASE MHD COMPUTER CODE (MGMH) TO PREDICT AND ESTABLISH THRUSTER THREE-DIMENSIONAL ELECTRICAL AND HYDRODYNAMIC PERFORMANCES

69

* MGHM CODE IS A THREE-DIMENSIONAL MULTIGRID SINGLE-PHASE ELECTRIC AND HYDRODYNAMIC SOLVER DEVELOPED AT ANL FOR THE ANALYSIS OF MHD GENERATORS AND DIFFUSERS

VIEWGRAPH 30

ANALYSIS AND MODELING TASKS

TASK 1

THREE-DIMENSIONAL ELECTRICAL SOLUTION (THRUSTER CORE AND END EFFECTS)

1.1 MODIFICATION OF THE THREE-DIMENSIONAL ELECTRICAL SOLUTION FOR THRUSTING OPERATION MODE

- IMPOSED VOLTAGE OPERATION MODE ; FIND THRUST
- IMPOSED INLET FLOWRATE MODE ; FIND VOLTAGE

1.2 MODIFICATION OF THE ELECTRICAL SOLUTION TO PREDICT END LOSSES

- IMPLEMENTATION OF A THREE-DIMENSIONAL ELECTRICAL SOLUTION BY REPLACING THE PRESENT TWO-DIMENSIONAL INFINITE SEGMENTATION MODEL
- IMPLEMENTATION OF MIXED BOUNDARY CONDITIONS

1.3 CODE VALIDATION WITH ANALYTICAL SOLUTIONS, EXPERIMENTAL DATA OR OTHER ANALYSES

VIEWGRAPH 31

ANALYSIS AND MODELING TASKS (CONT'D)

TASK 2 NEAR ELECTRODE BUBBLE MODEL

2.1 IMPLEMENT THE SOLUTION OF A BUBBLE CONSERVATION EQUATION (CONVECTIVE-DIFFUSION EQUATION) WITH UNSAGER'S GENERALIZED DIFFUSION COEFFICIENTS ASSOCIATED WITH THE MAIN DRIVING FORCES (MAGNETIC PRESSURE-DROP, BUOYANCY, INTERPHASE DRAG, ...)

2.2 ESTABLISH TWO-PHASE TURBULENT LAW OF THE WALLS WITH IMPLEMENTATION OF TWO-PHASE TURBULENT KINETIC ENERGY AND ITS DISSIPATION RATE MODELS

2.3 PREDICT BUBBLE CONCENTRATION IN THRUSTER, LOCAL CONDUCTIVITIES, ELECTRODE VOLTAGE DROP AND THRUST EFFICIENCY LOSS DUE TO PRODUCTION OF BUBBLES BY ELECTROLYSIS

THIS PAGE IS INTENTIONALLY BLANK

**SUPERCONDUCTING ELECTROMAGNETIC
THRUSTER FOR SEAWATER PROPULSION**

Presented by

Dr. J.C.S. Meng



SUPERCONDUCTING ELECTROMAGNETIC THRUSTER FOR SEAWATER PROPULSION

ONR/DARPA MHD SUBMARINE PROPULSION WORKSHOP

16,17 NOVEMBER 1989

**SUBMARINE WARFARE SYSTEMS DIRECTORATE
NAVAL UNDERWATER SYSTEMS CENTER
NEWPORT, RHODE ISLAND 02841-5047**

**Principle Investigator:
DR. J.C.S. MENG, CODE 804
(401) 841-3560**



PRESENTATION OUTLINE

OVERVIEW

**HISTORICAL BACKGROUND
RATIONALE FOR NAVY'S INTEREST
JAFSA'S PROGRAMS
DOD (DARPA, ONT, NUSC) PROGRAMS**

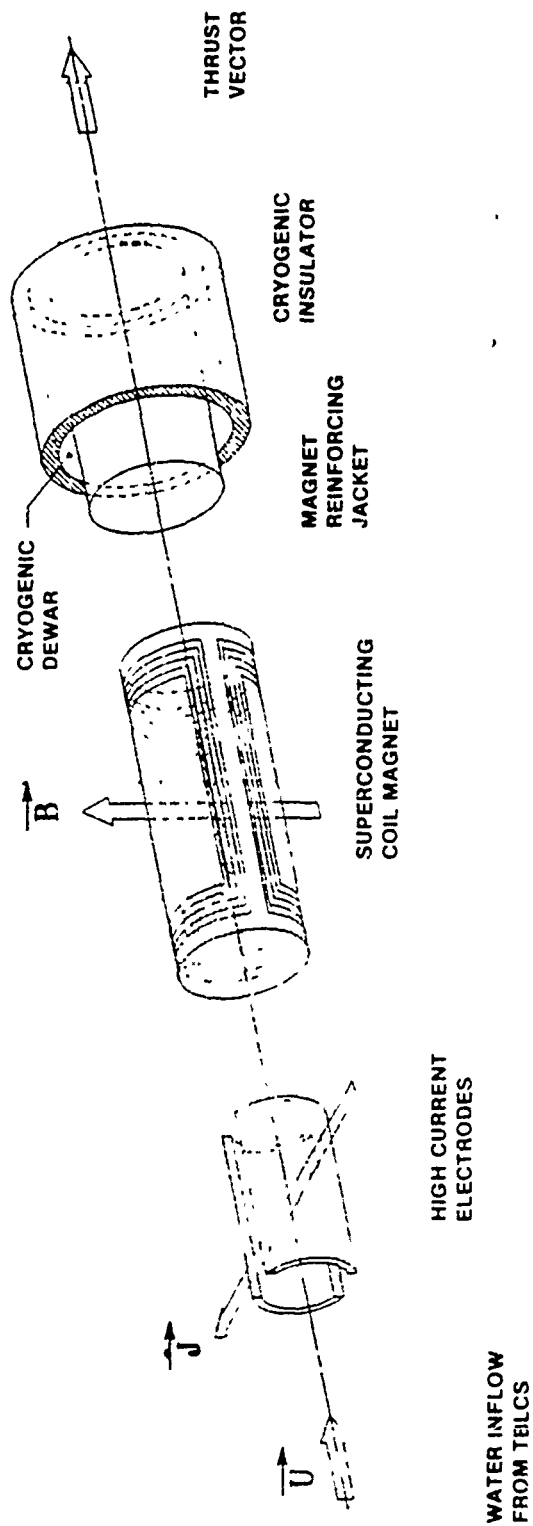
TECHNOLOGY AREAS AND GOALS

**PROPULSOR
HIGH CURRENT DENSITY SEAWATER ELECTRODE AND
POWER SOURCE
SUPERCONDUCTING MAGNET
CRYOSTAT
ESTIMATES OF SIZE AND WEIGHT AND INTEGRATION
CONFIGURATIONS**

FUTURE DIRECTIONS



BASIC SCEMT COMPONENTS





RATIONALE FOR SCENT

ELIMINATION OF PROPELLER

- EMT EXERTS FORCE OVER THE ENTIRE THRUSTED WATER VOLUME VERSUS PROPELLER ON WATER OVER BLADES.
- NATURE'S MOST EFFICIENT UNDERWATER PROPULSORS, WHALES, DOLPHINS WHICH ARE QUIET, PRODUCE LITTLE TURBULENCE AND EVOLVED OVER 10⁶ YEARS DO NOT RESEMBLE ANYTHING LIKE A PROPELLER.

SIMPLICITY

- NO MOVING PARTS, NO MECHANICAL NOISE, NO MECHANICAL WEAR.
- MATURED TECHNOLOGY, DRAW FROM THE EXISTING DATA BASE OF NMR (MEDICAL), AND MHD PUMP FOR LIQUID METAL (FAST BREEDER REACTOR).
- CRYOSTAT SHELF LIFE UP TO A YEAR WITHIN REACH.

POTENTIAL

- SHOULD, IN PRINCIPLE, BE THE QUIETEST UNDERWATER PROPULSION, AND WILL BRING THE RADIATED NOISE TO THE TBL NOISE FLOOR, WHICH CAN FURTHER BE REDUCED BY TBLCS.
- QUANTUM LEAPS IN SUPERCONDUCTING MATERIAL DEVELOPMENT PROJECTS GREAT INCREASE OF EMT EFFICIENCY (FROM 1% NOW TO 70%)



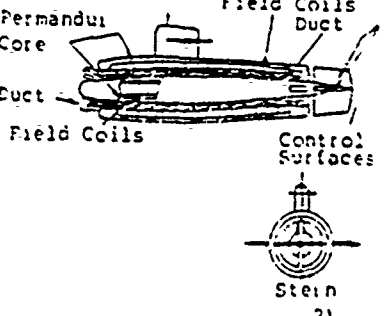
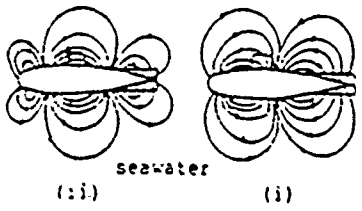
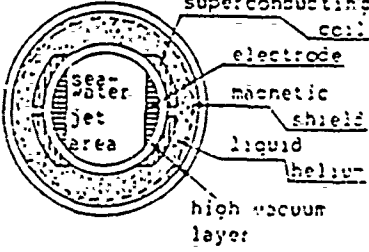
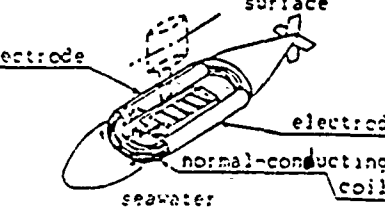

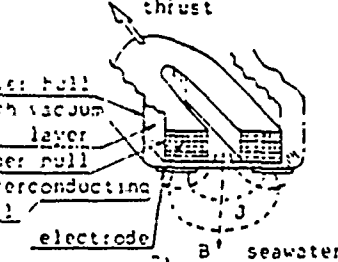
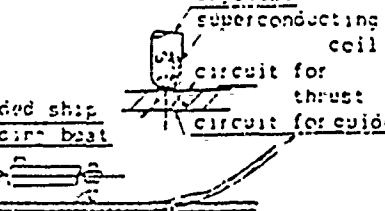
HISTORICAL BACKGROUND

ELECTROMAGNETIC THRUSTER (EMT)

- W. RICE OBTAINED A U.S. PATENT IN 1961.
- G. BACKUS FROM MIT PROPOSED AN EXTERNAL EMT CONCEPT, AND O.M. PHILLIPS (1962) REVIEWED IT, AND CONCLUDED THE LIMITING FACTORS ARE WATER'S LOW ELECTRIC CONDUCTIVITY AND THE MAXIMUM AVAILABLE B (0.6T THEN).
- WAY (1968) CONSTRUCTED A 10' LONG SUBSCALE SUBMARINE, WITH $B = 0.015T$ AND PROPELLED IT AT 0.4 M/SEC.
- HUMMERT (1979) CONDUCTED AN EVALUATION OF DC EMT IN SEAWATER AND SHOWED PROMISING INCREASE OF EMT EFFICIENCY IF B CAN BE INCREASED TO 5T.
- TADA AND SAJI (1983) CARRIED OUT EXPERIMENTS ON A SUBSCALE SHIP SCENT WITH $B = 2T$ AND CONCLUDED THAT ONLY A BREAKTHROUGH IN SUPERCONDUCTIVITY CAN BRING ABOUT EMT'S ADVANCES.



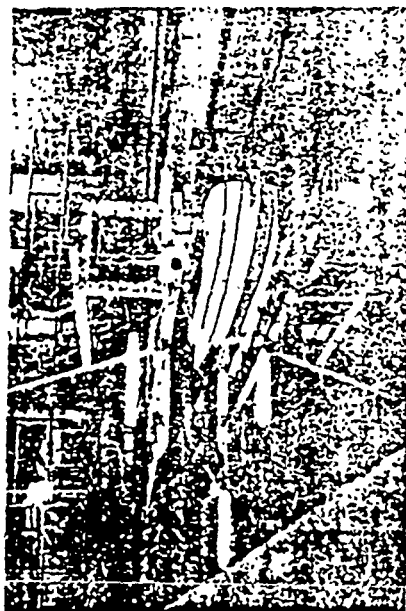
TYPES OF HYDRODYNAMIC SCENT

active region magnetic field	inner type	outer type
AC group	 <p>(b) AC-inner duct type²⁾</p>	 <p>(i) (ii)</p> <p>seawater</p> <p>(iii) is approximately one-fourth cycle after (i).</p> <p>(a) A.C. magnetic field type²⁾</p>
	 <p>(c) inner field type³⁾</p>	 <p>(d) bipolar coordinate type⁴⁾</p>
DC group	 <p>(e) charging melting metal type⁶⁾</p>	 <p>(f) panel type⁷⁾</p>
		 <p>(g) charging circuit type⁸⁾</p>



EXPERIMENTAL MODELS OF HYDRODYNAMIC EMT

ST-500
(TADA & SAJI, 1983)



EMS-1
(WAY, 1968)



HIGHLIGHTS OF JAFSA'S SCEMT

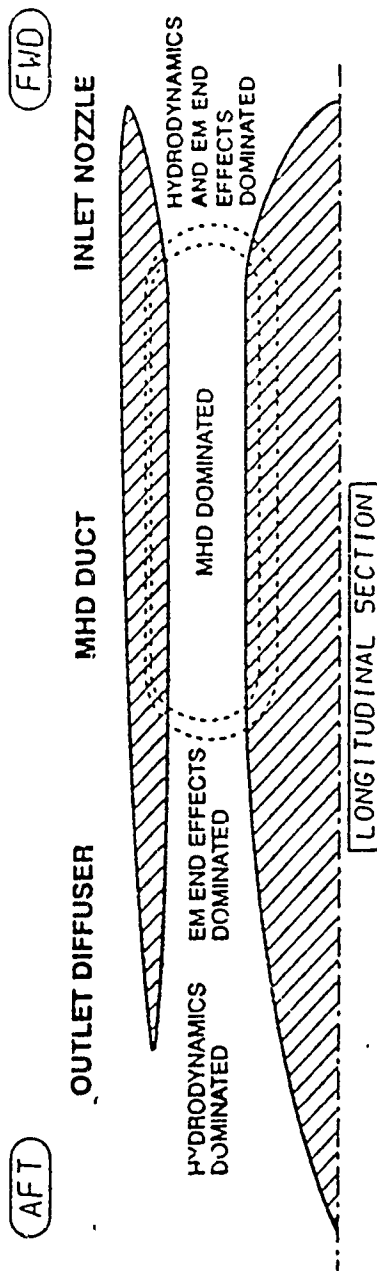
EXPERIMENTAL SHIP (TEST PLATFORM)

- HULL FORM: CATAMARAN LIKE MONO-HULL
- DIMENSIONS: 30m IN LENGTH, 10m IN BREADTH
- DISPLACEMENT: 185 TONS
- SPEED: 8 KTS

EXPERIMENTAL SHIP SCEMT PROPULSOR

- CONFIGURATION
 - 2 PROPULSION UNITS, EACH CONTAINS 6 SMALL SCEMT'S
 - 1.8m IN OUTSIDE DIAMETER, 5m IN LENGTH
- SC MAGNET
 - 26cm IN DIAMETER, 5m IN LENGTH
 - MAGNETIC INDUCTION IN SEAWATER: 4 TESLA
- ELECTRODES
 - ELECTRICAL CURRENT IN SEAWATER: $2 \times 10^3 \text{ A/m}^2$ (200 mA/cm^2)
 - UNKNOWN PARAMETERS: VOLTAGE, DIMENSIONS, MATERIAL, ETC.
- THRUSTER
 - TOTAL WEIGHT: 100 TONS
 - TOTAL THRUST: EXPECTED TO BE 8000N ($1.8 \times 10^3 \text{ LB,}$) FROM 2 UNITS
 - ΔP SCEMT: $\sim 8 \times 10^4 \text{ N/m}^2 \approx 11 \text{ PSI}$
 - EFFICIENCY: $\sim 4\%$

PHENOMENOLOGY AND DESIGN FACTORS FOR MHD CHANNEL DYNAMICS



PHENOMENOLOGY

- DECELERATION DUE TO EXPANSION
- INTERACTION WITH $J \times B$ END EFFECTS
- FLOW SEPARATION
- VORTEX CONTRACTION
- $J \times B$ DOMINATE OVER VISCOUS EFFECTS
- FLOW ACCELERATION
- FORMING PROGRESSIVELY LAMINAR CORE FLOW
- GAS GENERATION DUE TO ELECTROCHEMISTRY
- BUBBLE LAYER FORMATION OVER ELECTRODES
- ACCELERATION DUE TO CONTRACTION
- INTERACTION WITH $J \times B$ END FIELD
- VORTICITY STRETCHING
- TURBULENCE DAMPING

DESIGN GOALS

- UNIFORM OUTFLOW
- NO FLOW SEPARATION
- MAX PRESSURE THRUST
- MINIMUM MISALIGNMENT OF $J \times B$ END FIELD WITH DIFFUSER PROFILE
- MAXIMUM PRESSURE INCREASE AND THRUST
- TAILOR B TO PROVIDE UNIFORM $J \times B$ FORCE DENSITY
- MAXIMUM INTERACTION PARAMETER TO DAMP TURBULENCE
- MINIMUM BUBBLE EFFECTS
- UNIFORM INFLOW
- MINIMUM TURBULENCE
- MAXIMUM ALIGNMENT TO $J \times B$ END FIELD

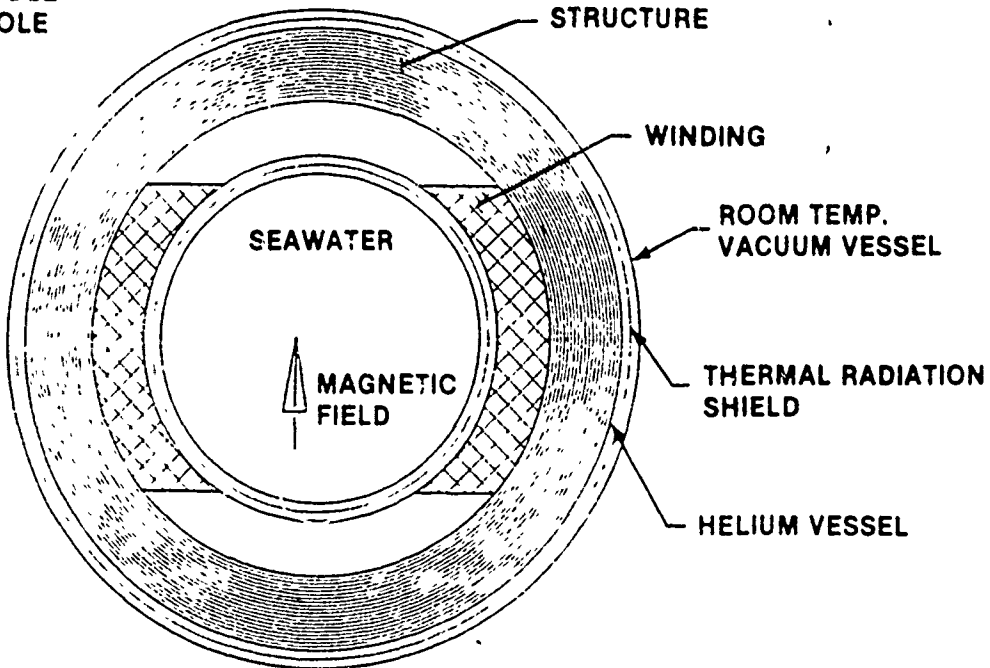
RELEVANT PHYSICS FOR SCEMT AND SEAWATER MHD

HYDRODYNAMICS	ELECTRODYNAMICS	MAGNETOHYDRODYNAMICS
<ul style="list-style-type: none"> • INVISCID EFFECTS <ul style="list-style-type: none"> - INLET/OUTLET FLOW DISTRIBUTIONS - PRESSURE FIELD - THRUST DISTRIBUTION • VISCOUS EFFECTS <ul style="list-style-type: none"> - FLOW SEPARATION AT INLET/OUTLET - TURBULENCE GENERATION AND DAMPING - PRESSURE LOSS EFFECTS ON THRUST DISTRIBUTION • THRUST AUGMENTATION <ul style="list-style-type: none"> - MOMENTUM THRUST vs PRESSURE THRUST - FLOW NOISE vs UNSTEADY THRUST NOISE - CONSISTENCY AMONG HYDRODYNAMIC AND MHD FRINGE FIELD EFFECTS 	<ul style="list-style-type: none"> • ELECTROHYDRODYNAMICS <ul style="list-style-type: none"> - GENERATION OF SECONDARY FLOWS - TURBULENCE GENERATION • ELECTROCHEMISTRY <ul style="list-style-type: none"> - DIFFERENT CHEMISTRIES - ELECTRODE CORROSION - GAS GENERATION RATES - ELECTRIC FIELD FRINGE EFFECTS - ENERGY BUDGET REDUCTION - NEAR ELECTRODE EFFECTS - MASS TRANSFER MECHANISMS - LIMITING CURRENT AND VOLTAGES • BUBBLE IN SEAWATER <ul style="list-style-type: none"> - GENERATION RATE - SIZE SPECTRUM - GROWTH/DISSOLUTION RATES - ELECTROSTATIC CHARGE - DEPTH PRESSURE EFFECTS - TURBULENT DAMPING DUE TO BUBBLES - REDUCTION EFFECTS ON ELECTRICAL CONDUCTIVITY 	<ul style="list-style-type: none"> • MAGNETIC EFFECTS <ul style="list-style-type: none"> - TURBULENCE DAMPING - INDUCED LORENTZ FORCE (HARTMANN EFFECT) - TBL THINNING - FRINGE FIELD DISTRIBUTION • THRUST AUGMENTATION <ul style="list-style-type: none"> - J X B DISTRIBUTION - TOTAL PRESSURE INCREASE - CONSISTENCY AMONG THRUSTER AND EM FRINGE FIELD EFFECTS • SEAWATER MHD <ul style="list-style-type: none"> - MAXIMUM TURBULENCE DAMPING - CHARGE ACCUMULATION IN TBL DUE TO $\vec{\omega} \cdot \vec{B}$ - CHARGED BUBBLE/SEAWATER 2-PHASE FLOW

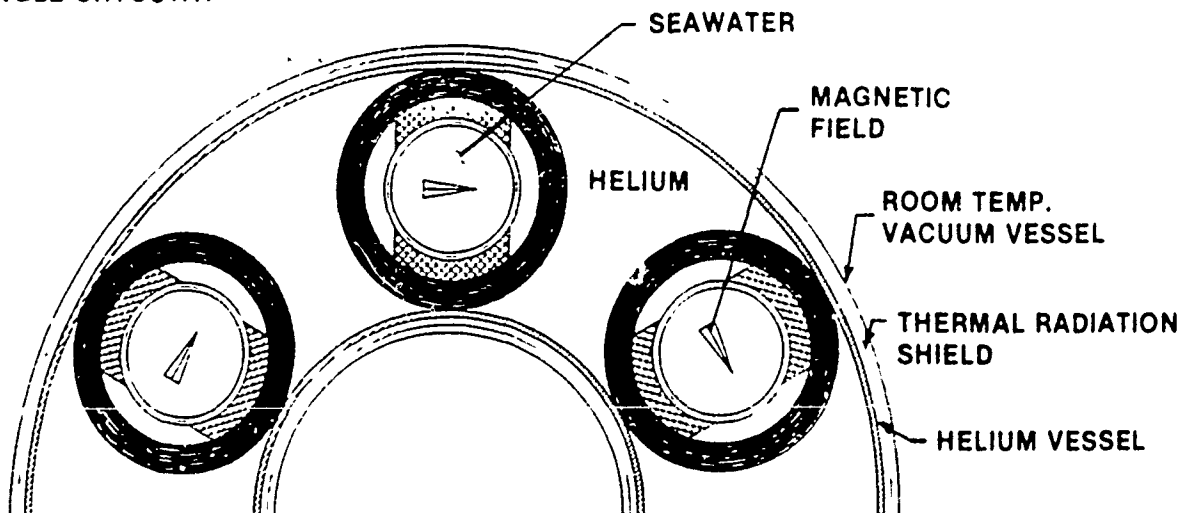


CROSS SECTIONAL VIEW OF SINGLE AND CLUSTER OF SADDLE DIPOLES

SADDLE DIPOLE



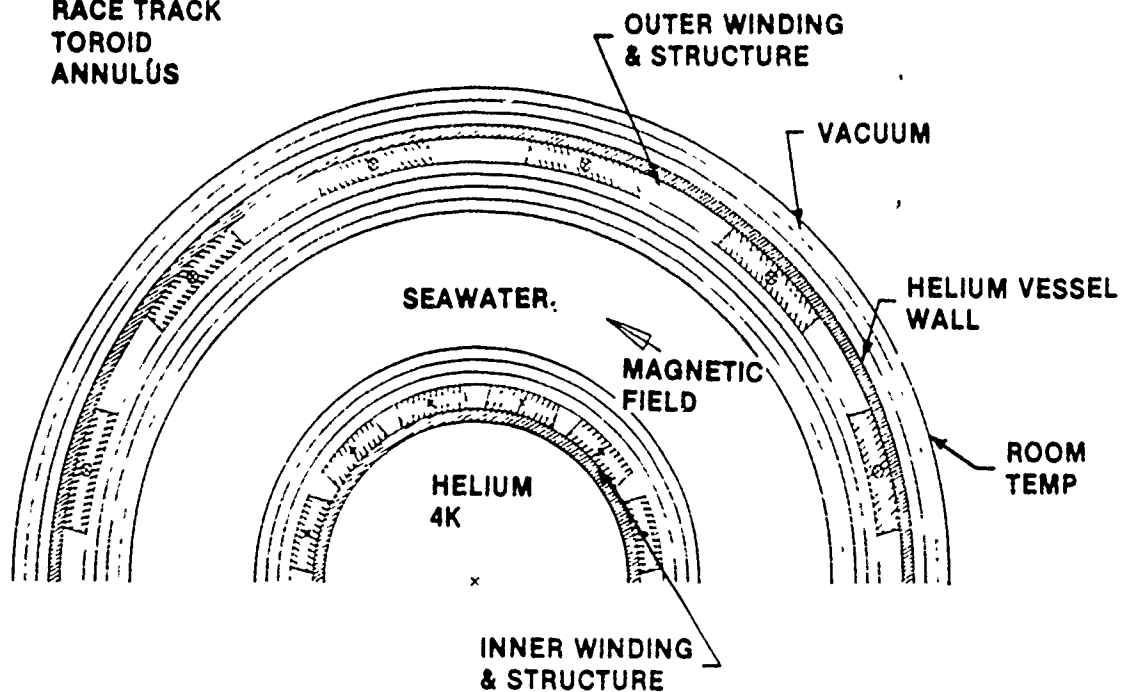
SADDLE DIPOLE CLUSTER
SINGLE CRYOSTAT



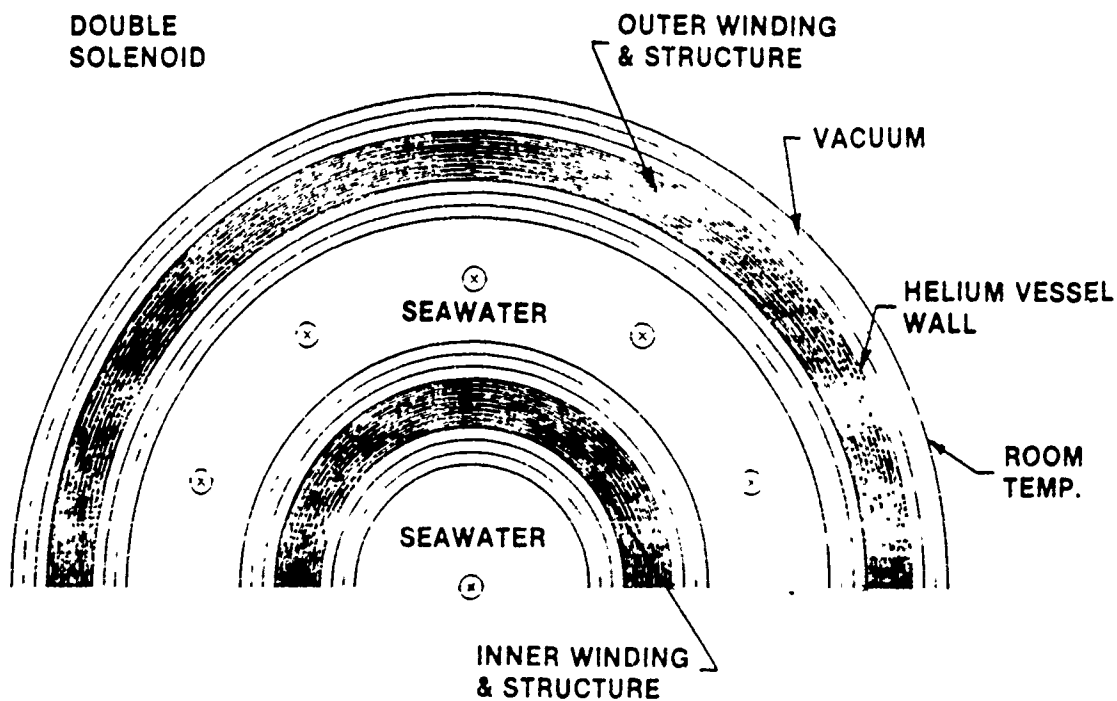


CROSS SECTIONAL VIEW OF TOROID AND SOLENOID

RACE TRACK
TOROID
ANNULUS

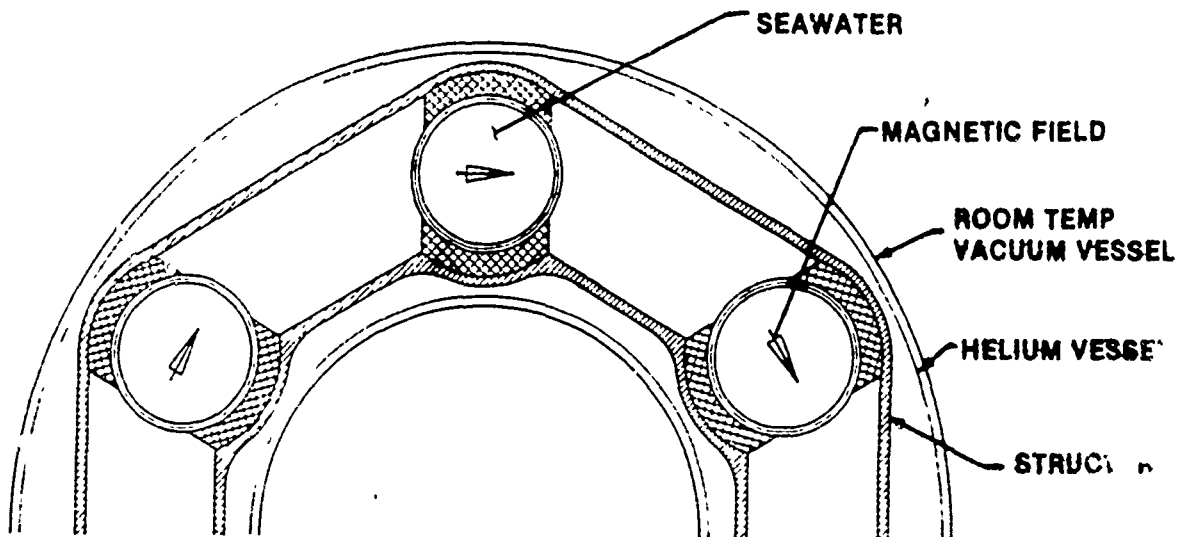


DOUBLE
SOLENOID

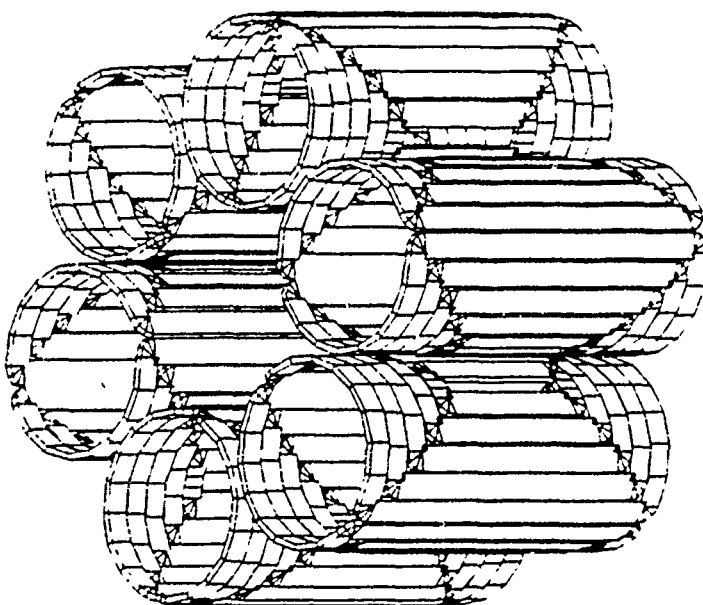




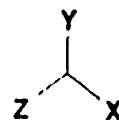
INTEGRATED STRUCTURE AND FINITE ELEMENT SIMULATION PANELS (SADDLE DIPOLE CLUSTER)



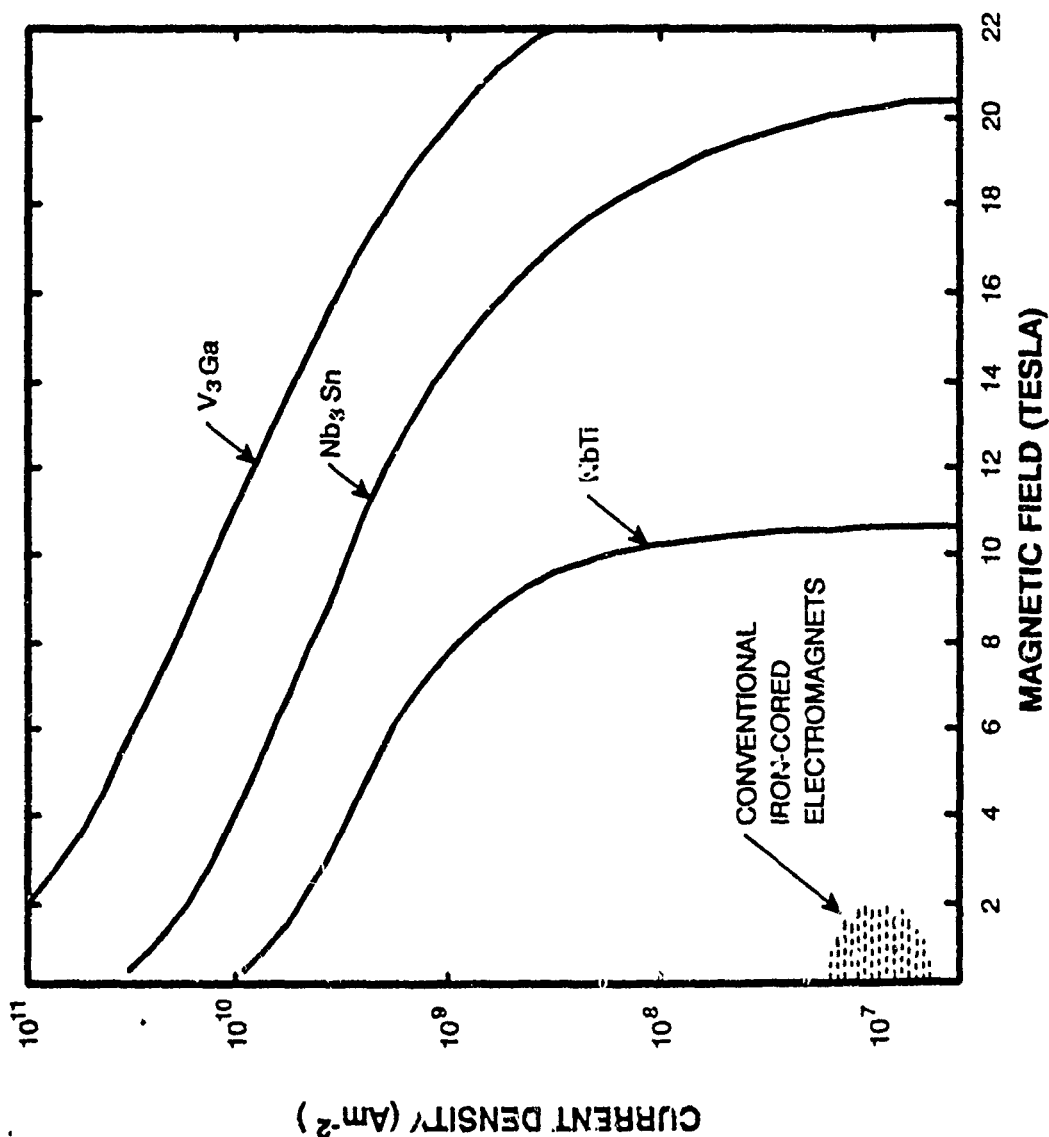
FINITE ELEMENT PANELS



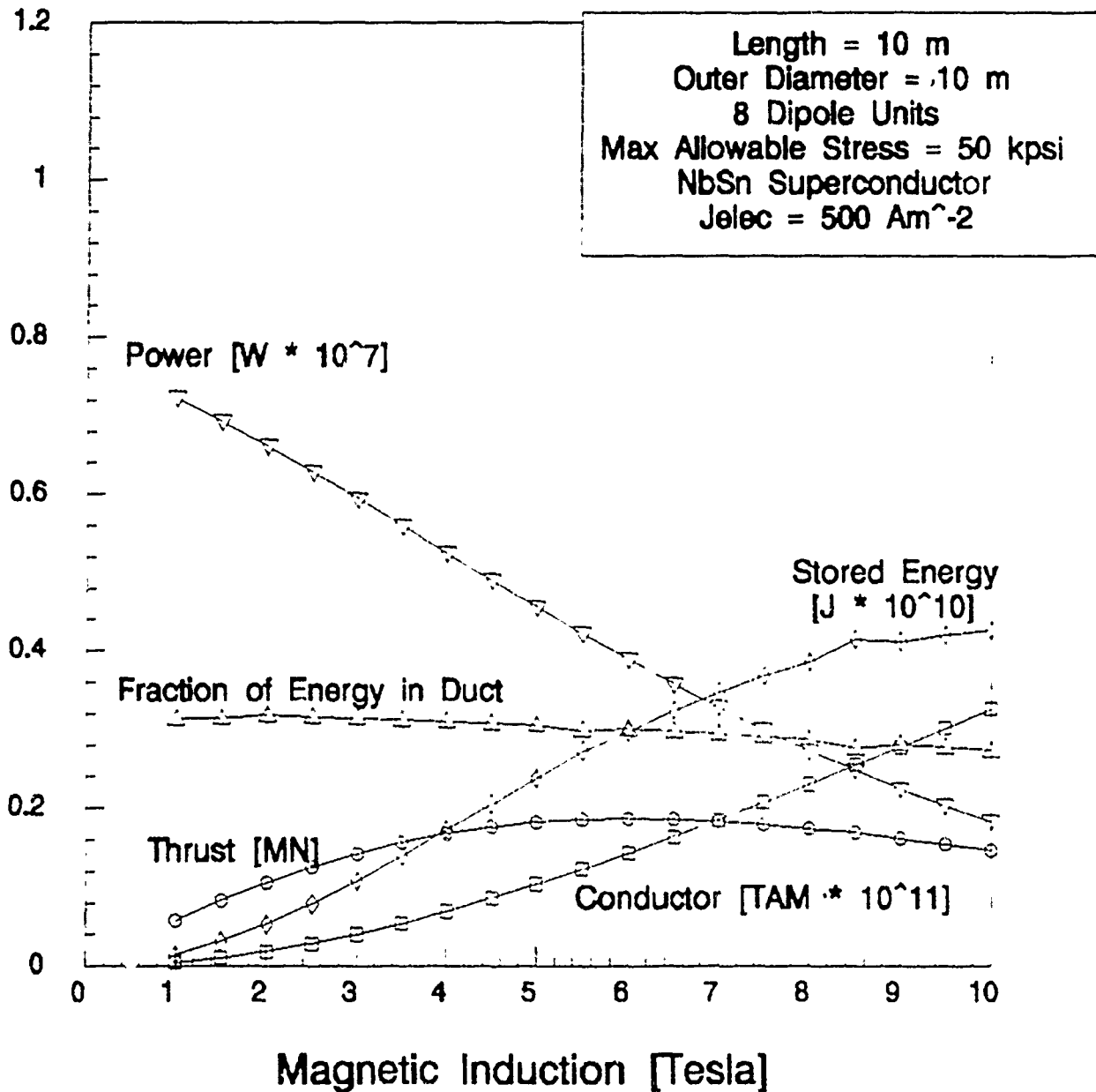
C	AT	
0.00	0.00	0.00



CRITICAL CURVES FOR THREE COMMON SUPERCONDUCTORS AT A CONSTANT TEMPERATURE OF 4.2 K

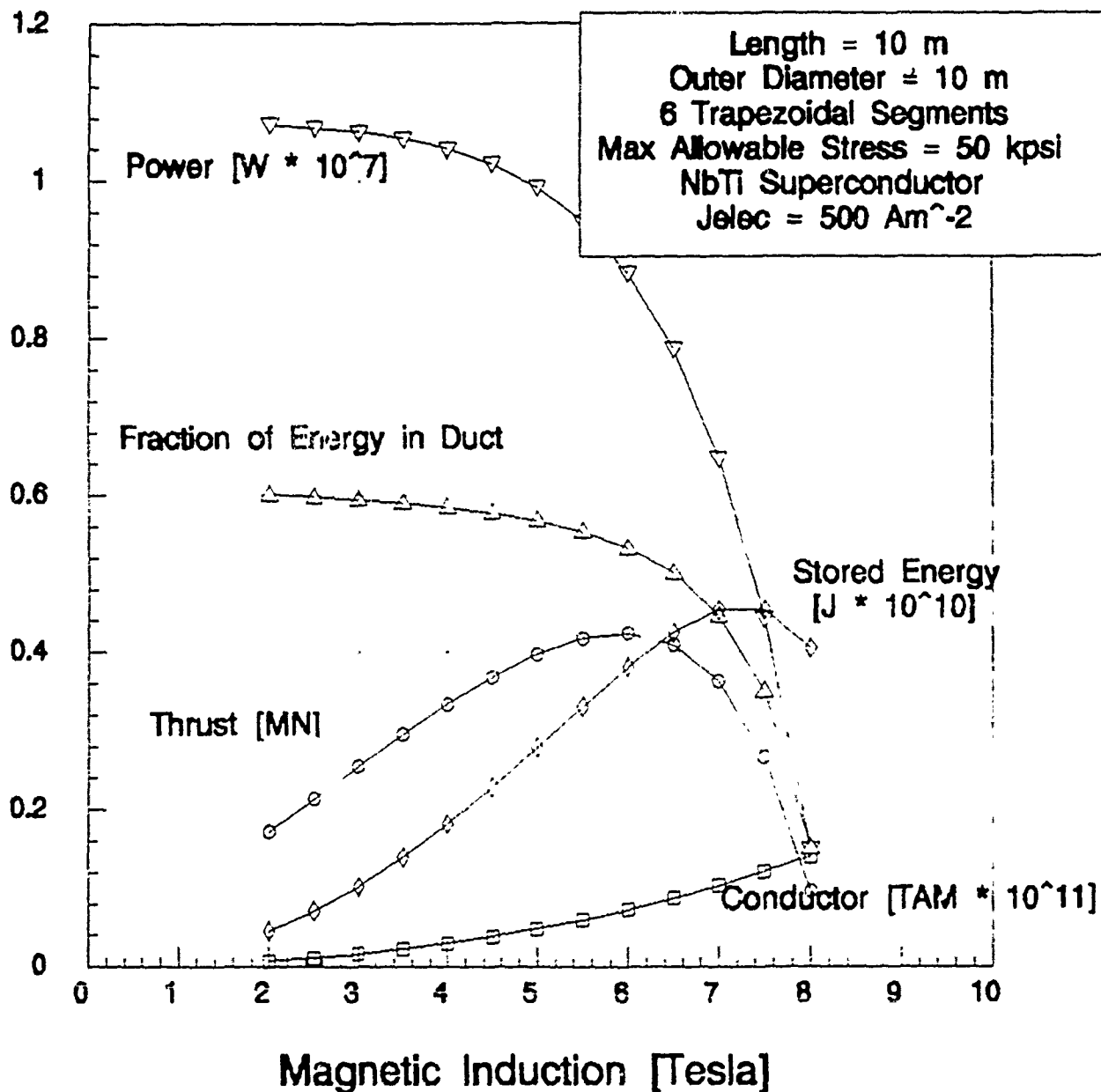


CLUSTERED DIPOLE PERFORMANCE CHARACTERISTICS



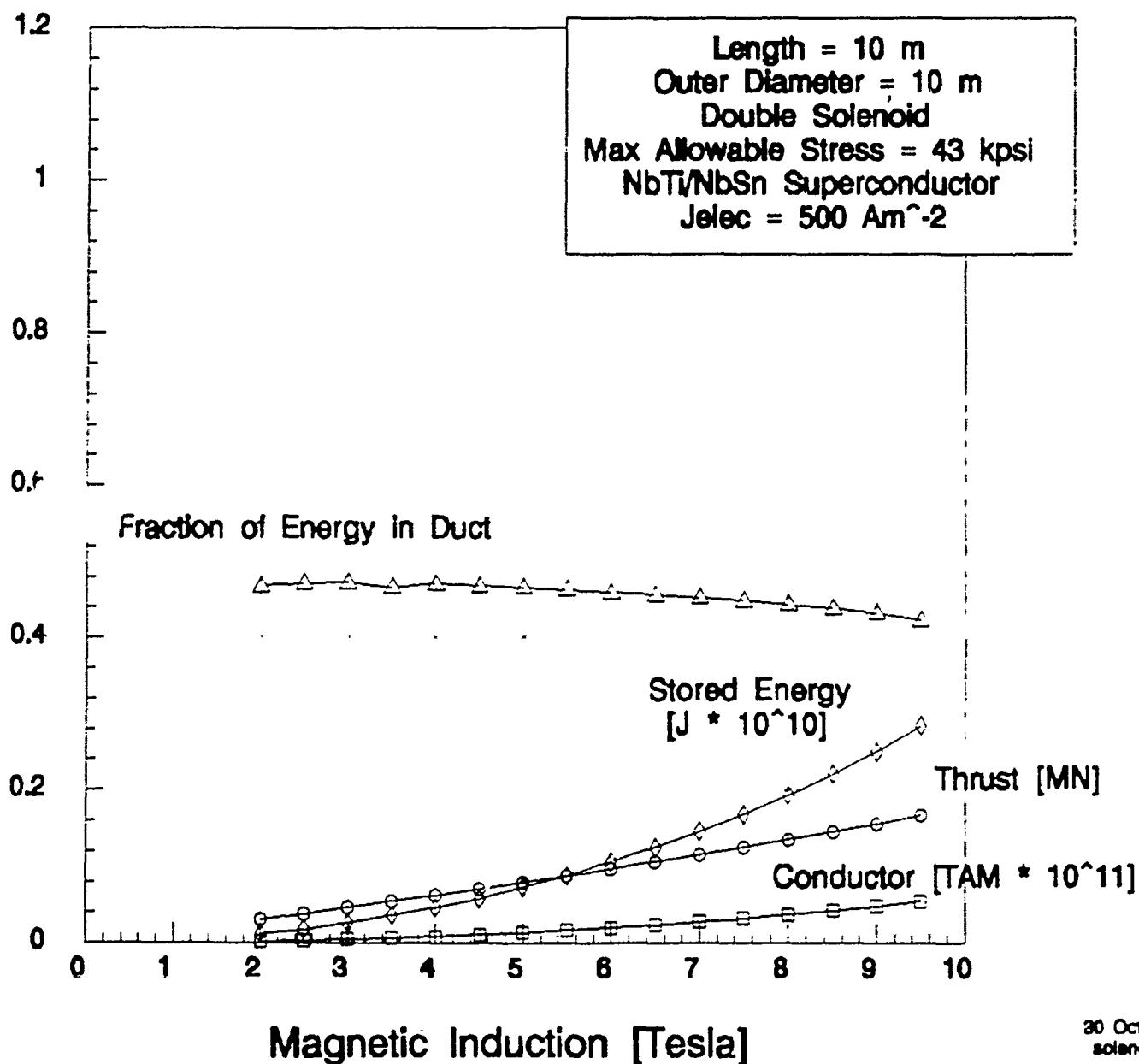
30 Oct 89
dipole

RACETRACK TOROID PERFORMANCE CHARACTERISTICS



30 Oct 89
toroid

SHIELDED SOLENOID PERFORMANCE CHARACTERISTICS

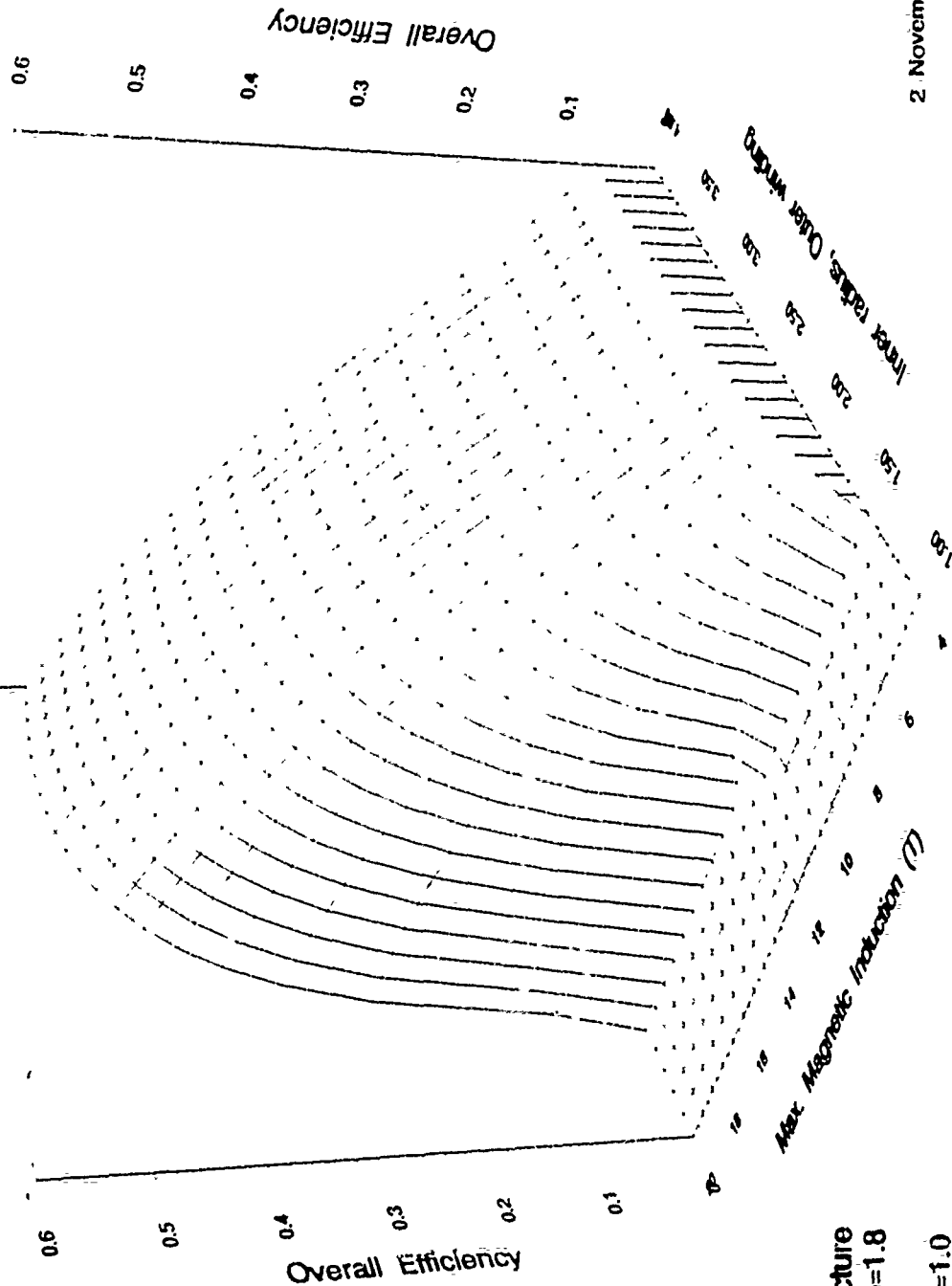


30 Oct 89
solenoid

(90)107.11



6-CHANNEL TOROID OVERALL EFFICIENCY

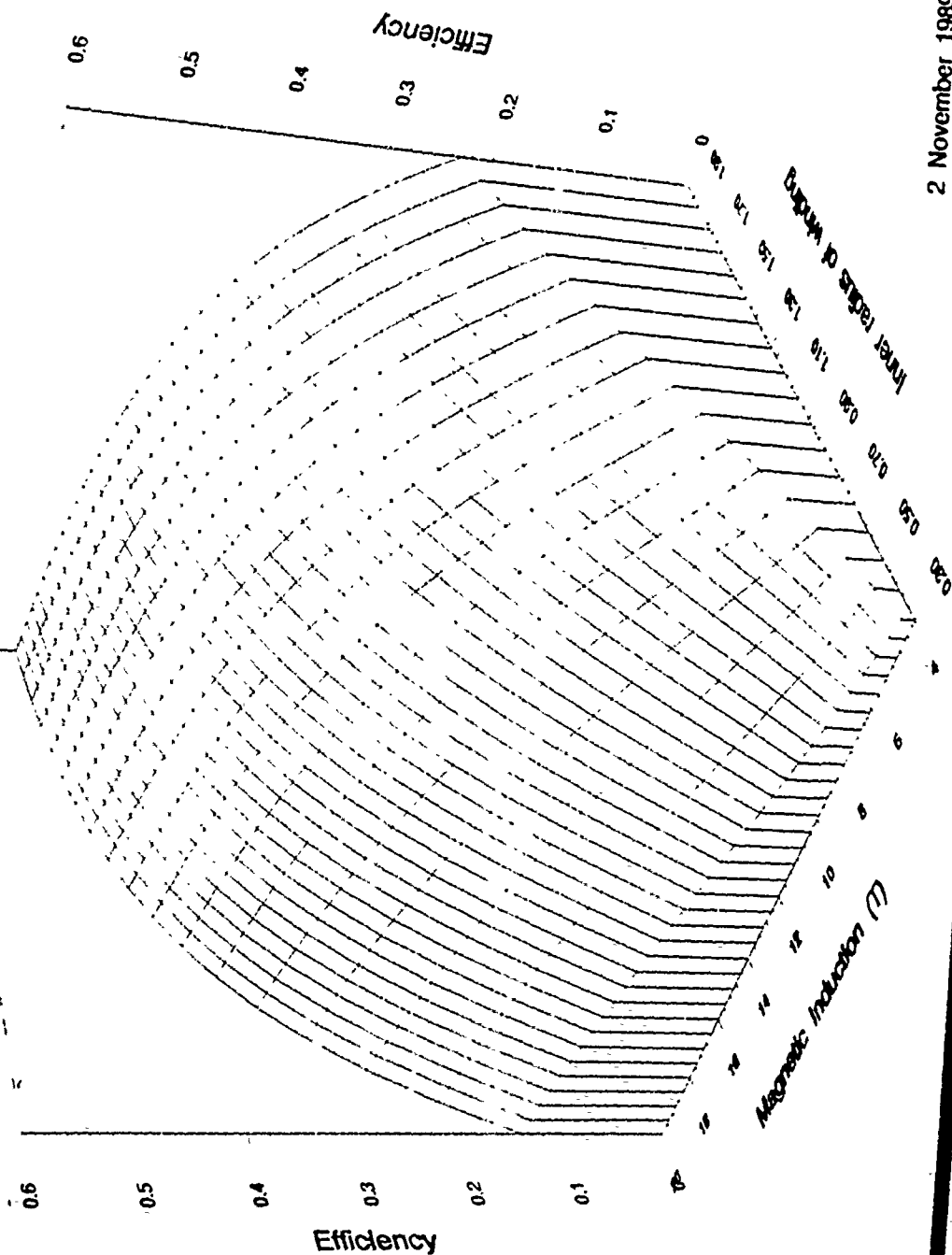


composite structure
 $\sigma = 500k, \rho = 1.8$
 $j_{wind} = 10^8$
 $l = 10, u_0 = 10, r_i = 1.0$

2 November 1989
 ntat



CLUSTERED DIPOLE (8 UNITS) OVERALL EFFICIENCY



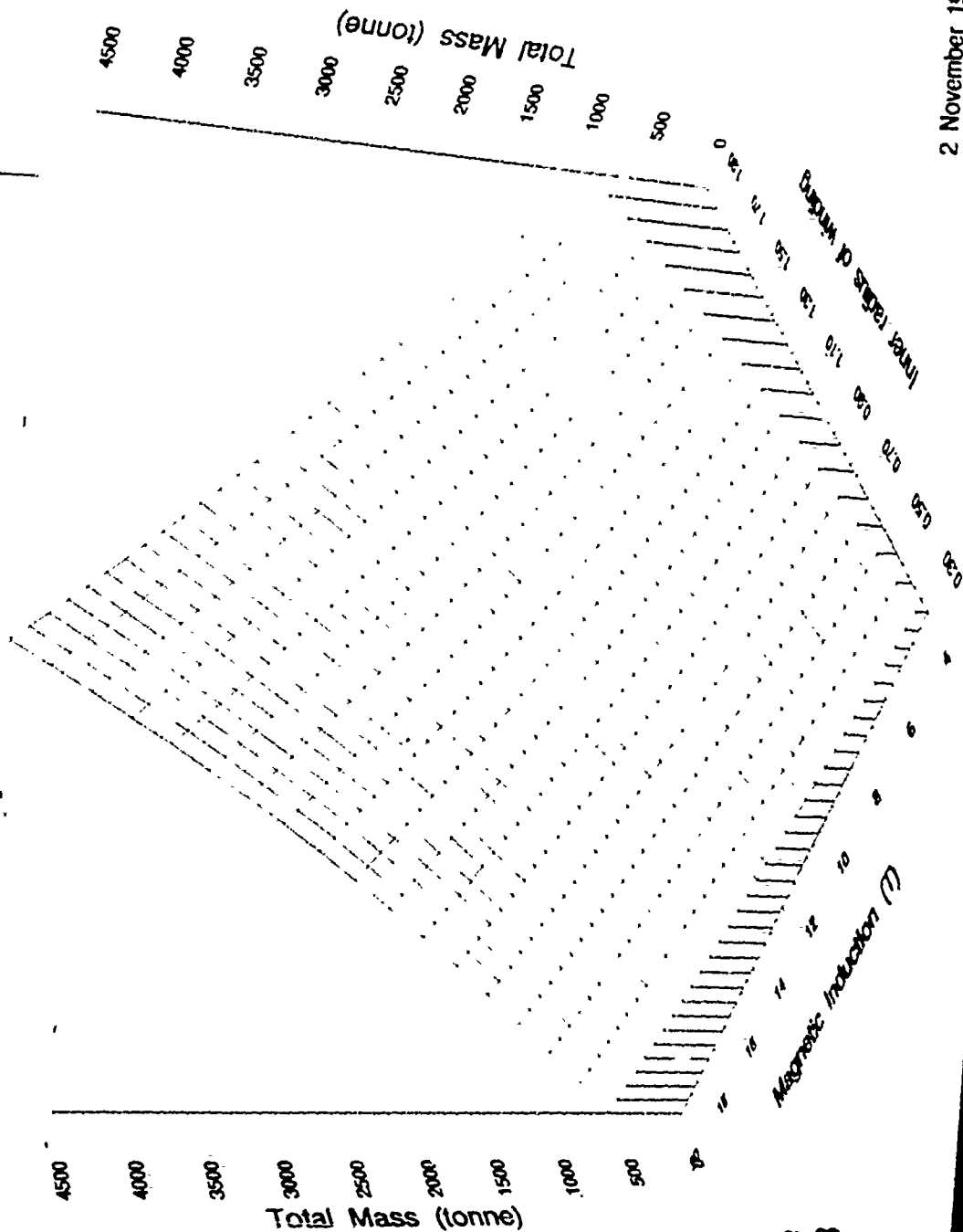
composite structure
 $\sigma = 500k, \rho = 1.8$
 $j_{wind} = 10^8$
 $l_e = 10, u_0 = 10$

N0211-GA-90(N) 0128.1

2 November 1989
 cfad



CLUSTERED DIPOLE (8 UNITS) TOTAL MASS



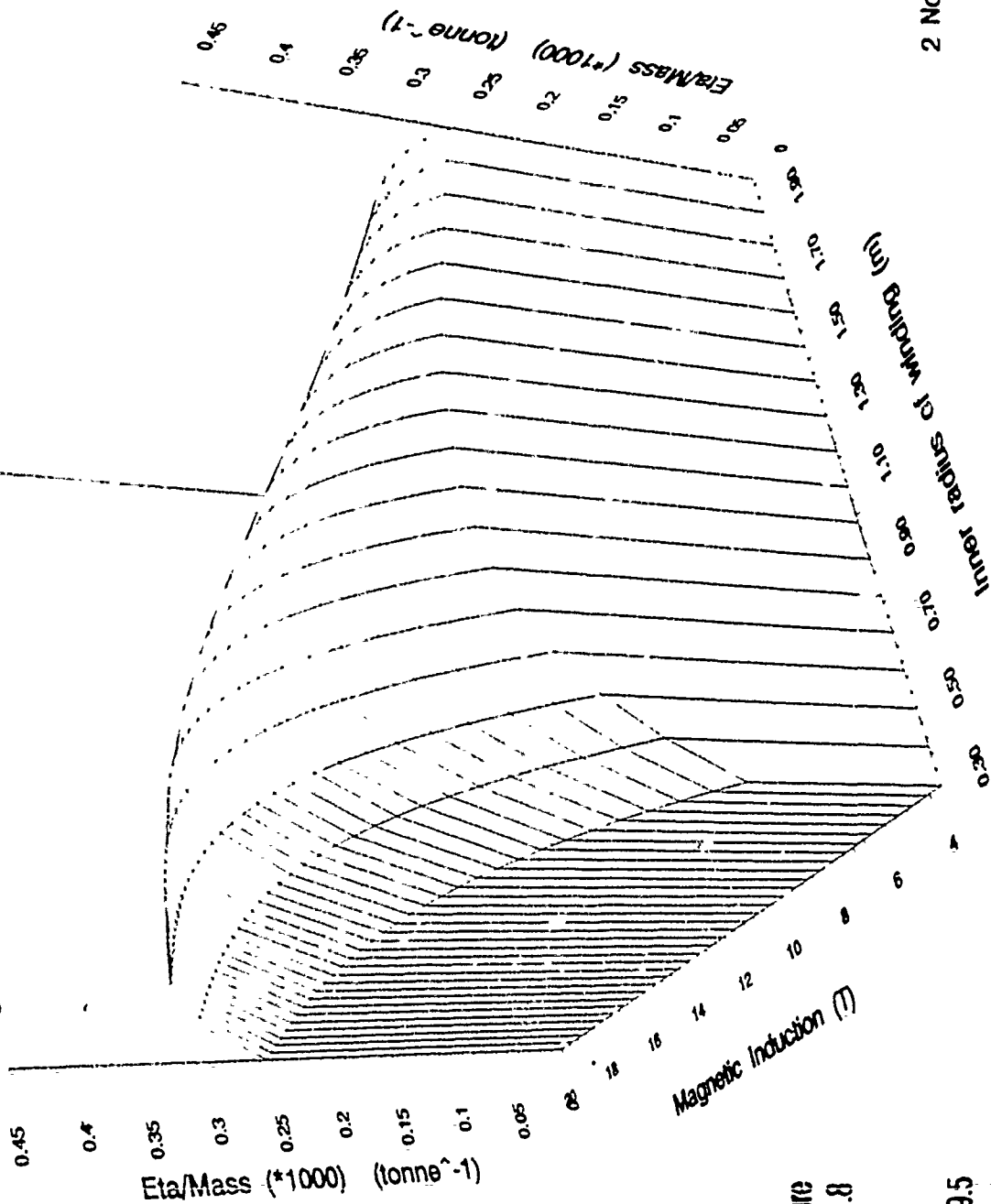
composite structure
sigma=500k, rho=1.8
jwind=10^8
le=10, u0=10

2 November 1989
massd

N0211-GA-90(M) 0128.5



CLUSTERED DIPOLE (8 UNITS) EFFICIENCY/TOTAL MASS

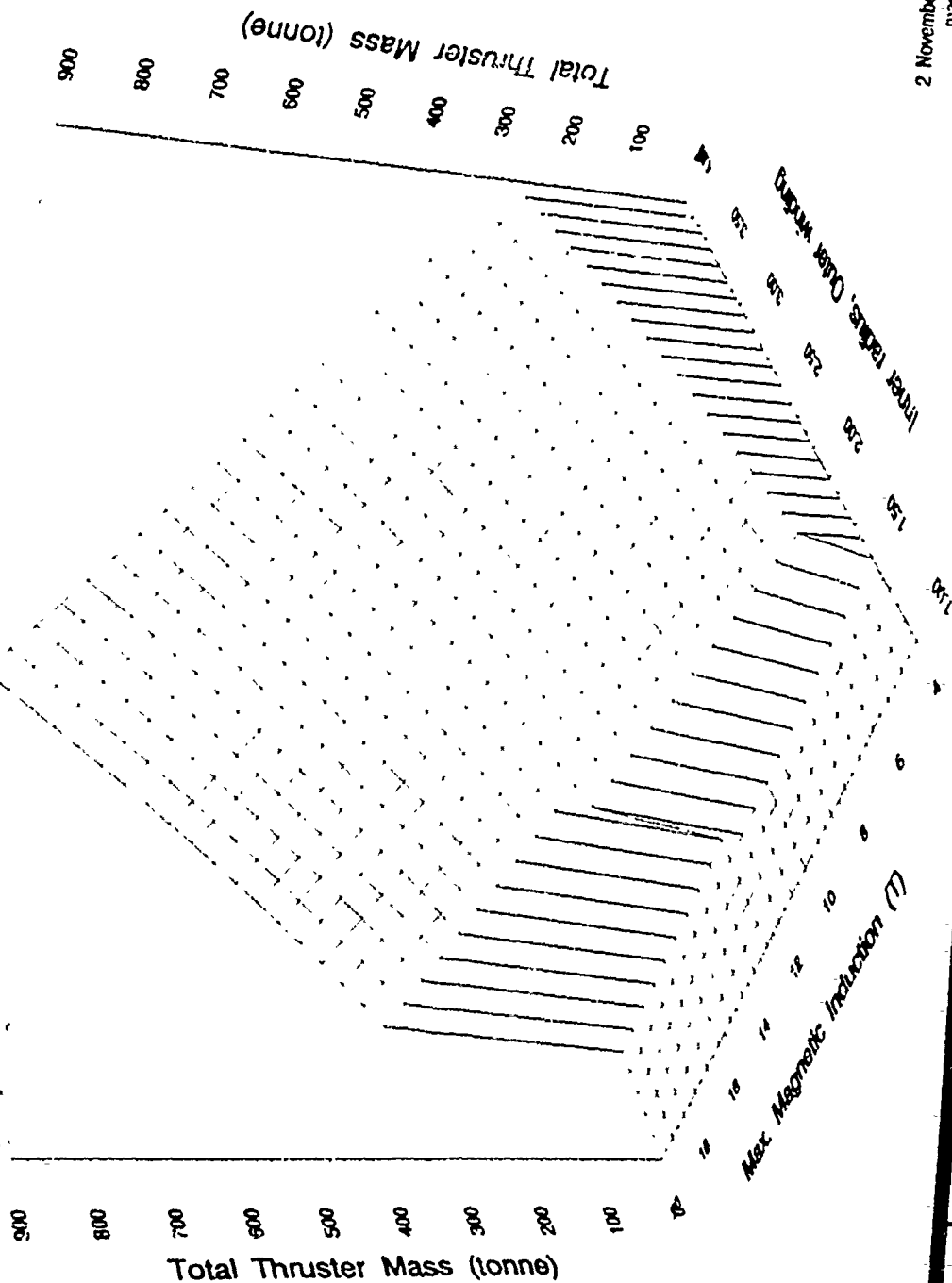


composite structure
 $\text{sigma}=500\text{k}, \text{rho}=1.8$
 $j_{\text{wind}}=10^8$
 $I_e=10, I_0=10$
 max. 4329 at 7.9.5

2 November 1989
 etamd



6-CHANNEL TOROID TOTAL MASS



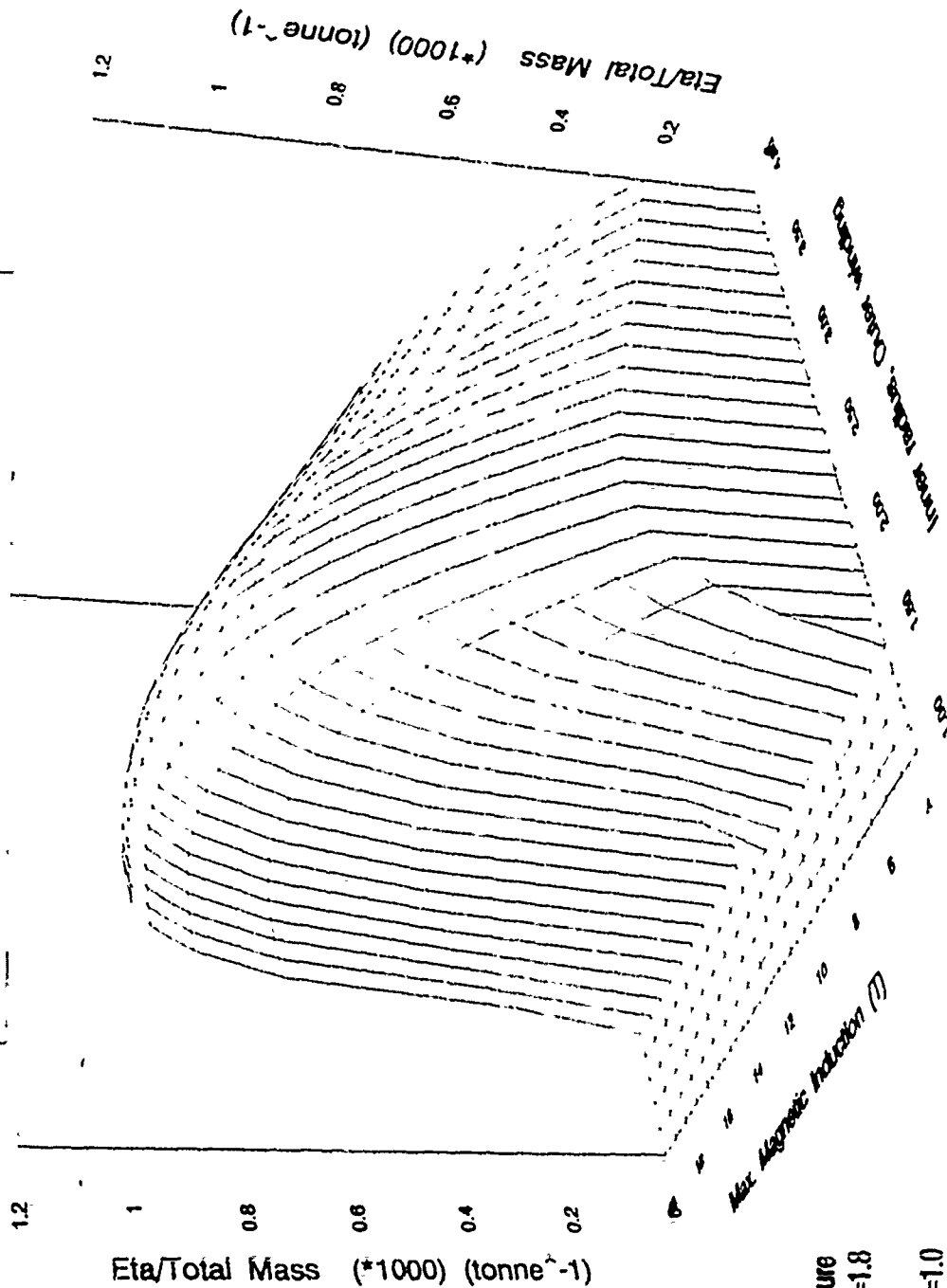
composite structure
 $\sigma_{max}=500k$, $\rho_0=1.8$
 $j_{wind}=10^8$
 $k_e=10$, $u_0=10$, $r_{i1}=1.0$

2 November 1989
 masst

N0211-GA-90(N) 0128.3



6-CHANNEL TOROID EFFICIENCY/TOTAL MASS



composite structure
sigma=500k, rho=1.8
jwind=10⁻⁸
le=10, u0=10, r1=1.0
max. 1.028 at (2.375, 15.2)

2 November 1989
etamf

N0211-GA-90(N) 0128.2

NUSC/INDUSTRY SCEMT WORKSHOP

WHEN, WHERE, WHO

- ◆ MARCH 21, 1989
- ◆ NUSC, NEWPORT, R.I.
- ◆ ORGANIZED AND CHAIRED BY DR. MENG

PARTICIPANTS

- ◆ INDUSTRY: 21 REPRESENTATIVES FROM GA, GE, GD, IGC; ELTECH; AVCO; WECO; KOCH, JANIS
- ◆ UNIVERSITY: 6 REPRESENTATIVES FROM MIT, AND USNA
- ◆ NATIONAL LABS: 10 REPRESENTATIVES FROM ANL, ONL, NUSC, DTRC, ONR, ONT

WORKSHOP SUBGROUPS

- ◆ MHD THRUSTER SYSTEM (DR. SWALLOM, AVCO)
- ◆ SUPERCONDUCTING MAGNET SYSTEM (DR. STEKLY, IGC)
- ◆ SEAWATER ELECTRODE SYSTEM (MS. NIKSA, ELTECH)
- ◆ CRYOGENIC SYSTEMS (DR. HUMMERT, WECO)
- ◆ UNDERSEA SYSTEMS INTEGRATION (MR. LONGDREGAN, EB)

NUSC/INDUSTRY SCENT WORKSHOP MHD THRUSTER SYSTEM SUBGROUP REPORT

KEY ISSUES

I. TECHNOLOGY

- THRUST AUGMENTATION VIA:
 - UNIFORMIZATION OF LORENTZ FORCE DENSITY WITHIN MHD DUCT
 - EM END EFFECTS ARE INCONSISTENT WITH HIGH THRUST HYDRODYNAMICS
- DRAG REDUCTION VIA:
 - TURBULENCE REDUCTION DUE TO MHD EFFECTS
 - REDUCTION OF EM EDDY CURRENT INDUCED WATER DRAG
- BUBBLE EFFECTS ON MAXIMUM CURRENT THROUGH SEAWATER

II. OPERATION

- EFFICIENCY FALLS OFF AS SPEED INCREASES
- BRACKISH WATER LIMITS POWER OUTPUT
- STALL DURING TRANSIENT START-UP WITH ZERO INITIAL VELOCITY
- WEIGHT AND VOLUME CONSTRAINTS

FUTURE DIRECTION

- EXPLORE POSSIBILITY OF A LAMINAR EMT JET BASED ON MHD TURBULENCE DAMPING EFFECT
- CONDUCT SMALL SCALE MODEL TESTS USING NUSC SEAWATER MHD AND NASA LANGLEY TOWING FACILITIES
- CONDUCT TRADE-OFF STUDIES OF MAXIMIZING THRUSTS VS. MINIMUM THRUSTER JET NOISE AND DRAG
- CONFIGURE SUPERCONDUCTOR TO GENERATE UNIFORM LORENTZ FORCE DENSITY

NUŠC/INDUSTRY SCENT WORKSHOP SEAWATER ELECTRODE SUBGROUP REPORT

KEY ISSUES

I. TECHNOLOGY

- PREFERRED ELECTROCHEMISTRY (Cl_2 VS. O_2)
- GASLESS ELECTRODE DEVELOPMENT
- MAXIMUM ELECTRICAL CURRENT DENSITY AND ELECTRIC FIELD ACROSS ELECTRODES
- ELECTRODE GEOMETRY VS. EFFICIENCY (PLANAR VS SADDLE)
- GAS BUBBLE FORMATION, TRANSPORT AND EFFECT ON THRUST AND NOISE
- THRUST ENHANCEMENT BY INCREASING CONDUCTIVITY USING ON-BOARD REVERSE OSMOSIS
- THRUST REVERSAL BY POLARITY REVERSAL

II. OPERATIONAL

- MUST PROVIDE MORE ON-BOARD ELECTRICAL POWER
- ELECTRODE LIFE IN HIGH SPEED SEAWATER
- SCALING AT CATHODE SURFACE (Ca, Mg) AT HIGH SPEED

FUTURE DIRECTION

- DETERMINE PREFERRED CHEMISTRY
 - MINIMIZE GAS PRODUCTION, TOXICITY, SCALING
 - MAXIMIZE MASS TRANSFER, ALLOWABLE CURRENT DENSITY
- DEVELOP GASLESS SEAWATER ELECTRODE SYSTEM
- IDENTIFY FEASIBILITY OF ON-BOARD SYSTEM FOR ENHANCEMENT OF ELECTRIC CONDUCTIVITY
- ESTABLISH PERFORMANCE OF UNCOATED ELECTRODES IN SMALL MODEL TO ESTABLISH A DATA BASE, THEN PROCEED TO LARGE SCALE DSA ELECTRODES

NUSC/INDUSTRY SCEMT WORKSHOP SUPERCONDUCTING MAGNET SUBGROUP REPORT

KEY ISSUES

I. TECHNOLOGY

- **MAGNET DESIGN:**
 - DESIGN PRINCIPLE BASED ON CRYOSTABILITY, WILL BE IMPRACTICAL
 - DESIGN BASED ON LOW CURRENT DENSITY WILL BE IMPRACTICAL
- **MAGNET RELIABILITY:**
 - THREE KEY FACTORS ARE: STABILITY, QUENCH PROTECTION AND STRUCTURAL INTEGRITY
 - CLOSELY RELATED TO SUPERCONDUCTORS AND CRYOSTAT DESIGN
 - RECOVERY TO OPERATION AFTER QUENCH IS CRITICAL
 - MODULAR DESIGN WITH ADEQUATE REDUNDANCY IS PREFERRED
- **SUPERCONDUCTOR:**
 - $J = 10^4$ A/CM² USED IN SSC AND MRI ARE RELIABLE
 - ALUMINUM STABILIZED CONDUCTOR APPEAR TO BE PROMISING FROM THE STABILITY AND WEIGHT POINTS OF VIEW
- **STRUCTURE:**
 - HIGH STRENGTH $R_u = 400$ KSI COMPOSITE MATERIALS CAN BE USEFUL FOR HIGH FIELD MAGNETS

II. OPERATION

- **SHOCK RESISTANCE OF MAGNET/CRYOSTAT AT DIFFERENT DEPTHS**
- **ALLOWABLE SIGNATURES (MAGNETIC, ELECTRIC, CHEMICAL, THERMAL, HYDRODYNAMICS, ACOUSTIC)**

NUSC/INDUSTRY SCEMT WORKSHOP SUPERCONDUCTING MAGNET SUBGROUP REPORT

FUTURE DIRECTION

- **MAGNET DESIGN**
 - MAGNET DESIGN BASED ON DRY ADIABATIC STABILITY OR LESS THAN THE FULL CRYOSTABILITY SHOULD BE PURSUED
 - SUPERCONDUCTORS AT HIGH CURRENT DENSITY AND ALUMINUM STABILIZED CONDUCTORS SHOULD BE CONSIDERED AS CANDIDATE IN MAGNETIC DESIGN
 - MAGNET DESIGN BASED ON COMPRESSIVE YIELD STRESS ONLY SHOULD BE EXPLORED
 - POSSIBILITIES OF USING HIGH STRENGTH COMPOSITE MATERIALS SHOULD BE EXPLORED IN FUTURE HIGH FIELD MAGNET DESIGNS
 - SHOCK RESISTANCE AND ALLOWABLE SIGNATURES SHOULD BE QUANTIFIED AND INCORPORATED AS PART OF MAGNET DESIGN SPECIFICATION
 - TAILORING THE B FIELD TO MAXIMIZE THE TRUST SHOULD BE EXPLORED
 - QUICK RECOVERY FROM QUENCH
 - SHOULD PURSUE MODULAR DESIGN WITH ADEQUATE REDUNDANCY
- **NEAR-TERM FOCUS**
 - SINCE THE TORPEDO APPLICATION IS THE SMALLEST SYSTEM, IT SHOULD BE THE INITIAL FOCUS
 - A SCALED MODEL USING ALL THE ABOVE SUGGESTED METHODOLOGY SHOULD BE BUILT AND TESTED
 - DUE TO THE MULTI-FACET ASPECT OF THE PROGRAM, A MULTI-DISCIPLINARY GROUP APPROACH WITH SIGNIFICANT SYSTEMS INPUT MUST BE ESTABLISHED

NUSC/INDUSTRY SCEMT WORKSHOP CRYOGENIC SYSTEMS SUBGROUP REPORT

KEY ISSUES

I. TECHNOLOGY

- **STRUCTURAL LOAD DISTRIBUTION:**
 - EXTRAPOLATION FROM NMR AND FR DESIGNS IS MISLEADING
 - MUST BE ADDRESSED FROM AN OVERALL SYSTEM REQUIREMENTS FIRST
- **PRESSURE IN CRYOSTAT**
 - CRYOSTAT MUST PROVIDE SHELL STRENGTH TO WITHSTAND DEPTH PRESSURE
 - POSSIBLE DIMENSIONAL CHANGE WITH DEPTH

II. OPERATIONAL

- **SYSTEMS REQUIREMENTS:**
 - CLOSELY RELATED TO THE MAGNETIC ENERGY STORAGE LEVEL AND MAGNET CONFIGURATIONS
 - THE REFRIGERATION RATE AND CRYOGEN STORAGE LEVEL
 - VENTING DURING QUENCH AT VARIOUS DEPTH PRESSURE
 - SPACE, WEIGHT, VOLUME, SHOCK LOADING, RELIABILITY
 - SAFETY, MAINTENANCE SERVICE
 - COST

FUTURE DIRECTION

- **DEFINE OVERALL SYSTEMS REQUIREMENTS FIRST, THEN EXAMINE CRYOGENIC SYSTEM ASPECTS**
- **CONSIDER MISSION DURATION RESTRICTIONS ON SYSTEMS DESIGN**
- **CONSIDER CRYOGEN GENERATION RATE, STORAGE LEVEL, RATES OF DUMPING OR VENTING OVERBOARD DUE TO QUENCH, REPLENISHING RATE RESERVE LEVEL FOR EMERGENCIES**

NUSC/INDUSTRY SCEMT WORKSHOP UNDERSEA SYSTEMS INTEGRATION SUBGROUP REPORT

KEY ISSUES

I. TECHNOLOGY

- HULL PENETRATIONS OF LARGE CURRENT CABLES, FLOOD OUT FAILURES MUST BE ELIMINATED TO PREVENT SHORTING, SELF DESTRUCTION AND BREACH OF HULL INTEGRITY
- EFFECT OF MAGNETIC FIELD ON POSSIBLE CORROSION ENHANCEMENT OVER ADJOINING DISSIMILAR HULL MATERIALS
- SHOCK EFFECTS ON CRYOGEN STORAGE AND SUPERCONDUCTING MAGNETS

II. SAFETY

- SAFE STORAGE AND CONTROLLED BOIL-OFF OF CRYOGEN FLUIDS IN A CLOSED SHIPBOARD ATMOSPHERE
- EFFECTS OF MAGNETIC FIELD ON PERSONNEL AND SHIPBOARD HARDWARE, SUCH AS ELECTRIC MOTORS, CONTROLLERS AND ELECTRONICS
- HANDLING OF BY-PRODUCT GASES, O₂, H₂, AND HYPOCHLOROUS ACIDS

III. OPERATION

- RESTRICTED OPERATION IN BRACKISH WATER
- EFFECTS ON STEEL HULL SUPPORT VESSELS (e.g. TUGS)
- ACCUMULATION RATE OF MAGNETIC PARTICLES INSIDE THE THRUSTER

FUTURE DIRECTION

- ENGINEERING INVOLVEMENT OF SHIPBUILDER SHOULD BE IMPLEMENTED AT AT PROGRAM INCEPTION TO ESTABLISH REQUIREMENTS FOR THE SCEMT AS WELL AS THE SHIP
- ESTABLISH SHOCK-RESISTANCE REQUIREMENTS TO THE CRYOSTAT AND CRYOGEN STORAGE SYSTEMS
- THRUSTER MUST BE BASED ON MAXIMUM MAGNETIC FIELD CONFINEMENT, INDICATING THE MULTI-POLE APPROACH IS MANDATORY

THIS PAGE IS INTENTIONALLY BLANK

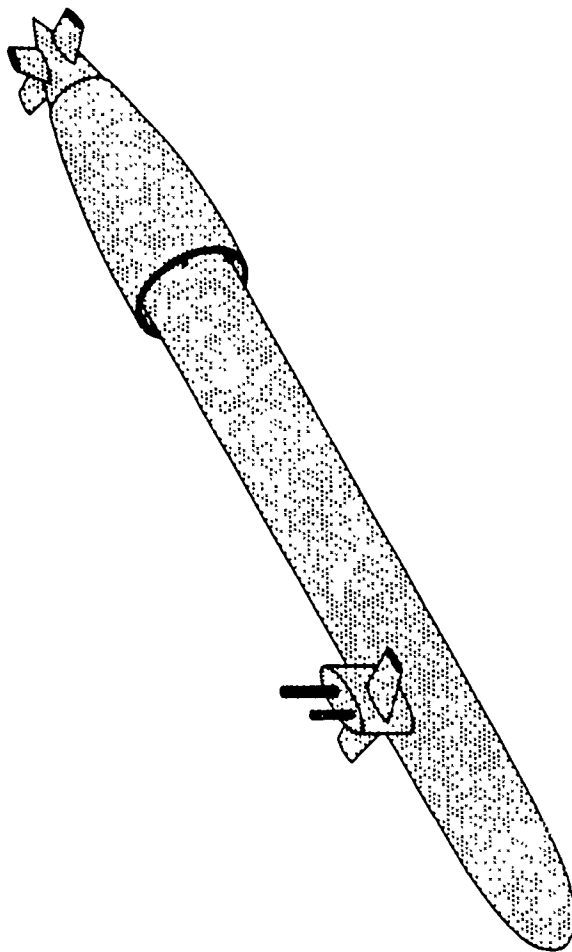
**MAGNETOHYDRODYNAMIC
SUBMARINE PROPULSION**

Presented by

Dr. Daniel W. Swallom

MAGNETOHYDRODYNAMIC SUBMARINE PROPULSION

Dr. Daniel W. Swallom
Director of Military Power Programs
Dr. Isaac Sadvnik
Principal Research Scientist
Avco Research Laboratory, Inc.
Subsidiary of Textron Inc.
Everett, Massachusetts 02149



Avco Research Laboratory **TEXTRON**

Avco Research Laboratory, Inc. Subsidiary of Textron Inc.

MAGNETOHYDRODYNAMIC SUBMARINE PROPULSION SYSTEM PROGRAM

The program results discussed in this presentation are based on the technical effort from a program sponsored by the Defense Advanced Research Projects Agency and administered by the David Taylor Research Center (ARPA Order No. 6660; Contract Number N61533-89-C-0067). The overall objective of the program is the development of magnetohydrodynamic thruster systems for use as submarine propulsion systems. The results presented herein are from the preliminary conceptual design task of Phase 1.

MAGNETOHYDRODYNAMIC SUBMARINE PROPULSION SYSTEM PROGRAM

- **INTRODUCTION AND BACKGROUND**
- **PERFORMANCE CHARACTERISTICS**
- **OVERALL PROGRAM**

AVCO MAGNETOHYDRODYNAMIC SUBMARINE PROPULSION SYSTEM PROGRAM PLAN

The overall magnetohydrodynamic thruster development program consists of two phases with the objective of an open ocean test of an untethered vehicle during Phase 2. The first phase, which is currently in progress, provides for the design of an integrated magnetohydrodynamic thruster system for submarine applications and a feasibility and performance assessment to identify critical key technology issues and the overall performance characteristics. The second phase of the program is directed toward a feasibility demonstration. This phase consists of three tasks. The first task is a risk reduction experimental program to provide for the resolution of the key critical technology issues and to establish an engineering data base. The second, and most important task, is the design, fabrication, and testing of an actual untethered, open-ocean test vehicle using a magnetohydrodynamic propulsion system. The third and final task is the completion of the overall thruster integration and detailed conceptual design and the technology transfer plan for transitioning to the next step in the development program.

AVCO MAGNETOHYDRODYNAMIC SUBMARINE PROPULSION SYSTEM PROGRAM PLAN

PHASE 1

TASK 1 - INTEGRATED CONCEPTUAL DESIGN

TASK 2 - FEASIBILITY AND PERFORMANCE ASSESSMENT

PHASE 2

TASK 1 - RISK REDUCTION EXPERIMENTAL PROGRAM

TASK 2 - PERFORMANCE AND FEASIBILITY DEMONSTRATION TASK

TASK 3 - OVERALL THRUSTER INTEGRATION AND TECHNOLOGY TRANSFER

ADVANCED SUBMARINE TECHNOLOGY TEAM ASSIGNMENTS

The prime contractor for the Magnetohydrodynamic Submarine Propulsion System Program is Avco Research Laboratory, Inc. The major subcontractors are General Dynamics Space Systems Division and General Dynamics Electric Boat Division. Avco is responsible for the magnetohydrodynamic propulsion system, the power requirements and system integration, the non-magnetic signature effects, the hull/thruster system hydrodynamics, and the hull model. General Dynamics Space Systems Division is responsible for the magnet system including the cryogenic system, the structure, and the magnetic signature effects. General Dynamics Electric Boat Division is responsible for major submarine issues and the submarine/propulsion system integration.

ADVANCED SUBMARINE TECHNOLOGY TEAM ASSIGNMENTS

AVCO

- MHD PROPULSION SYSTEM
- POWER REQUIREMENTS
- POWER SYSTEM INTEGRATION
- SIGNATURE EFFECTS
- HULL/POWER SYSTEM HYDRODYNAMICS
- HULL MODEL

GENERAL DYNAMICS

- SPACE SYSTEMS
 - MAGNET SYSTEM
 - STRUCTURAL

- ELECTRIC BOAT
 - PROPULSION SYSTEM/SUBMARINE INTEGRATION

MAGNETOHYDRODYNAMIC SUBMARINE PROPULSION SYSTEM DEVELOPMENT, OPERATIONAL, AND STEALTH ISSUES

The major development issues for the magnetohydrodynamic thruster include magnet scaling, the cryogenic system, the electrode system design and development, and the multiple hull penetrations. The magnet scaling issue is one of size, magnetic field level (stored energy), and robustness. Superconducting magnets of this size and field strength have not been built before. In addition, the magnet system must possess the robustness characteristics of a fighting vehicle. Hence, the magnet system, while based on similar operational magnets, represents a challenging engineering problem. The cryogenic system consists of the dewar, the refrigeration system, and all of the connecting piping and controls and provides the liquid helium for thermal management. The electrode system must provide the required current density for the thruster without performance degradation during the operational lifetime. Several electrode materials have been tested in various industrial applications and some have operated in these static conditions for lifetimes commensurate with the submarine requirements. The magnetohydrodynamic thruster concept eliminates the large, dynamic hull penetration and replaces it with many smaller, static hull penetrations. Thus, the number of penetrations for elective current feed lines and for cryogenic flow pipes may be large.

The operational issues are primarily performance and system lifetime. Performance is necessary for the submarine to perform its existing mission requirements. Thus, the submarine top speed must be sufficiently high to satisfy the existing mission requirements. Operationally, the system must have sufficient lifetime characteristics to operate without any major repairs between the scheduled shipyard overhaul cycles. Since superconducting magnet systems have demonstrated more than five years of continuous operation, and electrode materials have operated for similar periods of time in static applications, the lifetime requirements should be able to be satisfied.

Stealth, which is a major feature of all submarine activity, requires that all submarine generated signatures be minimized. The major areas of concern are related to acoustic, magnetic, and optical signatures. These signatures can be observed by various means and care must be taken in the design of the magnetohydrodynamic thruster system to insure that the overall submarine signature requirements are satisfied.

MAGNETOHYDRODYNAMIC SUBMARINE PROPULSION SYSTEM DEVELOPMENT, OPERATIONAL, AND STEALTH ISSUES

- **DEVELOPMENT ISSUES**

MAGNET SCALING

CRYOSTAT SYSTEM

ELECTRODE SYSTEM DEVELOPMENT

HULL PENETRATION

- **OPERATIONAL ISSUES**

PERFORMANCE

LIFETIME

- **STEALTH**

ACOUSTIC SIGNATURE

MAGNETIC SIGNATURE

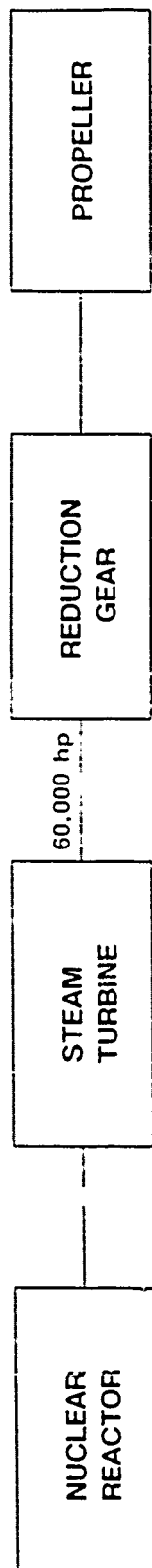
OPTICAL SIGNATURE

COMPARISON OF CONVENTIONAL AND MAGNETOHYDRODYNAMIC SUBMARINE PROPULSION SYSTEMS

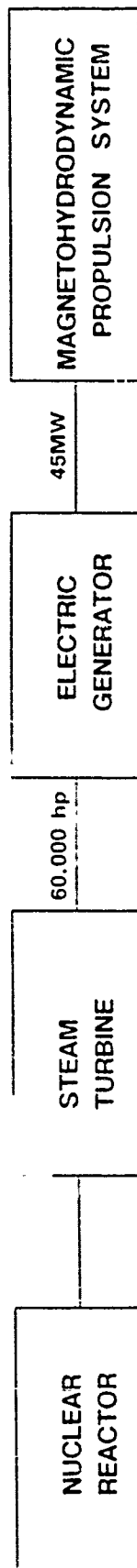
The design of the magnetohydrodynamic propulsion system is based on using the existing submarine power plant, which consists of the nuclear reactor and steam turbine set. The conventional reduction gear, drive shaft, and propeller are eliminated from the submarine. These components are replaced by an electric generator, the magnetohydrodynamic propulsion system and the cryogenic system. Thus, the output of the steam turbine is used to drive an electric generator rather than rotate the drive shaft.

COMPARISON OF CONVENTIONAL AND MAGNETOHYDRODYNAMIC SUBMARINE PROPULSION SYSTEMS

CONVENTIONAL SUBMARINE PROPULSION SYSTEM



MAGNETOHYDRODYNAMIC SUBMARINE PROPULSION SYSTEM

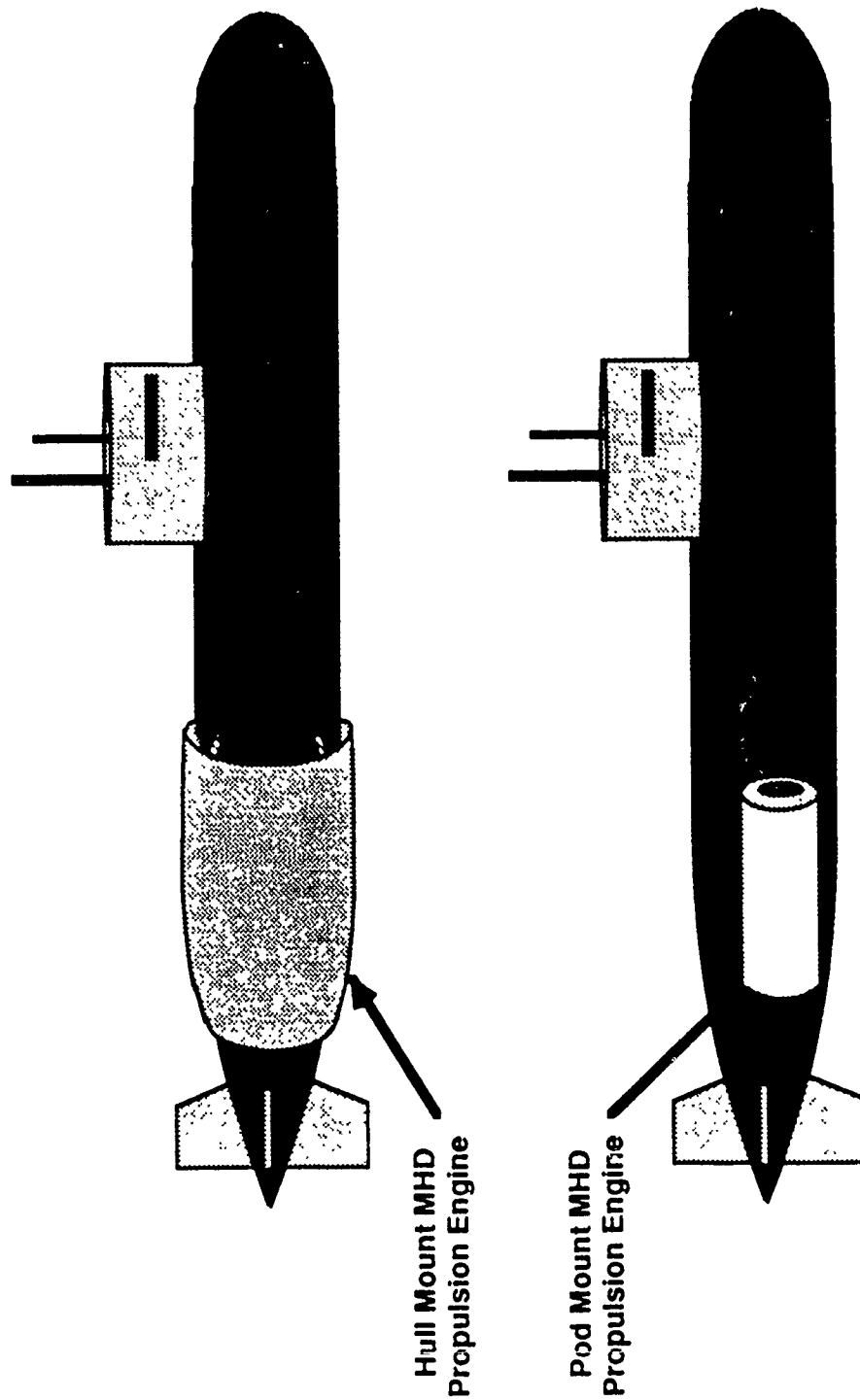


N4800

COMPARISON OF VARIOUS PROPULSION SYSTEM MOUNTING CONCEPTS

A variety of concepts - external hull mount, internal hull mount, and pod mount for example - can be considered. Of all of the concepts considered, two of the more appropriate ones are the external hull mounted concept and the pod mounted concept. Both of these concepts could be mounted at any axial position along the length of the submarine. Conventional submarine layout and operation probably favors stern mounted locations, but amidships or bow mounted systems might be attractive for "completely new design" submarines. Many features of these concepts are similar, but there are major differences between them. Because of the characteristics of magnetohydrodynamic thrusters and the performance requirements of the submarine, the annular hull mounted thruster system is the most attractive approach.

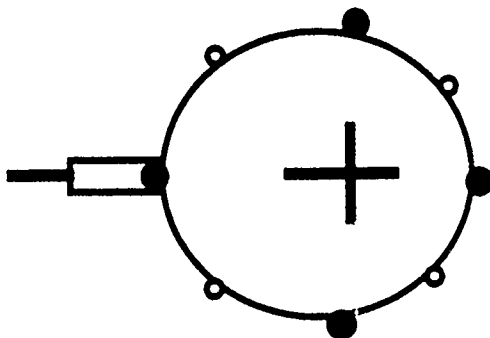
COMPARISON OF VARIOUS PROPULSION SYSTEM MOUNTING CONCEPTS



HULL CONFIGURATIONS - AFT VIEW

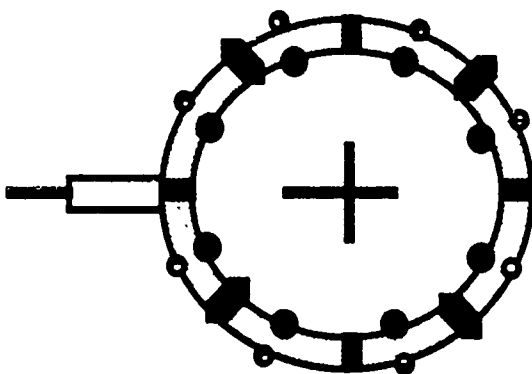
For externally mounted hull configurations, two configurations are possible - the squirrel cage and the annular hull mount. In the first magnetohydrodynamic thruster experiments performed by Stewart Way, the squirrel cage configuration was used. This approach was successful in propelling a vehicle through seawater. The annular hull mount concept offers several improvements - such as higher efficiency, lower magnetic field signature, and lower current density - over the squirrel cage configuration.

HULL CONFIGURATIONS – AFT VIEW



Squirrel Cage

N4508

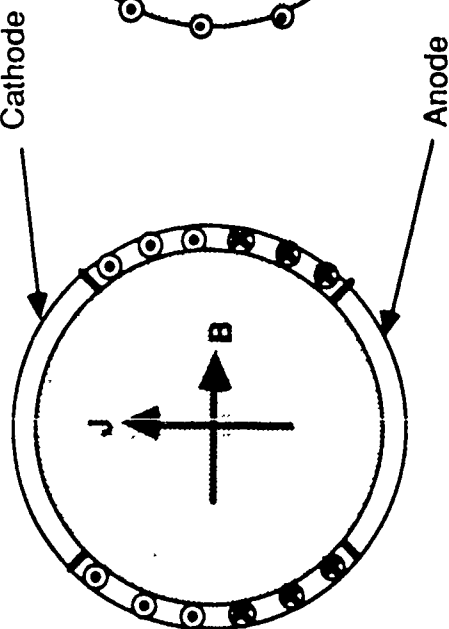


Annular Hull Mount

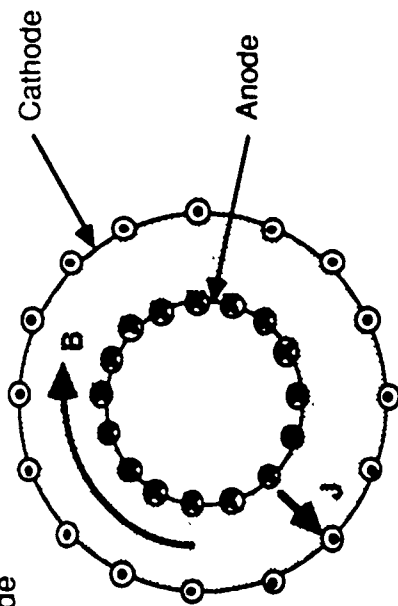
B FIELD AND CURRENT DENSITIES FOR THE THREE CONFIGURATIONS

The three configurations are shown conceptually. The gray area is the region where the seawater is flowing. In all three cases the resulting $j \times B$ force is perpendicular to the plane of the paper. The magnetic field leakage is greatest with the linear case and is minimized with the annular configuration. Because in the actual submarine application produces the highest performance most easily maximize the flow volume, the annular configuration produces the highest performance of the three configurations. Since this high performance is combined with other attributes such as the lowest magnetic field signature, the annular magnetohydrodynamic thruster is the preferred approach for the submarine propulsion system.

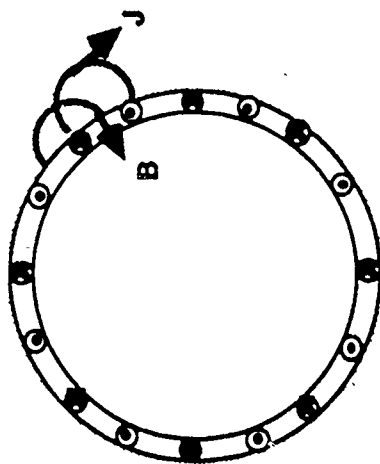
B FIELD AND CURRENT DIRECTIONS FOR THE THREE CONFIGURATIONS



Linear



Annular



Squirrel Cage

N4804

USS BUFFALO (SSN-715)

The USS Buffalo is typical of the Los Angeles attack class submarines. With a total length of 110 m, a diameter of 10.1 m, and a submerged displacement of 6900 tons, this submarine can achieve submerged speeds of 30+ knots with its existing power plant of ~ 35,000 shaft horsepower.(1)

(1)Captain Richard Sharpe, OBE, RN, Janes Fighting Ships, 1988-89,
Jane's Publishing Company Limited, London, England

USS BUFFALO (SSN - 715)



U.S. NAVY PHOTOGRAPH
BY CHRIS OXLEY

NB486

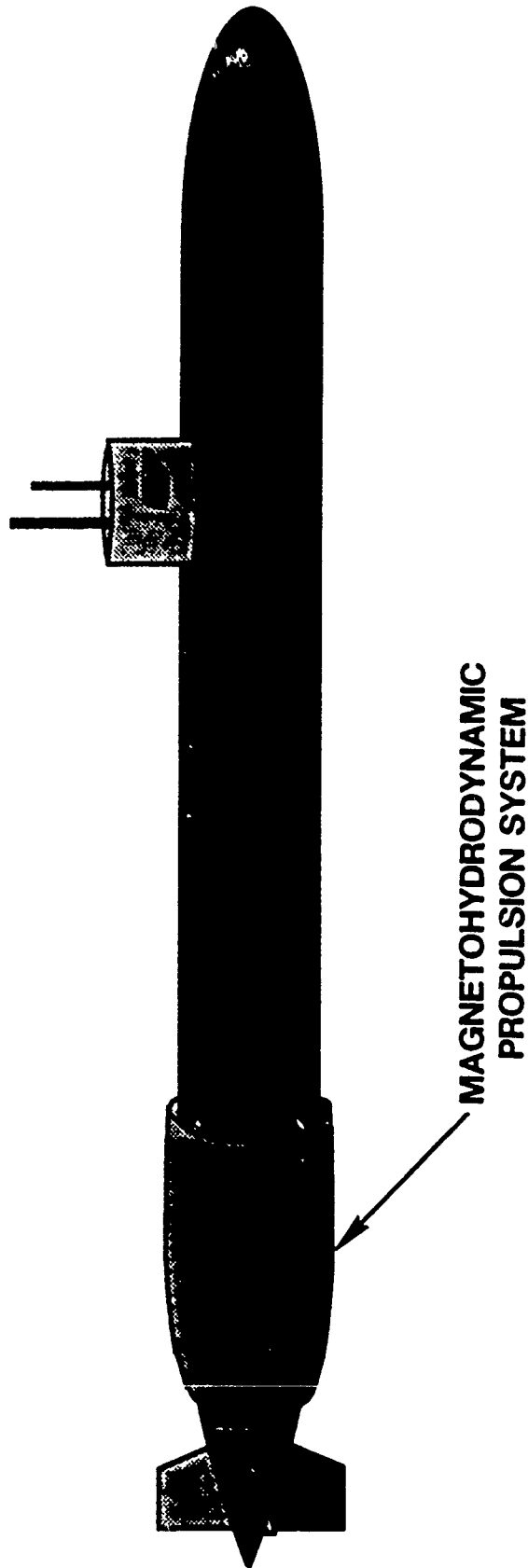
Avco Research **TEXTRON**

MAGNETOHYDRODYNAMIC PROPULSION SYSTEM FOR SUBMARINES

An annular magnetohydrodynamic thruster configuration is shown on a Los Angeles attack class submarine (SSN 688 Class). The thruster is approximately 20% of the total length of the submarine. It is segmented to provide for enhanced maneuverability as well as increased survivability. Because the configuration has maximized the enclosed volume of the thruster, the velocity difference between the submarine and the water flowing through the thruster has been minimized. The resultant propulsion system can provide performance approaching the conventional propulsion system, but the magnetohydrodynamic thruster offers the potential for much quieter operation.

MAGNETOHYDRODYNAMIC PROPULSION SYSTEM FOR SUBMARINES

LOS ANGELES CLASS SUBMARINE



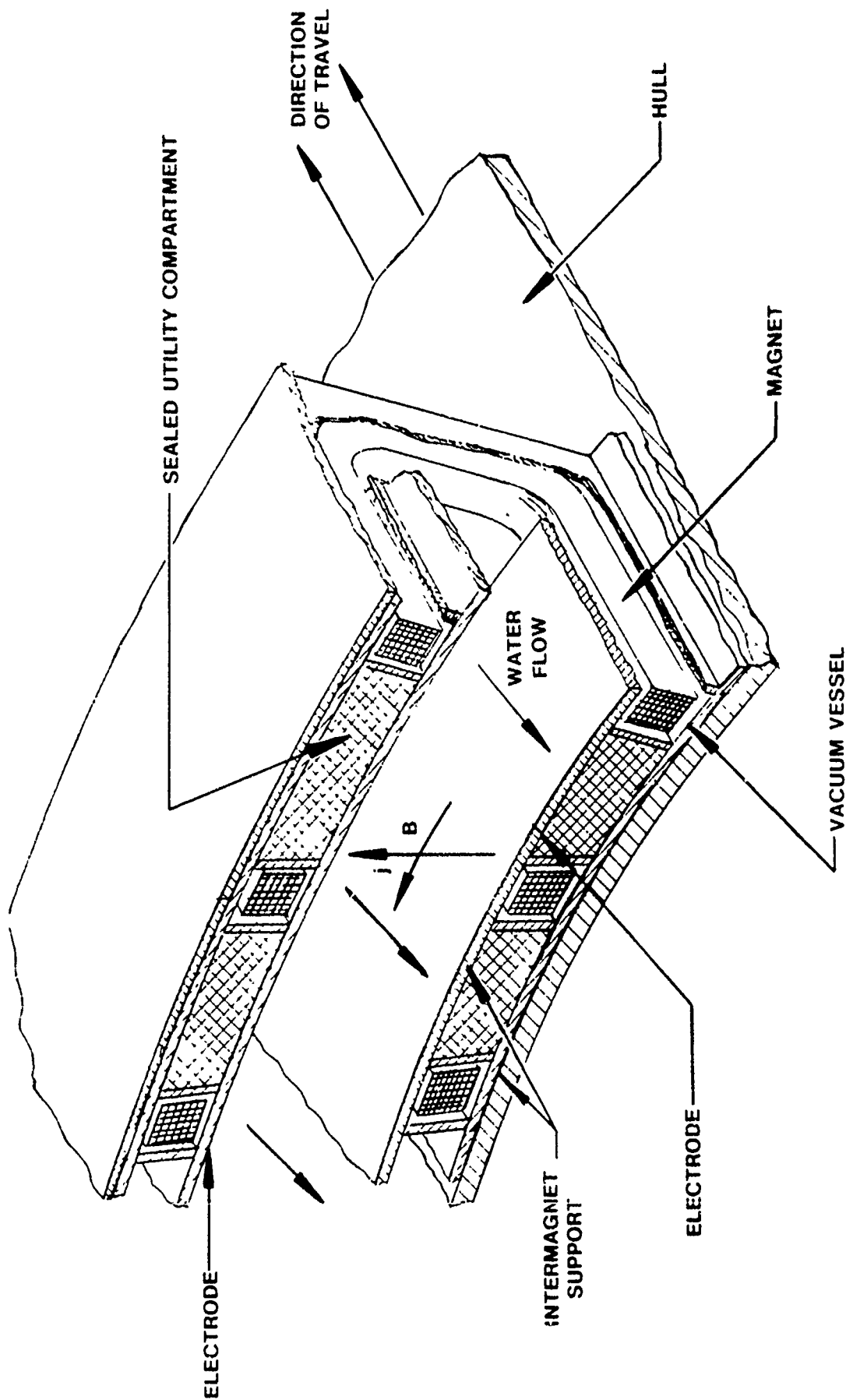
N4704

Avco Research **TEXTRON**

ANNULAR HULL-MOUNTED CONCEPT FOR MAGNETOHYDRODYNAMIC SUBMARINE PROPULSION

The figure shows the conceptual features of the annular configuration. The current flows in the radial direction. Large magnet coils provide a magnetic field in the azimuthal direction. The resultant $\mathbf{j} \times \mathbf{B}$ force is in the axial direction and provides the thrust to propel the submarine. The entire thruster unit is mounted exterior to the submarine hull. The electrodes are mounted on the inner and outer surfaces of the flow volume. The actual design would most likely consist of magnet coils that are much thinner in the radial direction and much thicker in the azimuthal direction.

ANNULAR HULL-MOUNTED CONCEPT FOR MAGNETOHYDRODYNAMIC SUBMARINE PROPULSION



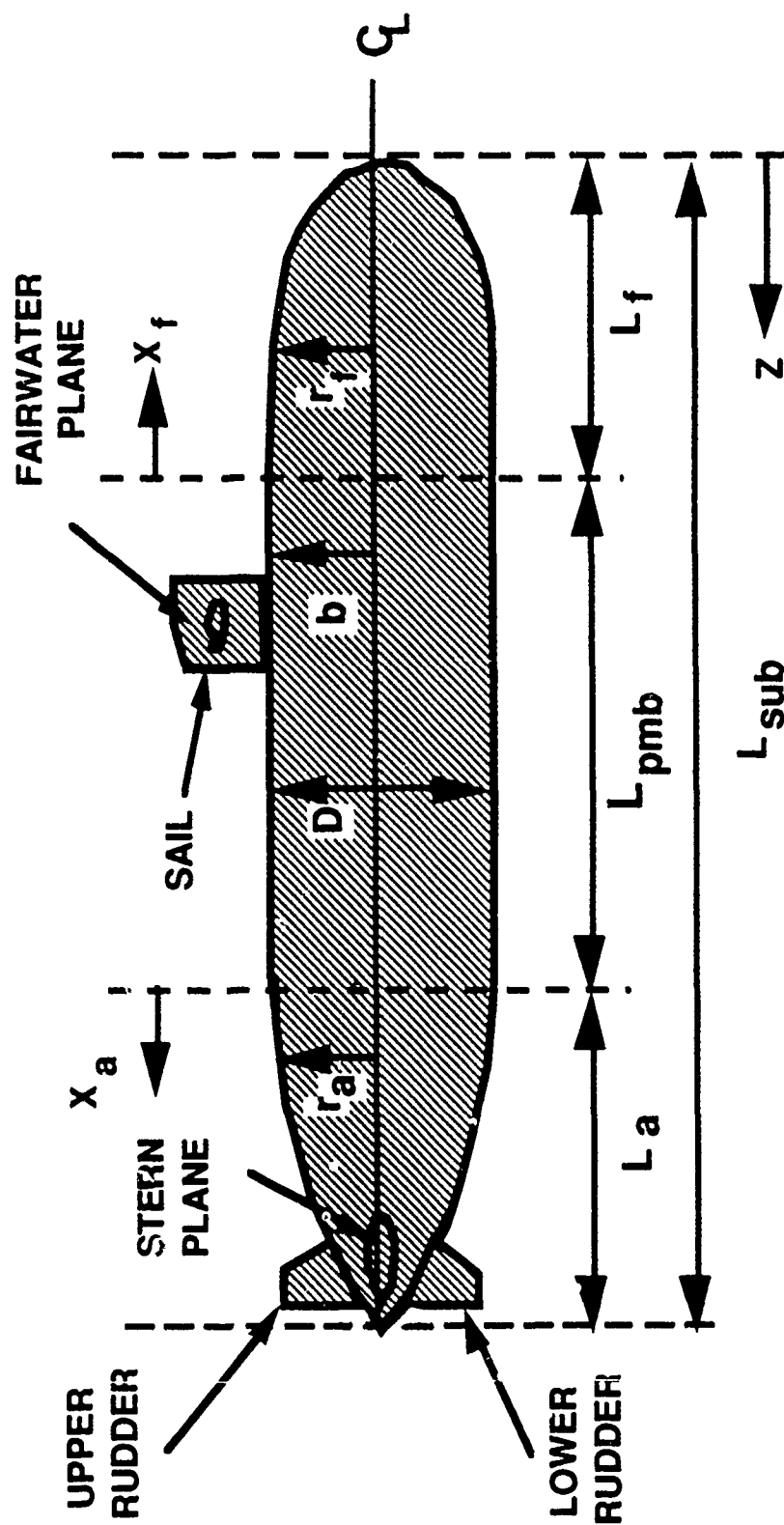
N4811

Avco Research **TEXTIRON**

QUASI - 1 D MODEL - THRUST AND DRAG

An optimization model has been developed to determine the optimum magnetohydrodynamic operating conditions and configurations for a given submarine power level, mass and volume. The submarine is modeled by using an ellipsoid for the bow of the submarine and a paraboloid for the aft section. The middle section is the parallel midbody. Stern planes, fairwater (sail) or bow planes, and upper and lower rudders are included as separate appendages with a characteristic drag coefficient and surface. Similarly, the sail drag coefficient and surface area are also included in the model. The submarine performance can then be determined for a variety of speeds, power levels, thrust requirements, and hull shapes.

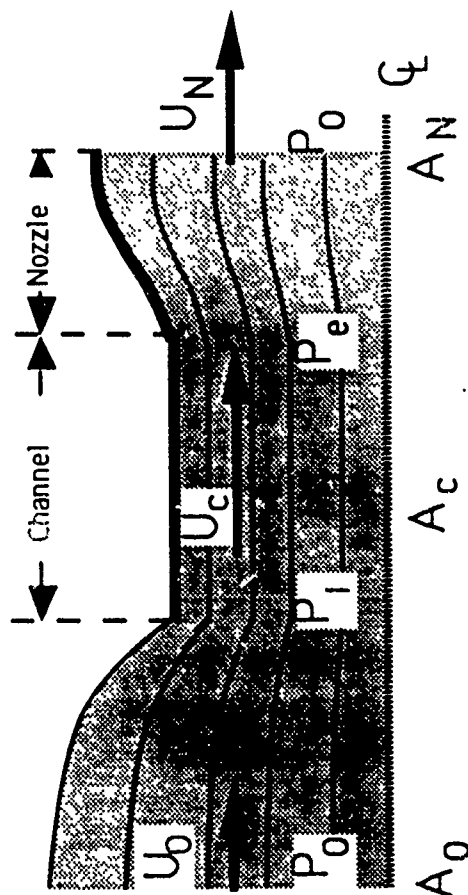
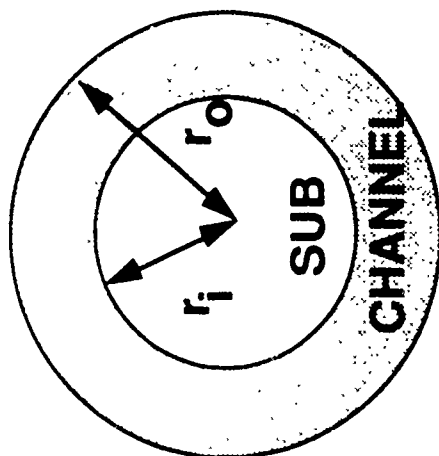
QUASI-1 D MODEL - THRUST AND DRAG



OPTIMIZATION MODEL

An optimization model has been developed to conduct studies to investigate the potential for various thruster operating conditions. The model is nondimensionalized and is used to define the major geometry characteristics of the thruster system. Three of these, which are discussed in the following figures, are the optimum thruster length, thruster radial width ratio, and thruster exit nozzle. These three parameters are used to develop the detailed thruster design. The optimum thruster length is the ratio of the thruster length to the submarine length. The channel radial width ratio is the difference of the inner and outer radii divided by the submarine length. The nozzle area ratio is the ratio of the nozzle exit area to the channel exit area.

OPTIMIZATION MODEL



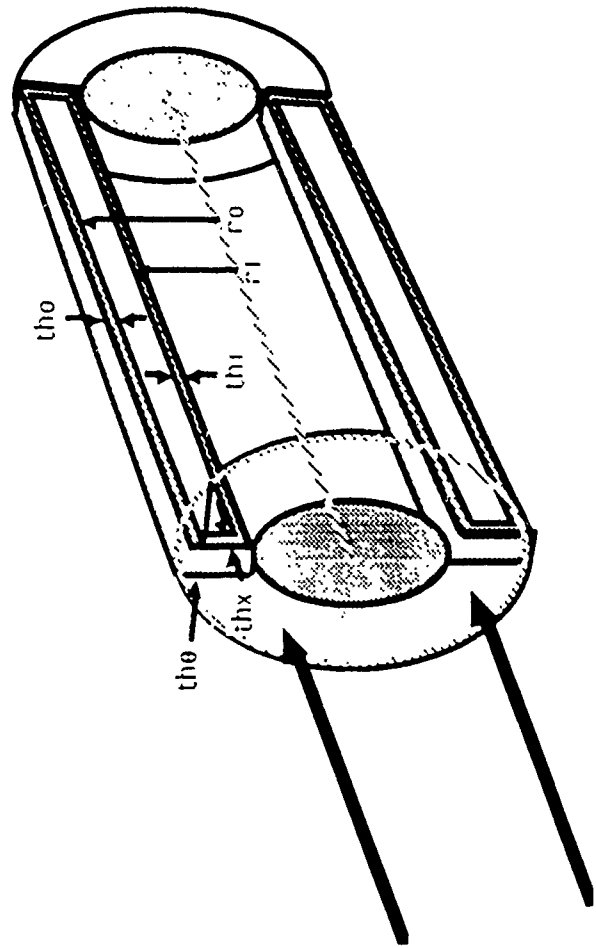
1-D MODEL INPUTS

The model uses the characteristic of seawater - electrical conductivity, density, and viscosity - for the working fluid. The submarine characteristic - length and diameter - as well as the bow and aft section profiles are used to determine the submarine shape. The magnet characteristic - magnetic field, number of magnet end turns, number of segmented partitions, the axial thickness of the end turns, and the thickness of the partitions - are used to model the magnet. The magnetohydrodynamic thruster is characterized by the thruster length, thruster inner radius, thruster outer radius, thickness of the inner coil, thickness of the outer coil, and the coil thickness in the azimuthal direction. In addition, the program can assess the merits of including a converging or diverging nozzle.

For the submarine propulsion system investigated for this optimization analysis, the submarine length was approximately 100 m and submarine diameter was 12.2 m. The seawater conductivity used was 4 mho/m and the magnetic field was 8 Tesla. The drag coefficient that was used was 0.003.

1 D MODEL INPUTS

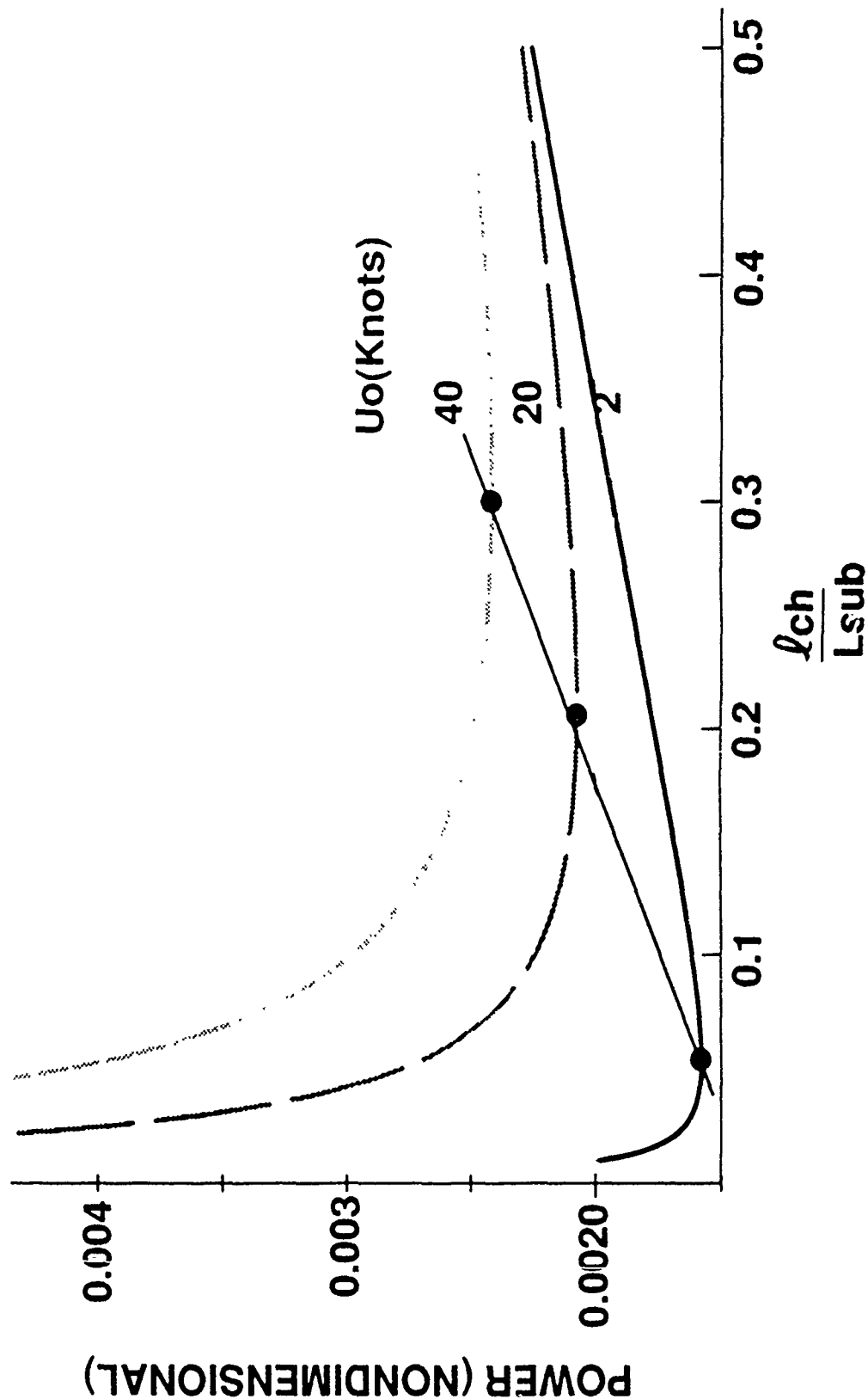
- WATER : σ, ρ, μ
- SUBMARINE : L_{sub}, D_{sub}
- MAGNET : $B(x), N_p, N_p, th_x, th_p$
- CHANNEL : $X_{ch}, L_{ch}, r_i(x), r_o(x), th_i, th_o, th_\theta$
- NOZZLE : $L_{noz}, A_{noz}/A_{chex}$



OPTIMUM CHANNEL TO SUBMARINE LENGTH RATIO

The determination of the ratio of the optimum magnetohydrodynamic thruster length to the total submarine length is important in the optimization of the thruster system. As expected, very low submarine velocities require very short thruster lengths for optimum performance. At velocities of a few knots, a thruster length of 5% of the submarine length is the optimum. As the submarine speed increases, the optimum thruster length also increases. At a speed of 40 knots, the optimum length is approximately 30% of the submarine length. As the length of the thruster increases, the added drag of the thruster increases faster than the added thrust developed from the additional length. For the submarine design investigated in this effort, a thruster length of 15% of the submarine length was selected to optimize overall performance at all velocities.

OPTIMUM CHANNEL TO SUBMARINE LENGTH RATIO



N8236

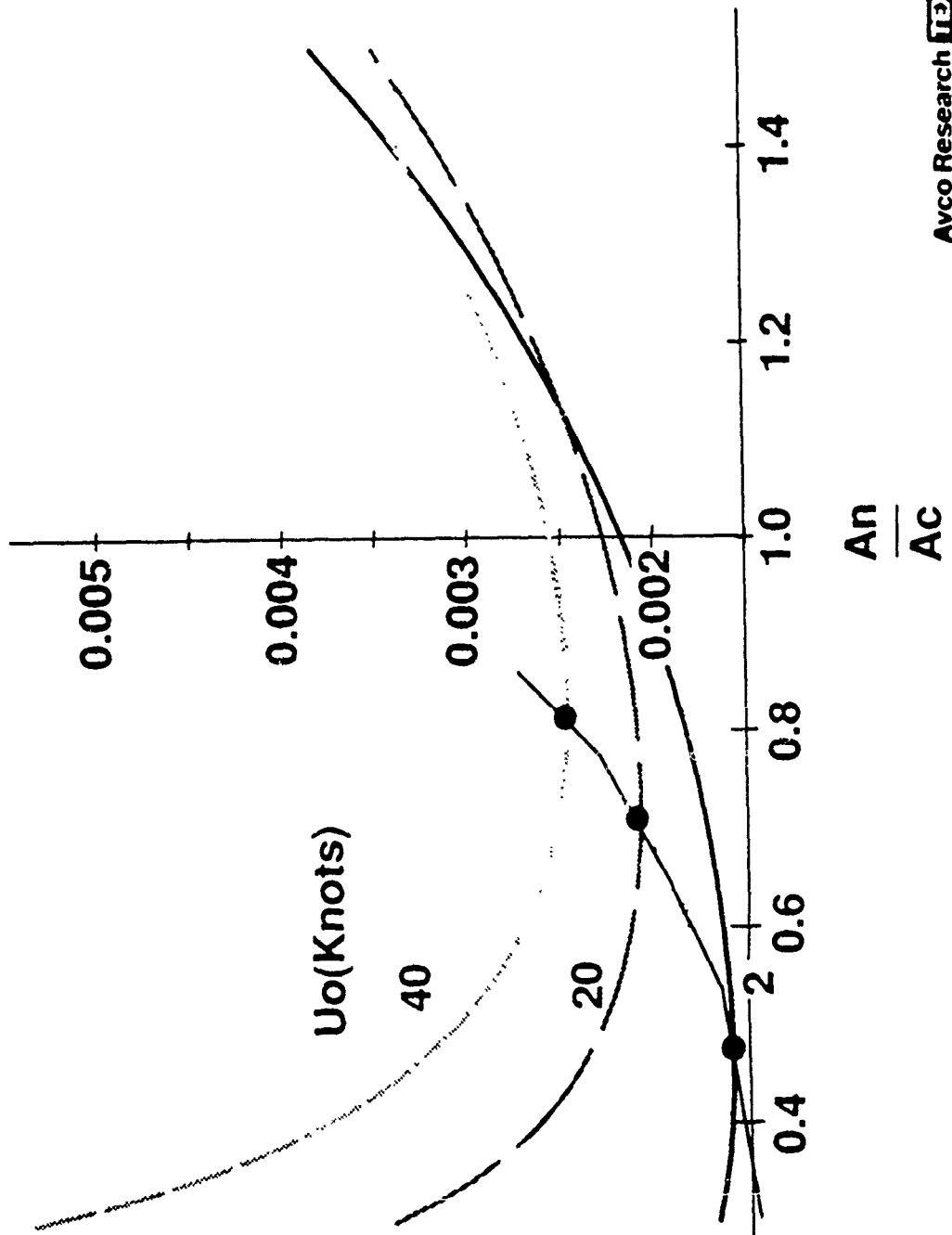
Avco Research **TEXTRON**

OPTIMUM NOZZLE AREA RATIO

Similarly, an assessment can be completed of the benefits obtained by using an exit nozzle in the aft section of the thruster. Again, at low submarine speed, the converging nozzle is of most benefit. As the velocity increases, the amount of nozzle convergence is reduced significantly. For the 40 knot velocity, the optimum area ratio is approximately 0.8. This area ratio was selected for the subsequent more detailed design analysis.

OPTIMUM NOZZLE AREA RATIO

POWER (NONDIMENSIONAL)



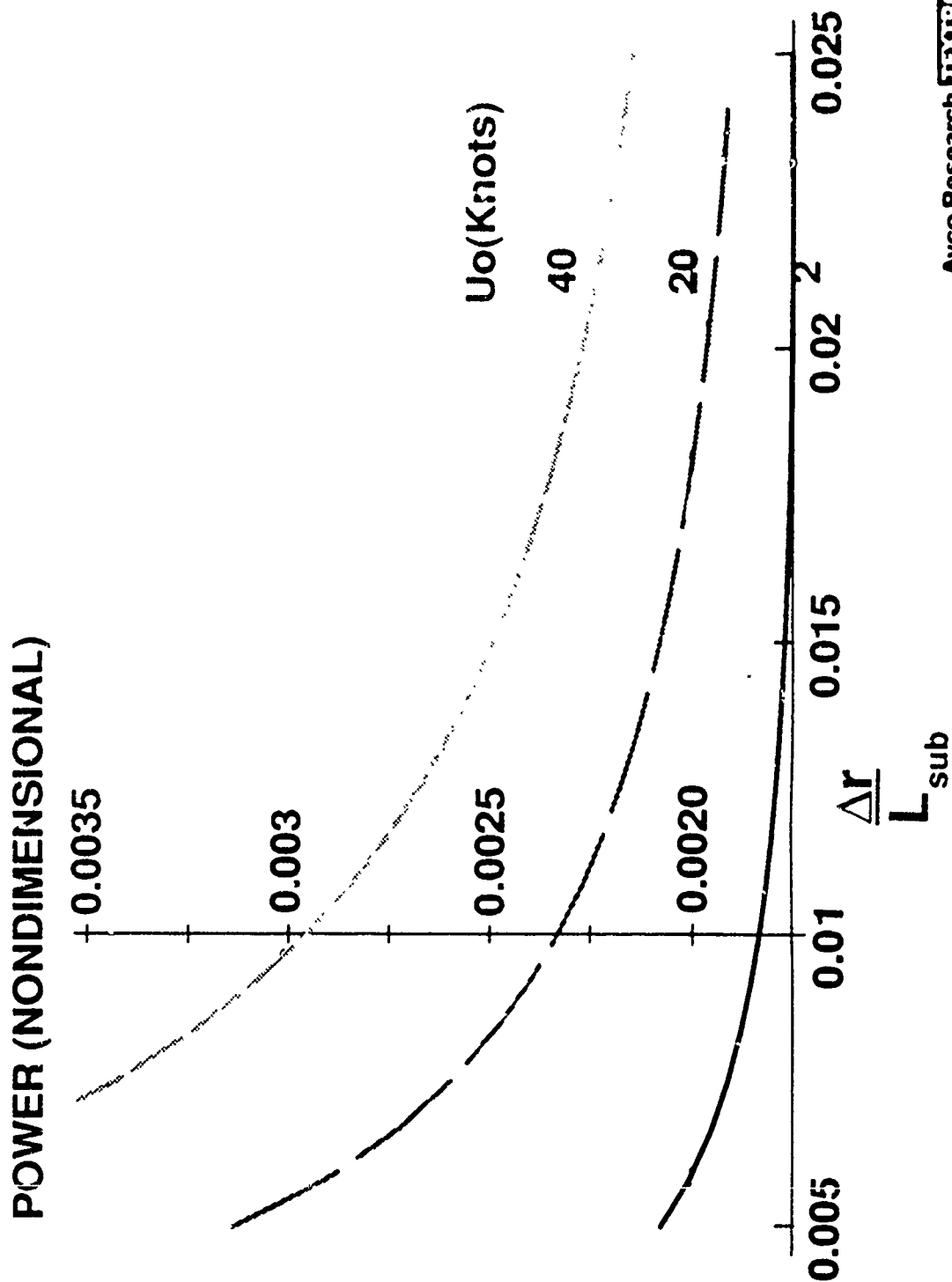
N8235

Avco Research **TEXTRON**

VARIATION WITH CHANNEL RADIAL WIDTH RATIO

The opening in the magnetohydrodynamic thruster region was also investigated as a function of submarine length. The nondimensional power versus nondimensional thruster opening is plotted for three velocities. As expected, increasing the size of the inlet area, which increases the thruster volume, increases the performance and decreases the nondimensional power requirements. On the other hand, larger values of inlet area require greater thruster diameter, and hence, magnet stored energy. Thus, some consideration must be given to these offsetting characteristics. For this reason the radial width ratio was selected to be 0.015. For this size, nearly all of the potential thruster performance increase obtainable from larger sizes has been achieved.

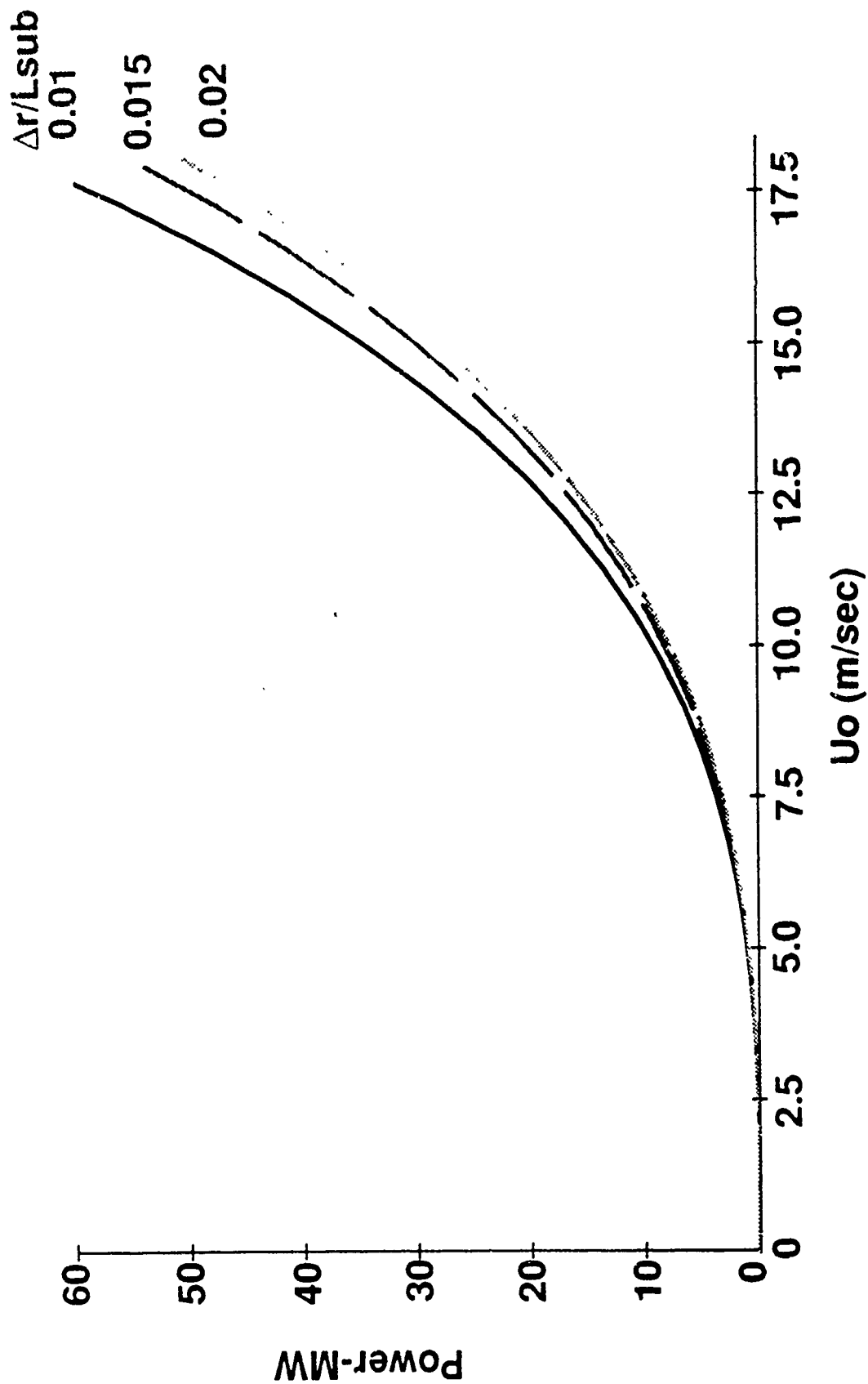
VARIATION WITH CHANNEL RADIAL WIDTH RATIO



POWER (MW) VS. SUBMARINE VELOCITY

The electrical power required for various submarine velocities is shown in the figure. Three values of channel radial width ratio are shown. For the 0.015 channel radial width ratio and a magnetic field of 8 Tesla, 45 MW of electrical power provides a submarine velocity of 17 m/sec or 34 knots. Increasing the channel radial width ratio to 0.02 increases the submarine speed by one knot. On the other hand, increasing the submarine speed by one knot through an increase in electrical power requires an additional 7 MW.

POWER (MW) VS. SUBMARINE VELOCITY



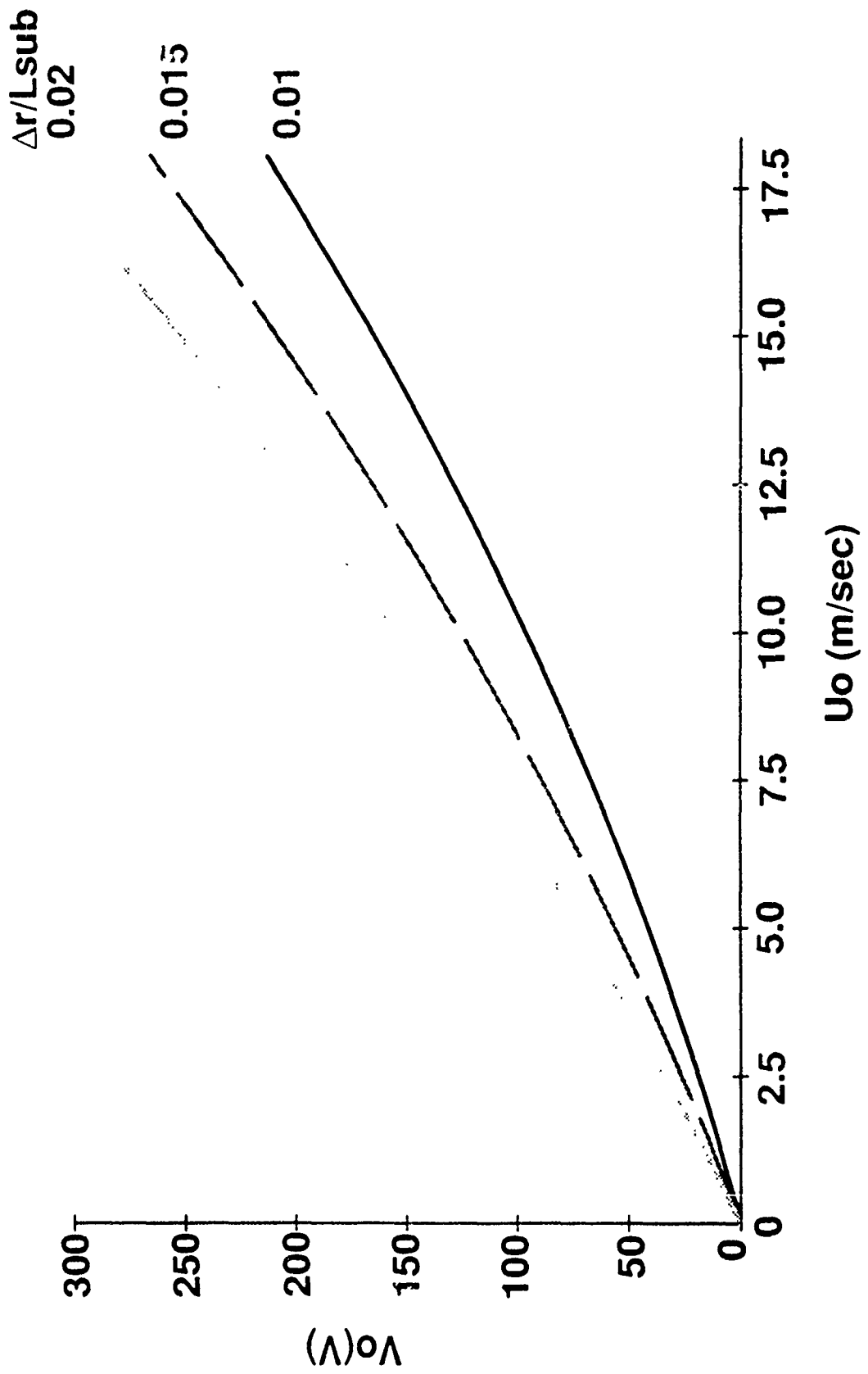
Avco Research **TEXTIRON**

N8231

VOLTAGE (V) VS. SUBMARINE VELOCITY

The resultant voltage for the magnetohydrodynamic submarine propulsion system is 250 volts at 17 m/sec (34 knots). The voltage, of course, is much more sensitive to the channel radial width ratio than the power is. Consequently, significant changes in the voltage occur when this ratio is increased or decreased. However, in all cases, the electric field is small and is well below any electric field limitations.

VOLTAGE (V) VS. SUBMARINE VELOCITY



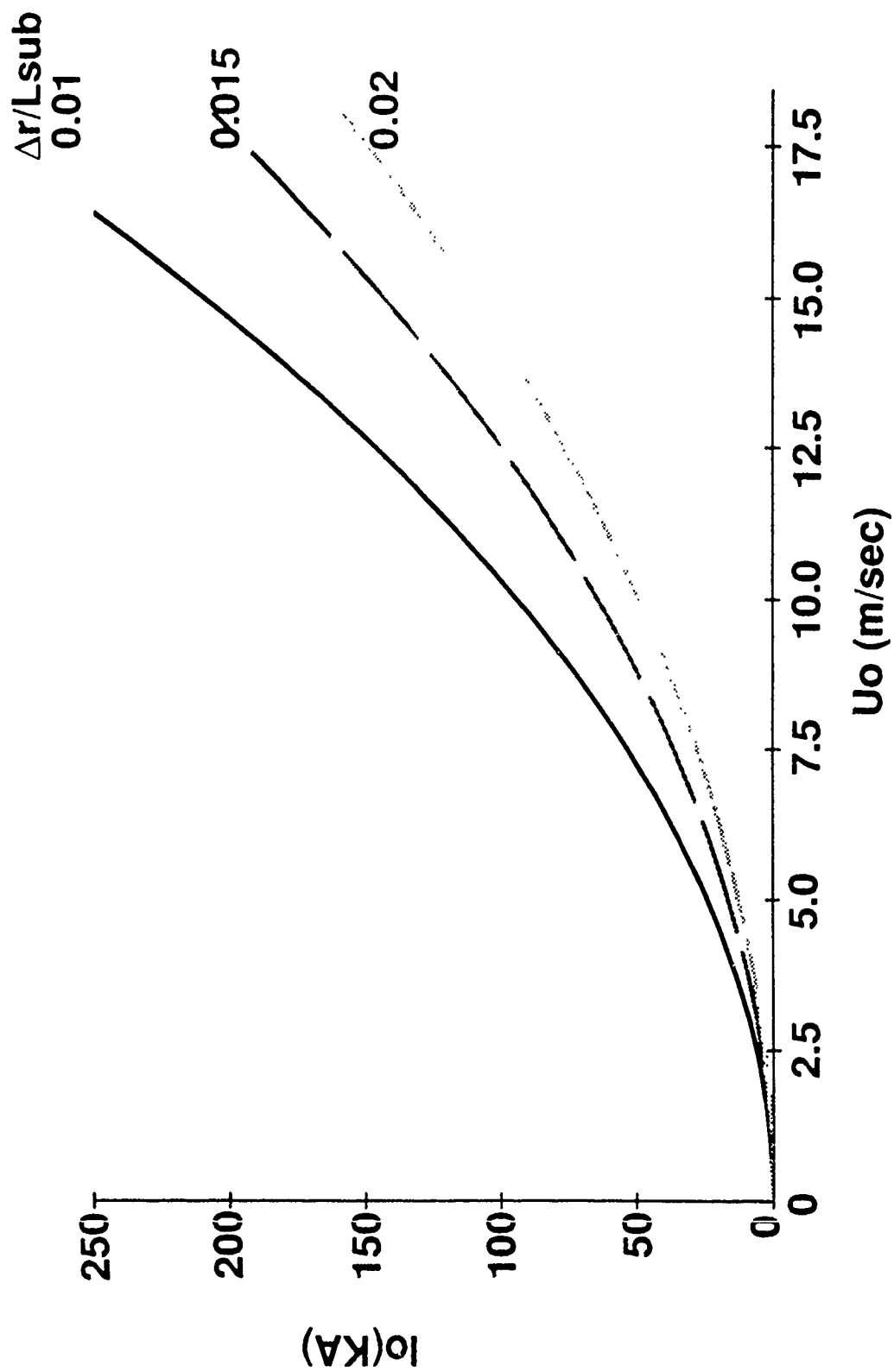
Avco Research **TEXTRON**

N8232

CURRENT (KA) VS. SUBMARINE VELOCITY

The resultant current for the magnetohydrodynamic submarine propulsion system is 180,000 A for 17 m/sec (34 knots). Again, as was the case with the required voltage, the current is relatively sensitive to the channel radial width ratio. Consequently, significant changes in current occur when this ratio is increased or decreased. For this current level, the current density is quite low - a few hundred amperes per square meter - because of the large surface area being used to transport the current.

CURRENT (KA) VS. SUBMARINE VELOCITY



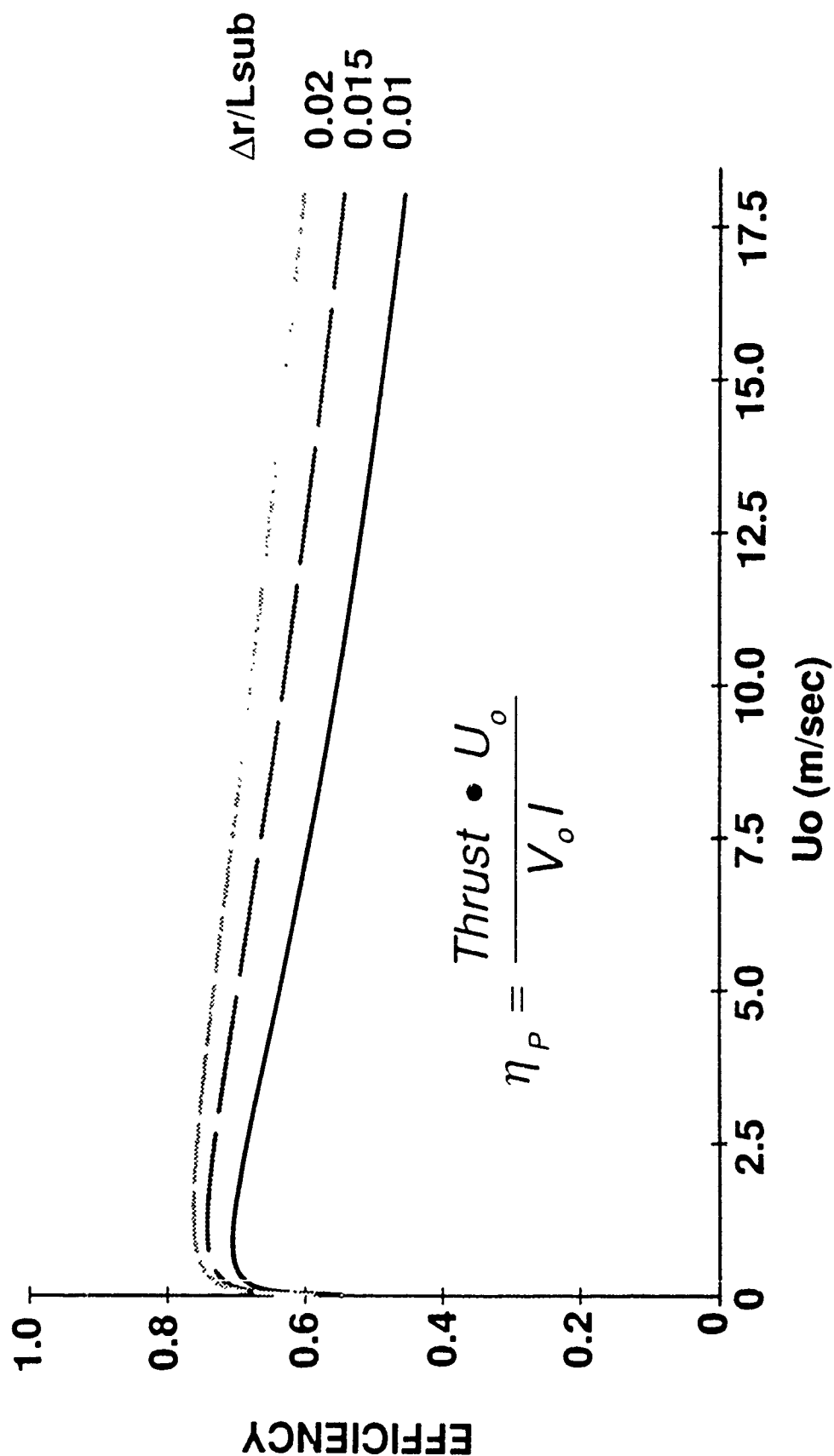
N8218

Avco Research **TEXTRON**

PROPULSION EFFICIENCY

The magnetohydrodynamic propulsion efficiency varies as a function of velocity. For the case of the channel radial width ratio equal to 0.015, the efficiency varies from ~70% at 1 knot to ~60% at 17 m/sec (34 knots). Again, this curve is for an applied magnetic field of 8 Tesla and an electrical power level of 45 MW. As expected, larger values of channel radial width ratio have higher efficiencies and lower values of this ratio have lower efficiencies.

PROPULSION EFFICIENCY



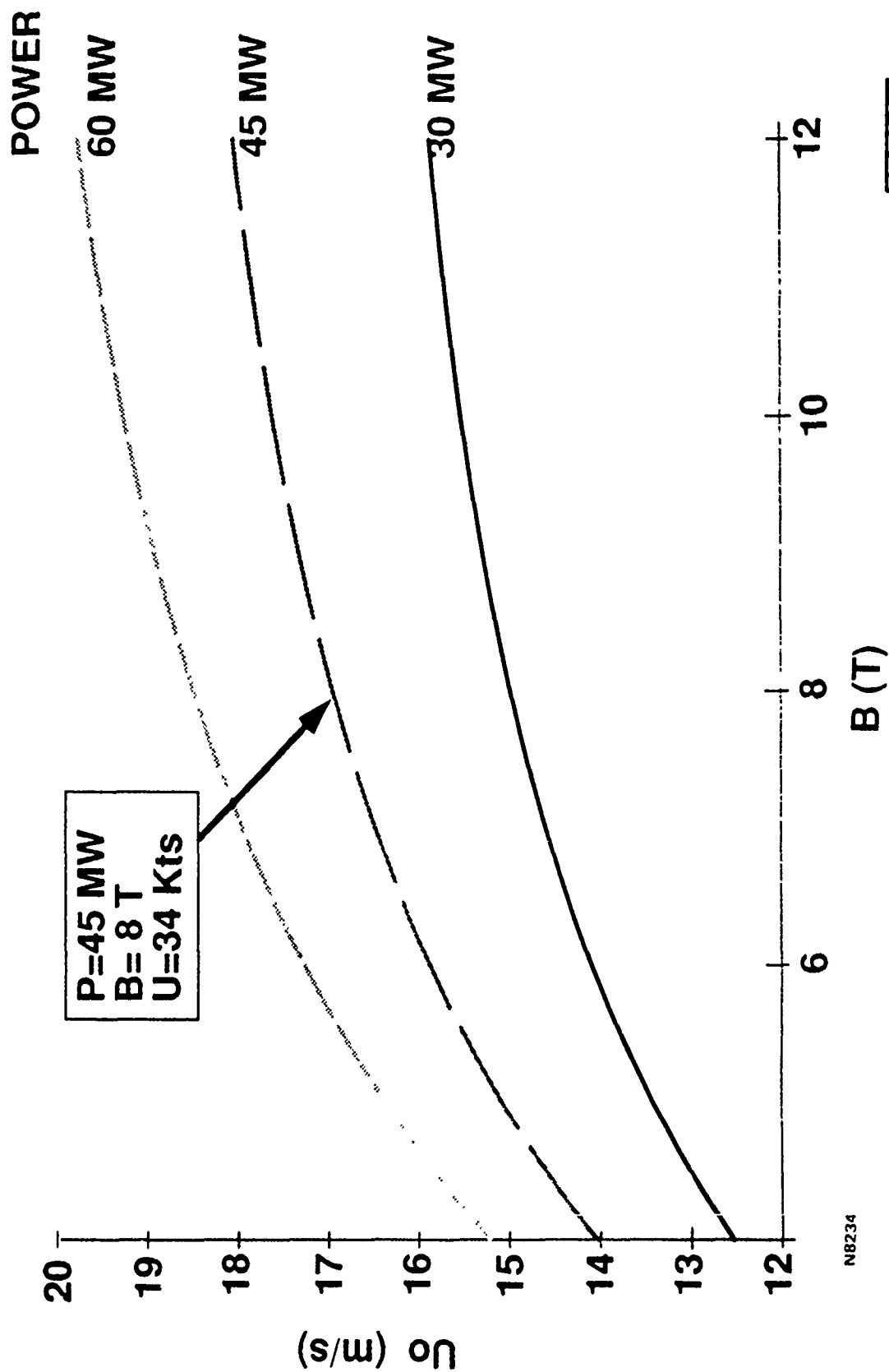
N8233

Avco Research **TEXTIRON**

MAXIMUM SUBMARINE VELOCITY VS. MAGNETIC FIELD

The results for a variety of power levels are summarized. The increased magnetic field provides an increase in the maximum submarine velocity for a given power level. The design point of 8 Tesla with 45 MW of electrical power provides a maximum speed of 17 m/sec (34 knots). Higher speeds can be obtained with higher power levels. Thus, 15 MW of electrical power addition can increase the submarine velocity by 1 1/2 to 2 m/sec (3 to 4 knots). This increase in power, of course, is achieved at the cost of an increase in the mass of the submarine power plant.

MAXIMUM SUB VELOCITY VS. MAGNETIC FIELD



N8234

Avco Research **TEXTRON**

MAGNETOHYDRODYNAMIC SUBMARINE PROPULSION SYSTEM MASS BALANCE

In order for the submarine to operate properly, the overall impact of the addition of the magnetohydrodynamic thruster must result in neutral buoyancy being maintained. The credits are mass removed by the removal of the propeller, drive shaft, and reduction gear and by the added buoyancy from the added displaced sea water volume of the thruster unit. The debits are the addition of electrical generation equipment and cryogenic equipment added to the submarine and the addition of the magnetohydrodynamic thruster external to the submarine. Thus, neutral buoyancy is maintained. No credit has been taken for any reduction in engine room volume or engine room packing efficiency.

MAGNETOHYDRODYNAMIC SUBMARINE PROPULSION SYSTEM MASS BALANCE

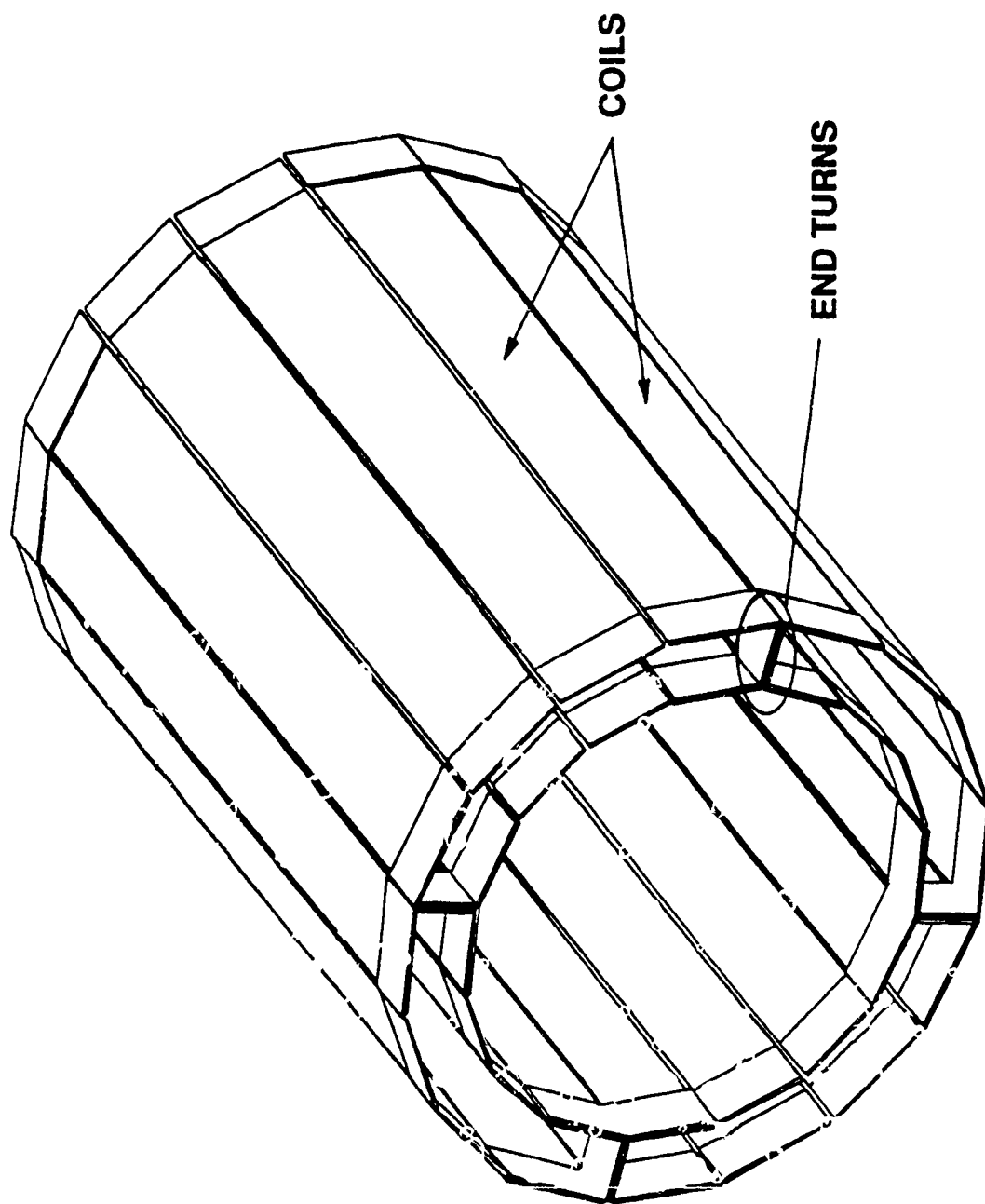
<u>CREDITS *</u>		<u>DEBITS</u>
RIP OUT (INTERNAL)	5 UNITS	ADD BACK (INTERNAL) 1 UNITS
ADDED BUOYANCY	<u>5 UNITS</u>	THRUSTER <u>10 UNITS</u>
10 UNITS	~ NEUTRALLY BUOYANT ~	11 UNITS

* NO CREDIT TAKEN FOR ANY REDUCTION OF ENGINE ROOM VOLUME,
OR ENGINE ROOM PACKING EFFICIENCY

MAGNETOHYDRODYNAMIC SUBMARINE MAGNET MODELING GENERAL DYNAMICS SIXTEEN ELEMENT MODEL

The sixteen coils in the conceptual design are shown with the finite element models that were used. The electrical current flow in the magnet coils was used to calculate the central field, end turn fields, and past magnetic fields. These contributions were summed to determine the total near and far field magnetic field signatures.

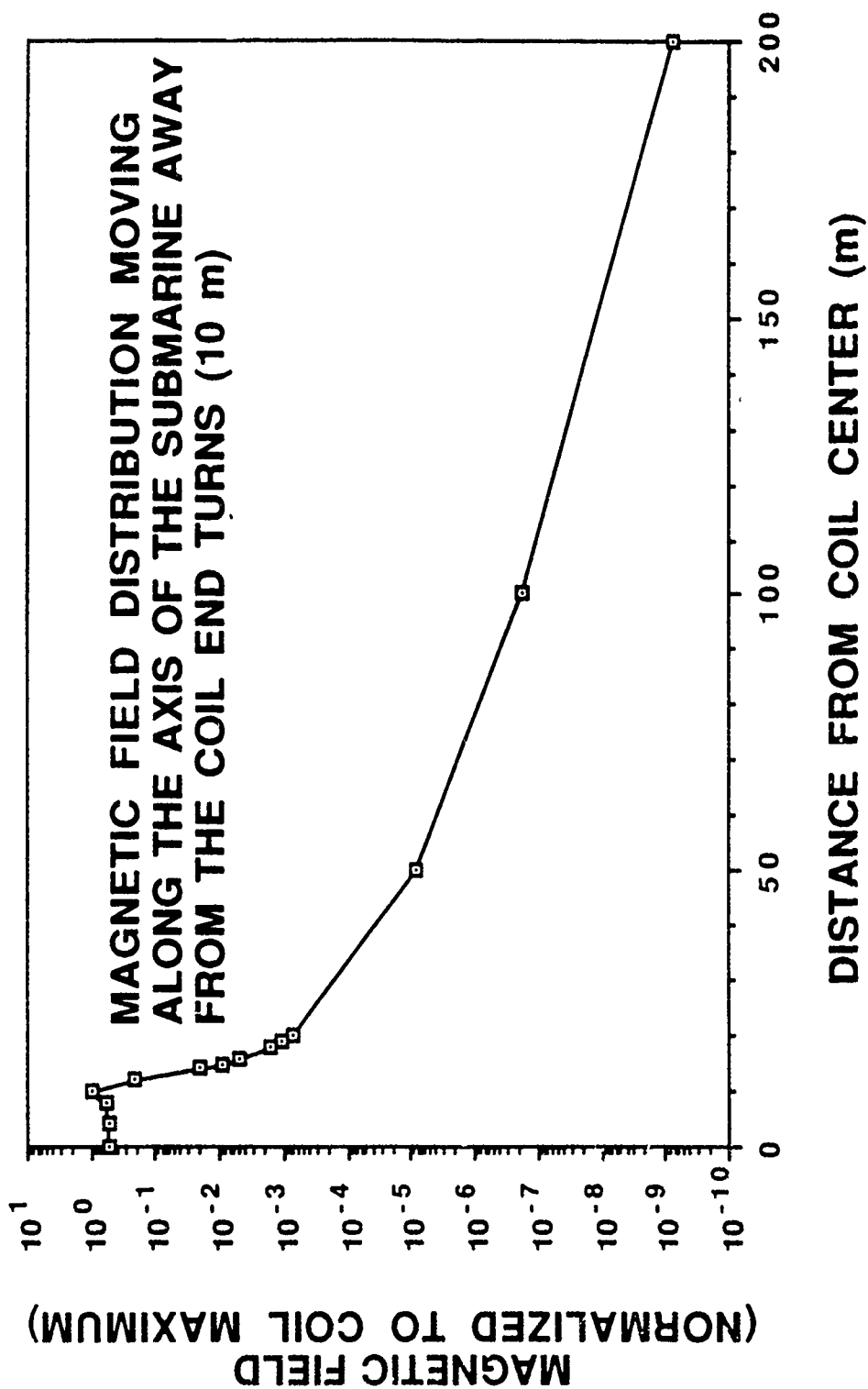
MAGNETOHYDRODYNAMIC SUBMARINE MAGNET MODELING GENERAL DYNAMICS SIXTEEN ELEMENT MODEL



NORMALIZED AXIAL MAGNETIC FIELD LEAKAGE PROFILE

The normalized axial magnetic field is shown as a function of the distance from the magnet coil end turns. The magnet coil extends from 0 to 10 m along the x axis of the figure. This plot is symmetrical about the axial center of the magnet coils. The calculation does not include any iron or any active or passive shielding. Thus, the submarine hull has been ignored in these calculations. With the proper design of shielding, the magnetic field profile may be reduced.

NORMALIZED AXIAL MAGNETIC FIELD LEAKAGE PROFILE



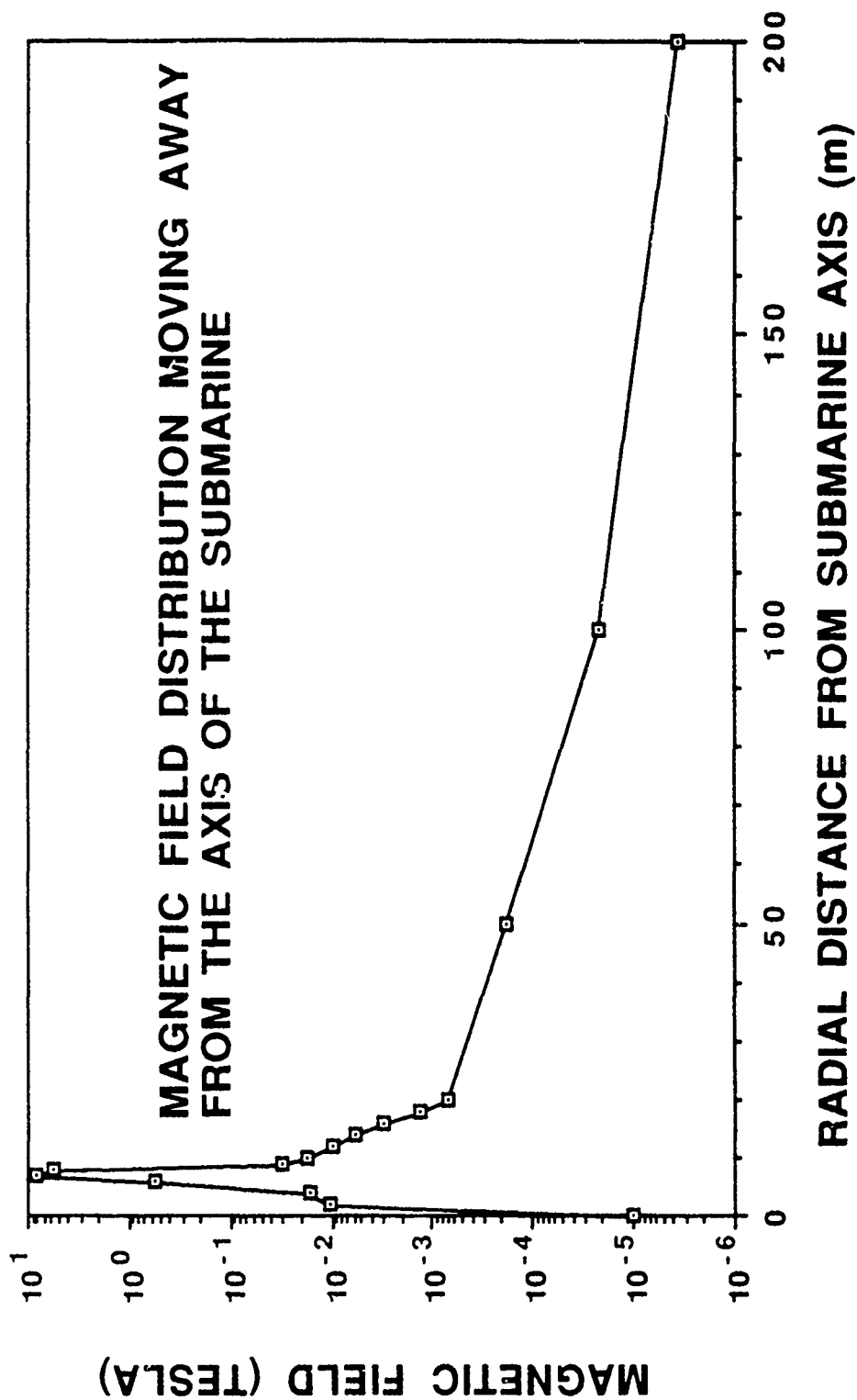
N8491

Avco Research **TEXTRON**

RADIAL MAGNETIC FIELD LEAKAGE PROFILE

The radial magnetic field is shown as a function of the radial distance from the center of the submarine. The region of magnetic field in the thruster extends from 6 to 7.5 m along the x-axis in the figure. The calculation does not include any iron or active or passive shielding. Thus, the submarine hull has been ignored in these calculations. With the proper design of the shielding, the magnetic field profile may be reduced.

RADIAL MAGNETIC FIELD LEAKAGE PROFILE



AVCO MHD PROPULSION CAN FAVORABLY IMPACT ENTIRE SUBMARINE SYSTEM

The Avco magnetohydrodynamic submarine propulsion system can favorably impact the total submarine system. In the area of hydrodynamics, the thruster is compatible with the use of any proposed boundary layer control techniques such as bubbles, polymers, etc. In addition, the thruster can be mounted at any axial location on the submarine.

In the areas of stealth and speed, the magnetohydrodynamic thruster offers the potential for a much reduced acoustic signature and a substantially reduced wake signature. In addition, the annular configuration provides a very low magnetic field signature. With regard to speed, the magnetohydrodynamic thruster is not limited by cavitation effects.

Because the magnetohydrodynamic thruster can be segmented, the thruster can be used to enhance the rates of diving, surfacing, and turning. Because the thruster system has a minimum inertia, thrust reversal is possible with a minimum delay. This same potential for segmentation can also provide for enhanced survivability. Because a loss of one segment does not render the submarine incapable of maneuvering, the submarine can retain a "fight while hunt capability".

The design of the magnetohydrodynamic thruster is compatible with current and planned submarine architectures. No new inventions are required to develop the thruster. In addition, because the magnetohydrodynamic thruster is an electric drive system, the propulsion system components can be located wherever convenient. Thus, more efficient uses of submarine engine spaces may be possible.

Lastly, the magnetohydrodynamic thruster contains a substantial amount of stored energy in the magnet system. This stored energy can be used as an emergency propulsion source in the case of a total power plant failure. Thus, the magnet in effect acts as a large storage battery to provide sufficient stored energy to propel the submarine at a velocity of a few knots for several hours.

AVCO MHD PROPULSION CAN FAVORABLY IMPACT ENTIRE SUBMARINE SYSTEM

- **HYDRODYNAMICS**
 - **BOUNDARY LAYER CONTROL (BUBBLES/POLYMERS)**
 - **FLEXIBLE CONFIGURATION**
- **STEALTH**
 - **VERY LOW MAGNETIC SIGNATURE**
 - **WAKE REDUCTION**
- **SPEED**
 - **NO PROPELLER CAVITATION LIMIT**
- **MANUEVERABILITY**
 - **ENHANCED RATES OF DIVING, SURFACING, TURNING**
 - **THRUST REVERSAL (MINIMUM INERTIA)**
- **SURVIVABILITY**
 - **FIGHT WHILE HURT CAPABILITY**
- **HM&E**
 - **COMPATIBLE WITH EXISTING AND PLANNED ARCHITECTURES**
 - **NO INVENTIONS REQUIRED**
 - **FLEXIBLE LOCATION**
- **EMERGENCY PROPULSION**
 - **STORED ENERGY IN MAGNET CAN PROPEL SUBMARINE**

N7156-1

Avco Research **TEXTRON**

AVCO MAGNETOHYDRODYNAMIC PROPULSION SYSTEM CHARACTERISTICS

In summary, the Avco submarine thruster is a segmented, annular concept. This approach minimizes the velocity difference in the water and maximizes the water mass flow rate; thus, maximizing efficiency and minimizing acoustic noise. The thruster can be mounted at a variety of axial locations on the submarine hull. The current design is matched to the existing submarine power plants. And finally, the magnetohydrodynamic thruster is an all electric drive with no external moving parts.

AVCO MAGNETOHYDRODYNAMIC PROPULSION SYSTEM CHARACTERISTICS

- SEGMENTED, ANNULAR CONCEPT
- MINIMIZES WATER ΔU , MAXIMIZES WATER FLOW
- FLEXIBLE MOUNTING LOCATION
- MATCHED TO EXISTING SUBMARINE POWER PLANT
- ALL ELECTRIC DRIVE, NO EXTERNAL MOVING PARTS

**FLOW CHARACTERISTICS INSIDE MHD
SEAWATER THRUSTERS**

Presented by

Ezzat Doss

FLOW CHARACTERISTICS INSIDE MHD SEAWATER THRUSTERS

Ezzat Doss
Argonne National Laboratory
Argonne, Illinois 60439, U.S.A.

ABSTRACT

A three-dimensional MHD fluid flow computer model has been developed and applied to study the concept of MHD seawater propulsion. The effects of strong magnetic fields on the current and electrical fields inside the MHD duct and their interaction with the flow fields, particularly those in the boundary layers, have been investigated. Results of parametric studies for variables influencing the flow field characteristics and the overall performance of the propulsion systems are discussed. Such parameters include the magnetic field, and electrical loading of the MHD thruster. The results of the calculations performed indicate the sensitivity of the thruster performance to the load factor. The distribution of J_y current density in the Hartmann layers of the insulating sidewalls causes the flattening of the velocity particles of sidewall boundary layers relative to the velocity profiles over the electrode walls. These nonuniformities in the flow field give rise to nonuniform distribution of the skin friction along the walls of the thrusters, where higher values are predicted over the sidewalls relative to those over the electrode walls. The extent of such nonuniformities of the flow fields and the corresponding differences in the skin friction between the sidewalls and electrode walls diminishes as the magnetic field or load factor decreases. Careful considerations should be given to the calculation and magnitude of frictional losses because of their impact on the efficiency of MHD thrusters.

BACKGROUND

There is considerable renewed interest in the possibility of using the MHD concept for propelling submarines or surface ships. This idea has been examined in the past by several investigators (Refs. 1 - 6), and it was found to have sufficient merit to warrant further studies, provided the applied magnetic field is high.

MHD seawater propulsion offers several advantages over conventional mechanical propellers. For

example, the absence of a mechanical propeller system will lend to a reduced vibration level in the ship or submarine; thus to a reduction in the mechanical noise generated. Also, the speed of conventional propellers is limited by cavitation. Such a restriction does not exist in MHD propulsion system. Therefore there is a potential to operate submarines and ships at higher speeds. Quiter and faster ships or submarines are desirable for obvious reasons. MHD seawater propulsion has the potential to achieve these goals at high propulsion efficiencies.

Magnetohydrodynamic seawater propulsion depends on the conductivity of the seawater to carry the electric currents. The applied magnetic field interacts with the electric current to produce the Lorentz forces, ($J \times B$), necessary to provide the propulsion force. In order to increase the propulsion efficiency, the MHD forces have to be large. This can be achieved basically by either increasing the fluid electrical conductivity or by increasing the magnetic field. One can enhance the conductivity of seawater by any seeding procedure. However this has a drawback of leaving a detectable trail of high conductivity fluid behind the surface ship or submarine, unless it should be possible to recover the conducting fluid at the stern. This option may not be practical for continuous normal operation. This conclusion leaves the other option of increasing the magnetic field as an open possibility.

The effect of magnetic field strength on the propulsion efficiency has been studied by different researchers in the past using simple physical relationships. For example, Phillips (Ref. 1) carried out a feasibility study of MHD ship propulsion using different magnet configurations for propelling 600 ft. submarines. He found that the overall efficiency of the propulsion system of the submarine moving at a speed of 10 knots with a conventional iron-core magnet of 0.6 T is only 8%. His conclusion was that low efficiency and thrust would make it unlikely to be useful as auxiliary propulsion unless a very large magnetic field is applied.

To demonstrate the need for higher magnetic fields, Doragh (Ref. 2) carried out an investigation in which he showed that a system propulsion efficiency of 60% can be achieved at a speed of 10 knots with a magnetic field of 10 Tesla. All the above studies, and also simple back of the envelope calculations using basic physics laws lead to one conclusion: i.e., a superconducting magnet with a high magnetic field must be used if one hopes to achieve a practical MHD propulsion efficiency. Stewart Way of Westinghouse (Ref. 3) was a pioneer in this application. He carried out a successful experimental test on a submarine model, 10 ft. long of 900 lb. displacement to demonstrate the proof-of-concept of MHD propulsion. He has also performed a parametric study for submarine tankers having submerged displacements of 25,000, 50,000 and 100,000 tons. The corresponding computed propulsion efficiencies for a magnetic field of 7

Tesla, and a cruise speed of 29 knots were 86%, 83%, and 79% in that order. Similar results regarding the enhancement of propulsion efficiency have been discussed by Hummert (Ref. 5) and Cott, et al (Ref. 6).

Outside the U.S., Japan and the Soviet Union are very interested in MHD propulsion. For example, Saji, et al (Ref.4) performed a parametric study for a 10,000 ton submarine tanker. They varied the magnetic field between 1 and 10 Tesla and the submarine velocity between 10 and 60 knots. Their calculations agreed with Doragh's prediction of 60% efficiency with a magnetic field of 10 Tesla. Also their calculations indicated that the system propulsion efficiency drops significantly to less than 5% for a magnetic field strength of 1 T.

All previous studies of MHD propulsion lead to one conclusion, i.e., a superconducting magnet with a high magnetic field (10-20 Tesla) must be used if one hopes to achieve a practical and superior MHD propulsion efficiency. However, operation of magnets using superconducting materials required cryogenic cooling with liquid helium, i.e., operation at 4.2K. Also, sophisticated magnet designs operating in the 5 to 6 Tesla range were not generally available on a large scale production basis. Furthermore, because of the requirement of extreme cryogenic environment with its accompanying cumbersome refrigeration and containment system, MHD propulsion was judged to be infeasible at that time. Recent developments in high temperature superconducting materials have renewed interest internationally in reviving the concept of electromagnetic ship propulsion. The critical temperature for the new types of superconductors now extends to about 100K which is well above the 77K boiling point of liquid nitrogen. Cryogenic cooling with liquid nitrogen is significantly simpler and cheaper than cooling with liquid helium and nitrogen can be easily liquified and stored in ships or submarines.

This conclusion, however, i.e., the need for superconducting magnets with high magnetic fields (10-20 T), opens the door for very important technical issues. One of them is how much can those high magnetic fields alter or modify the flow fields inside the MHD duct. Will those flow fields be distorted sufficiently to invalidate the expectation of higher propulsion efficiencies? Phillips (Ref. 1) presented a brief discussion about this subject and indicated that the magnetic field can influence the stability of the boundary layer, the wall friction, and the boundary layer velocity profile. His discussion was qualitative, very simple, and was not backed up by any quantitative numerical analysis. In order to answer those questions, three-dimensional computer models are needed to solve for the electrical and current density fields in the cross-section of the MHD ducts and include these as an integral part of three-dimensional calculations of the flow fields. That is the purpose of this paper.

COMPARISON OF FLOW PARAMETERS BETWEEN MHD SEAWATER THRUSTERS AND OPEN-CYCLE MHD GENERATORS

Exhaustive work has been done on MHD channel flow for open-cycle plasma power generation, but there has been minimal research effort on duct flow for seawater MHD propulsion. However, MHD flow inside ducts is subject to $\mathbf{J} \times \mathbf{B}$ forces whether the duct is an MHD generator or an accelerator. In the first case, electrical power is extracted from the interaction of the fluid flow with the magnetic field. In the accelerator case, energy is supplied to the duct by applying an external electrical field, and the resulting electrical currents interact with the magnetic field to produce a driving force that pushes the fluid through the duct. This is the case of MHD propulsion. There are obviously some differences between the flow medium and the operating conditions between the two cases; however, the governing equations and the physical phenomena are quite similar.

In order to place the flow parameters for seawater propulsion in perspective, a comparison is made between the expected operating parameters for ship propulsion and those for open-cycle MHD power generation. Table I lists these parameters. In turn, these physical parameters can be used to estimate several important dimensionless groups which govern the flow fields inside MHD ducts and, hence, the MHD thrust efficiency. The dimensionless groups include the following:

- Reynolds Number -- $R_n = \rho U D / \mu$
- Magnetic Reynolds Number -- $(R_n)_m = \mu_0 \sigma U L$
- Hartmann Number -- $H_a = (\sigma B^2 D^2 / \mu)^{1/2}$
- Interaction Parameters -- $(I_U = \sigma B^2 L / \rho U, I_p = \sigma U B^2 L / P)$

It can be seen from Table I that there are many similarities between the applications of MHD for open-cycle power generation and for seawater propulsion. The values of the dimensionless parameters indicate that, in some cases when strong magnetic interaction with the flow occurs, the velocity fields may be distorted.

In MHD generators, the flow and electrical fields are inherently three-dimensional for a variety of reasons. The aspect ratio of practical generators is close to unity so that all four boundary walls of the duct affect the flow development. The interaction of the MHD electrical forces ($\mathbf{J} \times \mathbf{B}$) with the fluid flow leads to flow distortions. The cross-sectional nonuniformity of the axial component of the Lorentz force ($\mathbf{J} \times \mathbf{B}$) is directly responsible for flattening the velocity profile along the insulating sidewalls and for the possible generation of velocity overshoots in the boundary layers. The nonuniformity in the magnetic field direction of the Lorentz force due to Hall current produces

secondary flows which in turn lead to flow asymmetry. The tensorial nature of electrical conductivity and the sidewall boundary conditions produce nonuniform Joulean dissipation, thereby distorting the temperature field. The distortion of the flow and temperature fields is enhanced by the mutual coupling between the flow and electrical fields. The extent and nature of flow distortions also depends on the electrical loading. Such unusual nonuniform flow fields have been investigated in the past using three-dimensional models such as those described in Refs. 7-9.

Table I

Operating Parameters for Open-Cycle Power MHD Generation and Seawater Propulsion

<u>Parameter</u>	<u>QC-MHD</u>	<u>Seawater Thruster</u>
mode	generator	accelerator
(electric load factor)	< 1.0	(> 1.0)
working fluid	combustion gases	sea water
seed	potassium	none
U (m/s)	700 - 1100	10 - 40
T (K)	2200 - 3000	300
Δp (atm)	6-10	0.5 - 5
ρ (kg/m ³)	~ 1	~ 10 ³
L (m)	8 - 15	10 - 30
D (m)	0.5 - 2.0	1 - 3
B (Tesla)	4 - 8	5 - 20
σ (S/m)	4 - 10	4 - 5
β	0.3 - 4.0	0
electrode	segmented	continuous
R_n ($\rho U D / \mu$)	> 10 ⁷ - 10 ⁸	~ 10 ⁷ - 10 ⁸
$(R_n)_m$ ($\mu_0 \sigma U L$)	<< 1.0	<< 1.0
H_a ($\sigma B^2 D^2 / \mu$) ^{1/2}	~ 10 ³	~ 10 ² - 10 ³
I_p ($\sigma U B^2 L / \Delta p$)	> 1.0	~ 0.1 - 1.0
I_u ($\sigma B^2 L / \rho U$)	> 1.0	~ 0.1 - 1.0

For MHD seawater thrusters, however, the electrical conductivity of seawater is expected to be practically uniform across and along the thruster, and the Hall parameter is negligible. Therefore one might anticipate that such flow nonuniformities would not be manifested strongly inside the ducts much as is the case of plasma generators. In order to investigate the extent of such flow nonuniformities in the thrusters, three-dimensional calculations of the flow and electrical fields are needed.

MHD THREE DIMENSIONAL THRUSTER MODEL

A three-dimensional MHD generator model incorporating fully the interaction between the flow and the electrical fields inside the channel has been developed at Argonne National Laboratory (Refs. 8 & 9) and has been applied for several open-cycle MHD generators. The flow fields are represented by the parabolic form of the three-dimensional compressible, turbulent Navier-Stokes equations and their solution is coupled to the solution of the electrical field in the cross-flow direction.

The equations solved in this model consist of the mass conservation equation, the three momentum equations, the equations for enthalpy, turbulence kinetic energy and dissipation rate, the Maxwell and Ohms law equations. This set of coupled equations is solved by the use of a finite-difference calculation procedure. The turbulence is represented by a two-equation model of turbulence in which partial differential equations are solved for the turbulence kinetic energy and its dissipation rate. Full descriptions of the equations and the method of solution are given in Ref. (9).

This three-dimensional model has been adapted for the application of seawater propulsion. A continuous electrode configuration has been used in this application where the electric field E_x is assumed to be zero. This assumption is reasonable since the Hall parameter, β , for seawater is negligible. An applied electric field, in terms of a load factor, is specified as the boundary condition for the electrode walls, while the sidewalls are assumed to be insulators. The electrical fields are computed at each crosssectional plane perpendicular to the flow. Locally the axial variation of the electrical fields and current densities are assumed to be negligible in comparison with their variations in the cross-plane. This assumption may not be accurate where there are strong variations of the magnetic field, flow velocity, or where there are abrupt changes in the boundary conditions. Such situations may exist near the ends of the MHD thrusters.

APPLICATIONS AND RESULTS

Operating Conditions

Computations have been performed using the three-dimensional model for MHD thruster operating in the continuous electrode mode with insulating sidewalls. The general operating parameters for the computational cases considered are listed in Table II. The thruster is assumed 10 m long, with constant cross sectional area of $1 \times 1 \text{ m}^2$. The magnetic field is assumed to be constant along the duct. The flow at the entrance of the thruster is assumed to be that of a plug flow.

Table II

Operating Condition for the Illustrated Examples

Thruster geometry:

• length	10	m (rectangular)
• height and width	1×1	m^2
• wall roughness	2.5	mm
Wall temperature	300	K
Fluid temperature	300	K
Working fluid	Seawater	
• electrical conductivity	4.8	S/m
• mass density	1025	Kg/m^3
• viscosity	$1.1 \cdot 10^{-3}$	Kg/(m.s)
• specific heat	3994	$\text{J/(m.s.}^\circ\text{C)}$
Flow velocity	30	m/s
Mass flow rate	30750	Kg/s
Magnetic field	0 - 20	T
Duct loading	continuous electrode with insulating sidewalls	
• average electric load factor	0 - 20	
• load potential	0 - 6000	V

The physical properties of seawater are documented in Ref. (10) and the values used are for a temperature of 20°C .

Parametric Study

A parametric study has been performed by varying the magnetic field up to 20 Tesla and the average electric load factor between 1 and 20. The average electric load factor K is defined as

$$K = \langle E_y \rangle / \langle UB \rangle$$

where E_y is the electric field across the duct between the two electrode walls, U is the axial flow velocity, and B is the magnetic field.

No restrictions have been imposed on the flow conditions at the exit of the thruster. The computations proceed to compute the flow fields and the pressure increase along the thruster regardless of the actual ambient pressure. Practically, for steady-state conditions, the flow velocity inside the thruster is a floating parameter that will be determined by the input and boundary conditions of the propulsion system. The cruise velocity will be reached when there is balance between the total thrust generated and the total surface drag of the ship or submarine. Furthermore, we will concentrate the discussion more on cases of high magnetic fields (20 T) where flow distortions are more likely to occur.

Effect of Load Factor on the Global Performance Parameters

Figure 1 presents the results for the pressure gain along the thruster for different load factors for the case of $B = 20$ T. Also presented on Fig. 1 is a curve for the accumulated frictional losses along the duct of the thruster. There is a linear dependence of the pressure gain on the axial distance along the duct. Such linear dependence is expected since the physical properties and the average axial velocity are constants along the duct. For simple MHD flows with no Hall effects ($\beta = 0$), the pressure rise is given as

$$\Delta p = (J_y B) L = \sigma U B^2 (K-1) L$$

This simple relationship indicates that the pressure gain varies linearly with the distance L , and increases with the load factor. This does not mean that MHD thrusters should operate at higher

values of the load factor, because this leads to lower efficiencies.

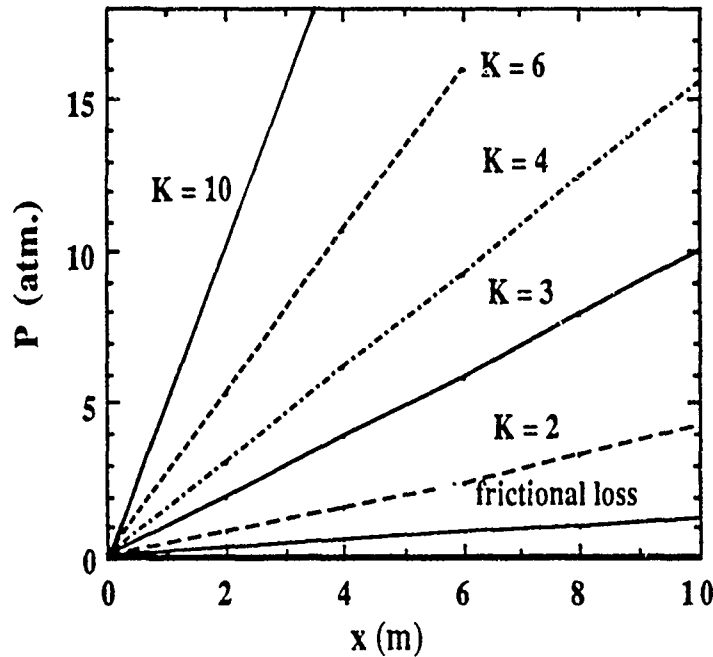


Figure 1 Pressure rise along the thruster. ($B = 20$ T, $U = 30$ m/s)

Figure 2 demonstrates the variation of the electrical efficiency with the load factor for $B = 20$ T. Two curves are shown on this figure, the top curve is for the ideal electrical efficiency and the bottom curve is the result of the three-dimensional calculations of the flow fields. In general, the thruster electrical efficiency is defined as:

$$\eta_e = \frac{\Delta p Q}{VI}$$

where Δp is the pressure rise in the duct, Q is the volumetric flowrate, V and I are the applied external voltage and currents. Physically this efficiency represents the net resulting MHD push power (after subtracting the frictional losses) divided by the input power.

For ideal situations where the flow is treated as one-dimensional with constant properties and neglecting frictional losses, one can show that the thrust efficiency is

$$\eta_{ideal} = UB/E_y = 1/K$$

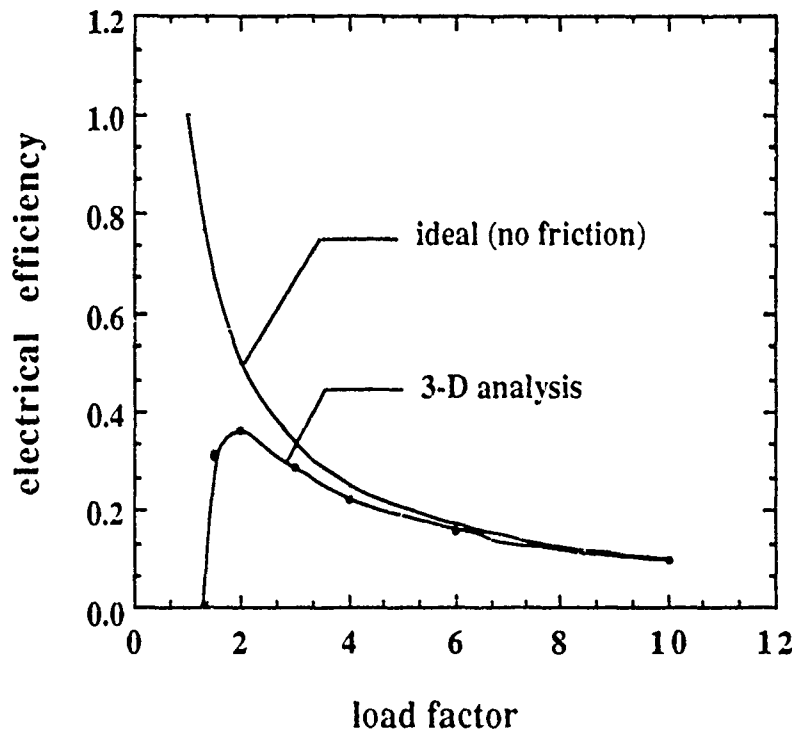


Figure 2 Variation of electrical efficiency with load factor ($B = 20 \text{ T}$, $U = 30 \text{ m/s}$)

This simple relationship is shown in Fig. 2, and it indicates, as expected, that the ideal efficiency is 100% for a load factor of 1 (open circuit). However in this case, no thrust is being generated. If frictional losses are included in the analysis, the thruster efficiency decreases as shown in the figure. However, since the frictional losses along the duct are almost the same for all values of K (as shown in Fig. 1), the deviation of the computed values of the thruster electrical efficiency from the ideal values gets larger as the load factor K decreases. As a matter of fact the curve for the computed efficiency will eventually reach a peak and then will change its slope at lower values of K when the net pressure gradient (after subtracting the frictional losses) becomes negative. This situation takes place when the MHD $\mathbf{J} \times \mathbf{B}$ forces become less than the frictional losses. This argument suggests that a greater attention should be given to the calculation of the frictional losses at lower values of the load factor K , particularly for K between 1 and 2. Also one should try to minimize the frictional losses if higher efficiencies are required. This should be a subject of further study in the future.

Flow Fields and Friction Factor

In order to predict the frictional losses accurately, one has to solve for the development of the flow

fields inside the MHD thruster. Figure 3 shows surface plots for the axial velocity distributions at several crossections along the duct. At first, one may think that these plots are typical for normal turbulent flow development in a duct. Figure 4 illustrates ,however, that there is a difference between the shape of the axial velocity profiles along the electrode and those along the sidewalls. As shown in this figure, the velocities near the insulating sidewalls are relatively higher than those near the electrode walls. Clearly this distortion is a result of the MHD $J_y B$ forces acting in the momentum equations.

In order to understand this behavior further, it is necessary to first consider the development of the J_y distribution between the two insulating sidewalls. The current distribution depends on several factors, mainly, the electrical connection, electrical conductivity distribution, and velocity field. In the present study, the thruster is connected in the Faraday mode with continuous electrodes and with electrically insulating sidewalls. Therefore, there is no flow of current through the sidewalls. If all properties and flow fields were uniform, J_y would be uniform, and a uniform accelerating force would have been imposed on the flow. However, in our case, the velocity field is not uniform, while the conductivity is constant. For the present application, where the Hall parameter is zero, Ohms law gives the following

$$J_y / \sigma = (E_y - UB)$$

Qualitatively, one can argue that $E_y(z)$ can be assumed constant for a Faraday connection with continuous electrodes, where

$$\int_0^H E_y(z) dy = \text{applied voltage} = \text{constant}$$

where H is the height of the duct (distance between the electrodes). Consequently, J_y will be higher in magnitude near the sidewall than at the center of the flow. Furthermore, if the load factor for simplicity is defined as $K = E_y / (U_{cl} B)$, where U_{cl} is the centerline velocity, then

$$J_y|_{z=0} / J_y|_{z=W/2} = K / (K-1)$$

where W is the duct width (distance between sidewalls).

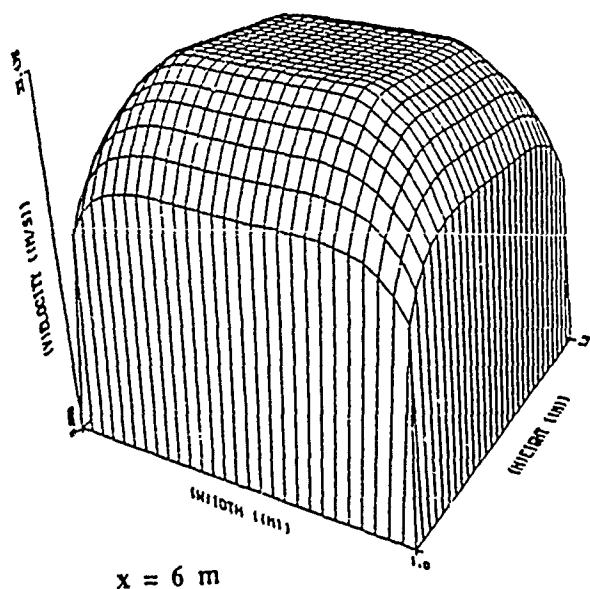
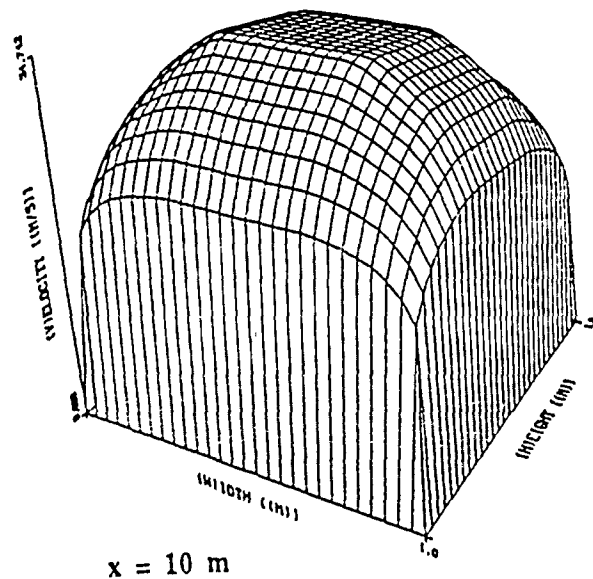
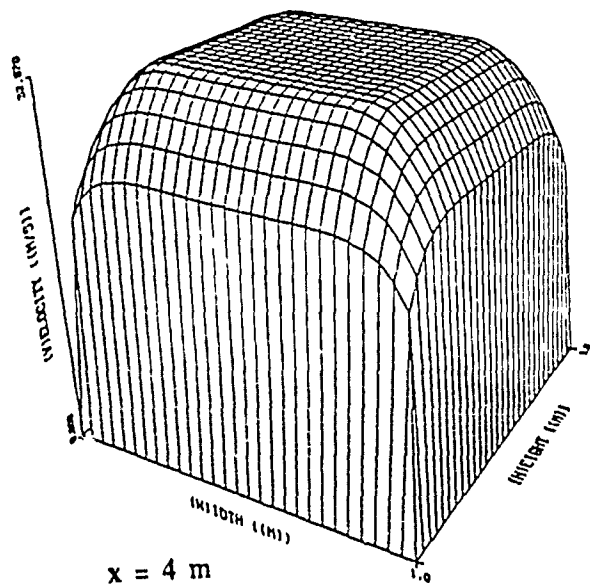
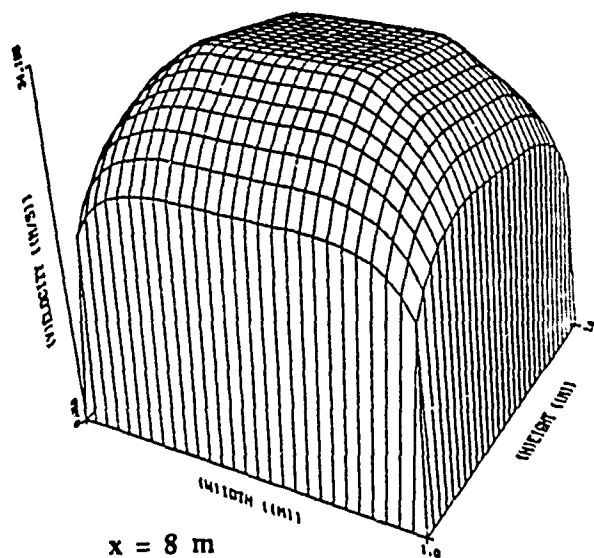
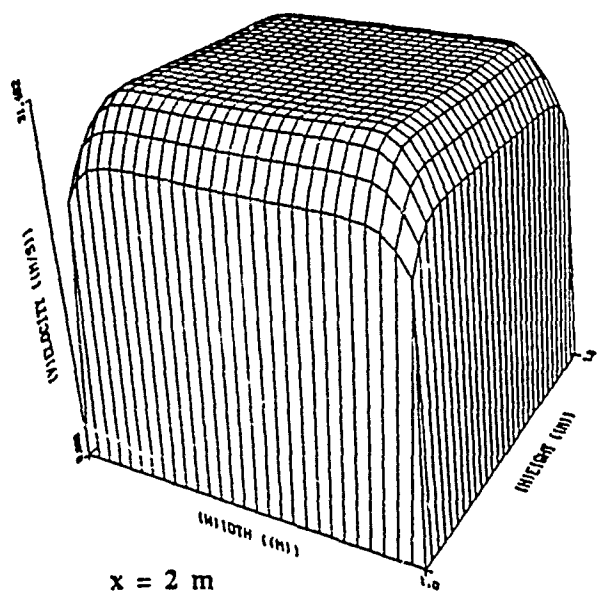


Figure 3 Flow development in MHD thruster
($B = 20 \text{ T}$, $U = 30 \text{ m/s}$, $K = 6$)

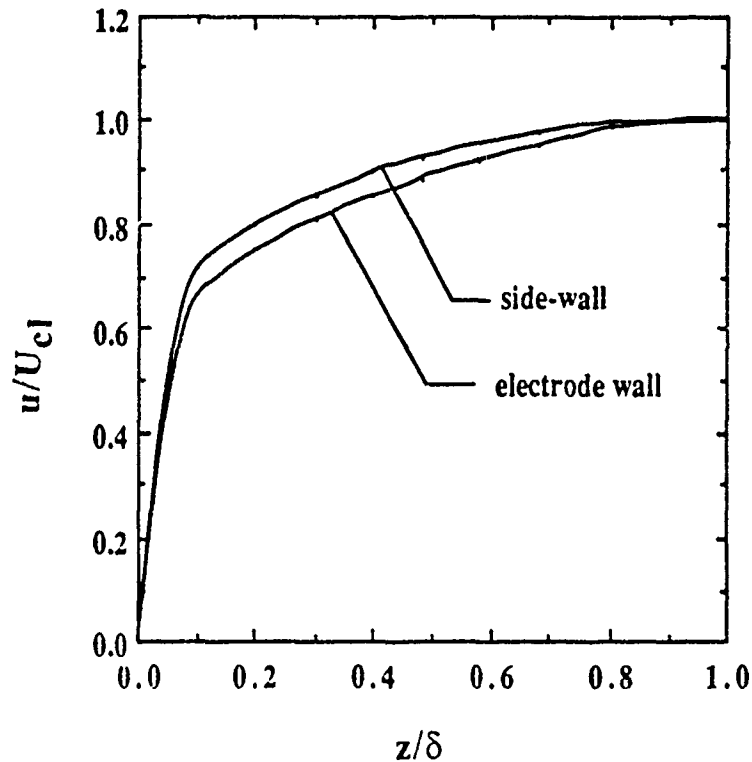


Figure 4 Normalized velocity profiles along thruster walls
($B = 20$ T, $U = 30$ m/s, $x = 10$ m)

The actual situation is more complex however, because of the corner regions and the three-dimensional effects. Figure 5 shows the distribution of the J_y - component of the current density (normalized to the centerline value) across the duct between the insulating walls at $x = 10$ m and for load factors $K = 2$ and 6 . This distribution, along the Hartmann layers of the sidewalls results in flow distortion. The nonuniform J_y distribution accelerates the flow differentially, exerting a larger force on the sidewall boundary layers, and leading to flatter boundary layer profiles in comparison to the electrode wall boundary layers. It seems logical to argue that, for conservation of mass, as the flow along the sidewall boundary layers is relatively accelerated, the flow along the electrode wall will be relatively decelerated. Such a behavior is depicted in Fig. 4.

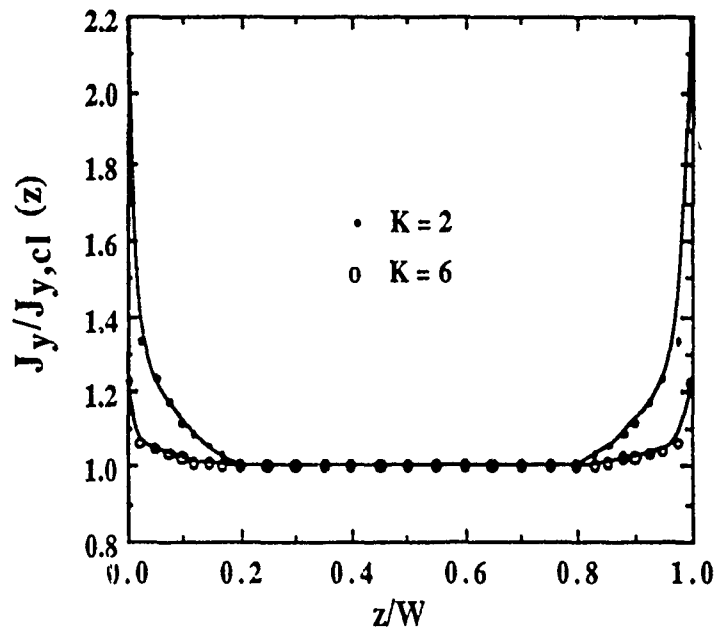


Figure 5 Normalized current density on the sidewall for different load factors
($B = 20$ T, $U = 20$ m/s)

As a result of such nonuniformities in the flow field, nonuniform distribution of the skin friction is expected along the duct walls. Figure 6 presents the variation of the friction factor (C_f) along the electrode wall and the sidewall of the thruster. The skin friction is higher on the sidewall.

The same mechanism responsible for the flattening of the boundary layers along the sidewalls and the increase of the skin friction factor for MHD thruster is the cause for the velocity overshoots in MHD plasma generators, albeit for different reasons. In MHD generators, the boundary layers are colder, and this leads to lower electrical conductivity in the near-wall regions. This leads to lower absolute values of the current density J_y . However the $J_y B$ forces act to retard the flow in MHD generators. This results in a larger retarding force in the central region of the flow. In a relative sense, the sidewall boundary layers are accelerated in relation to the central region, and this leads to the known phenomenon of velocity overshoots. Such a phenomenon was discussed earlier in Ref. 7.

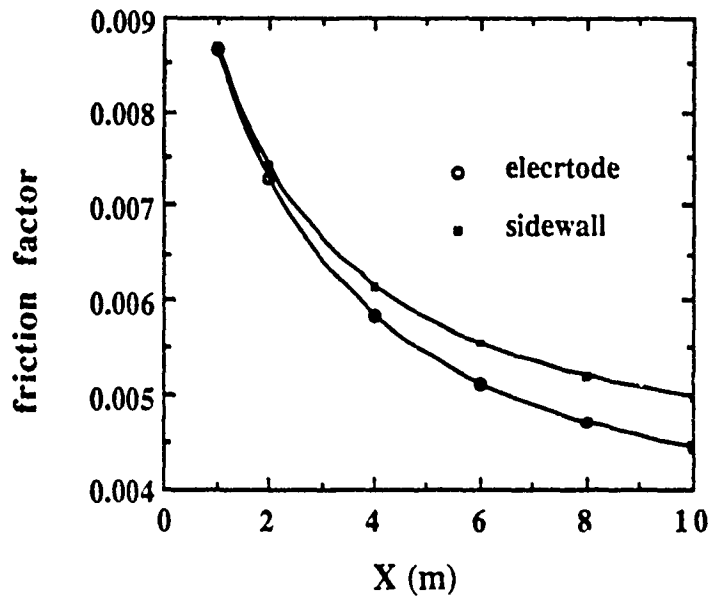


Figure 6 Variation of friction factor along thruster walls

Figure 7 illustrates the variation of the normalized current density $J_y(z)$ at the sidewall with the load factor K at the exit of the thruster for $B = 20$ T. The curve represents the previously given simple relationship, $K / (K-1)$, whereas the points represents the results of the three-dimensional calculations.

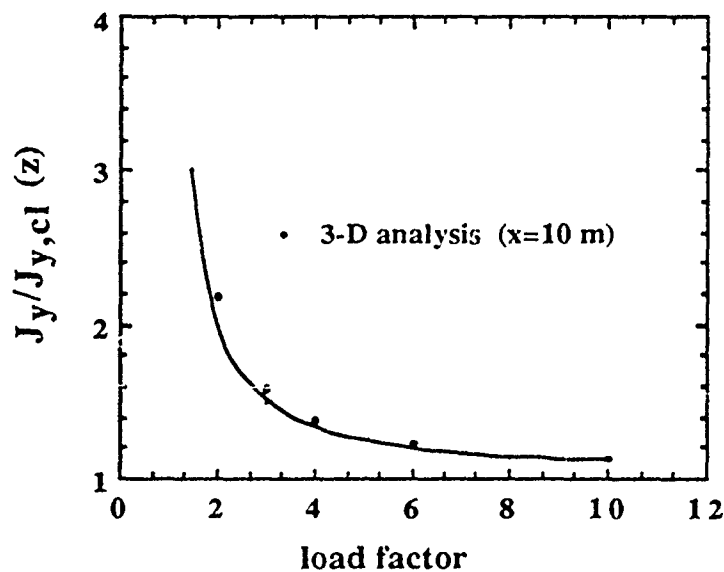


Figure 7 Effect of load factor on current density along sidewalls ($B = 20$ T, $U = 30$ m/s)

Finally, Figure 8 shows the effect of the magnetic field on the ratio of the skin friction between the sidewall and the electrode wall at the exit of the thruster ($x = 10$ m). The difference in behavior between the two walls, in terms of the skin friction factor, increases as the magnetic field increases.

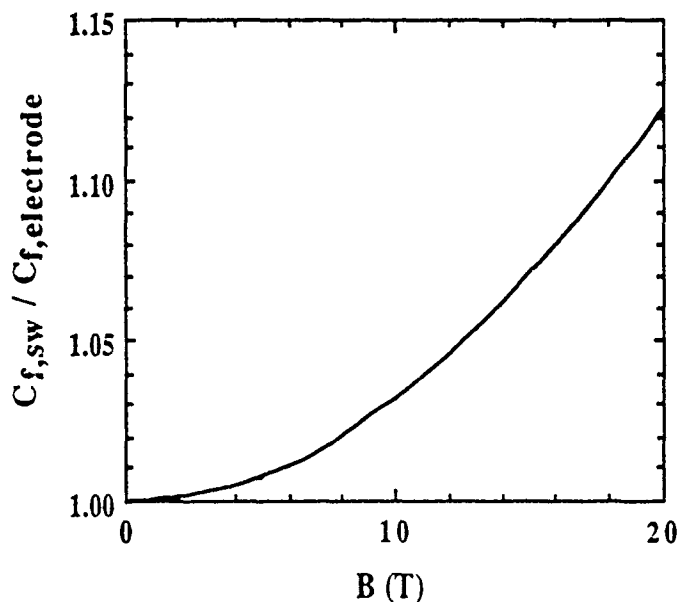


Figure 8 Effect of magnetic field and load factor on friction factor on thruster walls ($U = 30$ m/s, $x = 10$ m)

SUMMARY AND CONCLUSIONS

1. Parametric studies were performed by varying the load factor K , between 1 and 20, and the magnetic field between 0 and 20 Tesla in order to investigate their effects on the flow characteristics and thruster performance. The need to operate MHD thrusters with high magnetic fields has been established by previous investigations and has been discussed in the paper.
2. A three-dimensional MHD computer model has been developed and applied in the parametric study to investigate the concept of MHD seawater propulsion. A constant area duct with rectangular cross-section has been adopted in the applications of MHD propulsion. The thruster is assumed to operate in the Faraday mode with continuous electrodes and insulating sidewalls and with an external applied voltage.

3. As the load factor increases, the resulting $J \times B$ forces increase, thus giving larger pressure rise along the thruster. However, as the load factor increases, the thruster efficiency decreases. A balance between the efficiency and the thrust required must be taken into consideration in any application.
4. As the load factor decreases, the thruster efficiency increases. However, as the load factor keeps decreasing, a peak will be reached in the thruster efficiency curve, and then the efficiency will start to decrease rapidly as the MHD $J \times B$ forces becomes less than the frictional losses. Therefore, greater attention should be given to the calculation of the frictional losses at lower values of the load factor, K , particularly for K between 1 and 2.
5. The Hartmann layers on the insulating sidewalls are shown to have important effects on the current density and velocity distributions in the sidewall boundary layers. The velocity profiles are flatter over the sidewalls in comparison to the velocity profiles over the electrode walls.
6. As a result of the velocity nonuniformities, the average skin friction factor is enhanced along the sidewalls, in comparison with the skin friction factor along the electrode wall. However, the distribution of the average skin friction factor over all walls along the thruster is very close to the distribution predicted for non-MHD flow through the duct.
7. The difference in the skin friction between the sidewalls and the electrode walls increases as the magnetic field increases. Careful consideration must be given to the computation of the frictional losses along the thruster because of their impact on the MHD thruster efficiency.

REFERENCES

1. Phillips, O. M., "The Prospects for Magnetohydrodynamic Ship Propulsion," J. Ship Research, Vol. 43, March 1962, pp. 43-51.
2. Doragh, R.A., "Magnetohydrodynamic Ship Propulsion Using Superconducting Magnets," Proc. Naval Arch. and Marine Engineers Transaction, Vol. 71, 1963.
3. Way, S., "Electromagnetic Propulsion for Cargo Submarines," Journal of Hydraulics, Vol. 2, No. 2, April 1968, pp. 49-57.
4. Saji, Y., Kitano, M., and Iwata, A., "Basic Study of Superconducting Electromagnetic Thrust Device for Propulsion in Seawater," Advances in Cryogenic Engineering (Timmerhans, K.D. editor), Vol. 23, 1978, pp. 159-169.
5. Hummert, G.T., "An Evaluation of Direct Current Electromagnetic Propulsion In Seawater," Report ONR-CR168-007-1, Westinghouse Research Laboratories, Pittsburgh, Pennsylvania, July 1979.
6. Cott, D.W., et al, "MHD Propulsion For Submarines," CDIF External Report No. 2 DOE-MHD-D140, MSE Inc., Butte, Montana, October 1988.
7. Doss, E.D., and Curry, B.P., "Studies of the 3-D Coupled Flows Between the Electrode and Sidewalls of MHD Channels," AIAA paper 76-311, AIAA 9th Fluid and Plasma Dynamics Conference, July 1976.
8. Doss, E.D., and Ahluwalia, R.K., "Three-Dimensional Flow Development In MHD Generators At Part Load," AIAA-82-324, AIAA 20th Aerospace Sciences Meeting, January 1982.
9. Vanka, S.P., Ahluwalia, R.K., and Doss, E.D., "Three-Dimensional Analysis of MHD Generators and Diffusers," Report No. ANL/MHD-87-4, 1982, Argonne National Laboratory.
10. "McGraw-Hill Encyclopedia of Science and Technology," 6th Edition, Vol. 16, pp. 144-178, McGraw-Hill Book Company, New York, 1987.

ACKNOWLEDGEMENT

This work has been sponsored by the Office of Naval Research, U.S., under Contract No. N00014-89-F-0064.

THIS PAGE IS INTENTIONALLY BLANK

**SEA-WATER MAGNETOHYDRODYNAMIC PROPULSION
FOR UNDERWATER VEHICLES**

Presented by

T. Lin

Sea-Water Magnetohydrodynamic Propulsion for Underwater Vehicles⁺

T. F. Lin and J. B. Gilbert*

Applied Research Laboratory
The Pennsylvania State University
P. O. Box 30
State College, PA 16804

Abstract

To analyze underwater vehicle propulsion by applying Lorentz forces to the surrounding sea water. While this propulsion concept involves two different schemes, i.e. the external field method and the internal duct-type method, the current analysis focuses on the internal thruster scheme due to the space limitations and speed considerations. The theories of magnetohydrodynamic (MHD) pump jet propulsion are discussed. A so-called "dual control volume" analysis to model the MHD thruster, and calculations of vehicle velocity and power efficiency are presented. Different classes of underwater vehicles are considered. They include smaller vehicles such as torpedoes, remotely operated vehicles (ROV), underwater autonomous vehicles (UAV), up to larger ones such as submarines. The analytical results indicated that the speed performance increases proportionally with the seawater conductivity, and with the square of the magnetic field strength. At the same time, the energy efficiencies of vehicles appeared to favor larger systems with longer MHD channel.

Experimental investigations are also being planned to address important issues of the seawater MHD propulsion technology in underwater applications.

Nomenclature

A_{ex} exit area of the MHD channel (m^2).
 A_{in} entrance area of the MHD channel (m^2).
 A_{surf} surface area of the vehicle.

B magnetic field strength (Teslas).
 C nozzle discharge coefficient.
 C_D drag coefficient of vehicle surface.
 D electrode gap distance (m).
 D_H equivalent hydraulic diameter (m).
 E flow-induced counter electric field (volt/m).
 F velocity-of-approach factor of a nozzle.
 F_{em} Lorentz force (Newtons).
 f Darcy-Weisbach friction factor for pipe flows.
 I current across the electrodes (Amp).
 L active length of the MHD channel (m).
 m mass flowrate in an MHD channel (kg/s).
 N_{ch} number of MHD channels.
 P_e electrical power required by the MHD channel (watts).
 P_u mechanical power imparted to the sea water in the MHD channel (watts).
 p_{amb} ambient pressure of the vehicle (Pa).
 p_{in} entrance pressure of an MHD channel (Pa).
 p_{ex} exit pressure of an MHD channel (Pa).
 R resistance of sea water in the MHD channel (Ohms).
 s area ratio between the nozzle exit and the channel entrance (A_{ex}/A_{in}).
 T thrust of an MHD channel (Newtons).
 U_{ex} velocity of the sea water exiting from the nozzle (m/s).

⁺ ONR/DARPA Workshop on MHD Submarine Propulsion, Nov. 16 & 17, 1989, San Diego, California.

* Nuclear Engineering Department.

U_{in}	velocity of the sea water in the channel (m/s).
V	voltage across the electrodes (volts).
V_s	velocity of the vehicle (m/s or knots).
V_{ch}	active volume of sea water in the MHD channel (m^3).
W	width of the electrode (m).
Y	nozzle expansion coefficient.
Δp_{ch}	pressure rise or drop across the entire MHD channel (Pa).
Δp_N	pressure drop across nozzle (Pa).
η_e	electric efficiency.
η_{ind}	field induction efficiency.
η_t	total efficiency.
σ	electric conductivity of sea water ($1/(Ohm \cdot m)$).
ρ	sea water density (kg/m^3).

1. Introduction

Sea water conducts electricity in a modest scale by electrolytic ion exchange. While its conductivity is several orders of magnitude lower than metals, it is significantly higher than fresh water. By taking advantage of sea water's modest electric characteristics, the electromagnetic propulsion of marine vehicles has been a subject of technical speculation and study for some years (Refs. 1-6). The concept did not appear to hold much promise until the advent of the superconducting magnet. With such a magnet, the power requirement for excitation is virtually absent, and the weight penalty of the magnet is drastically reduced. Also, much stronger magnetic field than those previously attainable can be realized. Nevertheless, the only proof of its technical possibility was carried out more than twenty years ago by S. Way et al. (Ref. 6) In that, a vehicle 4-ft long and 18-inch in diameter was propelled by such an MHD propulsion principle at a speed only about 1 ft/s. The magnet used was a heavy electro-magnet, and S. Way had concluded that superconducting magnets are essential for the technology to be practical.

International activities in this subject were also visible. The U.S.S.R. have conceived its application in large icebreaker propulsion (Ref. 7). More recently, Japan has developed a strong program in researching the

electro-magnetic thrusters (EMT) for her future freighters (Refs. 8-10). With the recent advances in high- T_c superconductors and the possible simplification in cryogenics, it now appears that there is even more technical possibility in realizing a sea-water MHD propelled underwater vehicle. Whether such a vessel will be economically attractive or not is a question that must await further investigation. However, it is fair to predict that in certain naval applications where the importance of acoustic signature of a vehicle is outweighing other considerations, the MHD technology offers superior quietness because of its reduced mechanical moving parts.

In the consideration of duct-type internal MHD thrusters, the electric current and magnetic field in the sea water are normally arranged to be orthogonal to each other in the channel to provide an optimal Lorentz ($j \times B$) force. Sea water is being pumped in a straight active section of the channel. Immediately following that the sea water is pushed through a smooth nozzle that provides an adequate momentum thrust to makes the vehicle move. The following section of this paper discusses the detail theoretical background of this type of MHD pump jet propulsion. The vehicle's speed and efficiency performances are also discussed.

2. Theoretical Analyses

The general configurations of submerged vehicles with duct-type MHD thrusters can be shown in Figures 1(a) and 1(b). The basic pump jet propulsion principles are essentially the same in these two schemes. In both cases, the electric current and the magnetic field are arranged to be perpendicular to each other in an active region of the MHD channel. Sea water is brought in from the front end of a channel. As the Lorentz forces are applied to the channel, they pump the sea water downstream and eject it from the nozzle with a higher speed. The difference in speed between inlet and outlet of the channel creates the momentum thrust that pushes the vehicle forward. It is worth noticing that rotating machinery such as propeller is not required in such a system. In general, the annular channel thruster (Fig. 1(a)) provides a better efficiency because the amount of friction surface area per unit volume of fluid in the channel is

minimized. However, the scheme with separate rectangular channels provides the ability to steer and maneuver the vehicle by individually controlling the thrust of the channel.

2.1 Analysis of the MHD pump

A schematic of an MHD channel is shown in Figure 2, in that a simple rectangular thruster is illustrated. An analysis of annular thruster like the one shown in Fig. 1(a) will be very similar. The electric current is supplied by the electrodes from the top to the bottom, and the magnetic field is pointed into the paper so as to be perpendicular to the current. The Lorentz force is directed to the right to push the sea water through the nozzle. The net current flowing across the MHD channel between the electrodes is,

$$I = \frac{V - ED}{R}, \quad (1)$$

where D is the electrode gap distance, E is the flow-induced electric field whose direction is anti-parallel to I , and R is the electric resistance of sea water in the channel. If the width and length of the electrodes are W and L respectively, then the resistance is,

$$R = \frac{D}{\sigma WL}, \quad (2)$$

where σ is the electric conductivity of sea water ranging from 4 to 5 $1/(\Omega m)$. The first order magnetohydrodynamic approximations are then taken to assume only the induced electric field is significant, but not the induced magnetic field. Thus,

$$E = BU_{in}, \quad (3)$$

where U_{in} is the velocity of sea water in the channel. Defining the field induction efficiency to be,

$$\eta_{ind} = \frac{ED}{V} = \frac{BU_{in}D}{V}, \quad (4)$$

and the net current becomes,

$$I = \frac{1 - \eta_{ind}}{\eta_{ind}} \sigma BU_{in} WL. \quad (5)$$

The total Lorentz force pushing the sea water in the channel is,

$$F_{em} = IDB = \frac{1 - \eta_{ind}}{\eta_{ind}} \sigma B^2 U_{in} DWL$$

$$= \frac{1 - \eta_{ind}}{\eta_{ind}} \sigma B^2 U_{in} V_{ch}, \quad (6)$$

where V_{ch} is the active volume of the channel.

The mechanical power imparted on the sea water in the channel is,

$$P_u = F_{em} U_{in} = \frac{1 - \eta_{ind}}{\eta_{ind}} \sigma B^2 U_{in}^2 V_{ch}. \quad (7)$$

The electrical power supplied to the MHD channel is,

$$P_e = VI = \frac{1 - \eta_{ind}}{\eta_{ind}} \sigma B^2 U_{in} WL, \quad (8)$$

and the electrical efficiency is defined as, from Eqs. (7) and (8),

$$\eta_e = \frac{P_u}{P_e} = \frac{BU_{in}D}{V}. \quad (9)$$

This is identical to the field induction efficiency, η_{ind} . This, however, does not mean one can extract the most mechanical power from the MHD channel at η_e (or η_{ind}) being equal to 1. As one can see from Eq. (8), P_e approaches to zero as η_e approaches to unity. From Eqs. (7) and (9), the expression for the mechanical power under fixed channel dimensions and electrical potential would be,

$$P_u = (1 - \eta_e) \eta_e \sigma B^2 \frac{V_{ch}}{D^2}. \quad (10)$$

P_u can be optimized by taking the derivative of Eq. (10) with respect to η_e , and determining the value of η_e that satisfies a zero derivative. It turns out that P_u is optimized when η_e is equal to 0.5. That also means 50% of the electrical power will be consumed as heat by Ohmic loss. This is a condition that will always have to be taken into account in the thruster design.

2.2 Dual-control-volume analysis

In the past, the analyses of sea water MHD thrusters have been based on Bernoulli's equations in modeling momentum exchanges (Refs. 7 and 11). These analytical approaches basically ignored the viscous dissipation of fluid in the channel, and the pressures at the entrance and exit (p_{in} and p_{ex}) were taken to be the same as the ambient pressure. These, in

reality, were not quite justified. In our current analytical models, two separate control volumes are considered, to take into accounts the viscous dissipation in the channel and the relationship between the thrusts and the performances of the vehicle. In doing so, the pressure conditions at the inlet and outlet of each channel must be computed, instead of being assumed. Similarly to rocket propulsion, this would make up the pressure thrust portion of the total thrust.

The first control volume, shown as dotted lines in Figure 3, is the sea water volume enclosed by an individual MHD channel. The mass and momentum balances of flow around this control volume are discussed as follows. Assuming the ratio between the nozzle exit area and the MHD channel area is s , the mass conservation yields,

$$U_{ex} = \frac{U_{in}}{s} \quad (11)$$

and the momentum conservation yields,

$$\rho U_{in} A_{in} (U_{ex} - U_{in}) = IBD - \left(f \frac{L}{D_H} \frac{\rho U_{in}^2}{2}\right) A_{in} - \Delta p_N A_{in} + (p_{in} A_{in} - p_{ex} A_{ex}) \quad (12)$$

The second term in the right hand side (RHS) of Eq. (12) accounts for the friction loss in the straight channel, and the third term accounts for the nozzle loss. Also in Eq. (12), D_H is the equivalent hydraulic diameter of the channel, and f is the Darcy-Weisbach friction factor that is a function of the Reynold's number of the pipe flow. Although equivalent diameters are used in Eq. (12) for non-circular channels, f has been found to be slightly overpredicting the friction (Ref. 12). The nozzle loss is proportional to the square of the mass flowrate through it. It can be expressed as (Ref. 13),

$$\Delta p_N = \frac{1}{2\rho} \frac{\dot{m}^2}{(YFC A_{ex})^2} \quad (13)$$

where Y is the expansion factor which is unity for liquids. F is the velocity-of-approach factor defined as $F = 1/\sqrt{1-s^2}$. C is the nozzle discharge coefficient which has a value approximately equal to 0.98 for smooth nozzle transition at high Reynold's number. The last term

in the RHS of Eq. (12) is the net pressure force from both the inlet and outlet of a channel.

The thrust that is put out by an MHD channel can be written as, from the momentum principles (Ref. 14),

$$T = \dot{m}(U_{ex} - U_{in}) + (p_{ex} A_{ex} - p_{in} A_{in}) + p_{amb}(A_{in} - A_{ex}) \quad (14)$$

The first term in the RHS of Eq. (14) is the momentum thrust, and the combination of the second and third terms is the pressure thrust. p_{amb} is the ambient pressure of the vehicle, and is a depth-dependent quantity. From Eq. (12), Eq. (14) can be re-written as,

$$T = \Delta p_{ch} A_{in} + p_{amb}(A_{in} - A_{ex}) \quad (15)$$

where Δp_{ch} is the pressure rise (or drop) across the entrance and exit of the MHD channel. It is defined as,

$$\begin{aligned} \Delta p_{ch} A_{in} &= (p_{ex} - p_{in}) A_{in} \\ &= IBD - \left(f \frac{L}{D_H} \frac{\rho U_{in}^2}{2}\right) A_{in} - \Delta p_N A_{in} \end{aligned} \quad (16)$$

The relationship between the total thrust of all the MHD channels and the vehicle velocity can be obtained from the second control volume, shown as dotted lines in Figure 4. The skin friction of a vehicle is proportional to the square of its velocity, and must be balanced by the total thrust provided by the MHD thrusters at steady state. The equation describing the force balance in the second control volume is,

$$C_D A_{surf} \left(\frac{1}{2} \rho V_s^2\right) = N_{ch} T \quad (17)$$

where N_{ch} is the total numbers of MHD channels, A_{surf} is the total vehicle surface area. C_D is the drag coefficient at the vehicle surface, which is obtained from the standard values of International Towing Tank Conference (ITTC, 1957). The thrust in Eq. (14) can also be reduced to,

$$T = \dot{m}(U_{ex} - U_{in}) - (p_{in} - p_{amb})(A_{in} - A_{ex}) + \Delta p_{ch} A_{ex} \quad (18)$$

and the term $(p_{in} - p_{ex})$ can be approximated as an entrance pressure defect, from the Bernoulli's equation,

$$p_{in} - p_{amb} = \frac{1}{2}\rho(V_s^2 - U_{in}^2). \quad (19)$$

From Eqs. (18) and (19), Eq. (17) becomes,

$$C_D A_{surf} \left(\frac{1}{2} \rho V_s^2 \right) = N_{ch} (\dot{m}(U_{ex} - U_{in}) - \frac{1}{2} \rho (V_s^2 - U_{in}^2) (A_{in} - A_{ex}) + \Delta p_{ch} A_{ex}). \quad (20)$$

2.3 Solution procedures

In the discussion of the "dual control volume" analysis above, the pressures at the entrance and exit of an MHD channel were treated as unknowns. The relation between them was formulated in Eq. (16). If the vehicle dimensions and the MHD channel dimensions are given, the applied voltage that gives the optimal electric efficiency can be determined for given B and U_{in} from Eq. (4) by letting $\eta_{nd} = 0.5$. Then, Δp_{ch} can be calculated from Eq. (16) for a given s (nozzle area ratio). Eq. (20) in turn becomes a quadratic equation of V_s , which can be readily solved. However, there exists only a unique s for a given U_{in} to satisfy the condition in Eq. (15). It is also noted that Eq. (15) involves the ambient pressure of the vehicle. For a given depth, iterative procedures such as the generalized Newton's method or the bi-sectional method can be applied for the solution of s .

As a result, the performance of a vehicle with MHD thrusters can be analyzed by plotting the vehicle velocity, or the total efficiency against the sea water velocity in the channel. Here, the total efficiency is defined as,

$$\eta_t = \frac{N_{ch} T V_s}{P_e}. \quad (21)$$

For each point in a performance curve, there is a corresponding s to satisfy the conditions imposed by the conservation laws in both control volumes. This s value directly influence the nozzle design.

3. Results

Performance calculations were based on two classes of underwater vehicles. The first

class (class 1) is vehicles with dimensions similar to MK48 torpedoes. The common diameter and length were chosen to be 0.533 meter and 6.1 meters, respectively. The second class (class 2) is large submersibles such as submarines, with vessel diameter and length being 9.8 meters and 83 meters, respectively. Four rectangular MHD channels were attached to each vehicle 90 degrees apart from one another, and the channel lengths were always chosen to be two thirds of the vehicle lengths. For the first class vehicles, the electrode width and gap distance were 0.3 meter and 0.1 meter. For the second class vehicles, the electrode width and gap distance were 3 meters and 1 meter, respectively.

Figure 5 shows the dependence of class 1 vehicle velocity on the magnetic field strength and the sea water conductivity. It indicates that the vehicle velocity increases proportionally with σB^2 . The solid line represents the velocity performance at realistic sea water conditions. To achieve the torpedo speed (50 - 70 knots), the magnetic field needs to be as large as 15 to 20 Teslas. Nevertheless, it points to the possibility of low speed applications in ROV or UAV with more realistic magnetic fields. By increasing the conductivity of sea water in the active volume of the MHD channels, shown as dashed line, the velocity can be increased linearly. Similar curves can be generated for class 2 vehicles. For a reasonable submarine velocity, one only needs a magnetic field of about 5 Teslas. This will be further discussed next.

Figures 6 and 7 show the velocity and efficiency performances of class 1 vehicles, vs. the fluid velocity in the MHD channel at $B = 20$ Teslas. In general, the vehicle velocity increases with channel flow, as a result of increasing MHD pumping. As discussed in section 2 above, there can exist two satisfactory solutions for V_s at low U_{in} due to the quadratic nature of Eq. (20). One solution corresponds to the case of $s = 1$, where the MHD channel is straight and without any nozzle. This solution, shown as the upper curves in Figs. 6 and 7, often is not valid because η_t becomes larger than 0.5. This contradicts the imposed condition of optimal electric efficiency, as discussed in section 2.1. The other solution corresponds to a s value less than 1. It suggests that the existence of a smooth nozzle would create a

higher U_{ex} which in turn would generate the momentum thrust. This is a valid solution and is shown as the lower curves in the figures. Valid solution can also exist for $s = 1$ at higher velocity. In this situation, the vehicle thrust is mainly from the pressure thrust. Although the total efficiency generally decrease with increasing U_{in} , for class 1 vehicles, there appears to have an optimal efficiency near $\eta_t = 0.375$, Fig. 7.

Figures 8 and 9 show the velocity and efficiency performances of class 2 vehicles, i.e. submarines. It is noted that reasonable submarine velocity can be achieved with a magnetic field about 5 Teslas. For a submarine having a 35 knots velocity, the total power efficiency is about 0.355. This is largely due to the large size of the MHD channels. For class 2 vehicles, even larger MHD channels than the ones currently under consideration are possible. That would result in further increases in vehicle velocity and total efficiency.

4. Discussion

The purpose of this study is to assess the feasibility of sea water MHD propulsion for underwater vehicles. It is commonly acknowledged that magnetic fields higher than 10 Teslas are, although achievable, not practical in large scale engineering applications. Therefore, for smaller vehicles, the possible applications of sea water MHD propulsion are in low speed ROV's and UAV's, with lower magnetic fields. The electric sources can be from batteries, fuel cells, or generators driven by the long endurance version of the stored chemical energy propulsion system (SCEPS) concept. The high magnetic fields required by the torpedo applications seem to be still somewhat out of the reach of current technologies.

On the more encouraging side, a 5 Teslas magnetic field appears to be adequately suited for propelling a class 2 submarine with reasonable speed and efficiency, as shown in Figs. 8 and 9. The electric power will most likely be nuclear driven. A class 2 submarine going with a speed of 36 knots would need 66 Mw of electric power for its MHD channels. Assuming the Rankin cycle efficiency of the nuclear propulsion plant is 33%, the required reactor thermal power would be at least 200 Mw. This, of course, does not include any other ser-

vice power needed for the vehicle. Nevertheless, it is compatible in power capacity to the current nuclear submarine technologies (Ref. 15). In addition, a hybrid submarine having both the propeller screws and MHD channels may offer some strategic merits in underwater warfare.

Superconducting magnets are the essential elements of the sea water MHD propulsion technology, because they offer high fields at little electric consumption. They do need some cryogenic power to maintain low temperature. The liquid helium cooled superconducting magnets are somewhat hard to maintain due to helium leakage. The high- T_c superconducting materials offer the hope of more economical magnets, with much more cryogenic simplicity. Other important issues associated with sea water MHD propulsion are mainly in the electric conduction characteristics of the sea water. These are to be addressed in part in our future experimental studies.

5. Future Experimental Work

An experimental facility is currently being constructed to study the current conducting characteristics of sea water. It is a closed flow loop that circulates the salt water through a test section, as shown in Figure 10. The salinity of the salt water will be properly controlled to simulate that of sea water. The test section is a rectangular channel made of plexiglass, with two parallel electrodes mounted on opposing walls. The electrodes are made of copper and plated with 50 μ -inch of platinum layer. The platinum is plated to prevent the electrolytic dissociation of the electrode material, and to provide a good gas evolution which results in good current conduction.

As the current is being supplied to the electrodes, hydrogen and oxygen micro bubbles will be formed at the cathode and anode, respectively. Perhaps the most important issue to be addressed is how effective the current can be driven through the "flowing" salt water without saturating the electrolytic gas formation process. Since the performance of a thruster increases linearly with the sea water conductivity, enhancements of the fluid conductivity by seeding method or ionizing radiations become worthwhile.

The electrolytic micro-bubbles on the electrodes can have significant impact on the turbulent fluid structure of the MHD flow in the channel. Its influence on the drag of an internal channel flow also affect the performance of the thruster. These are the issues remained to be addressed in our future experiments.

6. References

1. W. A. Rice, U. S. patent 2997013, August 12, 1961.
2. J. B. Friauf, "Electromagnetic Ship Propulsion," *J. of Amer. Soc. of Naval Engrs.*, Feb., 1961, pp 139-142.
3. O. M. Phillips, "The Prospects for Magnetohydrodynamic Ship Propulsion," *J. of Ship Research*, March, 1962, pp 43-51.
4. R. A. Doragh, "Magnetohydrodynamic Ship Propulsion using Superconducting Magnets," Soc. of Naval Architects and Marine Engineers, Annual Meeting, New York, Nov. 14, 15, 1963.
5. S. Way, "Propulsion of Submarines by Lorentz Forces in the Surrounding Sea," Amer. Soc. of Mechanical Engrs. Paper 64 WA/ENER7, Nov., 1964.
6. S. Way and C. Devlin, "Prospects for the Electromagnetic Submarine," Collection of Technical Papers, AIAA 3rd Propulsion Joint Specialist Conference, Washington D. C., July 17-21, 1967, Paper # 67-432.
7. A. P. Baranov, "Future of Magnetohydrodynamic Ship Propulsion," *Sudostroyeniye*, No. 12, 1966, pp 3-6.
8. A. Iwata, Y. Saji and S. Sato, "Construction of Model Ship ST-500 with Superconducting Electromagnetic Thrust System," Proc. ICEC 8, 1980, pp 775-784.
9. E. Tada, Y. Saji, K. Kuroshi and T. Fujinaga, "Fundamental Design of a Superconducting EMT Icebreaker," *Trans. IMarE(C)*, Vol. 97, Conf. 3, Paper 6, pp 49-57, 1984.
10. Y. Sasakawa, K. Imaichi, E. Tada and S. Takezawa, "Japanese Experimental Ship with the Superconducting Electromagnetic Thruster," Paper presented in the Applied Superconducting Conference in Osaka University, Japan, Oct. 17, 1988.
11. G. T. Hummert, "An Evaluation of Direct Current Electromagnetic Propulsion in Sea Water," Office of Naval Research Project Report, 79-9B2-EMSUB-R1, 1979.
12. J. P. Waggner, "Friction Factor for Pressure Drop Calculation," *Nucleonics*, vol. 19, no. 11, 1961, pp 145-147.
13. G. L. Tuve and L. C. Domholdt, *Engineering Experimentation*, McGraw Hill, 1966, pp 369-381.
14. G. P. Sutton, *Rocket Propulsion Elements*, John Wiley & sons, 1976, pp 13-23.
15. T. Stefanick, "The Non-acoustic Detection of Submarines," *Scientific American*, vol. 258, no. 3, March, 1988, pp. 41-47.

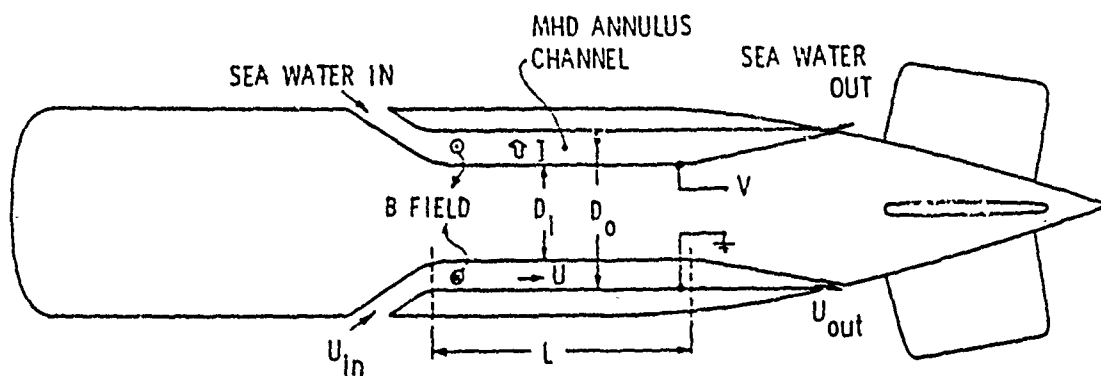


Figure 1(a) Submersible with an Annular MHD Channel.

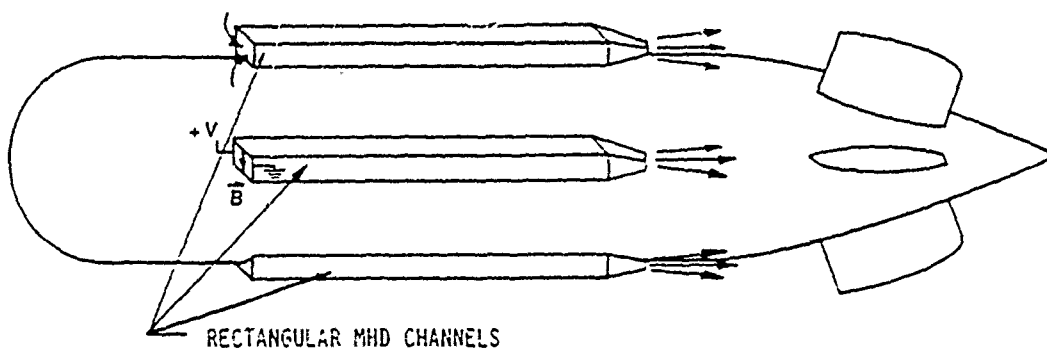


Figure 1(b) Submersible with Rectangular MHD Channels.

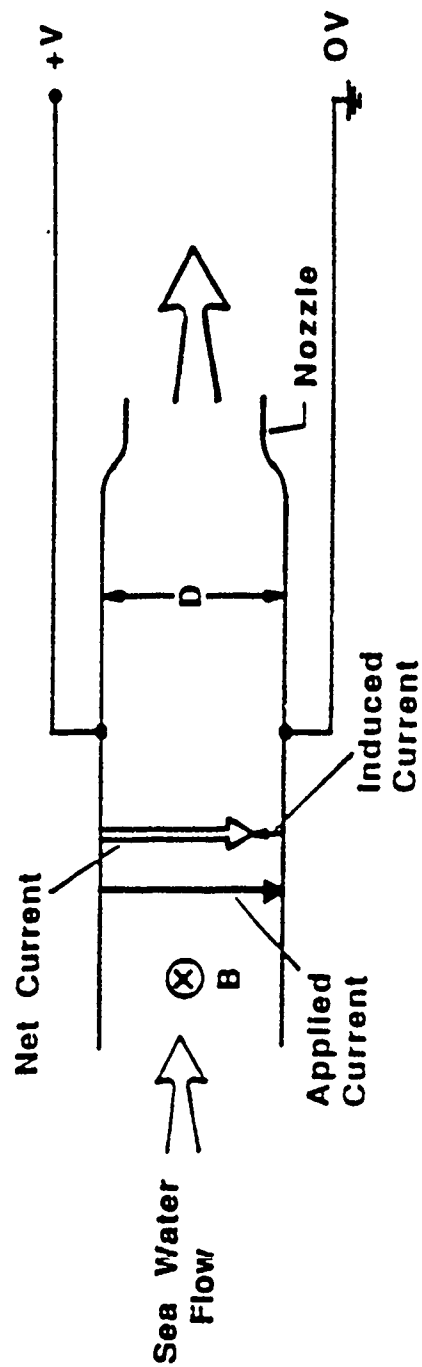


Figure 2 Schematic of a duct-type MHD Channel.

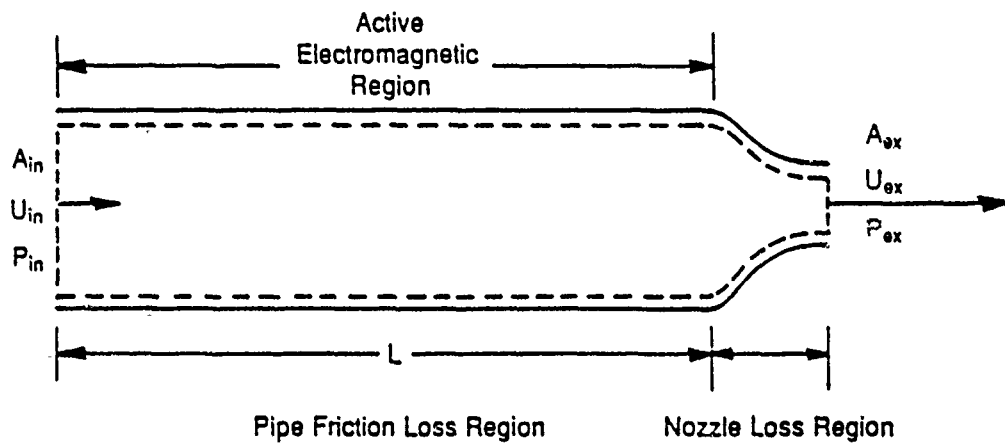


Figure 3 Control Volume #1.

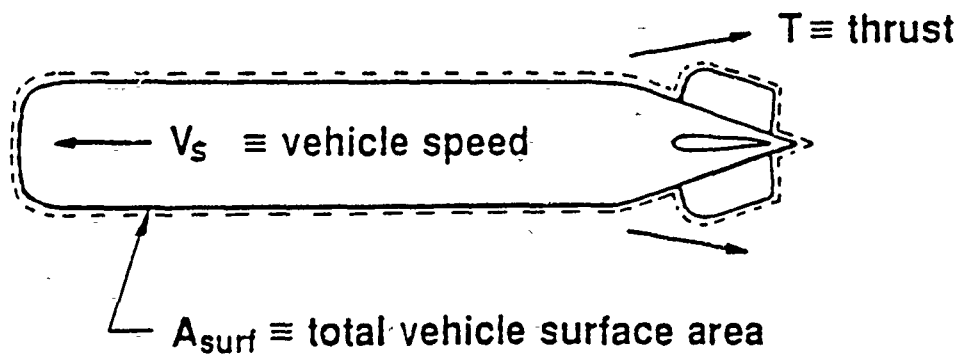


Figure 4 Control Volume #2.

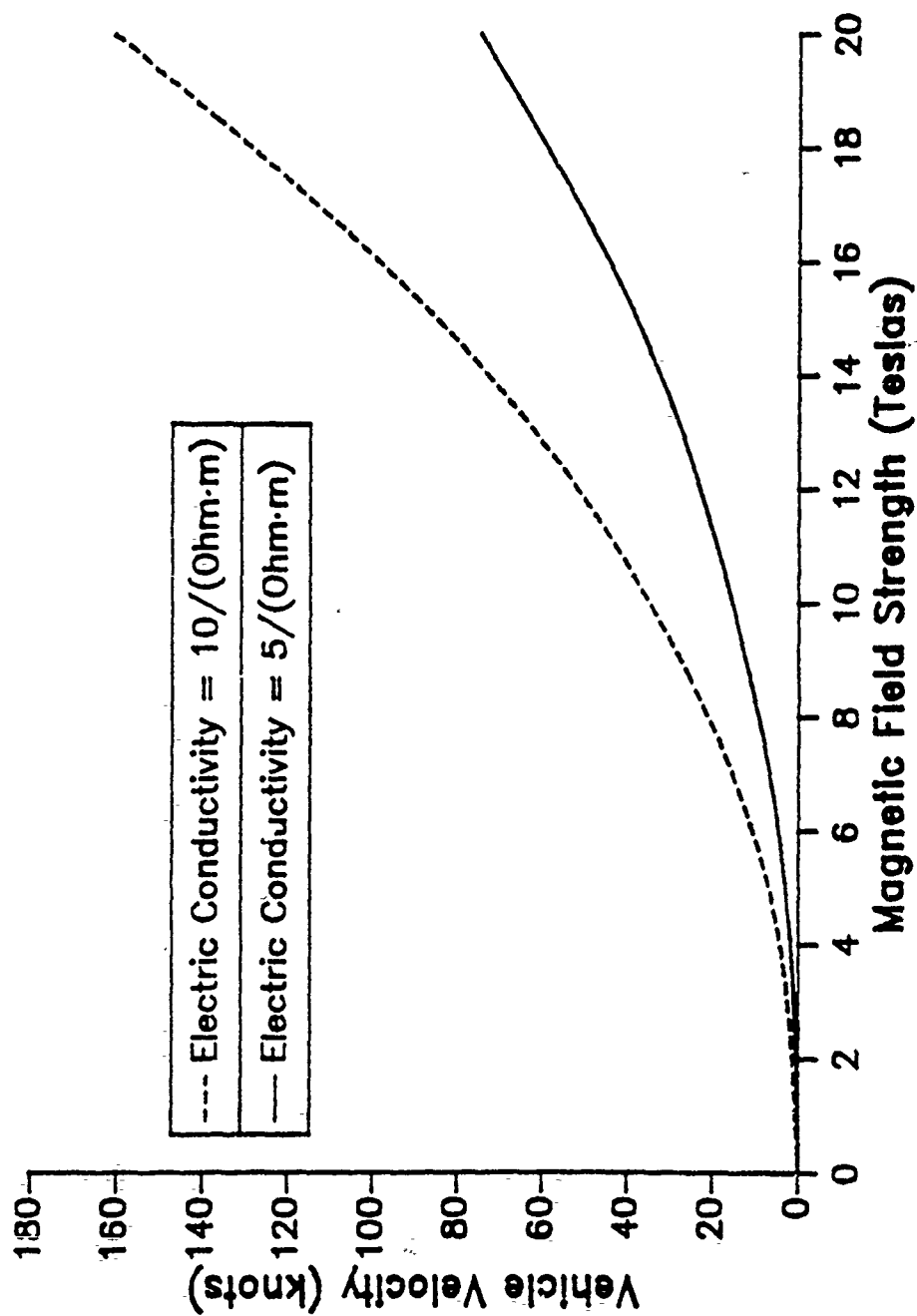


Figure 5 Velocity vs. Magnetic Field for Class 1 Vehicles.

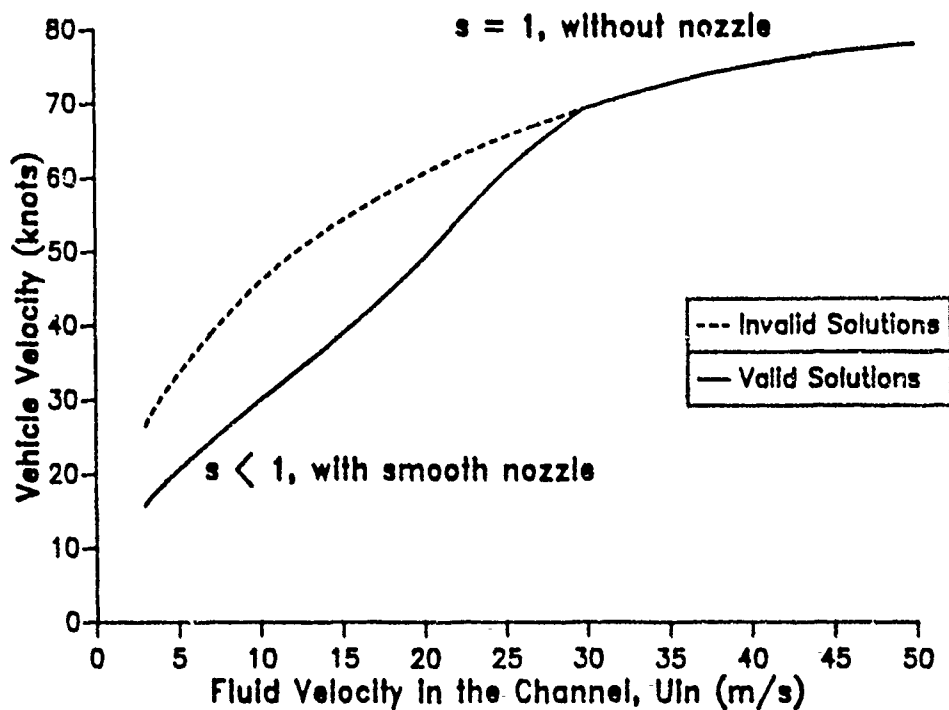


Figure 6 Velocity of Class 1 Vehicles at $B = 20T$

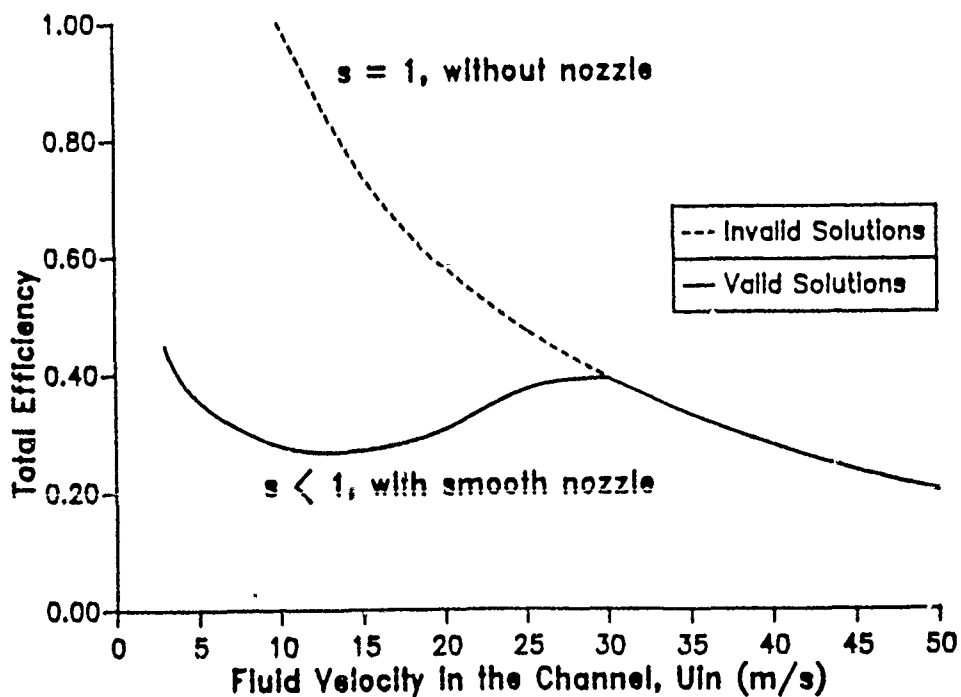


Figure 7 Total Efficiency of Class 1 Vehicles
at $B = 20T$.

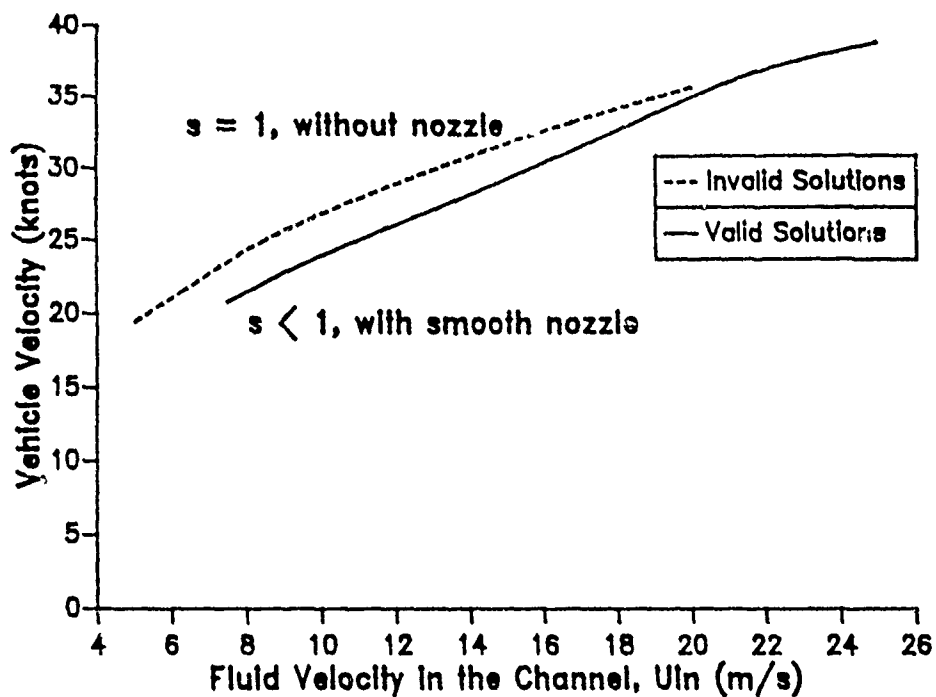


Figure 8 Velocity of Class 2 Vehicles at $B = 5T$.

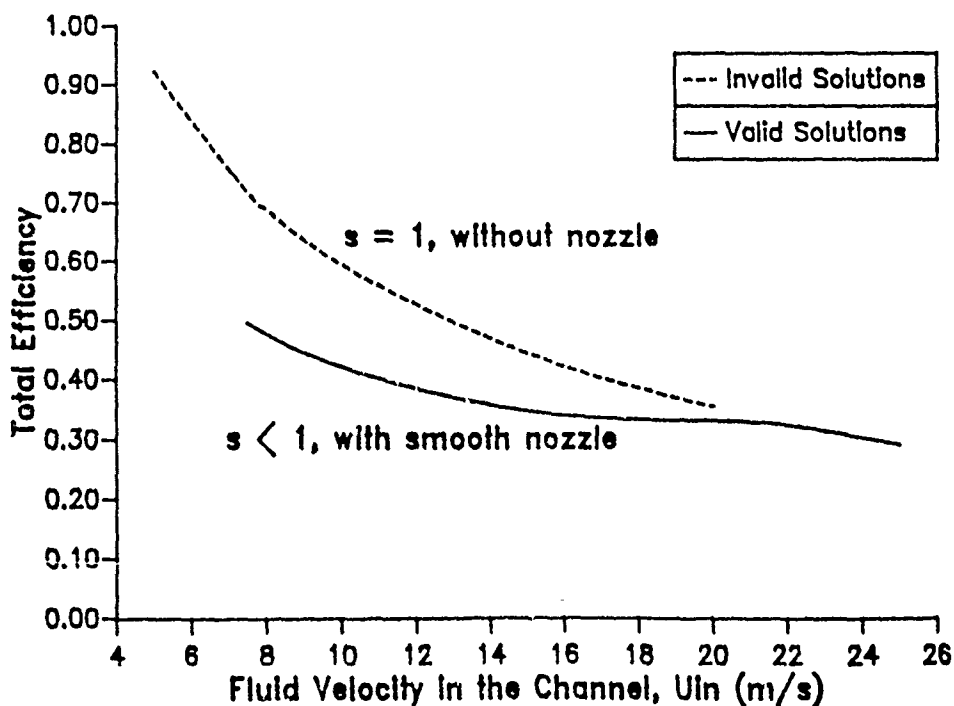


Figure 9 Total Efficiency of Class 2 Vehicles at $B = 5T$.

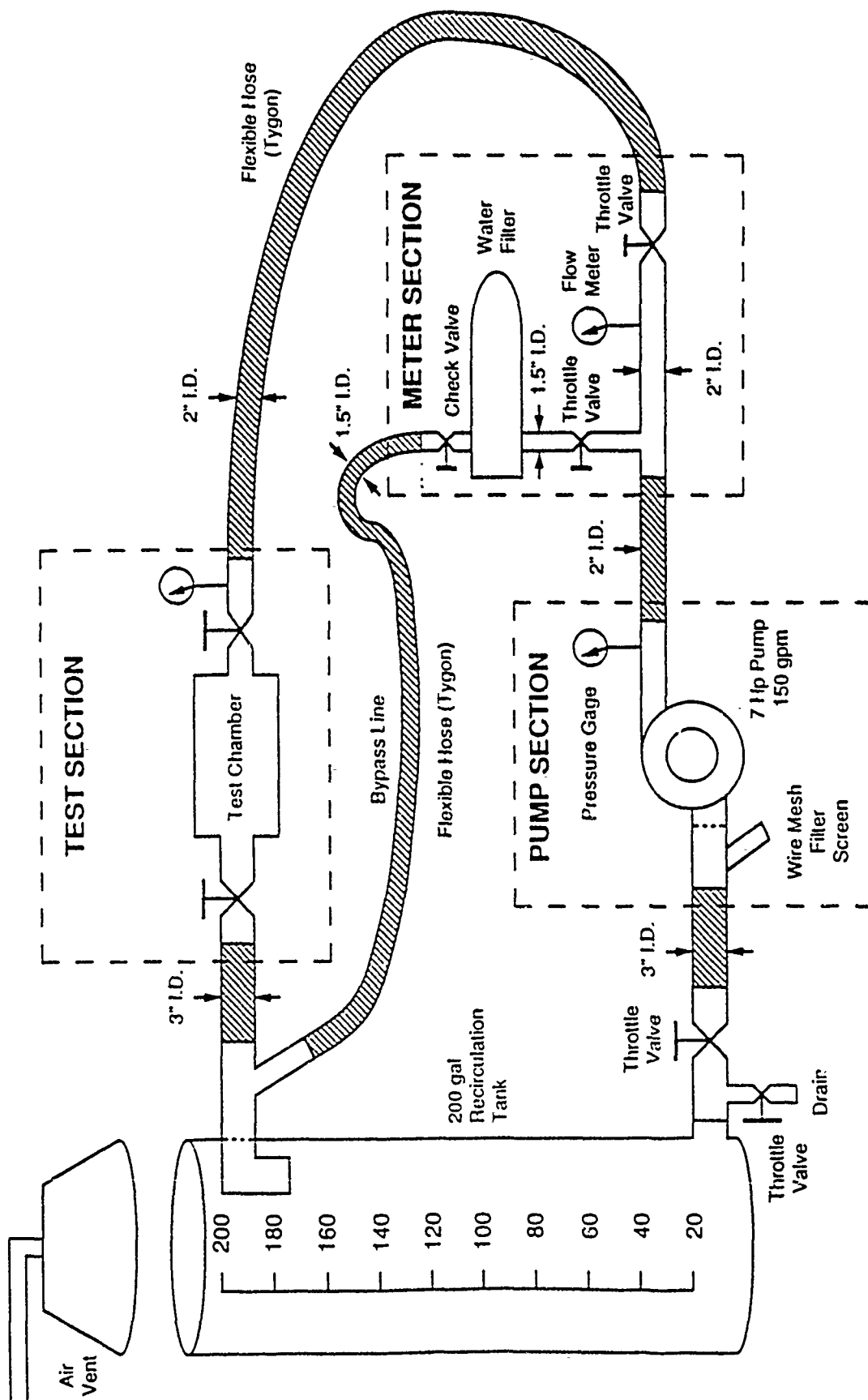


Figure 10 Schematic of the Salt-Water Test Loop.

THIS PAGE IS INTENTIONALLY BLANK

**MAGNETOHYDRODYNAMIC SUBMARINE PROPULSION
AT THE DAVID TAYLOR RESEARCH CENTER**

Presented by

David Bagley

Magnetohydrodynamic Submarine Propulsion at the David Taylor Research Center

**Presented by David Bagley
of the
Electric Propulsion and Machinery Systems Branch**

The purpose of this discussion is to introduce the David Taylor Research Center (DTRC) and describe our work in MHD propulsion. It is divided up into three sections; the first is an introduction to DTRC, the second is a description of our past and current involvement in MHD propulsion, and the third is a brief view of what we see in the future.

Introduction to the David Taylor Research Center

DTRC is the Navy's principal research, development, test, and evaluation center for naval vehicles. The viewgraph with the rather poor picture of Admiral Taylor lists some of the major areas of interest to DTRC. This is not by any means an exhaustive list; we work on everything that goes into a ship except weapons systems and nuclear reactors.

DTRC is actually made up of two geographically separate laboratories. The larger of the two labs is in Carderock, Maryland, just outside the Washington beltway. It employs about 1600 people, and houses the Ship Systems Integration Department, the Ship Hydromechanics Department, the Ship Electromagnetic Signatures Department, the Ship Structures Department, and the Ship Acoustics Department. These departments' facilities include the Anechoic Flow Facility, the Model Towing Basin Facility, and the Variable Pressure Cavitation Channels.

The second lab is located in Annapolis, Maryland on the north side of the Severn river, across from the U.S. Naval Academy. Approximately 800 people work there in

the Propulsion and Auxiliary Systems Department and the Ship Materials Engineering Department. Also located at the Annapolis site are the Deep Ocean Pressure Tanks, the Submarine Fluid Dynamics Facility, and the electric drive testcraft Jupiter II.

DTRC Strengths Applicable to MHD Propulsion

DTRC has great experience in many areas applicable to MHD propulsion. We have been a leader in the field of applied superconductivity and cryogenic systems and in the development of advanced electric drive for Navy vessels since the 1960's. (For more information on this subject, see chapter 9 of the recently-published book *Superconductivity: The New Alchemy*, by John Langone.) Also listed on this viewgraph are other areas of DTRC expertise that we feel will be important in the development of MHD propulsion.

Current MHD Propulsion Work

DTRC's current efforts in MHD propulsion fall into four areas. The first two of these are paper studies, one sponsored by the Office of Naval Technology (ONT), and the other by In-house R&D funding. These studies are idealized, one-dimensional analyses of MHD in seawater, and its suitability as propulsion for Navy vessels. They were also both learning exercises for their respective authors, and their reports are currently in preparation. Our third area of MHD activity is the small-scale experiments at the U.S. Naval Academy conducted by Visiting Professor Kenneth E. Tempelmeyer. Finally, DTRC has been providing technical and contractual support to the Defense Advanced Research Projects Agency (DARPA) in their MHD submarine propulsion development program.

ONT Submarine MHD Propulsion Assessment

The ONT study examines a simple duct of square-cross-section, with intake and exhaust shrouds for flow conditioning. The electric current, magnetic field, and seawater flow are all considered to be uniform over the active region. Electrical losses are assessed in the active region, hydrodynamic drag losses throughout, flow separation

losses in the exit diffuser (or nozzle), and a propulsive slipstream loss at the exit. The load for the propulsor was a typical nuclear attack submarine operating at full power. Three different magnetic field levels were considered, and four different duct sizes (the viewgraph shows the active part only). The study does not specify a particular arrangement scheme for integrating the MHD propulsor with the submarine, and does not modify the propulsive characteristics of the vehicle for any such installation.

The results show that propulsive efficiency increases with duct size and magnetic field (though this may be limited by end effects, which were ignored in this study), and decreases with ship speed (based on the much higher thrusts required for higher speeds). These trends, along with estimates of the accompanying magnet weights, seem to limit the propulsive efficiencies of MHD propulsors to levels significantly lower than those of conventional propellers. The question at this point is whether the as yet undefined acoustic benefits of MHD propulsion will be worth its weight and efficiency penalties.

IR&D Submarine MHD Propulsive Efficiency Study

This study, which was performed by Dr. Samuel Brown and Dr. Neal Sondergaard of DTRC, started with a classical propeller model, and adapted it to apply to an MHD propulsor. As in the ONT study, the seawater flow, electric current, and magnetic field were considered to be uniform in the active region, and end effects were ignored. The results, as expected, showed that high fields, large ducts, and low speeds were needed for high efficiency, and that, given these parameters, acceptable efficiencies could be achieved (this study did not address magnet weights).

USNA Small-Scale Experiments

During the past year, Dr. Kenneth Tempelmeyer of Southern Illinois University has been a Visiting Professor at the U.S. Naval Academy, and has been working with DTRC on MHD propulsion. In addition to providing valuable technical guidance to us, he has performed a series of small-scale experiments on the electrical characteristics of seawater. These experiments were carried-out in a USNA laboratory, using a small water-flow table and synthetic "Instant Ocean" seawater. DTRC has been providing

technical support for these experiments, and will be publishing two reports on their results. Dr. Tempelmeyer will be discussing his work and presenting some of the results.

DARPA Technical and Contractual Support

DTRC has been providing support to several areas of DARPA's MHD submarine propulsion program. We are the Technical and Contracting Agent for the DARPA-sponsored study at Avco Research Laboratory (which will be described in great detail by Dr. Daniel Swallom of Avco). In addition, Dr. Theodore Farabee, of our Ship Acoustics Department, has been providing technical support in acoustic data acquisition and analysis to the Large-Scale Experiment at Argonne National Laboratory (to be discussed by Dr. Michael Petrick of Argonne).

Future MHD Activity

In the future, DTRC intends to be involved in MHD propulsion in three separate areas. Firstly, our support to the DARPA programs, as described above, are expected to continue. Secondly, we have some small-scale in-house experiments planned. These experiments will be extensions and enhancements to Dr. Tempelmeyer's USNA experiments. They will be focused on electrolysis effects and signatures, and may include a magnetic field. Finally, we will be examining superconducting magnets and cryogenic systems for MHD propulsion under an ONT-sponsored superconductivity program.



David Taylor Research Center
Annapolis, Maryland

MHD Submarine Propulsion



David Taylor Research Center
Annapolis, Maryland

Introduction to DTRC

Current MHD Propulsion Work

Future MHD Activity

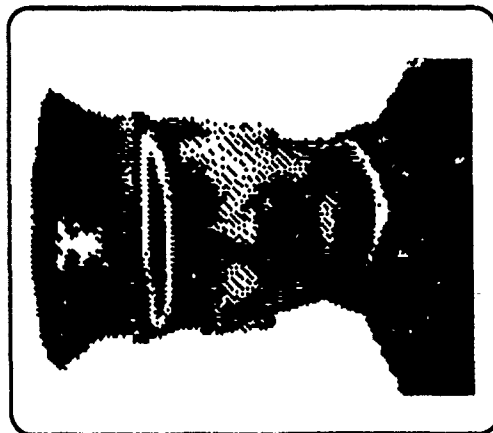


David Taylor Research Center

Annapolis, Maryland

The David Taylor Research Center

is the Navy's principal research, development, test, and evaluation center for naval vehicles.



Propulsion
Structures
Silencing
Materials
Hull-forms
Maneuvering
Seakeeping
Auxiliaries



David Taylor Research Center

Annapolis, Maryland

DTRC Strengths Applicable to MHD Propulsion

- Advanced Electric Propulsion Systems
- Superconducting Magnets and Support Systems
- Acoustic and Electromagnetic Signatures
- Ship Structures and Materials Engineering
- Hydromechanics and Ship Systems Integration



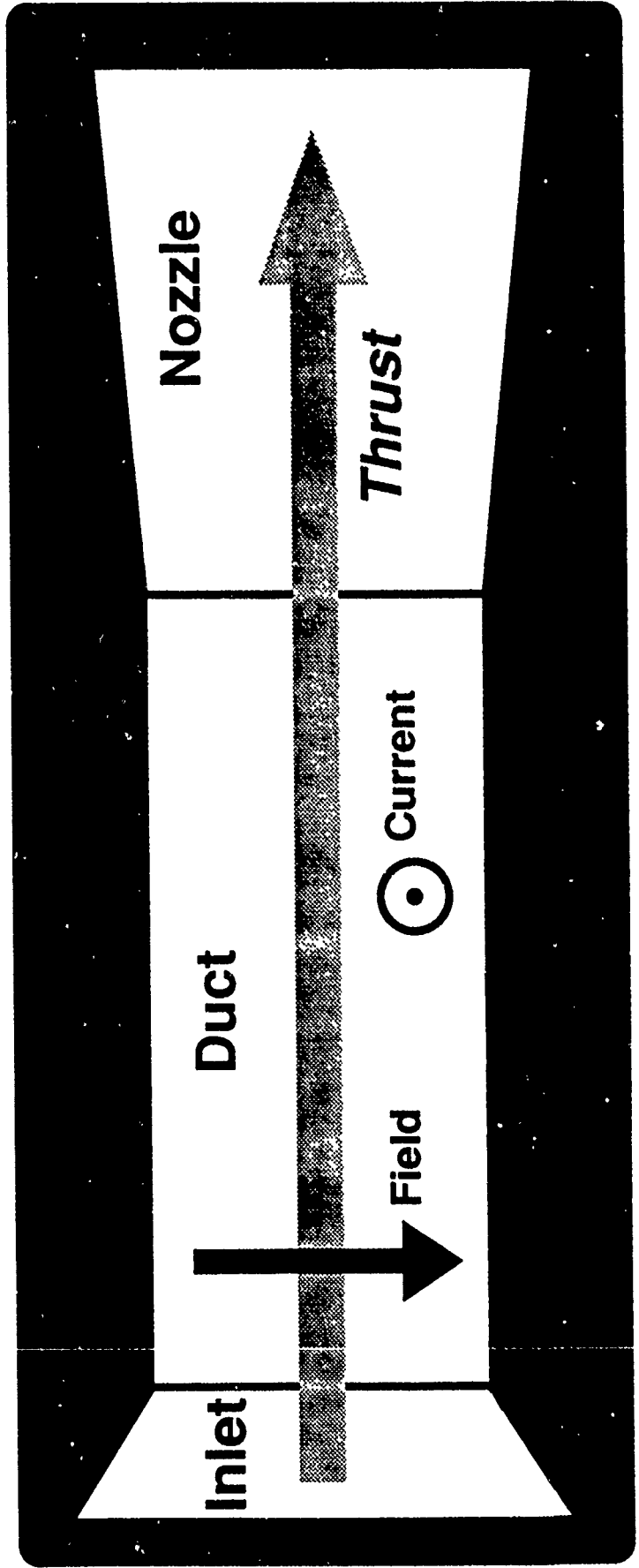
David Taylor Research Center

Annapolis, Maryland

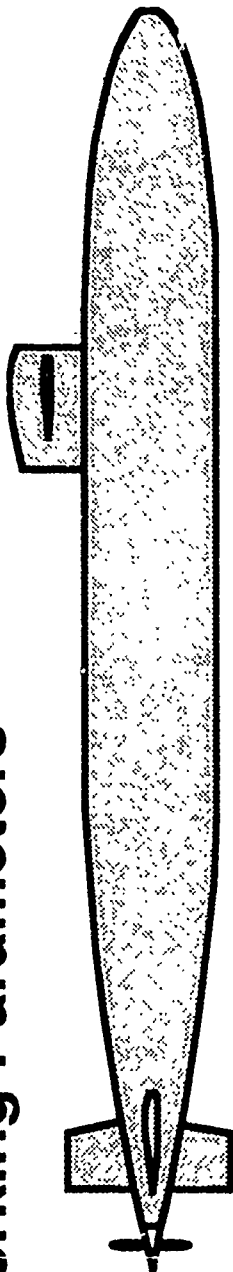
Current MHD Propulsion Work

- ONT Submarine MHD Propulsion Assessment
- IR&D Submarine MHD Propulsive Efficiency Study
- USNA Small-Scale Experiments
- DARPA Technical and Contractual Support

ONT Submarine MHD Propulsion Assessment



Working Parameters



Typical nuclear attack submarine

6900 tons, 110 m long x 10 m diameter, 31 knots at 30,000 SHP.

Data from *Modern Submarine Warfare*, David Miller and John Jordan,

Military Press, New York, 1987.

MHD propulsor duct sizes



5m x 5m x 20m



3m x 3m x 10m

1m x 1m x 3m



2m x 2m x 5m

MHD field levels



5 Tesla



10 Tesla

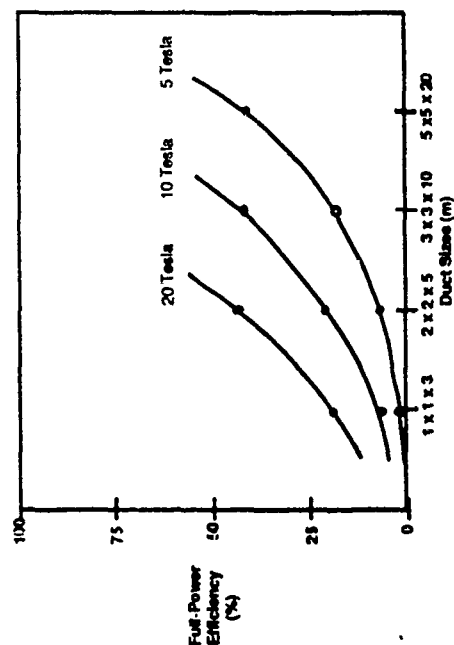


20 Tesla

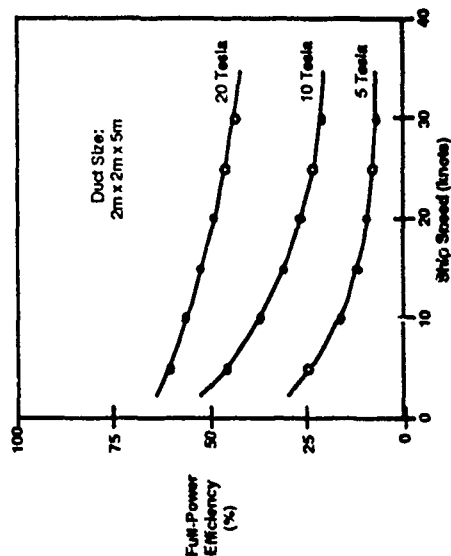


ONT Submarine MHD Propulsion Assessment

Efficiency vs. Size



Efficiency vs. Speed



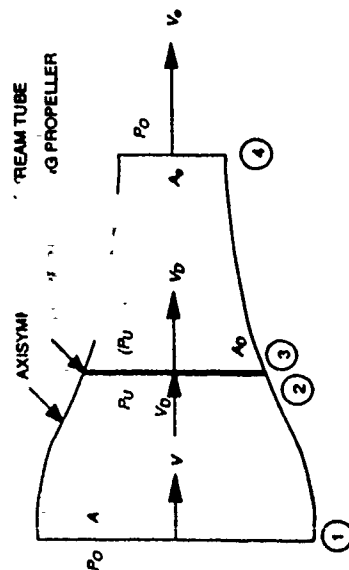


David Taylor Research Center

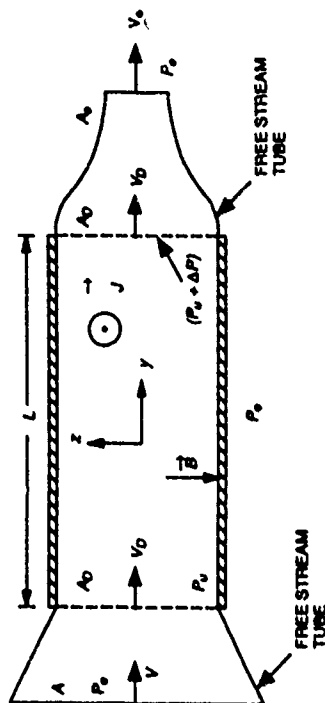
Annapolis, Maryland

IR&D Submarine MHD Propulsive Efficiency Study

Propeller System



MHD Propulsor

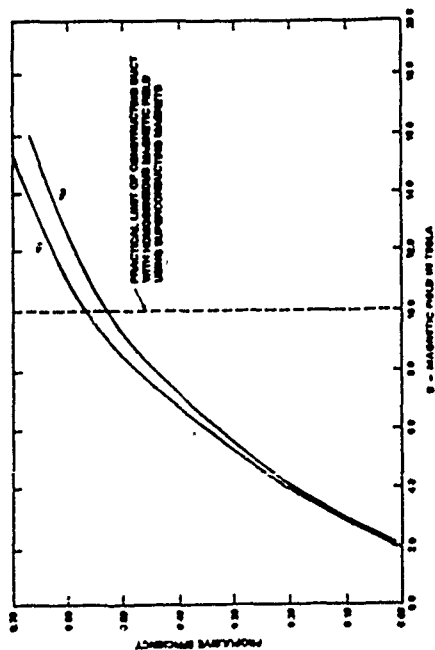




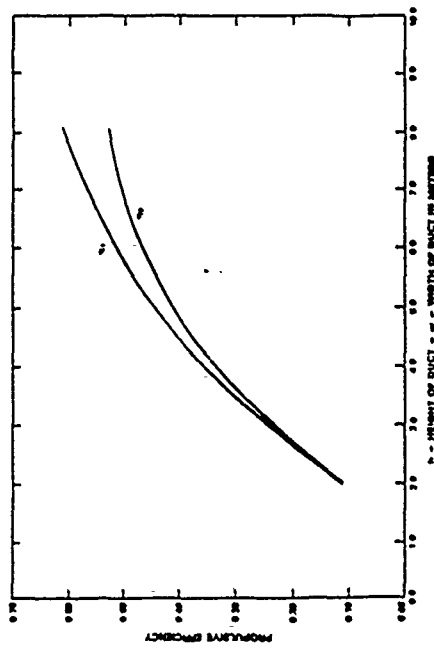
David Taylor Research Center

Annapolis, Maryland

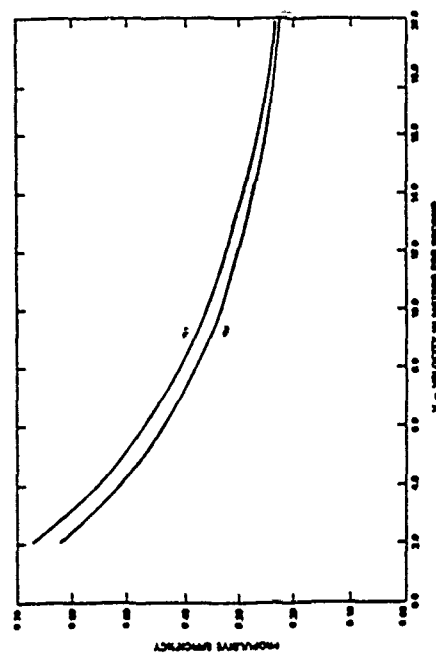
Efficiency vs. Mag Field



Efficiency vs. Duct Width



Efficiency vs. Vehicle Speed



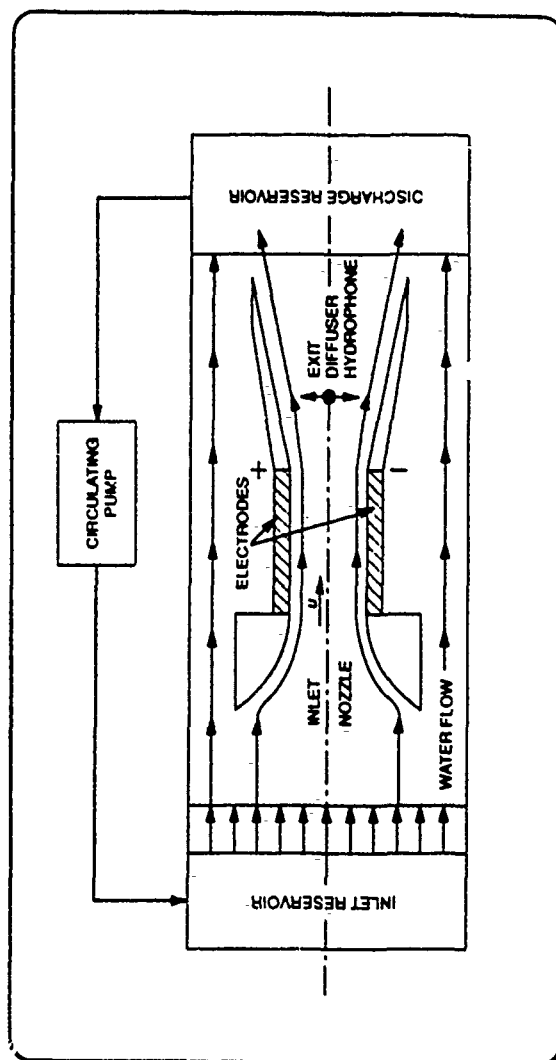


David Taylor Research Center

Annapolis, Maryland

USNA Small-Scale Experiments

- Duct electrical characteristics
- Electrode materials and corrosion
- Bubble generation, effects, and noise





David Taylor Research Center

Annapolis, Maryland

DARPA Technical and Contractual Support

- **Avco MHD Submarine Propulsion Study**
DTRC monitoring contract and providing technical support and review.
- **Argonne Large-Scale Duct Experiment**
DTRC providing technical support for acoustic data acquisition and interpretation.



David Taylor Research Center

Annapolis, Maryland

Future MHD Activity

- Support to DARPA MHD Efforts
- DTTC In-house MHD Experiments
- ONT Superconductivity Program



David Taylor Research Center

Annapolis, Maryland

Support to DARPA MHD Efforts

- Continued technical and contractual support to Avco MHD Submarine Propulsion study.
- Continued technical support in the area of acoustics to the Argonne experiment.
- General technical review/oversight for overall MHD program.



David Taylor Research Center

Annapolis, Maryland

DTRC In-house MHD Experiments

- Extension/enhancement to USNA tabletop experiments.
- Small seawater test loop and MHD pump using normally-conducting and super-conducting magnets.
- Will investigate electrolysis effects, electromagnetic end effects, and acoustic and non-acoustic signatures.



David Taylor Research Center
Annapolis, Maryland

ONT Superconductivity Program

- Superconducting magnet and cryogenic support system assessments, research, and technology development.

THIS PAGE IS INTENTIONALLY BLANK

DARPA REQUIREMENTS

Presented by

LCDR Richard Martin

MHD SUBMARINE PROPULSION PROGRAM

DARPA SUBMARINE TECHNOLOGY PROGRAM

**16 NOVEMBER 1989
MHD WORKSHOP**

LCDR RICHARD MARTIN, MECHANICAL & ELECTRICAL PROGRAM AREA MANAGER

DARPA MHD SUBMARINE PROPULSION PROGRAM

OBJECTIVE

TO DETERMINE IF MHD PROPULSION IS A VIABLE OPTION WITH THE FOLLOWING ATTRIBUTES:

- **MINIMUM ACOUSTIC, OPTICAL, AND MAGNETIC SIGNATURE**
- **ROBUSTNESS AND SURVIVABILITY IN HOSTILE ENVIRONMENT**
- **HIGH PERFORMANCE IN DIVERSE OPERATING CONDITIONS**
- **TECHNOLOGY BASE THAT ENABLES CONSTRUCTION OF SYSTEM AT REASONABLE COST**

DARPA MHD SUBMARINE PROPULSION PROGRAM

MAJOR THRUSTS OF PROGRAM

- **LARGE-SCALE, HIGH INTERACTION THRUSTER EXPERIMENT USING A HIGH B-FIELD (6 TESLA) SUPERCONDUCTING MAGNET AT ANL**
- **SUB-SCALE THRUSTER EXPERIMENT USING A NORMAL CONDUCTOR ANNULAR MAGNET (3 TESLA) AT AVCO**
- **INVESTIGATION OF KEY TECHNOLOGY ISSUES FOR MHD SUBMARINE PROPULSION IN FOLLOWING AREAS:**
 - **DEVELOPMENT OF ELECTRODE FOR MINIMUM SIGNATURE AND LONG LIFE**
 - **DEVELOPMENT OF ROBUST, LIGHTWEIGHT, HIGH PERFORMANCE SUPERCONDUCTING MAGNET WITH MINIMUM MAGNETIC SIGNATURE**
 - **DEVELOPMENT OF SEAWATER CONDUCTIVITY CONTROL TECHNIQUE**

DARPA REQUIREMENTS

LCDR Richard Martin
Program Manager for Mechanical Systems
Naval Technology Office
Defense Advanced Research Projects Agency

The items listed in the following table are of interest to DARPA. They are suggested for use in research programs proposed and conducted in magnetohydrodynamic submarine propulsion.

DARPA REQUIREMENTS

ITEM	GOALS	COMMENTS	TECHNICAL CHALLENGE
PROPULSION EFFICIENCY	50-70 %	DEPENDS ON VOLUME AND CONFIGURATION, SEA WATER CONDUCTIVITY	
SIGNATURE A) ACOUSTIC	ELIMINATE PROPELLER RELATED NARROWBAND AND BROADBAND NOISES, REDUCE BUBBLE EFFECTS		GASLESS ELECTRODES, MAGNET CONSTRUCTION
B) MAGNETIC	REDUCE TO AMBIENT, THE FAR FIELD MAGNETIC SIGNA- TURE AT D = 5 METER REDUCE INTERNAL MAGNETIC FIELDS TO ACCEPTABLE LEV- ELS FOR EQUIPMENT AND PEOPLE	DESIGN ENGINEERING SHOULD ACCOMMODATE THIS LEVEL.	MAGNETIC SHIELDING
C) OPTICAL	REDUCE/MINIMIZE BUBBLE EFFECTS		GASLESS ELECTRODES

DARPA REQUIREMENTS, CONTINUED

ITEM	GOALS	COMMENTS	TECHNICAL CHALLENGE
MAGNETIC FIELD	8-10 TESLA	USE OF LOW TEMP. SUPER-C SYSTEMS	COMPOSITES, DESIGN PHILOSOPHY, SCALING ISSUES
SIZE AND WEIGHT	NEUTRAL BUOYANCY	2-3 TONS/M ³ OF WARM BORE AREA	COMPOSITES
SYSTEM LIFE	30 YEARS OR BETTER		ELECTRODE LIFE
SURVIVABILITY	PRESENT REQUIRE- MENTS TO WITH- STAND UNDERWATER SHOCK EXPLOSION		CRYOSTAT DESIGN FOR SHOCK

**ELECTRICAL CHARACTERISTICS OF
A SEAWATER MHD THRUSTER**

Presented by

Kenneth E. Tempelmeyer

Electrical Characteristics of a Seawater MHD Thruster

by

Kenneth E. Tempelmeyer

Secretary of the Navy Fellow: U.S. Naval Academy

and

College of Engineering: Southern Illinois University

November 1989

ABSTRACT

There is renewed interest in the application of the MHD propulsion concept to surface ships and submarines. However, there is almost no experimental information concerning the major physical processes which will occur in a seawater MHD propulsion unit, such as (1) the seawater electrolysis process at operational conditions needed for ship propulsion, (2) the effects of bubble formation on the performance of a seawater thruster and (3) the effectiveness of the MHD interaction in seawater. Small scale tests of an MHD type channel but without an applied magnetic field have been carried out to provide information about the first two of these areas (1) seawater electrolysis and (2) the effect the H_2 bubbles generated during the electrolysis of seawater. Current/voltage characteristics were obtained with different electrode materials for current densities up to 0.3 amp/cm^2 . The effect of bubble formation on the channel current has been assessed over a range of operating conditions. Long-duration tests to 100 hrs. have been made to provide information on electrode durability and long-term operational problems.

INTRODUCTION

The acceleration of electrically conducting fluids by crossed electric and magnetic fields (i.e. electromagnetic pumps) has been proposed and investigated for many years. Commercially available liquid-metal pumps successfully utilize this concept but it has had limited success in other applications.

Because seawater is an electrical conductor, the application of this concept for ship propulsion (i.e. magnetohydrodynamic (MHD) propulsion) has been repeatedly suggested over the past three decades. (see refs. 1 through 5 for example). In 1968, Way⁶ constructed and operated a model of an MHD powered vessel which was probably the first demonstration of MHD propulsion for ships. More recently there have been several publications as well as news media accounts of MHD ship propulsion research in Japan. This activity is centered at and funded by the Japan Foundation for Shipbuilding Advancement (JAFSA). (See, for example, publications by Tada, et al⁷ and Motora⁸.) The Japanese effort has also resulted in the operation of a successful prototype which is reported to have two MHD thrusters each producing a Lorentz force of 8000 newtons with a 4 tesla superconducting magnet installed in a vessel having a displacement of about 150 tons.⁹

With the advent of superconducting magnets, which can produce fields of 6 to 10 tesla, the application of MHD thrusters for seawater becomes more feasible. As a result, there is an increasing interest in this propulsion concept at several naval labs and at the Defense Advanced Research Project Agency (DARPA). The interest in this ship propulsion concept is stimulated by the potentially quieter operation of an MHD thruster as compared to a conventional methods of providing mechanical power to shafts and propellers.

The David Taylor Research Center (DTRC) has been analytically studying the application of MHD thrusters for submarine propulsion over the past several months. To support this activity, an experimental test program of the electrical characteristics of an MHD thruster has been started at the U.S. Naval Academy in cooperation with DTRC using two conventional water tables in the Mechanical Engineering Fluids Mechanics Laboratory. The purposes of these tests were to: (1) determine the current-voltage characteristics of an MHD channel flowing seawater (without an applied magnetic field); (2) determine the electrical conductivity of simulated seawater and the electrode voltage drops; (3) investigate different types of electrode materials; (4) observe the dynamics of bubble formation, hydrogen on the cathode, and chlorine on the anode at various operating conditions, and; (5) make measurements of bubble noise downstream of the channel.

This report summarizes the electrical characteristics of a seawater MHD thruster configuration but without the applied magnetic field and (2) provides some comments on the suitability of some different electrode materials. A second DTRC report¹⁰ provides information concerning bubble formation, bubble dynamics and the noise potential of a seawater MHD propulsion unit.

BACKGROUND

Ohms Law for an MHD thruster may be written as:

$$\vec{J} = \sigma (\vec{E}_{app} + \vec{V} \times \vec{B}) \quad (1)$$

where \vec{E}_{app} represents the applied electric field provided by an external d-c power supply and $\vec{V} \times \vec{B}$ is the electric field induced by the motion of the conductor through the magnetic field. There was no applied magnetic field for the tests

described here ($B = 0$). As a result, the measured current-voltage characteristics for a constant-area rectangular channel are related by:

$$\frac{I}{(L)(W)} = \sigma \frac{V_{app}}{d} \quad (2)$$

where L and W are the length and width of the electrodes in contact with the salt water and d is the electrode spacing. The experimental current-voltage characteristics presented here are representative of what will occur in a seawater MHD thruster when E is interpreted as the sum of the applied and induced electric fields in an MHD unit.

As a voltage is applied across the electrodes, current begins to flow resulting in electrolysis of the salt water. While there has been no attempt in this investigation to study the electrochemical reactions in the electrolysis process, some background may aid in understanding the performance of various electrode materials and other phenomena that occur.

If the electrodes are inert, electrolysis of an aqueous solution NaCl results in the generation of chlorine gas at the anode and hydrogen gas at the cathode by the reactions.

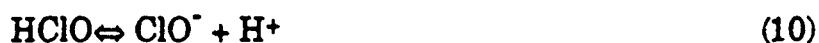


A surplus of electrons at the cathode creates conditions for chemical reduction in that region and the deficit of electrons at the anode results in the conditions for oxidation. However, if the anode material is oxidized, there will be material loss through reactions such as:



resulting in the formation of oxides of the anode material as the reacting anode material contributes metal ions to the solution. Thus, the principle results of passing an electric current through seawater are the production of H_2 at the cathode and the oxidation of reacting metals at the anode.

More complicated electrode reactions can also occur depending upon the electrode materials used and the level of current. Bennett¹¹ states that chlorine generated at the anode will very quickly be hydrolyzed and H_2 generated by the reactions:



Hypochloride, a disinfectant, is produced in this process which increases the pH of the solution.

At certain voltage levels O_2 generation at the anode may be favored over the production of chlorine through the reaction,



This apparently occurs at very low current densities ($j < 1 \text{ mA/cm}^2$) and is probably not important for the conditions of these tests.

The amount of hydrogen gas produced at the cathode is simple to calculate since one hydrogen atom is produced for every electron. The measurement of the electrolysis current was employed as an early means of determining Avogadro's Number. One Faraday of charge, F , (96,487 coulombs) will produce one mole or 1.008 gms of hydrogen. Thus, a current of 10 amps will result in 1.0443×10^{-4} gm of H_2 /sec. As a result, it can be shown that the volumetric production of H_2 is:

$$\dot{V} = \left(\frac{I}{F} \right) \times \left(\frac{RT}{2P} \right) \quad (13)$$

if H_2 is treated as a perfect gas. For typical run conditions of these tests, $T = 300^\circ K$, $p = 1 \text{ atm}$ and at a current of $I = 10 \text{ amp}$,

$$V \approx 1.28 \times 10^{-3} \text{ liters of } H_2/\text{sec} \quad (14)$$

were produced. This represents the maximum H_2 gas generation rate for these tests.

Additional chemical reactions also occur in the high pH region near the cathode. Magnesium and calcium salts which are present in seawater are hydrolyzed to form calcium and/or magnesium hydroxide. These oxides exist as a white gelatinous or colloidal material, and the reactions are more predominate with certain types of electrodes where the gelatinous products begin to adhere to surfaces in regions of low velocity. $Ca(OH)_2$ and $Mg(OH)_2$ form routinely in seawater electrolysis cells and are periodically removed by reversing the current.¹² The formation of these materials, however, may cause additional problems in seawater MHD thrusters.

Some additional information concerning seawater electrolysis is available in references 13 to 15.

TEST EQUIPMENT

WATER TABLE FACILITY

Tests were carried out using two water tables which produce a sheet of water having a specified depth. Wall guides were introduced to simulate a two-dimensional flow channel consisting of an intake nozzle, a constant area MHD channel (without B-field), and an exit diffuser, see Fig. 1. The channel dimensions were adjustable to accommodate investigation of different channel configurations and sizes. Two basic channel configurations were used:

1. Open-Top Channel - In this configuration the electrodes made up the sidewalls of the channel as shown in Fig. 1. The bottom wall or floor was made of an insulating material and there was a free, water surface at the top. Figure 2a is a photograph of this configuration.

2. Closed Channel - When this configuration was used, the bottom surface of the channel served as the cathode; the top surface as the anode; the sidewalls were made from non-conducting materials. This channel was fully submerged in the water flow. A photograph of the closed channel may be seen in Fig 2b.

ELECTRODE MATERIALS

Several electrode materials were investigated as summarized in the table below:

Table 1 - Electrode Materials Tested

Open-Top Channel

<u>Pair Number</u>	<u>Anode</u>	<u>Cathode</u>
1	Aluminum	Aluminum
2	Copper	Copper
3	Incoloy 800	Incoloy 800
4	Titanium Substrate Rare-Earth Oxide Coating*	Titanium Substrate Rare-Earth Oxide Coating*
5	Titanium Substrate Rare-Earth Oxide Coating*	Hastelloy C

Closed Channel

6	Aluminum	Aluminum
7	Copper	Copper

*Manufactured and provided by Eltech Corp. The oxide coating is believed to be ruthenium dioxide.

The width or height of the electrodes (W) varied from about 2 to 5 cm and the channel and electrode length (L) varied from about 12 to 20.5 cm. The electrode

spacing (i.e. the width of the channel) (d) was also varied but for most tests the spacing between electrodes was about 5 cm.

Long-duration (50 hr or 100 hr) tests were made for Electrode Pairs 4 and 5.

POWER SUPPLY AND INSTRUMENTATION

The electrodes were connected to a D.C. power supply. Applied voltages ranged from 0 to 30 volts; the corresponding current varied from 0 to about 12 amps. The electrode surface area could be varied by changing the depth of the water in the open channel and/or changing the length of the electrodes in the closed channels. Current/voltage measurements were made for each of the electrode pairs by applying various voltages up to the value which produced a current density of 0.2 to 0.3 amp/cm². Approximate calculation of the electrical characteristics of an MHD submarine thruster suggest that this level would be the upper limit of current density which would be of interest in a submarine MHD thruster.

Currents and voltages were measured with Fluke meters. The repeatability of the electrical measurements was well within 2%.

Approximate values of the flow velocity were obtained from (1) a water flow meter in the water table and (2) by timing the passage of a small floating object in the MHD channel. Test velocities varied from 0 up to about 90 cm/sec. The accuracy of the flow velocity measurement was no better than about $\pm 10\%$ of the values stated. Throughout these tests however there was no indication that the flow velocity had an important effect upon the measured current and voltage characteristics other than a small effect on the "starting voltage" which is discussed later.

Specific gravity of the simulated seawater was measured periodically with a calibrated hydrometer set and the pH of the water was regularly monitored with a pH cell and meter.

RESULTS AND DISCUSSION

SIMULATION OF SEAWATER

ELECTRICAL CONDUCTIVITY

The water tables were drained and filled with fresh tap water having a specific gravity of 1.000. Various potentials were applied across the electrodes with the fresh water flowing through the channel at a velocity of about 20 cm/sec. The current varied linearly with voltage. From the applied voltages and current measurements the fresh water was found to have an electrical conductivity of $\sigma = 0.0306$ mho/meter.

Salts (in the form of the commercial product named "Instant Ocean") were then added to the water in several steps. At each step the (1) specific gravity and (2) currents at various voltages were measured. As will be observed in subsequent figures, the current varied linearly with voltage for the salt water over the current range provided by the power supply. Figure 3 summarizes the measured electrical conductivity of the simulated seawater as a function of its specific gravity. At a specific gravity of 1.024, a typical value for seawater, the electrical conductivity was found to be 4.5 mho/m which is also consistent with typical published values for seawater. Moreover, the electrical conductivity of the simulated seawater varied linearly with the specific gravity of the water up to specific gravities corresponding to ocean water.

For experimental purposes it may be desirable to increase the electrical conductivity of the water well beyond that of seawater. One test was performed on a solution containing twice the amount of Instant Ocean needed to achieve an electrical conductivity of 4.5 mho/m. All of the salts were soluble and the resulting conductivity was slightly above 10 mho/m with a specific gravity of 1.05. This data point is also shown in Fig. 3. While no attempts were made to produce

higher conductivities, it is possible to do so by the addition of larger amounts of an appropriate salt compound. The specific gravity and electrical conductivity of the test medium were maintained near 1.024 and 4.5 mho/m respectively throughout the tests reported here.

SCALING COMPOUNDS

As will be discussed later, longer duration testing of the electrodes resulted in the formation of a gelatinous material on the cathode side of the channel. This material which was principally $Mg(OH)_2$ adhered to some of the cathode materials and to wall surface discontinuities and corners. Whether or not this material will be formed in an MHD thruster operating on seawater is not known. However, these tests indicate that it will form in facilities simulating seawater with Instant Ocean. It can provide some obstruction to the flow and reduce somewhat the effective electrode surface area. These effects are discussed later.

CURRENT/VOLTAGE CHARACTERISTICS

The current-voltage characteristics of several types of electrodes were obtained for the channel geometries and test conditions summarized below:

(a) Channel Length, L	12.7 to 20.5 cm
(b) Channel Width (Electrode Spacing), d	5 to 10 cm
(c) Electrode Width, W	2 to 5 cm
(d) Flow Velocity, V	0 to 90 cm/sec
(e) Electrical Conductivity, σ	4.1 to 4.5 mho/m

These data are given in Figs. 4 through 9 in terms of applied electric field (E) and current density (j) in order to generalize the variation of channel geometry. Data were obtained for current densities up to 0.2 to 0.3 amp/cm²

which will probably be the upper level of current density of interest in seawater MHD thrusters.

OPEN TOP CHANNEL CONFIGURATION

The electrical characteristics of five open-top channels with different electrode materials are given in Figs. 4 through 8. In all of these tests the electrodes served as the vertical sidewalls.

It was anticipated that the H_2 generation at the cathode might create a gas sheath over the electrode and produce a non-linear variation of current density with increasing electric field. Inspection of the Fig. 4 to Fig. 8 data however, illustrates that this does not occur. Small H_2 bubbles formed uniformly over the cathode surface. They rise due to their buoyancy, but remain in the electrode sidewall boundary layer until they reach the free surface. As they rise they are also convected downstream by the boundary-layer flow, but more slowly than would be expected. As the current increased the gas generation rate increases, (see Eq. 13,) but the bubbles continue to move away from the electrode surface such that voltage drop at the wall is not significantly effected.

Comparison of Figs. 4 through 8 illustrates that the electrical characteristics of all of the electrode materials tested are quite similar (with the exception of copper electrodes which formed oxide films, Fig. 6b. The copper oxide films severely limit the current. All electrode materials exhibit linear variations of current density with applied electric field. As might be expected each material had a somewhat different initiation voltage, V_I , (i.e. the voltage or electric field which must be applied before appreciable current will flow). The initiation voltage and "zero-current" electric field for each electrode pair tested are summarized below:

Table 2 - Approximate Electrode Voltage Drops

<u>Anode</u>	<u>Cathode</u>	<u>Initiation Voltage, volts</u>	<u>Zero Current Electric Field, volts/cm</u>
Aluminum	Aluminum	1.5	0.3
Incoloy 800	Incoloy 800	1.1	0.2
Copper	Copper	1.5	0.3
Eltech	Eltech	2.1	0.4
Eltech	Hastelloy C	1.9	0.45

The Eltech metal-oxide coated electrodes exhibited the highest V_I of the electrodes tested but there were no large differences between any of the electrodes. The values measured are consistent with the voltage drops measured in water electrolysis cells¹⁶.

The flow velocity of the water through the channel was varied from about 6 to almost 90 cm/sec. In addition, some current/voltage data were obtained under static conditions. Comparison of Figs. 4 through 8 illustrate that for the range covered in these tests, changing the flow-velocity did not alter the electrical characteristics in any significant way. Comparison of Fig. 5 with the data in Figs. 7 and 8 (see circle symbols in Figs. 7 and 8 corresponding to the start of the test series) illustrates that the E vs j data for velocities of 0, 20, 47 and 77 cm/sec are almost coincident when the differences of initiation voltage, V_I , are taken into account.

Data given in Figs. 4, 5, 6a, 7, and 8 for an open channel configuration having a free water surface, characterize the maximum current densities which may be expected in a seawater MHD propulsion unit, if the electric field shown by the figure is taken as the sum of the applied electrical field and the induced electric field ($V \times B$) in an MHD duct. Electrolysis effects however, can reduce the

current flow. (1) Trapped H_2 bubbles and gas in a closed channel, (2) oxidation products on the anode and (3) the products of other chemical reactions on the cathode will reduce the current density at a given value of the electric field from the values shown in these Figures. The causes of reduced current are discussed in subsequent sections.

CLOSED CHANNEL CONFIGURATION

Two constant-area closed channels which were fully submerged in the water flow were also investigated (see Fig 2(b)). For both channels the bottom wall was the cathode, the top wall the anode and the sidewalls (i.e., the B-walls) were made of electrically insulating material. Copper electrodes were tested first and then abandoned because copper oxide films which formed on the anode very quickly limited the current (see Fig. 6(b)). As a result, most of the closed channel data were obtained with channels having aluminium electrodes. The closed channel dimensions and test condition were:

Table 3 - Closed Channel Geometries

<u>Channel</u>	<u>Electrode Spacing cm</u>	<u>Electrode Height cm</u>	<u>Electrode Length cm</u>	<u>Flow Velocity cm/sec</u>
(a)	3.7	2.6	20.4	18 to 90
(b)	3.7	3.4	13.8	26 to 70

The channel flow was discharged into a diffuser with diverging sidewalls. For Channel (a) the top and bottom walls of the diffuser were parallel and horizontal. In later tests with Channel (b) the top diffuser wall was also diverged 2° .

CLOSED CHANNEL TESTS WITH HIGHER FLOW VELOCITIES

The variation of current density with electric field for the two closed channels is given in Fig. 9 when the channel flow velocities were 70 and 90 cm/sec. As occurred with the open-top channel the current density varied linearly with increasing electric field in the closed channel at these flow velocities. Comparison of the electrical characteristics of closed channels with aluminium electrodes (Fig. 9) to the electrical characteristics of the open-top channel with aluminum electrodes (Fig. 4) indicates that the closed channel had about the same initiation voltage (V_i) as measured for the closed channels, but at a given electric field the current densities in the completely closed channels were about 10% to 15% lower than measured in the open-top channel. The specific gravity and electrical conductivity of the simulated seawater were essentially the same for these two tests. This current decrease appears to be associated with the H_2 generation in the electrolysis process and represents a loss of performance in an MHD seawater thruster operating at these velocities. The cause of this current decrease is discussed fully in the section describing the observed bubble dynamics.

CLOSED CHANNEL TESTS WITH LOWER FLOW VELOCITIES

Channel (a) with a Horizontal Diffuser Top Wall

The current changed drastically when the water flow velocity was decreased. Figure 10 summarizes the time variation of the electrode current at two lower velocities (18 cm/sec and 34 cm/sec) for Channel (a) with a horizontal diffuser top wall. With the configuration of a horizontal diffuser top wall gas bubbles which are swept out of the channel rise to the top diffuser and become trapped against the top wall. Surface tension forces impede their movement downstream. As a result, large gas pockets were formed on the upper wall which grew back upstream into the MHD channel. The consequence is that the trapped

gas begins to cover part of the anode surface and causes the current to decrease. The gas pockets however do move slowly downstream and periodically escape from the diffuser exit. Thus, the channel-diffuser combination discharges H_2 gas pockets in a regular periodic fashion. When this occurs and a large pocket of gas escapes the current rises again to its initial value. Whereupon the current begins to again decrease as new gas pockets form.

As shown in Fig. 10, the period between H_2 gas discharges is quite regular. The period depends upon level of the applied voltage and the flow velocity. Increasing the applied voltage increases the current flow and gas generation rate (see Eq. 13). This in turn decreases the period of the discharge (see Fig. 10b). Increasing the flow velocity at constant applied voltage more rapidly convects the gas bubbles downstream so that the gas pockets build more slowly which increases the period (compare Fig. 10a with the middle curve in Fig. 10b). A horizontal top wall diffuser in a seawater MHD thruster is clearly undesirable since it would result in a low frequency "fluctuation" of the thrust at low operational velocities. At channel velocities of 70 cm/sec and above current oscillations as shown in Fig. 10 did not occur. Moreover, they also may be eliminated by diverging the diffuser top wall as described below.

Channel (b) with a Diverging Diffuser Top Wall

Channel (b) had the diffuser top wall diverged 2° (i.e. slanted upward). With this configuration the large gas pockets described above did not form along the diffuser top wall. Some H_2 gas bubbles coalesce forming larger bubbles but they move along the wall with sufficient velocity to prevent accumulation of large amounts of gas in the diffuser as occurred with a horizontal top wall. Consequently, the periodic discharge of gas pockets and the periodic variation of electrode current were eliminated.

The closed Channel (b) when operating at low velocity, however, exhibited a decrease in electrode current to a lower equilibrium value as shown in Fig. 11. The final equilibrium current level can be significantly less than currents achieved in the open-top channels and given previously in Figs. 4 to 8. The current decrease is again the result of bubbles or gas trapped on the electrodes (in this case the anode) as discussed in the next section. The time to reach the equilibrium current and the amount of the current decrease depends upon the flow velocity and the applied voltage (i.e. current level).

Thus, diverging the diffuser top wall eliminated the undesirable periodic discharge of gas in the flow channel. However, the longer residence time of the H₂ bubbles in the flow at lower velocity, decreases the current flow in a closed channel from what might be expected based upon the seawater conductivity (i.e. Figs. 4 to 8).

Summary

The following table summarizes the degradation of current density which for these tests occurred in a closed channel as a result of H₂ gas formation in the electrolysis process. Values of the maximum current density achievable in an open-top channel are also shown for reference purposes:

Table 4 - Summary of Current Density in Closed Channels
at Various Operating Conditions

<u>Velocity = 26 cm/sec</u>	<u>Electric Field. volts/cm</u>		
	<u>2.16</u>	<u>4.05</u>	<u>6.49</u>
Initial Current Density amp/cm ²	.068	.138	.220
Final Equil. Current Density amp/cm ²	.035	.085	.160
Time to Reach Equil., min.	7	3	2
Max. Current Density Possible, amp/cm ²	.082	.158	.270

Table 4 (Continued)

Velocity = 70 cm/sec and above

Initial Current Density amp/cm ²	.068	.138	.220
Final Equil. Current Density amp/cm ²	.060	.130	.220
Time to Reach Equil., min.	Nil	Nil	Nil
Max. Current Density Possible, amp/cm ²	.082	.158	.270

These test results are shown in a different way by Fig. 12 which compares the variation of the measured current density with electric field for a closed channel (cathode on the bottom wall) with the measurements for an open channel. This comparison illustrates that due to H₂ gas formation in the electrolysis process a higher applied voltage will be necessary to achieve a given current and hence propulsive thrust in a closed channel than would be ideally expected from the value of the seawater electrical conductivity. Because the channel flow velocities for these tests were much lower than would exist in a typical submarine thruster, there is a tendency to believe that this potential loss of performance will be greatly reduced and perhaps eliminated as flow velocities increase. However, the observations of bubble dynamics described in the next section clearly suggest that the current losses are due to the bubbles that move through low-velocity sidewall boundary-layer regions because of their buoyancy. They accumulate in the upper corner between an electrode and the sidewall and result in blocking a part of the electrode surface area. Simply increasing the overall flow velocity may not significantly alter the mechanisms which results in gas accumulation at the electrodes.

BUBBLE DYNAMICS

As shown by Figs. 4 through 12 four modes of current flow were observed during these tests:

- (1) A linear variation of current with voltage, with current levels corresponding to the ideal values expected for the salt water specific gravity and electrical conductivity. This result occurred in an open-top channel with a free surface and the electrodes served as the vertical sidewalls which allowed the H_2 to escape.
- (2) A linear variation of current with voltage for a closed channel but with currents about 10% lower than the ideal value. This result occurred when the closed channel velocity was greater than 70 cm/sec.
- (3) A periodic fluctuating current in a closed channel at velocities below about 40 cm/sec and with a horizontal top wall on the diffuser.
- (4) A significantly decreased but steady current in a closed channel at velocities below about 40 cm/sec and with a 2° diverging top wall on the diffuser.

All of these current modes were a function of gas generation rate in the channel and the bubble dynamics.

OPEN-TOP CHANNEL BUBBLE DYNAMICS

Observation of the bubble formation in the open-top channels clearly demonstrate that small diameter bubbles (probably less than 0.5mm in diameter) are generated uniformly over the cathode sidewall and to a lesser degree with some anode materials (the Eltech material and aluminum for example). The bubbles rise and move downstream in the electrode sidewall boundary layers under a balance of forces due to (1) shear in the boundary layer, (2) their natural buoyancy and (3) their surface tension with the wall. As they reach the water surface they coalesce into much larger bubbles and either escape from the free

surface into the atmosphere or float downstream on the surface and along the wall forming a "foam boundary layer". In any event with a free-surface the bubbles do not appear to move out of the sidewall boundary layers where they are generated and into the free-stream except when they reach the free surface.

Figure 13(a) is a photograph of bubbles formed in an open-top channel. It illustrates (1) the layer of small bubbles forming on the cathode surface, (2) the foam boundary layer at the free surface and (3) the absence of any bubbles in the free stream. A sketch of the bubble dynamics with this configuration is given by Fig. 13(b). The bubble formation and their movement does not significantly impact the electrical characteristics. At a given applied voltage the current that results is what would be expected from the conductivity of the water.

CLOSED CHANNEL BUBBLE DYNAMICS

In a closed channel the situation is different. Any gas that is generated at the top wall or rises through the sidewall boundary layers tends to be trapped against the top wall. Surface tension forces are enhanced on the top surface since the buoyant force pushes the bubble against the top wall. Shear forces in the top wall boundary layer are not sufficient to move the gas downstream very rapidly.

One brief test was conducted with a closed channel having the cathode as the top wall. Hydrogen generated at the cathode became trapped against the cathode surface due to its buoyancy and surface tension. This greatly reduced the current which could be passed through the seawater. No data were taken for this configuration because it didn't appear to be of practical interest. For all other closed channel tests the cathode was placed on the bottom wall and the anode served as the top wall. With this orientation most of the hydrogen produced at the cathode will rise through the cathode boundary layer because of its buoyancy and move into the free stream (see Fig. 14(a)).

Acoustic measurements, ref. 10, suggest that the size of the bubbles generated in these tests was in the range between 0.1 to 0.5 mm in diameter. This size range was also consistent with visual observations. Bubbles of this size will have a rise velocity between 1.5 and 5 cm/sec¹⁷. Assuming that the bubbles are spherical, they are subject to a vertical buoyant force (F_B) and a drag force (F_D) moving them horizontally. It can be easily shown that the ratio of F_B to F_D for "free" bubble is:

$$\frac{F_B}{F_D} = \frac{gD}{3C_D V^2}$$

where D is the diameter of the bubble, C_D is the drag coefficient for a sphere (which depends on Reynolds number), V is the flow velocity, and g is the acceleration due to gravity. For the conditions of these tests the ratio:

$$\frac{F_B}{F_D} \ll 0.1$$

Thus, the bubbles rising out of the cathode boundary layer and into moving the free stream (which had a velocity as high as 70 to 90 cm/sec) are swept downstream and out of the channel before they could rise to the top of the channel. (see Fig. 14(a)). Even at the lower velocities of these tests (near 20 to 30 cm/sec), a large portion of the bubbles generated on the bottom wall are swept out of the channel before rising to the top wall.

The situation is different however for bubbles formed at the cathode and sidewall corner. These bubbles will rise in the sidewall boundary layer and stay close to the sidewall. As a result many of these "boundary layer" bubbles reach the top before moving out of the channel since in this case:

$$\frac{F_B}{F_D} = (0)1$$

The migration of bubbles generated in the bottom corners is also sketched in Fig. 14(a). Bubbles which rise through the sidewall boundary layers create small gas

pockets at the corners between the sidewalls and the anode. The effect of these gas pockets is to reduce the effective surface area of the anode and reduce the current flow. This bubble flow pattern is responsible for the decrease in current measured for the closed channel operating at higher velocities. (Compare Fig. 9 with Fig. 4 or see Fig. 10)

As the channel flow velocity decreases, this effect becomes more pronounced; moreover, at the lower flow velocities some of the gas generated at the bottom of the channel may rise to the anode before leaving the channel and block even more of the anode area. This bubble behavior produces the larger current decrease with time as shown in Fig. 11 for a low, channel velocity.

Gas generated at the floor of the channel and swept into the diffuser can then rise further and be trapped against the diffuser top wall. When that wall was horizontal, large gas pockets accumulated which as outlined earlier cause the periodic fluctuation in current summarized in Fig. 10.

IMPLICATIONS FOR A SEAWATER THRUSTER DESIGN

The results of these tests (even though the scale and velocities were small) suggest potential performance problems with seawater MHD thrusters which will have to be considered. In addition, they also suggest channel geometries and orientations which may be more desirable.

Effect of Bubble Formation on Channel Performance

These tests have indicated a 10 to 15% reduction of current densities in closed channels having flow velocities as high as 90 cm/sec (see Fig. 12) due to bubble-induced gas blockage at the electrode. The end effect of the gas blockage in the channel is to reduce the electrical efficiency of a seawater MHD propulsion unit.

A simple analytical model which approximates the performance of an MHD submarine thruster has been developed by Bagley¹⁸ at DTRC. As an example, a particular calculation, using his model to estimate the performance of submarine MHD propulsion unit having a magnetic field of 5 tesla and a current density of 0.2 amp/cm², indicated a thruster electrical efficiency (the ratio of MHD power out to electrical power in) of about 24.3%. If 13% of the electrode surface area is blocked by a gas sheath, which is the reduction indicated by the Fig. 12 data, the thruster electrical efficiency would decrease to 21.8%. It should be emphasized that these values are approximate and that the scale and velocities used in these tests may cause a greater degradation of current than will occur in a full-scale configuration. Moreover, a complete MHD channel will produce the Lorentz force ($j \times B$) in the fluid and in the boundary layer which may act to move the bubbles in the boundary layer downstream more rapidly. This force on the fluid was absent in these tests since $B \approx 0$. However, the potential for decreased performance due to gas bubbles and/or gas pockets on the electrodes should not be dismissed lightly.

Channel Configuration

The observation of the H₂ bubble dynamics and the measurement of their effects provide some guide to the design of an MHD thruster. First, it would appear highly desirable to avoid horizontal or converging channel top walls (ceilings) in flow passages where H₂ bubble may exist which tends to trap bubbles due to surface tension effects and allows gas pockets to form. This suggestion would apply to the diffuser as well as the channel. Diverging the channel walls and particularly the top wall should decrease or minimize current losses due to gas blockage.

For a linear MHD channel it appears desirable to place the cathode at the bottom of the channel. (see Fig. 14(a)). This should maximize the possibility of the

bubbles getting into the free stream and being swept out of the channel before rising to the top electrode where they would provide a high-resistance blockage to the current flow. Since some anodes produce less gas than others, their use would also be desirable. As outlined later, those anodes which demonstrated good durability, however, also produced gas on the anode surface.

If the electrodes are at the sidewalls of a linear channel, larger amounts of the H_2 gas will be trapped in the boundary layers as illustrated in Fig. 14(b). These tests suggest that a linear channel with electrode sidewalls may inherently have lower performance unless some means is provided to remove the bubbles or gas pockets.

The concept of an annular MHD propulsion unit configuration which is wrapped around the hull of the submarine has been suggested several times over the past twenty-five years.^{2, 19, 20} This configuration has a number of advantages related to (1) a simpler magnet design and (2) minimizing the size and perhaps cost of the MHD propulsion unit appendage which would have to be added to a conventional submarine hull. A sketch of this configuration is shown in Fig. 15(a).

It's not yet clear how the outer annulus wall would be structurally supported. This sketch shows that the outer wall is supported by vanes in the inlet nozzle and exit diffuser which would enclose part of the magnet coil windings. The azimuthal magnetic field would be provided by several coils which would be enclosed in the outer wall, the end support vanes and then the inner wall. This arrangement would leave an unobstructed annular MHD flow passage as shown in Fig. 15(b). Such an arrangement would minimize the formation of H_2 gas pockets being trapped in the MHD channel and interfering with the current flow if, as sketched in the figure, the inner wall served as the cathode. Gas formed at the inner electrode would escape into the free steam and be swept

out of the channel before reaching the outer electrode. Thus, this arrangement would appear to be much less susceptible to current losses due to gas blockage effects described above.

If, however, it would become necessary to provide support walls over the length of the MHD channel between the inner body (the cathode) and the outer body (the anode), the annular passage would be partitioned or segmented. Should structural consideration make such support partitions necessary, or that it is done to subdivide the thruster for directional control purposes, the electrodes in each sector would be orientated in different directions with respect to the direction of the gravitation force. The observation of H_2 bubble dynamics in these tests and the tendency of the bubbles to remain in the low-velocity boundary layers suggest that the problem of trapped gases interfering with the current flow in some of the thruster segments could be quite severe with this configuration. The efficiency of the thruster would be reduced and should this occur, the thrust from each sector to the MHD propulsor could vary considerably. The end effect would appear to be a force couple acting in the nose-down direction.

LONG DURATION TESTS

Two long-duration electrode tests were carried out to obtain information concerning the durability of some electrode materials and to gain some insight into the operation of closed-loop facilities designed to evaluate seawater MHD thrusters. A 50-hour accumulative test was made with Electrode Pair 4 (Eltech Anode and Eltech Cathode) and 100 hours of operation of Electrode Pair 5 (Eltech Anode and Hastelloy C Cathode) was carried out.

50-HOUR TEST OF ELTECH ELECTRODES

Figure 7 summarizes the current/voltage characteristics of an Eltech anode and cathode combination over 50 hours of testing at an electric field of 6 volts/cm and a current density of approximately 0.25 amp/cm². There were no important changes of the electrical characteristics over the course of the tests. Changes in current at a given voltage shown in Fig. 7 were due to (1) increase of the water temperature during the run and (2) the formation of magnesium scaling products on the anode. Moreover, there was no visible or measurable degradation of the electrode surfaces over the 50-hour test.

Effect of Water Temperature

This 50-hour test was made up of several 6 to 10 hour continuous runs. Over the course of the run, energy is added to the water by the circulating pump and by the current passing between the electrodes and through the water. As a consequence, the temperature of the water rises a few degrees over the run. The electrical conductivity of the simulated seawater is relatively sensitive to the water temperature. Figure 16 shows the variation of current with time for the constant applied voltage of 30 volts. During a run the current rises as the water temperature rises. Then, overnight the facility was shut down and the water temperature returned close to its original value. This cycling or variation of water temperature with time resulted in the sawtoothed current history given in Fig. 16. With constant values of applied voltage, flow velocity, specific gravity of the water and channel geometry, it was possible to measure the resulting current at temperatures between about 65°F to 92°F. As illustrated by Fig. 17, a 25°F temperature variation resulted in about a 25% change in current. Consequently, one must exercise care in interpreting current data in a closed MHD thruster test facility in which the water or electrolyte temperature can change. Since the

current varies linearly with water (electrolyte) temperature, it would be simple to correct current data for changes in the water temperature.

Effect of Scaling Products at the Cathode

As noted earlier the very high pH condition which exists at the cathode results in the formation of magnesium and to a lesser degree calcium hydroxide. This material is glantinous and adhered to the Eltech cathode surface. Some observations over the course of the tests concerning these deposits are made in Fig. 18. While these scale deposits were wiped from the cathode between most of the run periods, they did nevertheless form a crust on the cathode surface as the test progressed as shown by Fig. 19.

This cathode scaling material $Mg(OH)_2$ is electrically insulating. So, as the $Mg(OH)_2$ scale accumulates on the cathode over a period time, it reduces the current. This effect can be seen in Fig. 16 by the decrease of the initial current at the start of each run period from the start of the test, up to a total run time of about 36.6 hours (i.e. the dash-dot line). Current data taken from Fig 16 is summarized below:

Table 5 - Current Variation with Time for Long-Duration Tests

<u>Accumulated Test Time, hr.</u>	<u>Current (T = 70°F), amp</u>
0	5.6
7.6	5.44
15.7	5.17
25.0	5.17
36.6	4.93
44.2	5.59
50.5	5.44

At an accumulated run time of 44.2 hours the cathode was removed from the channel, scrapped clean, re-installed and run for a short time with reversed polarity. Running the cathode as an anode for a short time effectively removed the

scale. With the cleaned cathode, Fig. 16 illustrates that the current increased to nearly the level measured when the cathode was new. Continuing to run the cathode for another 6.3 hours resulted in the current beginning to again decrease as more scale formed. Appendix A provides a chemical analysis of this scale material.

Other Long Duration Trends

Figure 18 summarizes the cathode and anode weights over the 50 hour test period. The cathode exhibited a slow weight increase as a scale crust accumulated. When the electrode polarity was reversed and the scale removed, the cathode weight returned to its original value. The weight of the anode appeared to vary slightly over the course of the test. The weight changes shown in Fig. 18 are believed to be due different moisture contents of the oxide coating and their mounts since the electrodes were just wiped dry and weighed. It is believed that the 50-hour test did not result in any measurable weight loss for either the Eltech anode or cathode.

The electrolyte pH was also recorded over the period of this test (see Fig. 18(b)). The pH was observed to rise initially over the first few hours of the test as hypochloride was produced. After that it continued to increase but rather slowly. It should so be noted that the slight odor of Cl_2 was present over the free-surface of the water from time to time when the electrodes were powered. Measurements just over the surface of the water and near the channel indicated Cl_2 concentrations of 3 to 5 ppm which is the level of its odor threshold. This electrolysis process did not generate any appreciable amount of free Cl_2 .

100-HOUR TEST OF ELTECH/HASTELLOY ELECTRODES

Tests of the stainless steel Electrode Pair 3 indicated that the $\text{Mg}(\text{OH})_2$ and $\text{Ca}(\text{OH})_2$ scaling products did not adhere to the electrode surface. Moreover,

discussions with others¹² indicated that commercially available electrolysis cells utilize stainless cathodes to reduce the scaling problem. For these reasons, a 100-hour test of a polished Hastelloy C cathode and an Eltech (ruthenium dioxide coating on titanium substrate) anode was made. This test consisted of several 8-hour to 24-hour continuous run periods. The purposes of the test were to (1) gain information about the durability of this electrode pair, (2) to observe the location and amount of scaling and (3) measure the electrical characteristics of this electrode pair, (Fig. 8).

Scale Formation

The magnesium scale formed near the cathode surface but it did not adhere to the polished steel surface to any important degree. At the entrance and exit of the channel, however, there were vertical wall seams where the channel was butted to the nozzle exit and diffuser entrance. These vertical seams on the cathode side of the channel represented small but finite wall discontinuities. Scaling products become attached to these discontinuities and grew upstream on the nozzle sidewall and downstream on the diffuser sidewall. They also grew outward from the wall in the form of a vane-like bulge that extended well beyond the wall boundary layer. The flow velocity was 77 cm/sec for these tests. The $\text{Mg}(\text{OH})_2$ scale also grew in the corner between the cathode sidewall and channel floor where velocities were relatively low and then outward across the channel floor to the anode. It primarily adhered to the floor rather than the cathode. Scale growth patterns are given in Fig. 19.

For the channel size and flow velocity of these tests the growth of the $\text{Mg}(\text{OH})_2$ scale was sufficient to create disturbance and blockage of the flow. After one 24-hour continuous run period the scaling material was collected from the nozzle/channel/diffuser walls and weighed, after it had been dried. During this test period the weight of the scale accumulation was about 0.22 gms per square

centimeter of cathode surface area. This corresponds to an accumulation rate in the channel region of roughly:

$$\dot{m}]_{\text{scale}} = 0.01 \text{ gm/hr/cm}^2 \text{ of cathode}$$

After 100 hours of running the $\text{Mg}(\text{OH})_2$ scale material coated most of the wetted surfaces in the test facility to some degree.

The use of a polished stainless steel cathode greatly minimize the formation of the scale material on the cathode surface. Moreover, the use of these electrodes almost eliminates the current reduction and loss of MHD channel performance due to scaling which occurred with an Eltech or aluminum cathode. However, the production of the magnesium and perhaps calcium oxides at the cathode may cause some losses of channel performance by creating blockage and flow disturbances which may lead to higher pressure drops in the exit diffuser. In addition, this material may cause some operational problems in closed-loop test facilities where it can accumulate and initiate disturbance to the flow. This may be particularly important in facilities where acoustic testing of MHD thrusters is to be done.

Electrode Durability

This electrode pair accumulated 109 hours running at a current density of 0.30 amp/cm^2 . A summary of the test periods is given below:

Table 6 - Summary for 100 Hour Test

<u>Date</u>	<u>Power On</u>	<u>Power Off</u>	<u>Run Time, hr</u>	<u>Total Time, hr</u>
9/7/89	9:35 am	8:20 pm	10.75	10.75
9/8/89	8:15 am			
9/9/89		9:35 am	25.25	36.0
9/9/89	9:50 am	5:50 pm	8.0	44.0
9/11/89	8:50 am			
9/12/89		7:05 am	22.25	66.25
9/12/89	7:05 am			
9/13/89		2:00 am*	15.1	81.35
9/13/89	7:25 am	6:50 pm	11.25	92.60
9/14/89	8:45 am	10:35 pm	14.8	107.40
9/15/89	8:45 am	10:45 am	2.0	109.4

*Anode power supply connection failed at about 2:00 am.

The performance of both the anode and cathode over this period was excellent.

Both electrodes were weighed before and after the test;

	<u>Eltech Anode</u>	<u>Hastelloy Cathode</u>
Beginning of Test	0.10180 lb.	0.47818 lb.
End of Test	0.10232 lb.	0.47626 lb.

The weight differences shown are within the overall measurement error.

SUMMARY AND CONCLUSIONS

Systematic tests of the seawater electrolysis process in an MHD type channel have been carried out. There was no applied magnetic field for these tests and the Lorentz force on the simulated seawater was absent. The current/voltage or current density/electrical field characteristics measured during these tests are similar to those which will occur in an MHD seawater thruster, if the electric field for these tests is taken to represent the sum of the applied field and induced field in an MHD channel. These tests have led to the following conclusions: 1. The product Instant Ocean can be used to produce a test medium for MHD thruster tests which has the same electrical conductivity and specific gravity relationship as sea water (i.e. $\sigma = 4.5$ mho/m and S.G. = 1.024). This product can also be employed to increase the electrical conductivity of the test medium to at least 10 mho/m, if it is desirable to evaluate a seawater MHD thruster over a wider range of MHD conditions.

2. The current or alternatively the current density with a seawater electrolyte vary linearly with applied voltage or electric field up to a current density of at least 0.3 amp/cm^2 when there is the means to remove the hydrogen bubbles generated at the electrodes (principally H_2 at the cathode). An electrode voltage drop of 1 to 2 volts occurs and may be thought of as an initiation voltage which must be applied before significant current will flow in the seawater electrolyte.

3. When the channel completely encloses the flow, H_2 gas generated at the electrodes can become trapped in the boundary layers. It rises to the top of the channel due to its buoyancy and forms pockets of gas. These gas pockets can, to a varying degree depending upon the orientation of the electrodes, cover a portion of the electrode surface and reduce the current flow. In this case the gas acts as an

insulating sheath over a part of the electrode and reduces the MHD thruster performance. For these tests the loss of electrical current was at least 10 to 15% and as high as 50%.

4. The current varied periodically with time for test configurations with horizontal top walls (ceilings) in the channel and diffuser as the channel periodically discharged pockets of gas which had become trapped at the top surface.

5. Careful consideration must be given to the geometric design of a seawater MHD thruster and its exit diffuser to avoid the formation of pockets of trapped H_2 gas and/or to provide the means to remove the gas. Diverging top walls for the channel and diffuser is believed to be essential for linear MHD thrusters in order to minimize gas blockage of the electrodes. The toroidal or annular MHD thruster configuration may have a configurational advantage in minimizing gas blockage, as long as it does not have to be portioned into segments. If, however, structural considerations dictate subdividing the annular passages into segments, to support the outer annular wall, some segments of the annular flow passage will in all likelihood have significantly reduced current. This would result in uneven thrust for the annular segments which is clearly undesirable.

6. Copper and aluminum anodes were severely eroded as copper and aluminum oxides formed. Moreover, the oxide film which quickly formed on the copper anode limited the current flow. Corrosion of other copper and aluminum materials used in the test facility was also rather severe. Stainless anodes were also oxidized, but to a lesser degree. An anode made of ruthenium dioxide on a titanium substrate (manufactured by Eltech Corp) proved to be quite durable in a

50-hour and 100-hour test. For both of these long-duration tests there was no visible or measurable loss of this anode material.

7. The principle problem at the cathode was the formation of a white gelanteous material from the salts in the electrolyte solution. The primary substance that formed during these tests was magnesium hydroxide, $Mg(OH)_2$ (Appendix A). This material formed at the high pH condition at the cathode and adhered to the aluminum and Eltech cathodes. Since it is an electrical insulator, it reduced the current flow as it accumulates over long run times. This material could be easily removed by reversing the polarity. The $Mg(OH)_2$ did not adhere as readily to two types of stainless steel electrodes which were tested. However, it did stick to and grow out from the nozzle, and diffuser walls as well as the insulated B-walls in regions where there were wall discontinuities and/or corners with low flow velocities.

8. An electrode pair made up of an Eltech anode (to minimize anode erosion) and a polished Hastelloy C cathode (to minimize the buildup of $Mg(OH)_2$) exhibited very good performance over a 100 hour test at a current density of about 0.3 amp/cm². Following this test there was no measurable loss or visual damage to either electrode. However, while the $Mg(OH)_2$ deposits did not form on the polished stainless cathode surface, these deposits did form in other parts of the flow channel to the point of creating significant flow disturbances. This electrode pair, a ruthenium dioxide coated anode and a polished stainless cathode is recommended for use in MHD seawater thrusters. It will provide good electrical performance and durability.

9. From the results of these tests it appears that it will be necessary to consider and control the formation of $\text{Mg}(\text{OH})_2$ and other compounds in the flow inlet nozzle and exit diffuser adjacent to the cathode surface. In addition, MHD thruster test facilities will have the problem of an accumulation of these materials throughout the test facility particularly in corners or other flow regions where velocities are low and/or flow discontinuities exist.

10. With the use of a ruthenium dioxide-coated anode, hypochloride (HClO) forms at the anode in which the Cl_2 produced at the anode is hydrolyzed to produce additional H_2 . This will have the effect of slowly increasing the pH of the seawater test medium in a closed MHD thruster test facility. In addition, in a closed test facility the temperature of the test medium will also increase with time as energy is added to the water by (1) joule heating of the electrolyte and (2) a circulating pump. The electrical conductivity of the seawater is quite sensitive to water temperature. As a result, the electrical conductivity of the test fluid and as a result the current at a given voltage will increase with time as the electrolyte temperature rises. A temperature correction to the current/voltage data taken over long runs will probably be necessary.

REFERENCES

1. Friauf, James B, "Electromagnetic Ship Propulsion" ASNE Journal, Feb 1961, p. 139-142.
2. Phillips, Owen M., 'The Prospects for Magnetohydrodynamic Ship Propulsion', Journal of Ship Research, March 1962, p. 43-51.
3. Doragh, R.A., "Magnetohydrodynamic Ship Propulsion Using Superconducting Magnets", Presented Annual Meeting of The Society of Naval Architects and Marine Engineers, Nov 14 & 15, 1963, New York, NY.
4. Way, S., "Propulsion of Submarines by Lorentz Forces in the Surrounding Sea" ASME Publication 64-WA/ENER7, Winter Meeting Nov 29 - Dec 4, 1964.
5. Hummert, George T., "An Evaluation of Direct Current Electromagnetic Propulsion in Seawater" Office of Naval Research Report ONR-CR168-007-1, July 1979.
6. Way, S., "Electromagnetic Propulsion for Cargo Submarines", Journal of Hydrodynamics, Vol. 2, No. 2, Apr. 1968.
7. Tada, Eiichi, et al "Fundamental Design of a Superconducting EMT Ice Breaker", Trans. I Mar E (C), Vol 97, Conf. 3, Paper 6, p. 49-56.
8. Matora, Seizo, "General View of the JAFSA Project", JAFSA Report 7/10/88.
9. Matora, Seizo, "Research and Development of Superconducting Electro-Magnetic Propulsion Ships" Japan Foundation of Shipbuilding Advancement, unpublished communication.
10. Tempelmeyer, Kenneth E., "Preliminary Measurement of Bubble Dynamics and Bubble Noise in a Seawater MHD Propulsion Unit", DTRC Report DTNSRDC 891 ____, Nov 1989.
11. Bennett, J.E., "Electrodes for Generation of Hydrogen and Oxygen from Seawater", Int. Journal of Hydrogen Energy, Vol 5, p. 401-408, 1980.
12. Nitsa, M., Eltech Corp., private communication, June 1989.

13. Bennett, John E., "On-Site Generation of Hypochloride Solutions by Electrolysis of Seawater, AIChE Symposium Series - Water, 1977.
14. El-Bassuoui, A.M.A., et al, "Hydrogen and Fresh Water Production from Seawater", Int. Journal of Hydrogen Energy, Vol 7, No. 12, p. 919-923, 1982.
15. Slepchenko, O.S., et al, "Effect of Anion Composition of the Electrolyte on Active Chlorine Current Yield in the Electrolysis of Sea and Brackish Waters" Khimiya i Tekhnologiya Vody (Translated to English) Vol. 9, No. 2 p. 150-152, 1987.
16. LeRoy, R.E., et al, "Time-Variation in Unipolar Water Electrolysis and Their Implications for Efficiency Improvement", Proceedings of the Symposium on Industrial Water Electrolysis, Vol. 78-4, p. 63-76, 1978.
17. Richardson, E.G. (Ed), Technical Aspects of Sound, Chap. 5, "Air Bubbles in Water" by E. Meger, p. 222-238, Elsevier Publishing Co., 1957.
18. Bagley, David, private communication, DTRC Report in Progress, Sep 1989.
19. Rice, Warren A., U.S. Patent No. 2,997,013, Aug 22, 1961.
20. Resler, E.L., "Magnetohydrodynamic Propulsion of Sea Vehicles", Seventh Symposium on Naval Hydrodynamics, Rome Italy p. 1437-1445, 1968.

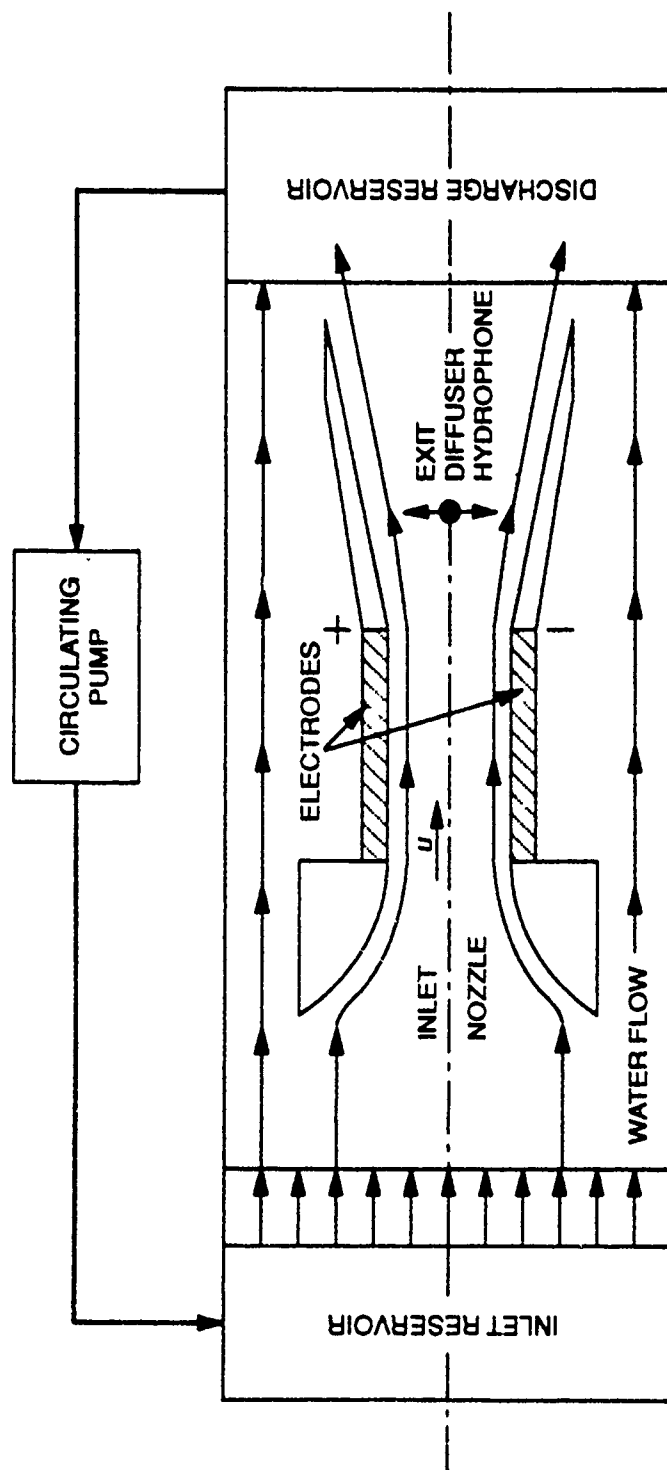
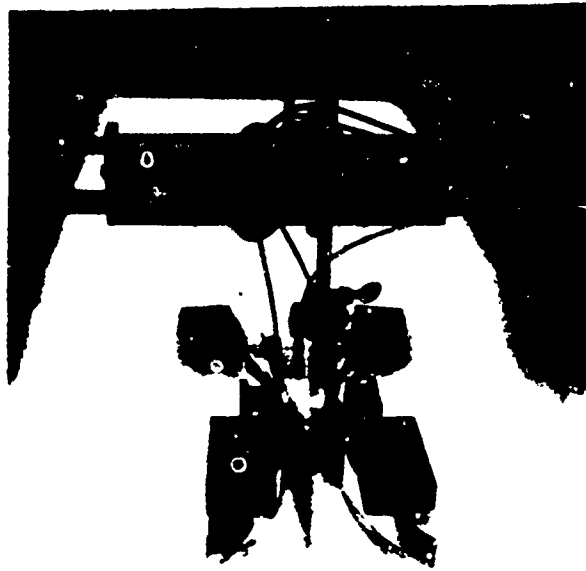
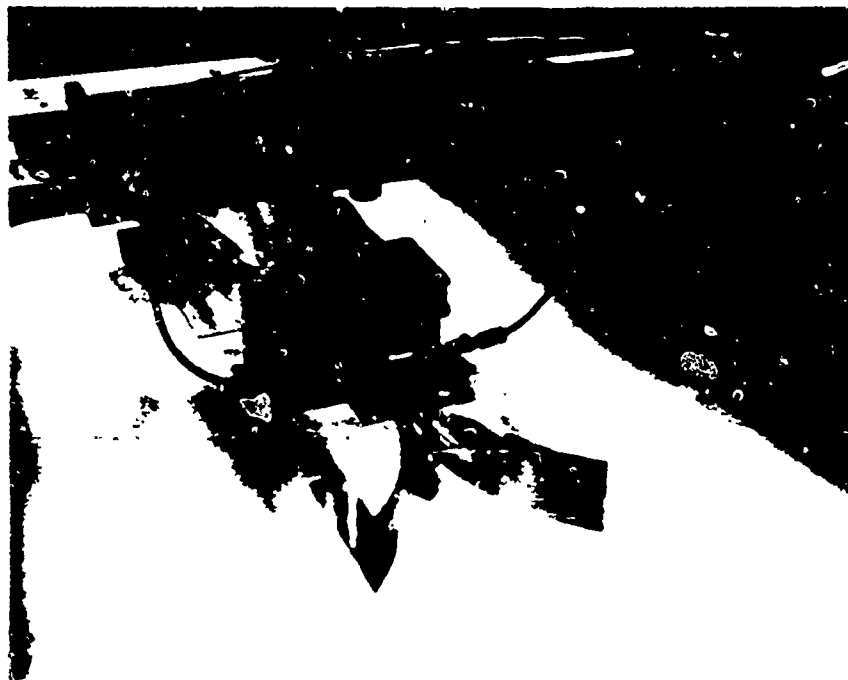


Fig. 1. Schematic of the test set-up for the open-top channel tests.



(a) Open-top channel.



(b) Fully enclosed channel.

Fig. 2. Photographs of the open-top and closed channel configurations.

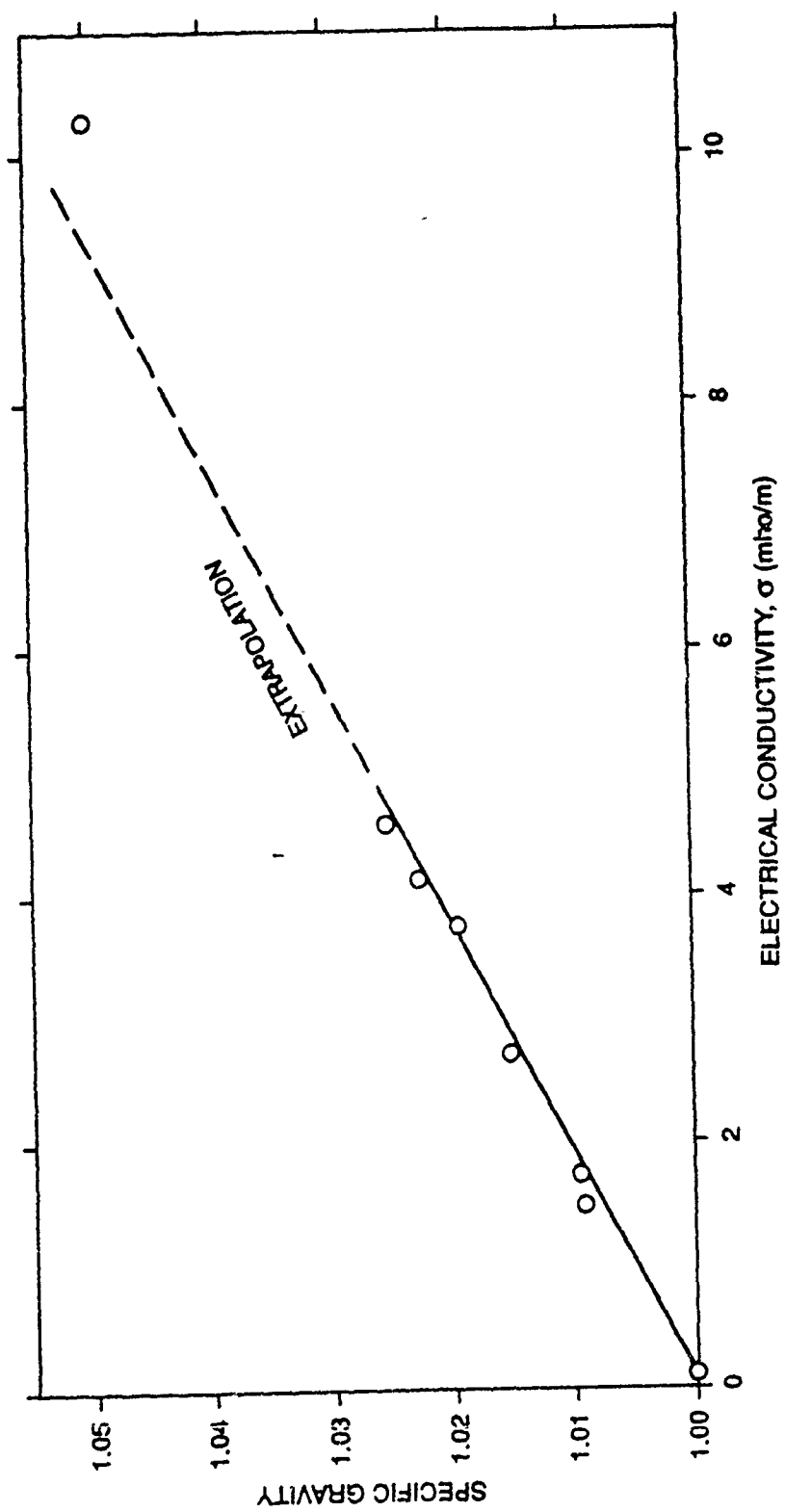


Fig. 3. Variation of measured electrical conductivity with specific gravity for simulated sea water.

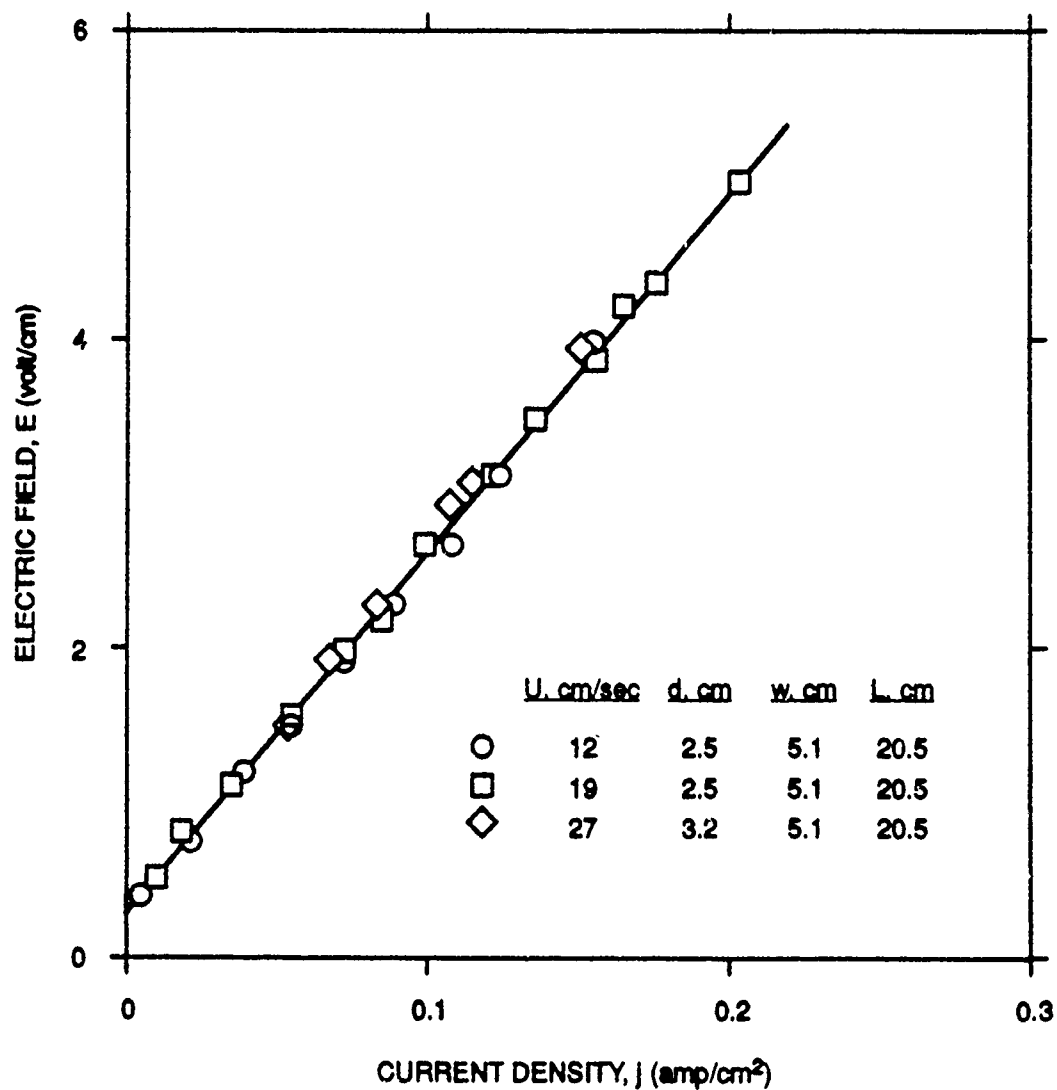


Fig. 4. Current density variation with electric field for aluminum electrodes and different channel geometries.

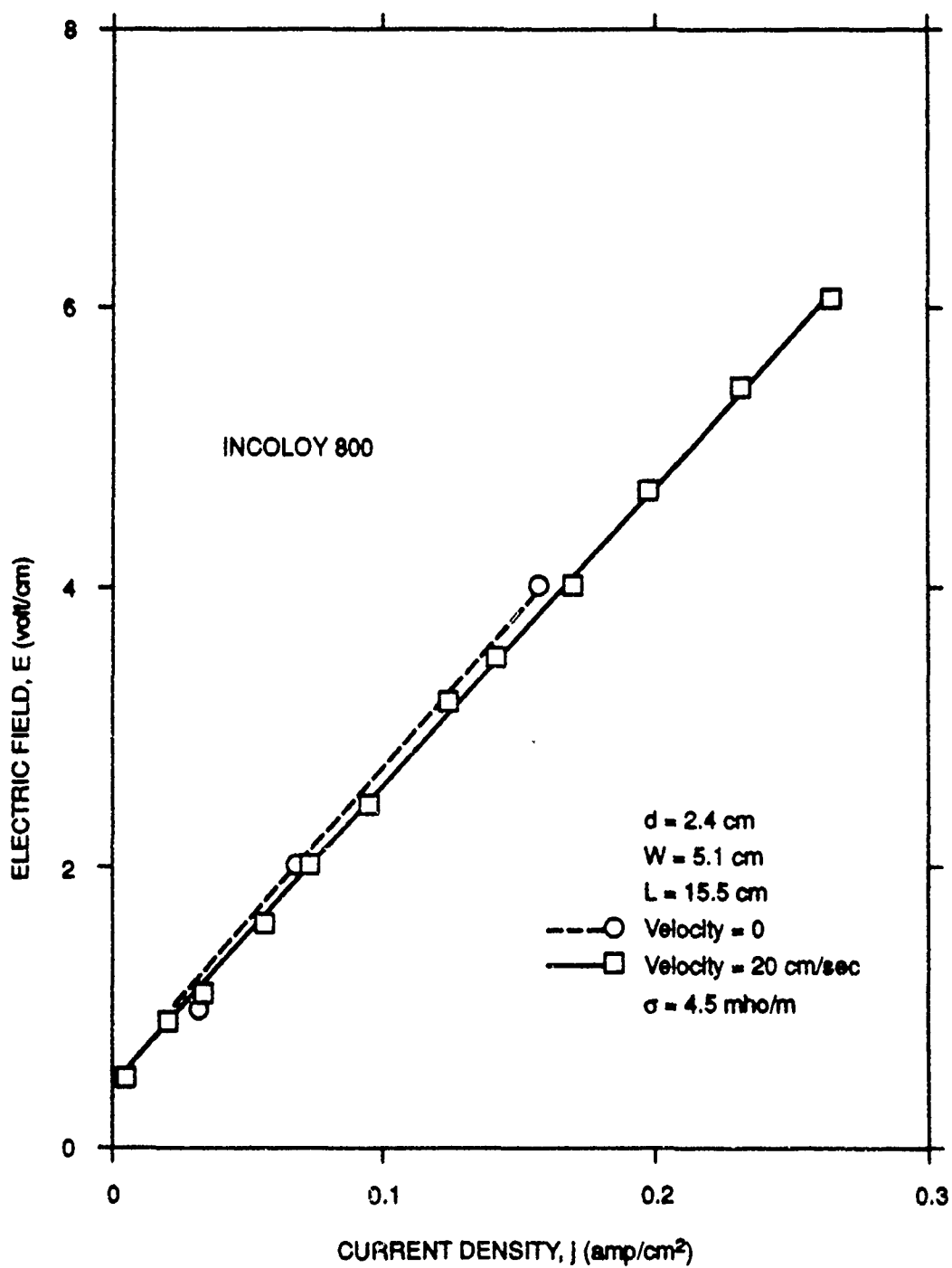
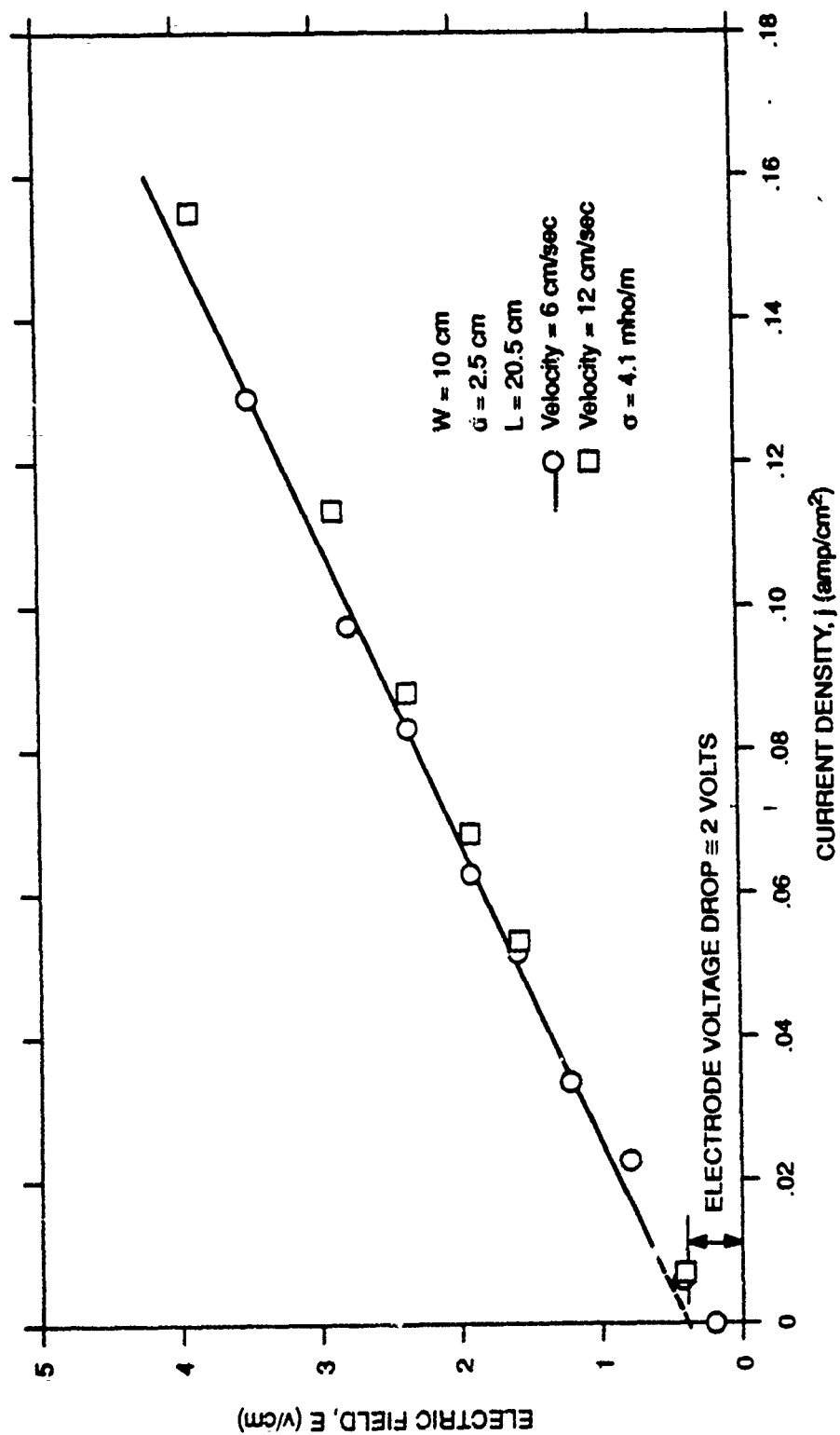
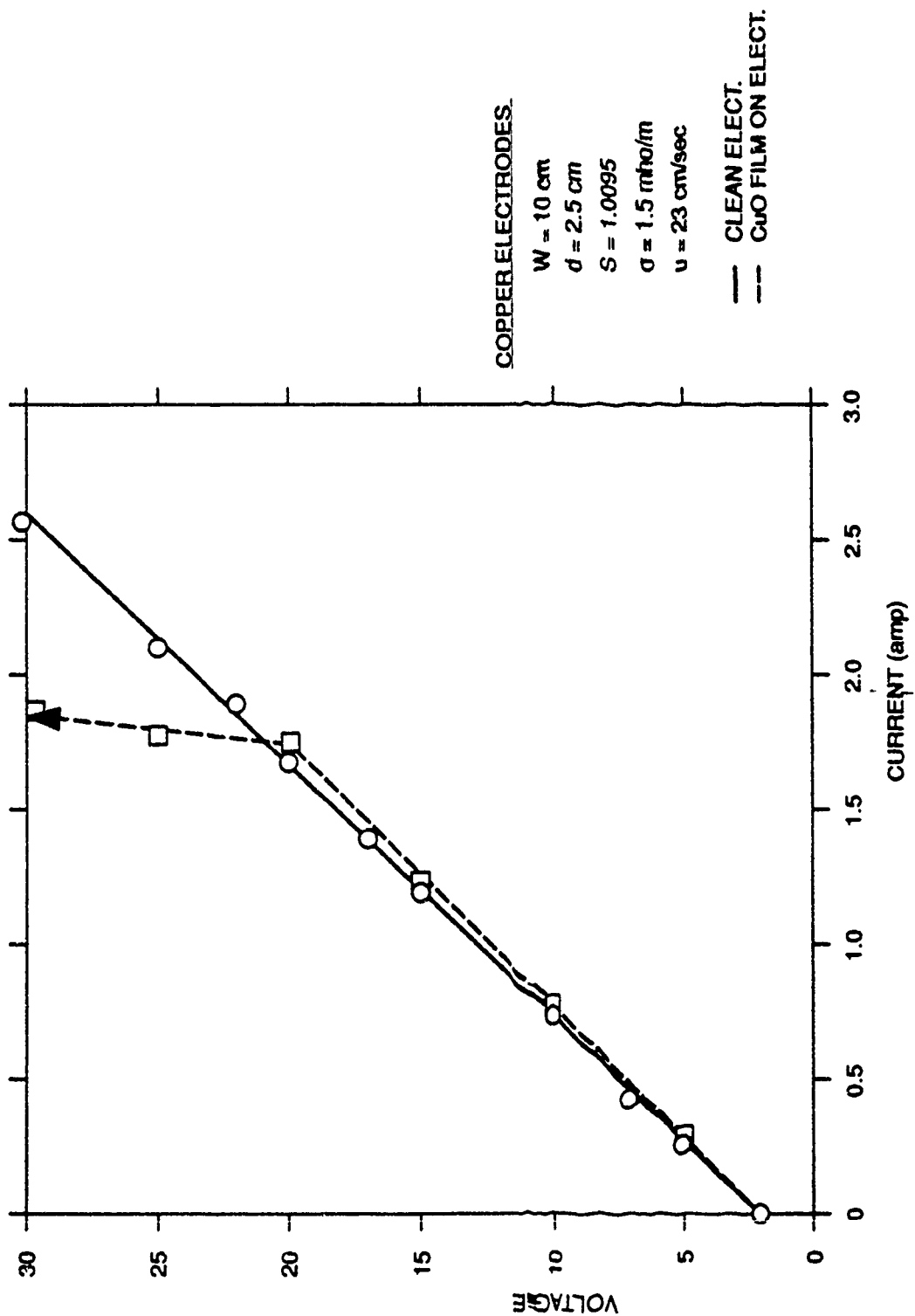


Fig. 5. Current density variation with electric field for Incoloy 800 electrodes at zero velocity and at 20 cm/sec.



(a) Current density variation with electric field with clean electrodes.

Fig. 6. Electric characteristics of copper electrodes in an open-top channel.



(b) Effect of copper oxide corrosion film on anode surface.

Fig. 6. (Continued)

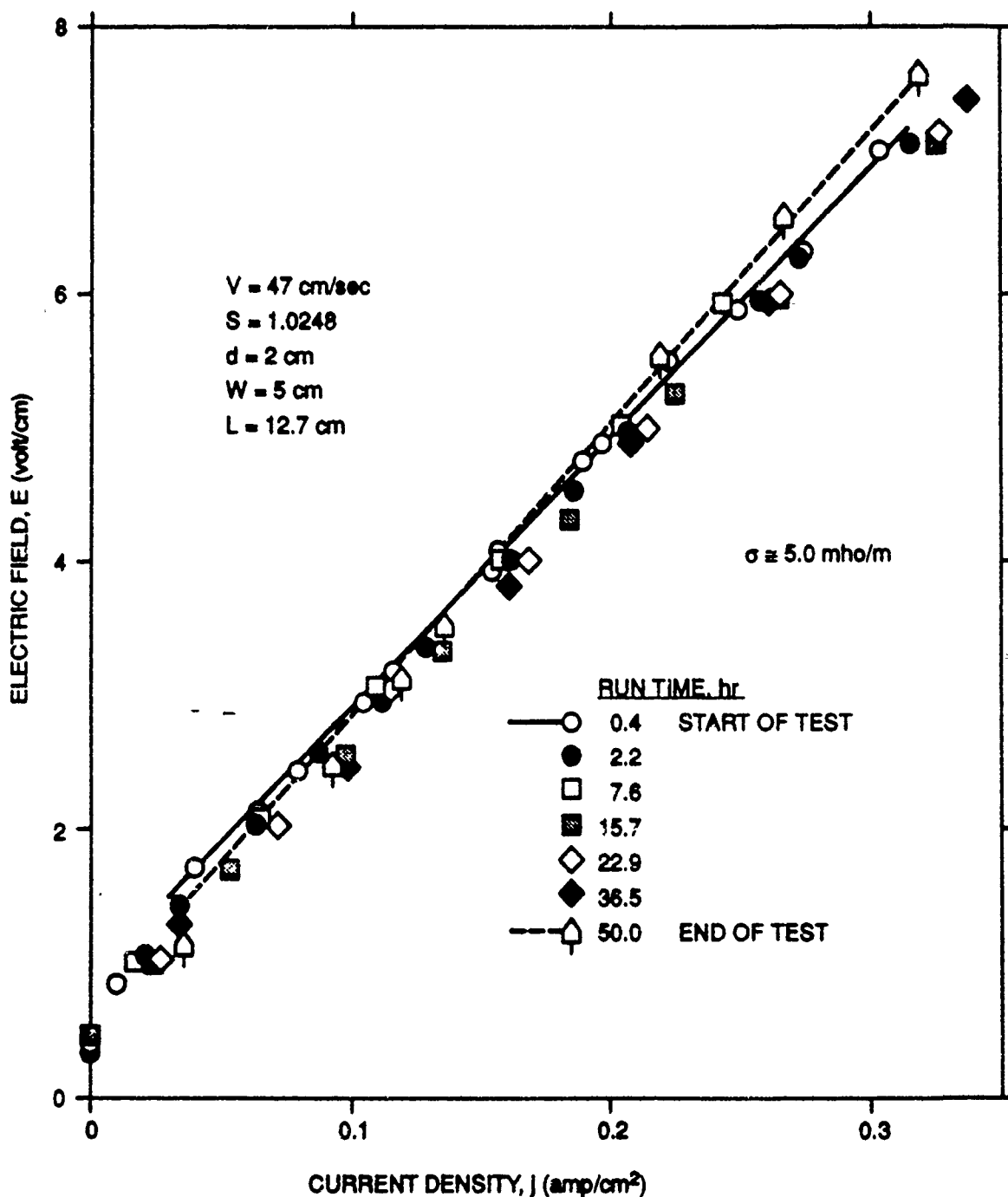


Fig. 7. Current density variation with electric field for Eltech electrodes (ruthenium dioxide coating on a titanium substrate).

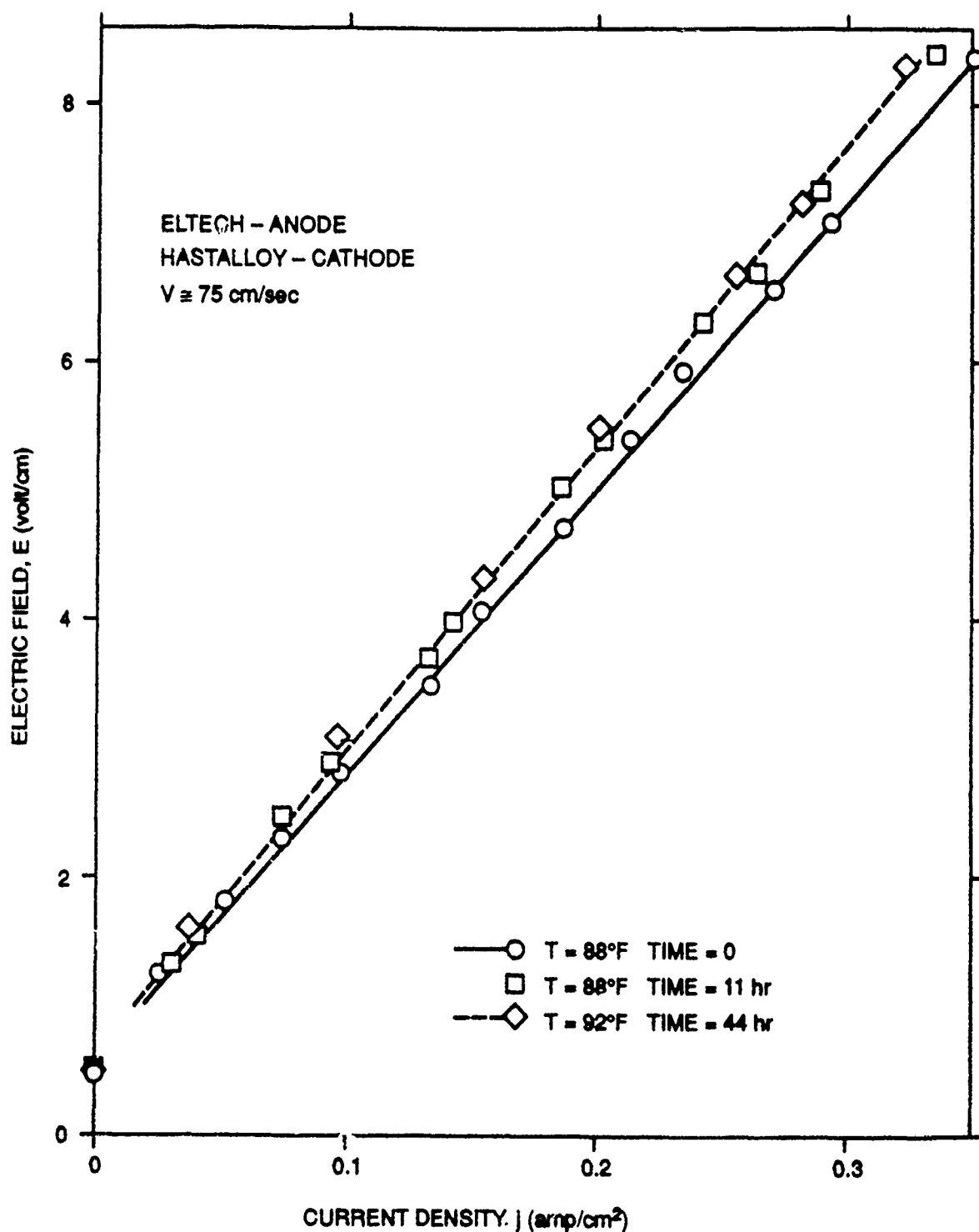


Fig. 8. Current density variation with electric field for an Eltech anode and a Hastalloy C cathode.

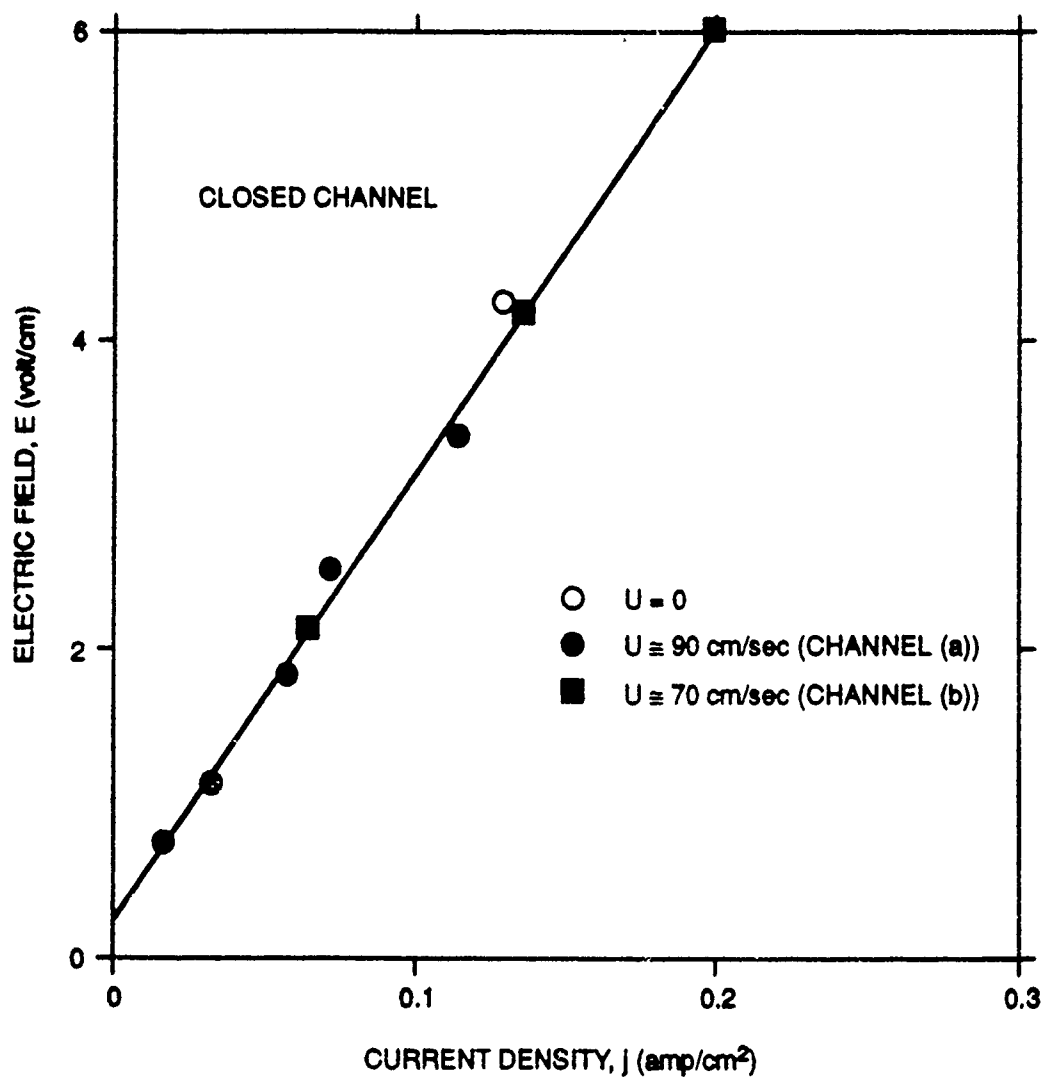


Fig. 9. Current density variation with electric field for an enclosed channel with aluminum electrodes.

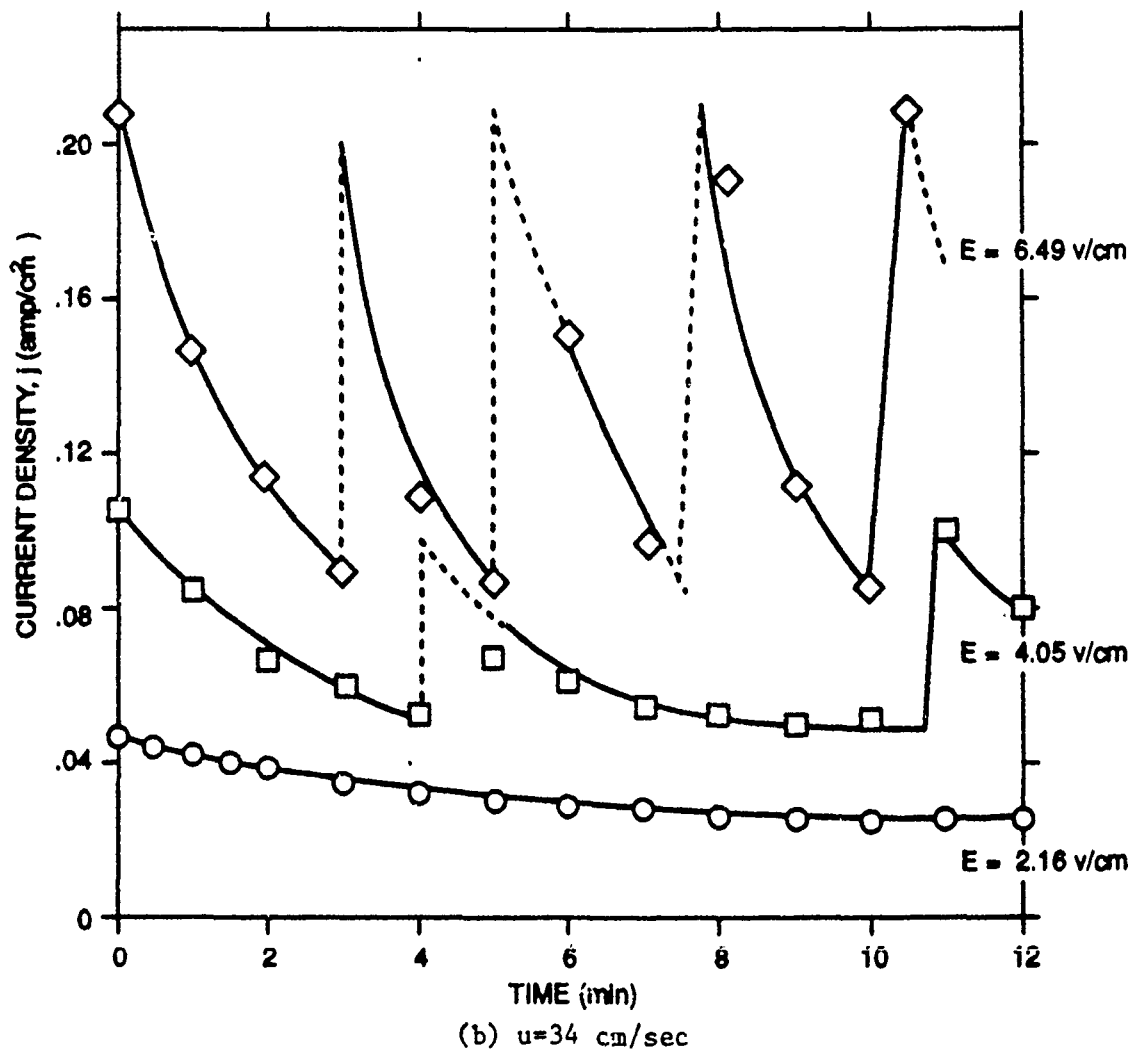
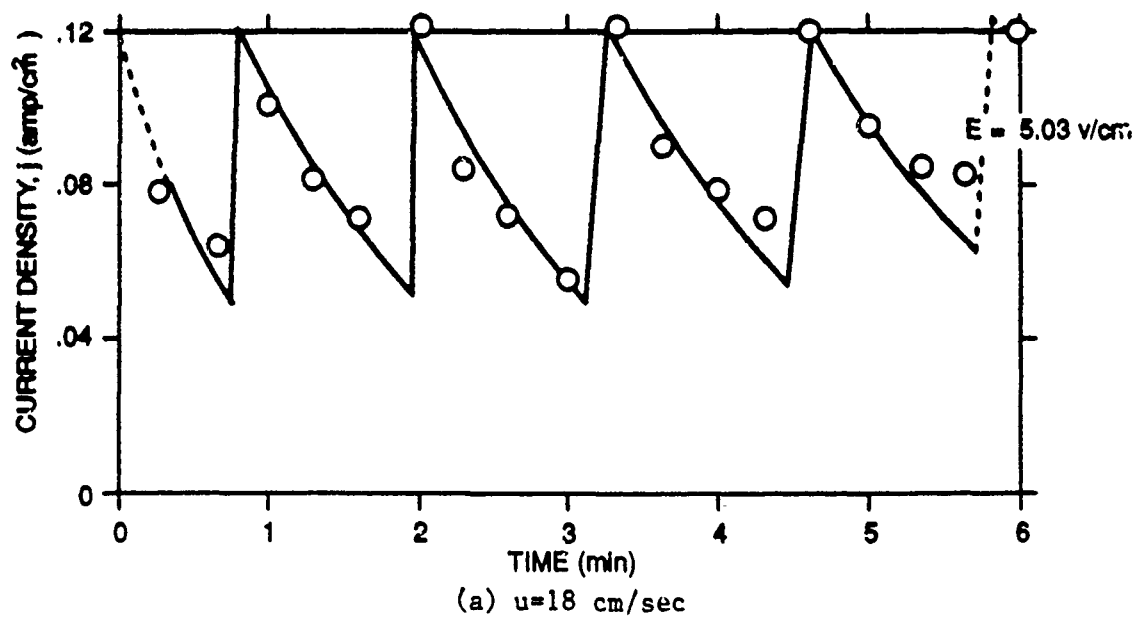


Fig. 10. Time variation of the current density in an enclosed channel with a horizontal top wall in the exit diffuser.

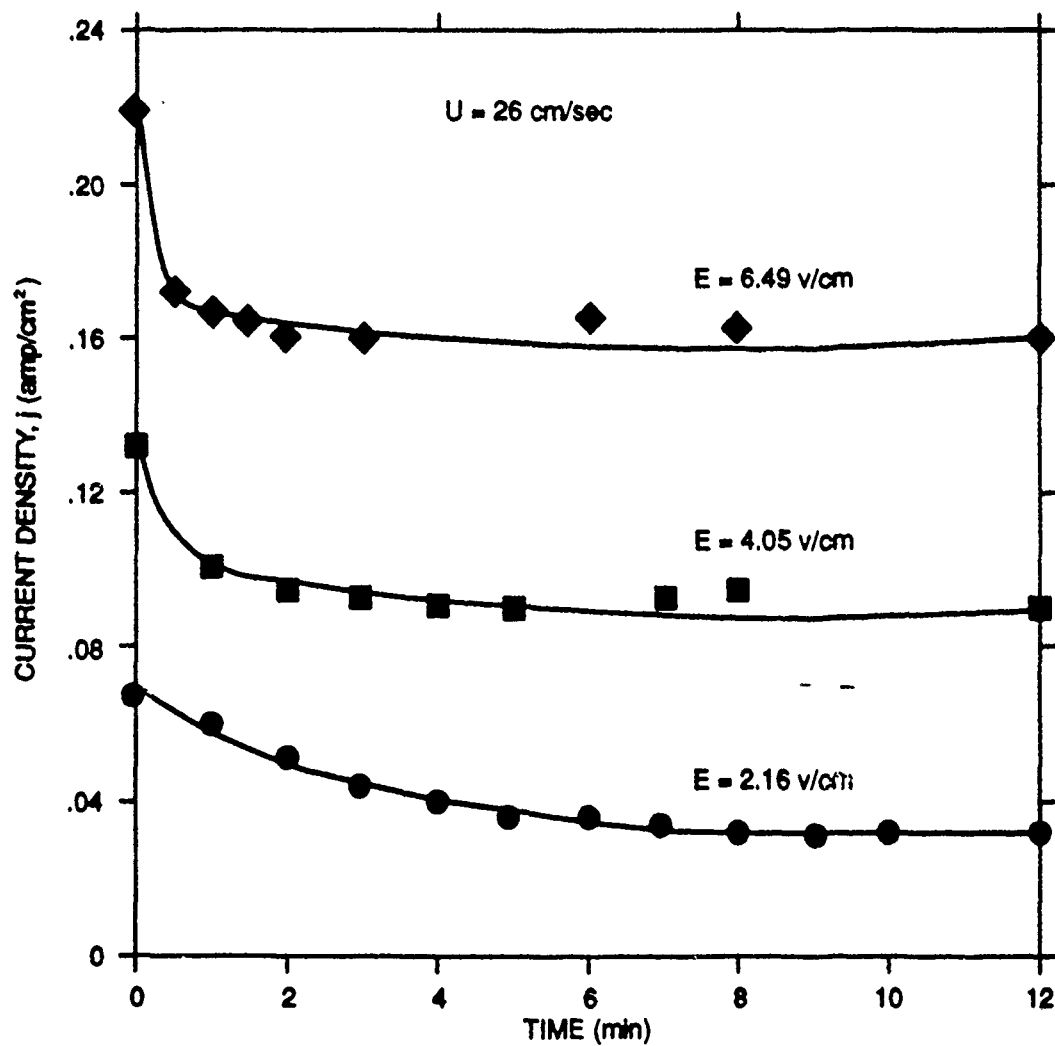


Fig. 11. Time variation of the current density in an enclosed channel with a 2° diverging top wall diffuser.

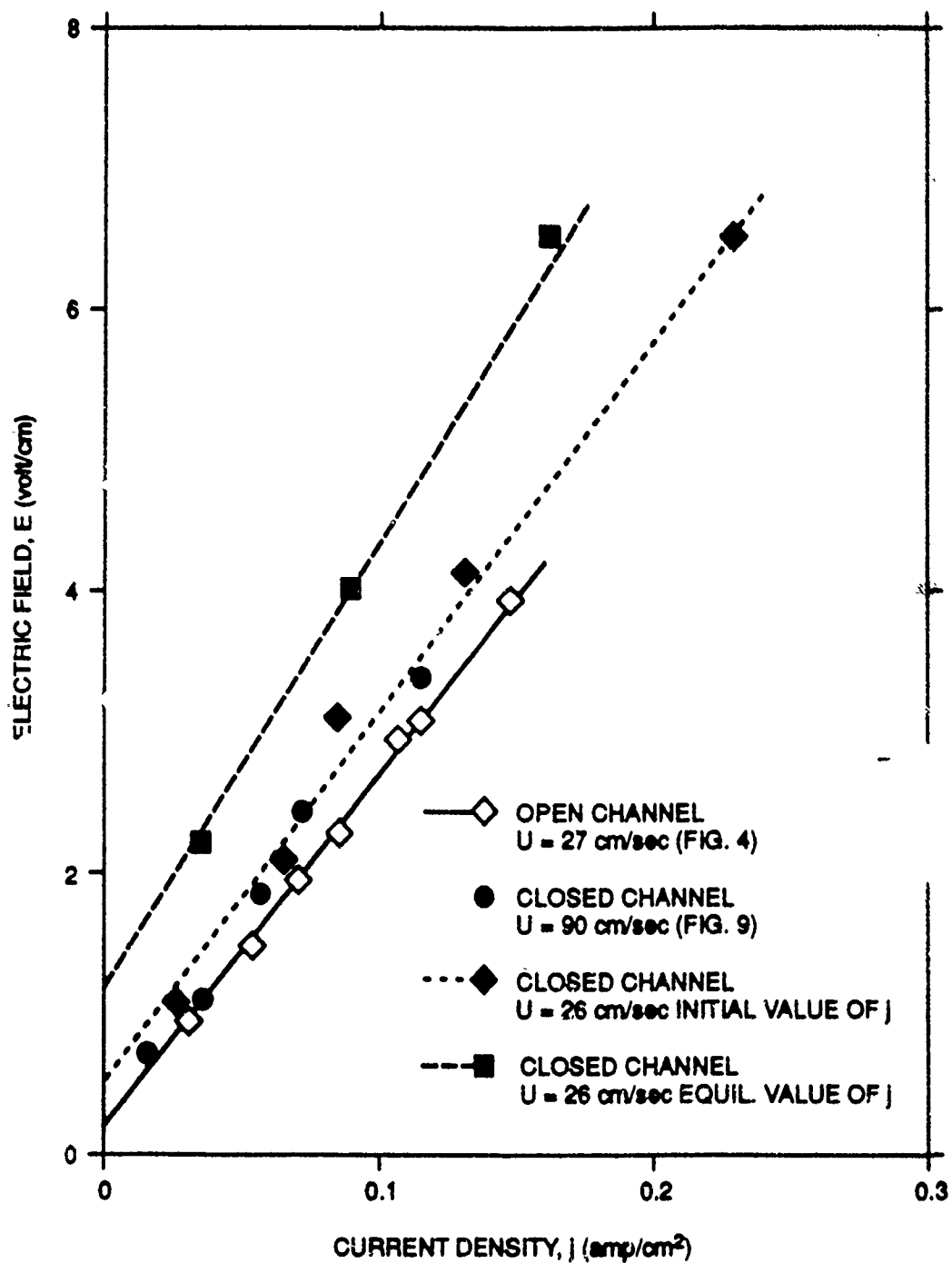
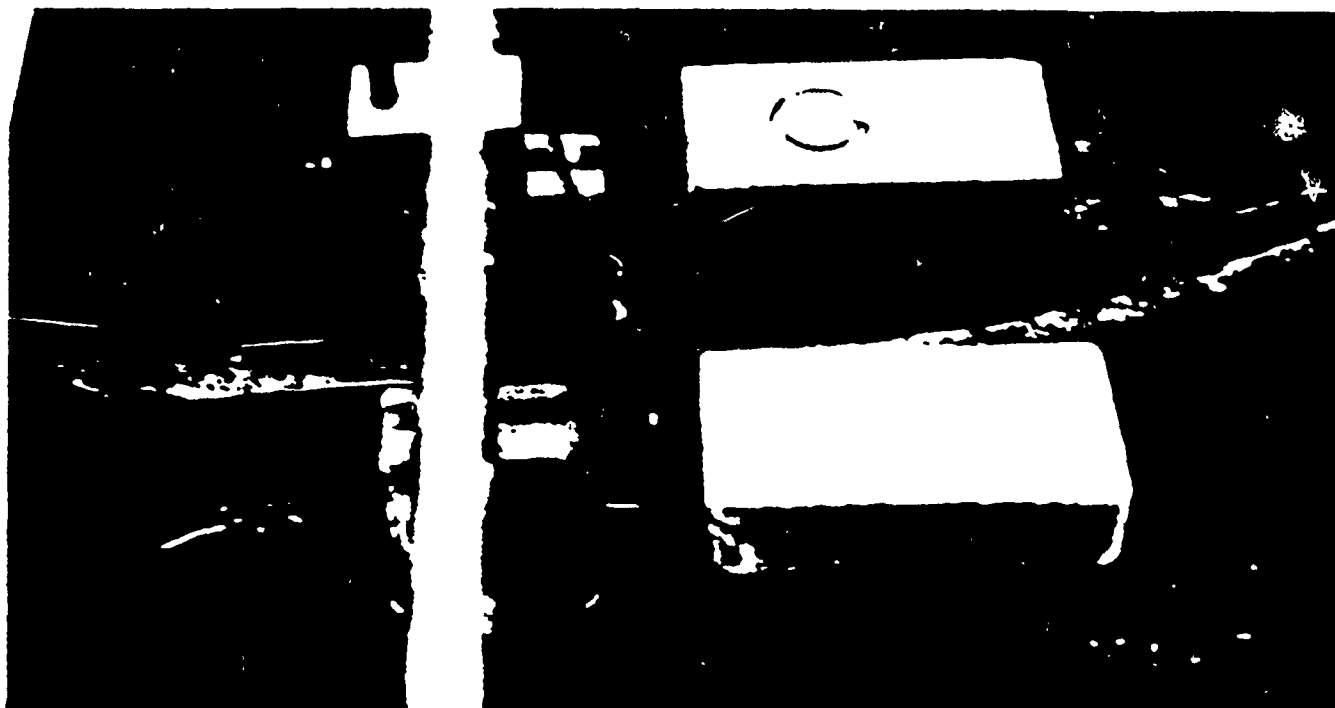
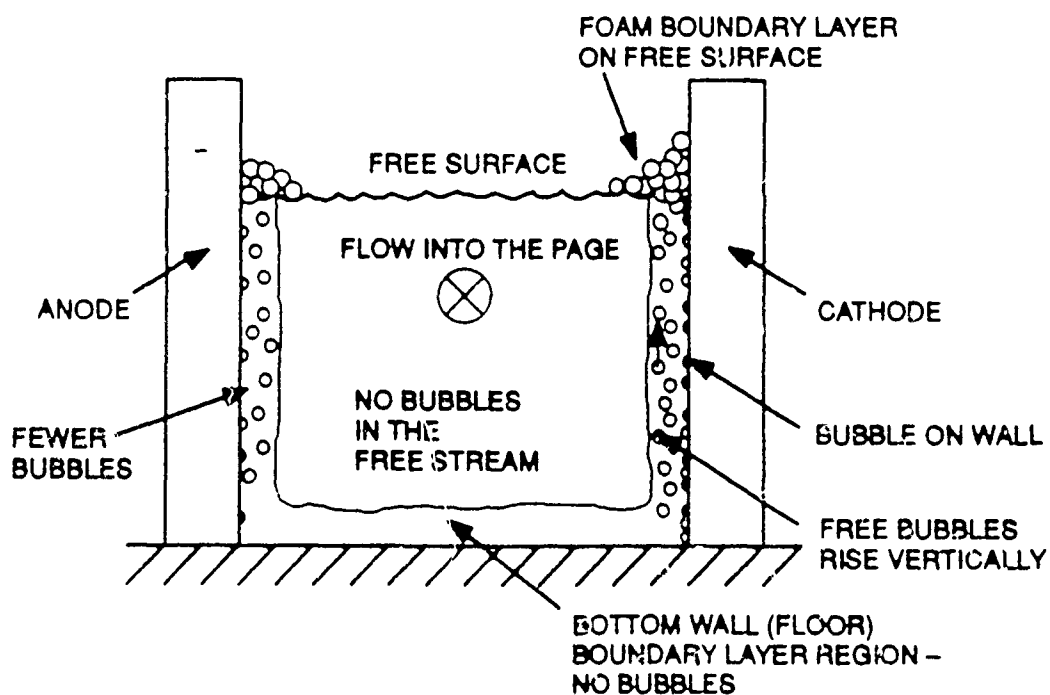


Fig. 12. Current density variation with electric field for an enclosed channel at various run conditions.

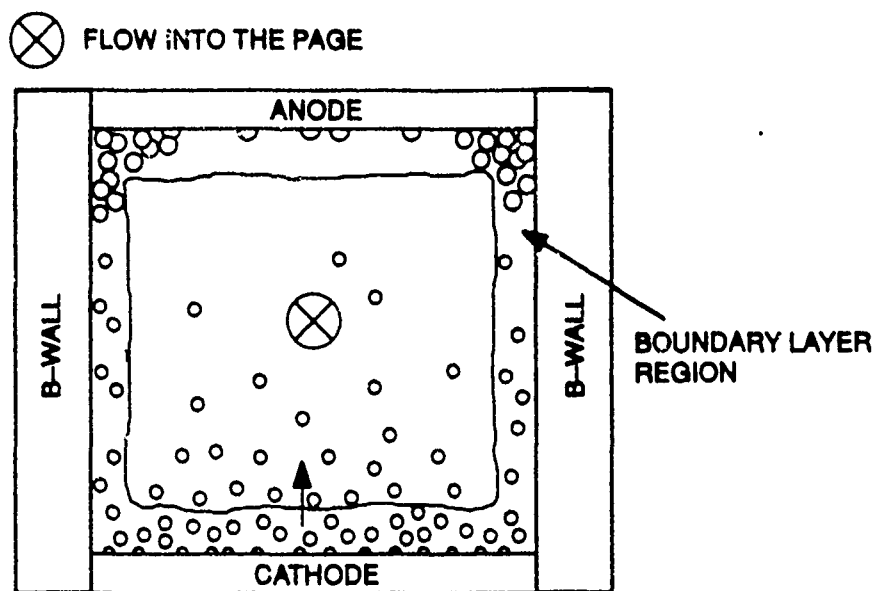


(a) Photo of surface foam on the cathode wall.

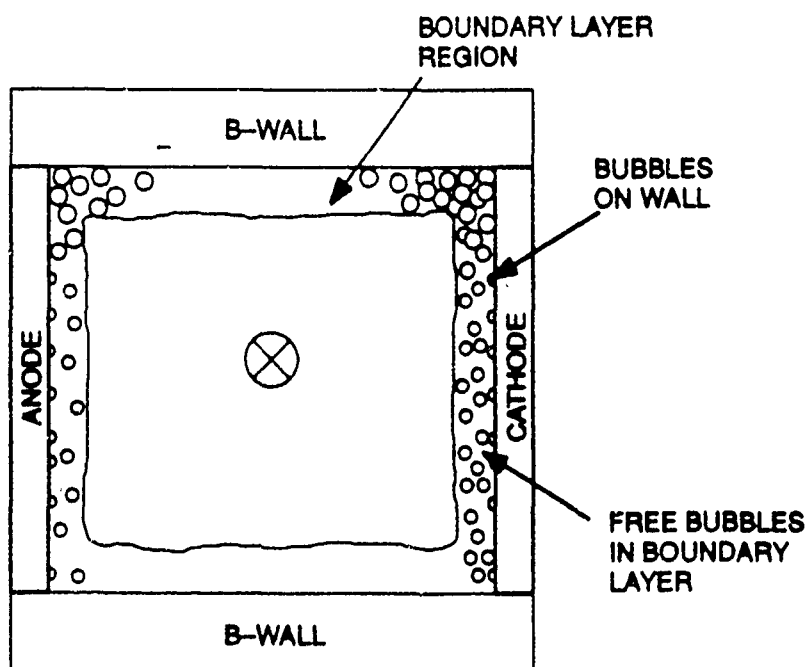


(b) Cross-sectional sketch of the bubble movement pattern.

Fig. 13. Hydrogen bubble dynamics in an open-top channel.



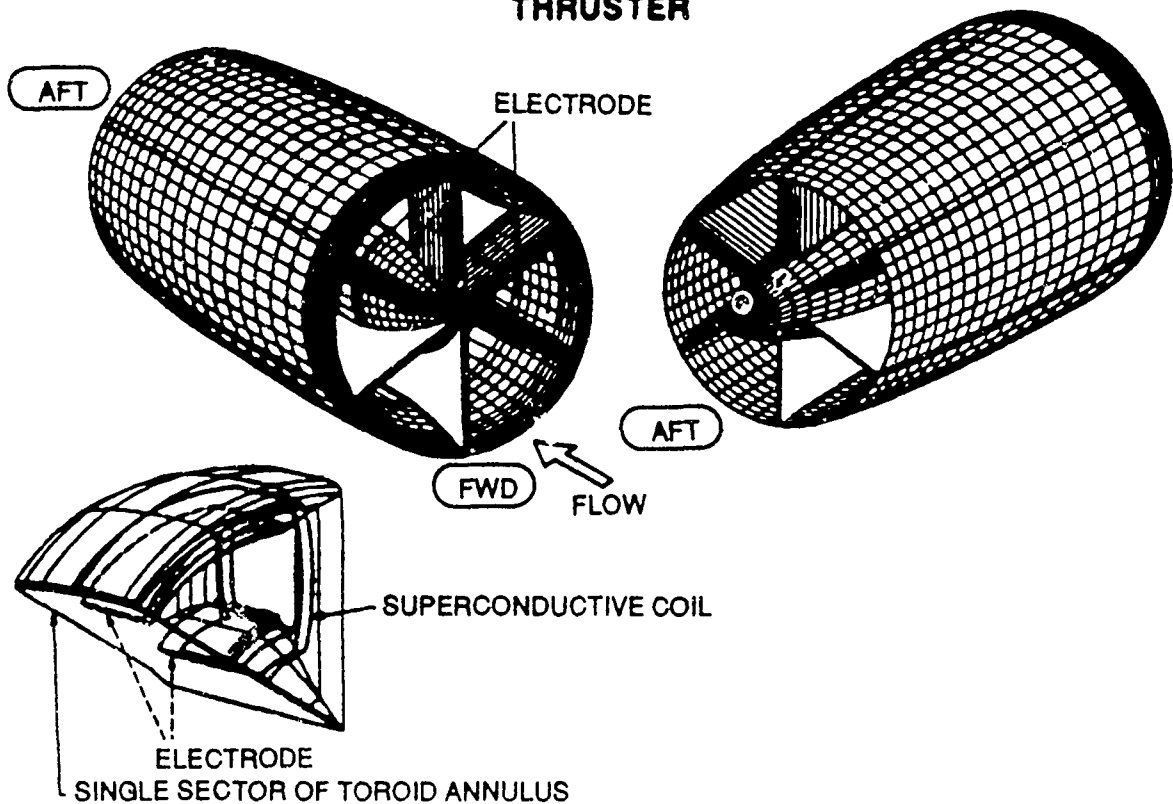
(a) Cathode floor and anode ceiling.



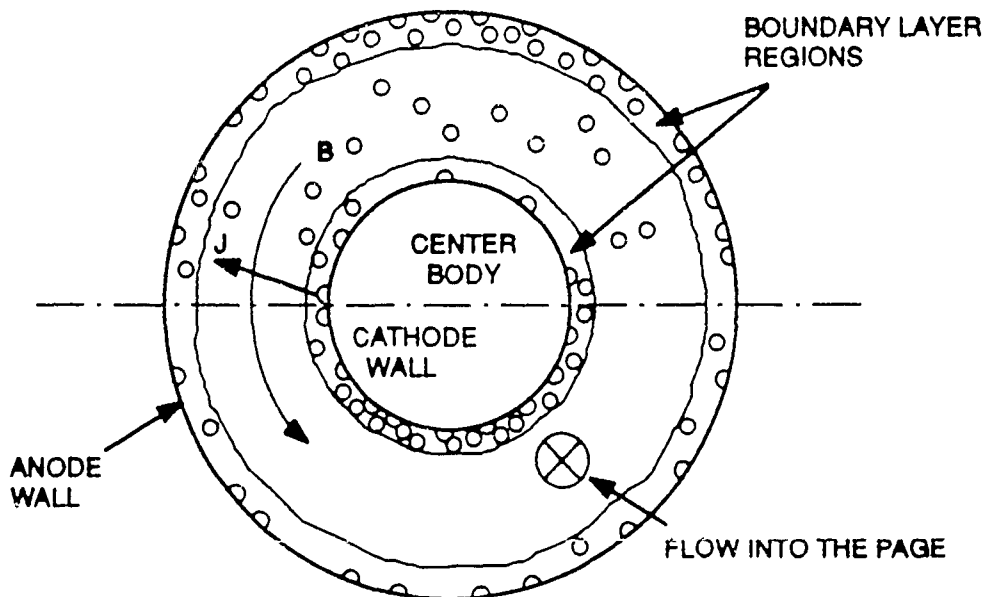
(b) Electrodes on the sidewalls.

Fig. 14. Hydrogen bubble dynamics in a closed channel with different electrode orientations.

TOROID ANNULUS THRUSTER



(a) Sketch of the toroid configuration (taken from ref-).



(b) Prospective bubble pattern with a toroid annulus thruster.

Fig. 15. Annular toroid configuration.

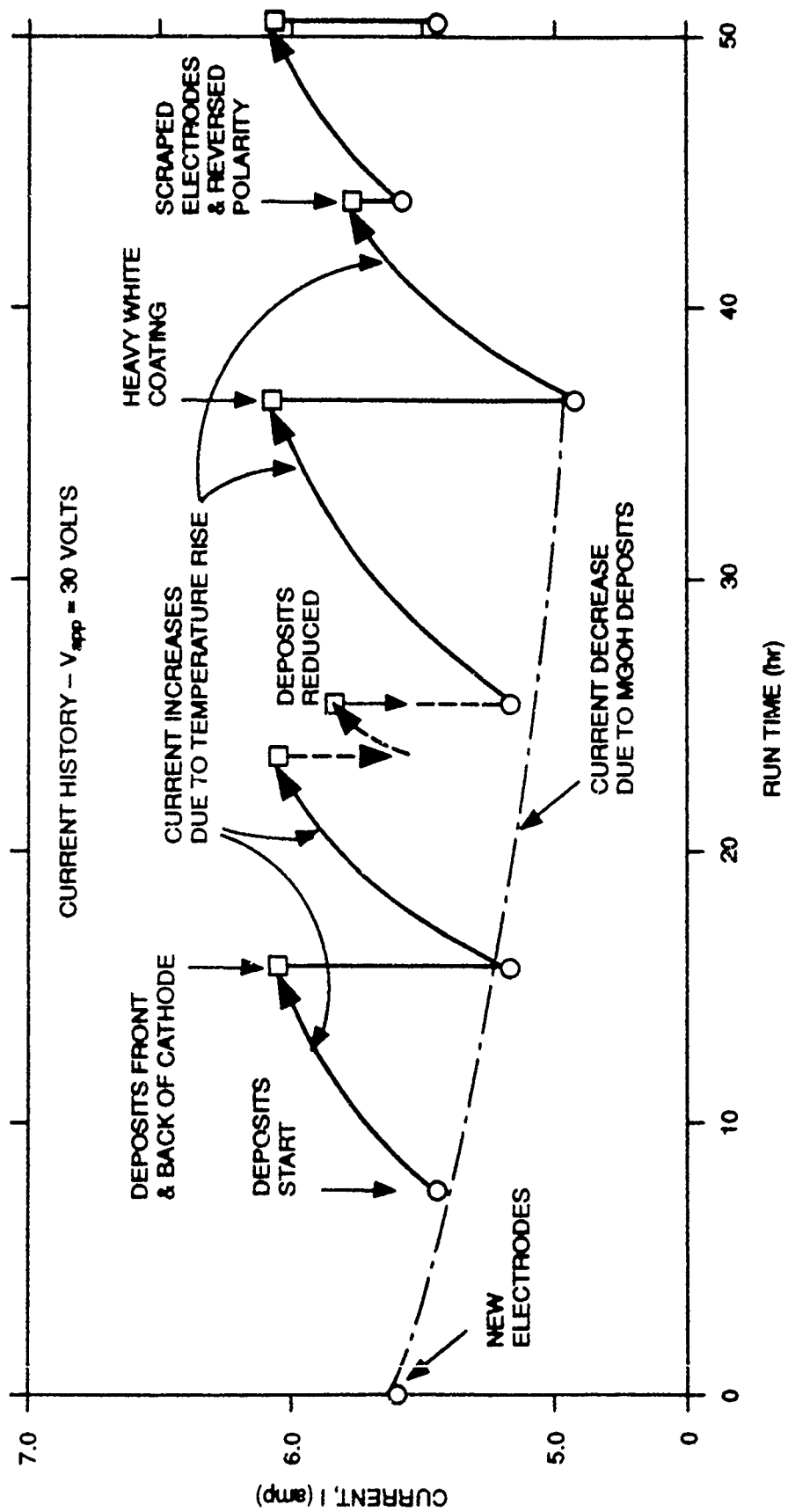


Fig. 16. Current history over a 50-hour test of Eltech anode and Eltech cathode.

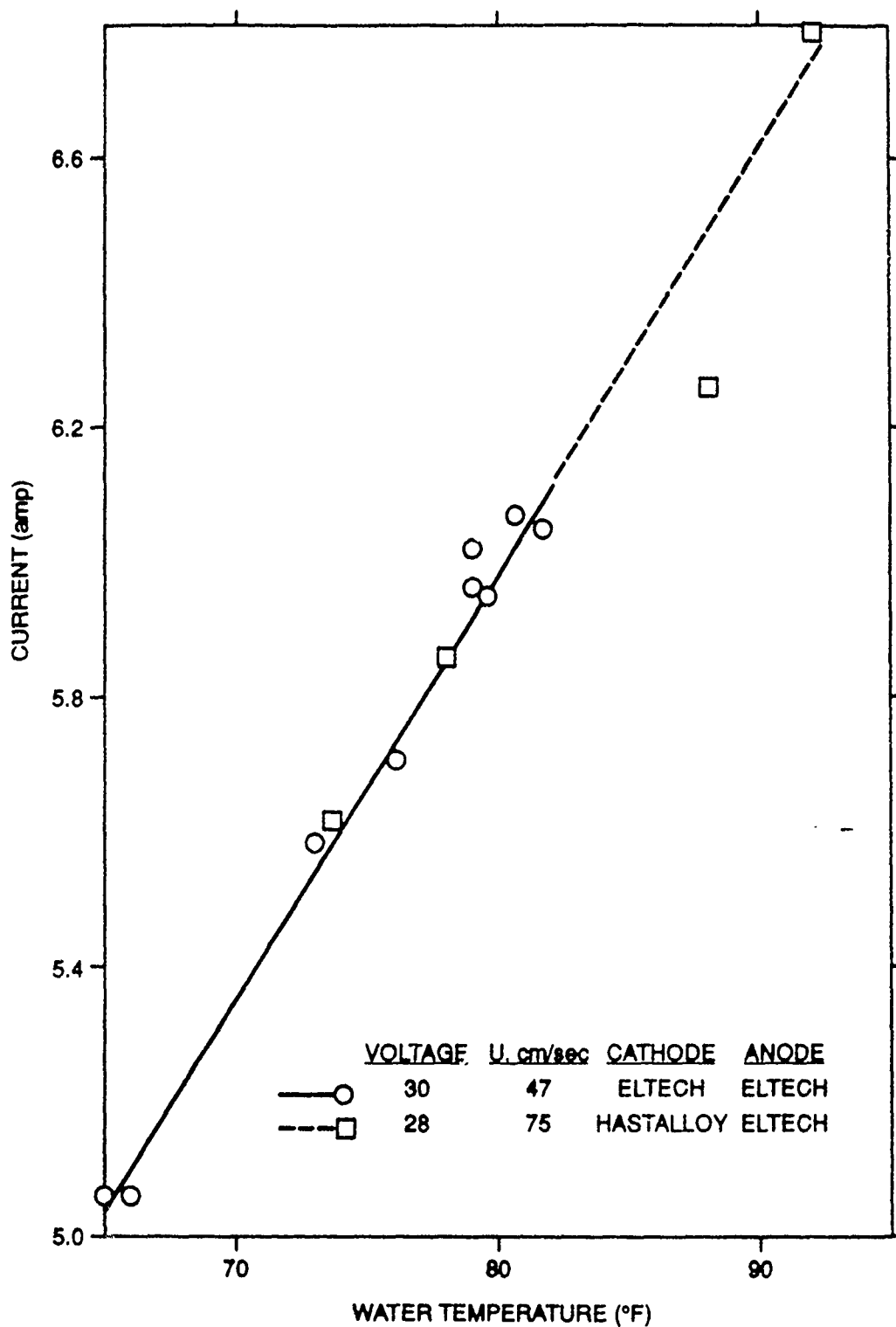


Fig. 17. Variation of electrode current with water temperature during long-duration tests.

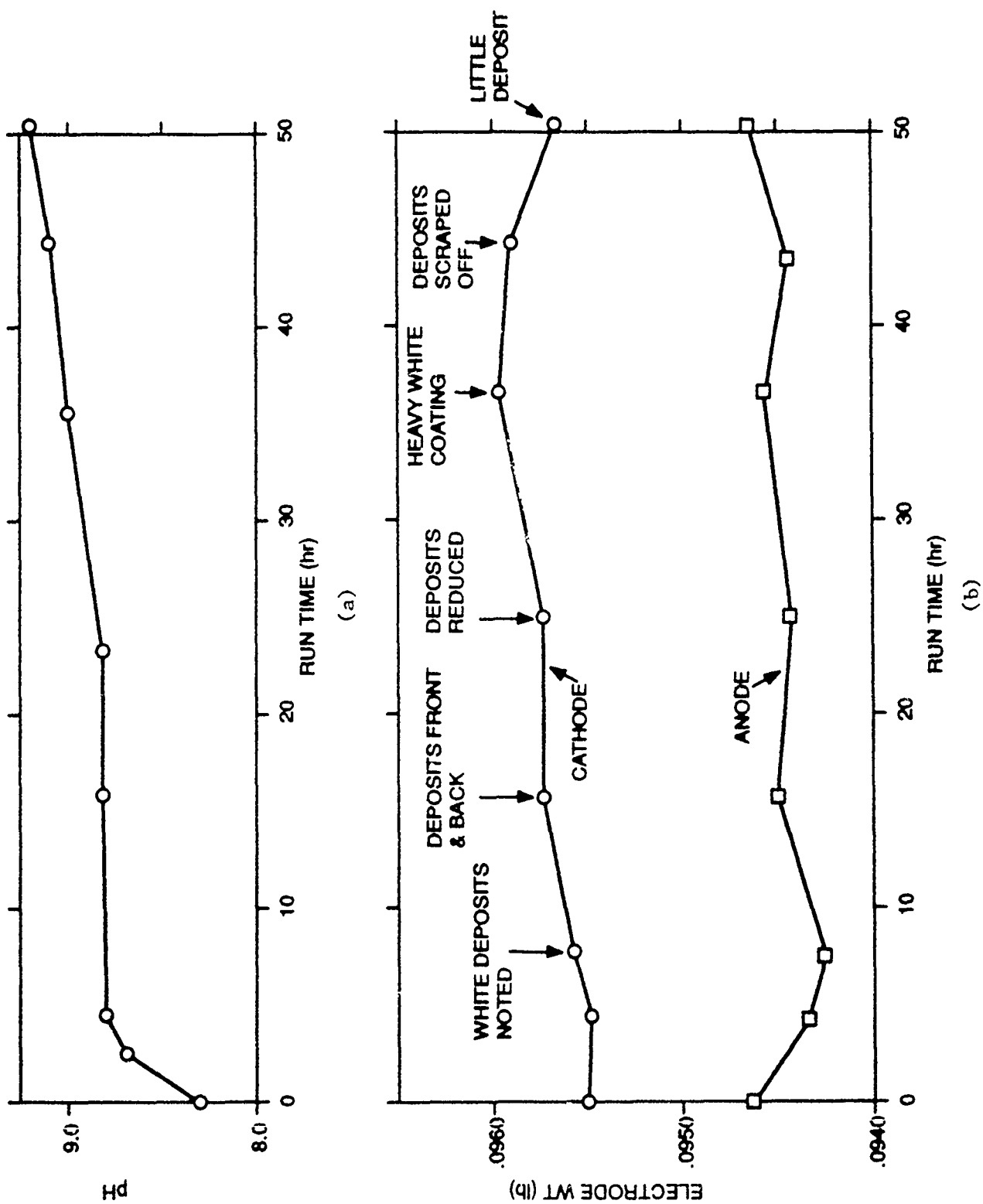
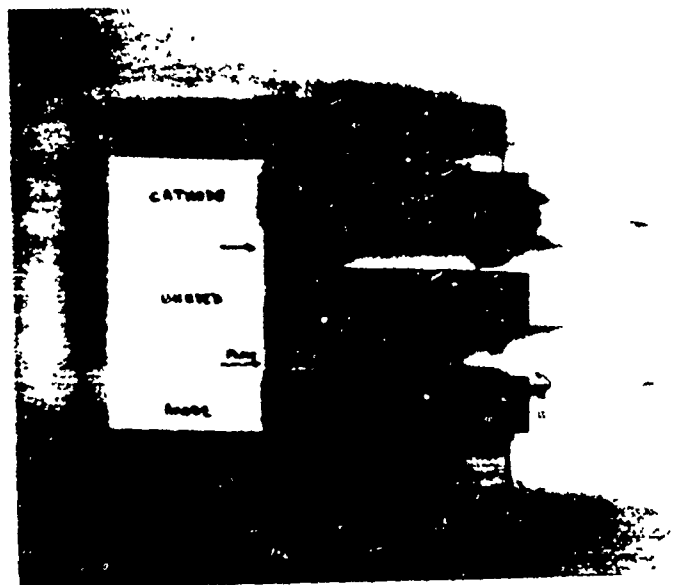
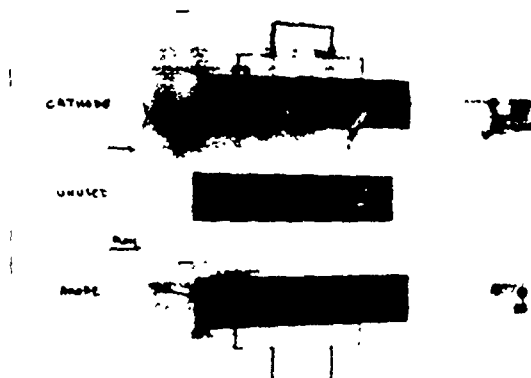


Fig. 18. Some results of long-duration testing.



(a) After 15.5 hours of testing

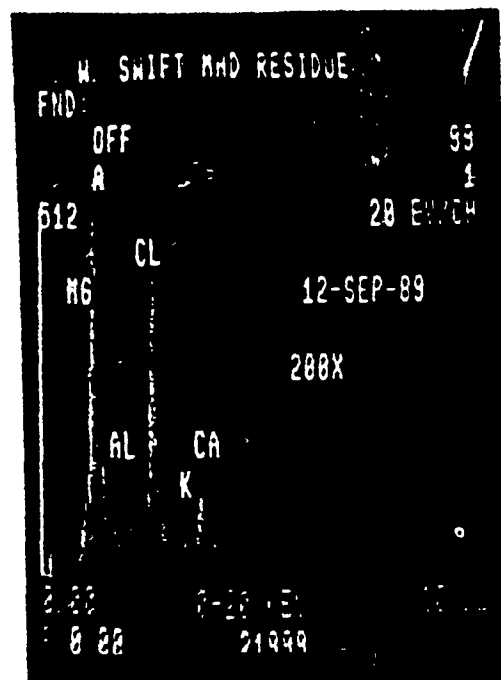


(b) After 36.3 hours of testing

Fig. 19. Photos of Eltech electrodes during 50-hour test.

APPENDIX A - CHEMICAL ANALYSIS OF CATHODE DEPOSIT

Bill Swift		white	
fa=1k	95357	material	
0.07	9/13/89		
2Theta	d	I	ID
11.5	7.741	22vd	m(100)
18.83	4.730	11d	h(90)
20.5	4.347	10vvd	
23	3.878	10vvd	m
26.4	3.385	4	ca(100)
27.3	3.275	2	ca
29.5	3.035	21s	cc(100)
33.15	2.708	5s	ca
34.8	2.583	23d	m
36.12	2.491	7s	ca
38.1	2.366	45	h(100)
39.45	2.288	25d	m,cc
40.6	2.226	3	
41.2	2.195	4	ca
43.2	2.097	5	cc
46	1.976	8d	ca
46.45	1.958	3	m
47.1	1.932	6	
47.5	1.917	7	cc
48.25	1.889	6	ca
48.6	1.876	6	cc
50.25	1.818	8du	ca
50.8	1.800	13vdu	h
53.05	1.728	7s	ca
58.75	1.573	25d	h
50.1	1.541	14vdu	
60.73	1.527	28d	m
61.55	1.508	18ud	m
62.05	1.497	27	h
h=Mg(OH)2 JCPDS 7-239			
m=Mg6Al2(OH)18(4.5H2O) 35-965 type			
cc=CaCO3 calcite 5-0543			
ca=CaCO3 aragonite 5-0453			
d=diffuse diffraction line			
vs=very; u=unresolved line			
s=sharp line			



Comments

XRD-
Major: Mg(OH)2,
Mg6Al2(OH)18(4.5H2O) type phase as per
JCPDS 35-965. note there are several
phases which have similar patterns to the above as
Mg6Al2CO3(OH)16(4H2O) JCPDS 14-191, and Al(OH)3
is possible.
An amorphous phase(s) also present
Minor: CaCO3 calcite and aragonite forms detected
note: Ca(OH)2, NaCl, CaCl2, MgCl2 not detected
The amorphous phase(s) maybe the chloride
containing component.

SEM-EDX-
Mg>Cl>>Ca,Al>K

THIS PAGE IS INTENTIONALLY BLANK

CONDUCTIVITY ENHANCEMENT OF SEAWATER

Presented by

Chris Young

CONDUCTIVITY ENHANCEMENT OF SEAWATER

Presented by
Chris Young

15 November 1989

Conductivity Enhancement of Seawater

MHD propulsion methods using seawater as the conducting medium has always been plagued by low efficiency estimates. This has largely been blamed on the lack of high magnetic fields but the root of the problem is the inherent low conductivity of seawater. The literature in the area of conductivity enhancement of seawater is all but nonexistent and one may well ask oneself why you would consider enhancing the conductivity of seawater apart from MHD applications.

Efficiency of Conductive MHD Propulsion

To get an understanding of the importance of conductivity enhancement, one must first look at the efficiency equation describing this process. The efficiency can be written in terms of the product of five contributing efficiencies or inefficiencies. The first efficiency is the efficiency related to the coupling of the momentum in a water jet to the surrounding medium to produce thrust. This factor is the limiting factor for all related jet propulsion mechanisms including propellers. The second efficiency is related to the conversion of electrical input power to a Lorentz force acting on the water. This term takes into account the fraction of the input energy which goes into joule heating of the conducting fluid. The third term in the efficiency equation relates the conversion of the Lorentz forces within the MHD channel to actual water movement. Not all of the applied Lorentz force results in fluid motion because of drag losses within the channel and outside of the ship. The fourth efficiency takes into account entrance losses and the fifth factor accounts for electrochemical reactions. The losses due to electrochemical reactions are typically small compared to all other losses. In the remainder of this presentation, no further mention will be made of these electrochemical losses.

EFFICIENCY OF CONDUCTIVE MHD PROPULSION

• Total Efficiency Given by Product of Five Efficiencies

$$-\eta_1 = \frac{\text{Thrust Power}}{\text{Mechanical Power}} = \frac{2}{1 + V_2/V_1}$$

$$-\eta_2 = \frac{\text{Electromagnetic Power}}{\text{Input Power}} \quad (\text{Joule Dissipation})$$

$$-\eta_3 = \frac{\text{Mechanical Power}}{\text{Electromagnetic Power}} \quad (\text{Drag Loss})$$

$$-\eta_4 = (\text{End Zone Losses})$$

$$-\eta_5 = (\text{Electrochemical Losses})$$

The efficiencies may be combine in an equation which can be written in terms of dimensionless quantities. " U " represents the ratio of the jet velocity to the torpedo velocity. " k " represents the losses associated with drag and entrance losses. " H " is a sort of interaction parameter. Here we notice that the conductivity has found its place within this interaction parameter. The higher the conductivity, the lower the value of H . The required electric field can be found using the equation second from the bottom and the last equation gives the duct diameter.

IMPORTANT MHD EFFICIENCY EQUATIONS

- Let $\eta_0 = \eta_1 \eta_2 \eta_3 \eta_4$

$$\eta_0 = \frac{2U(U-1)}{[(1+k)U^2-1] \{U+H[(1+k)U^2-1]\}}$$

where

$$U = \frac{\text{Velocity of Stream}}{\text{Velocity of Ship}}$$

$$k = \text{Pressure loss coefficient (drag + entrance/exit losses)}$$

$$H = \frac{\rho V_s}{2L\sigma B^2}$$

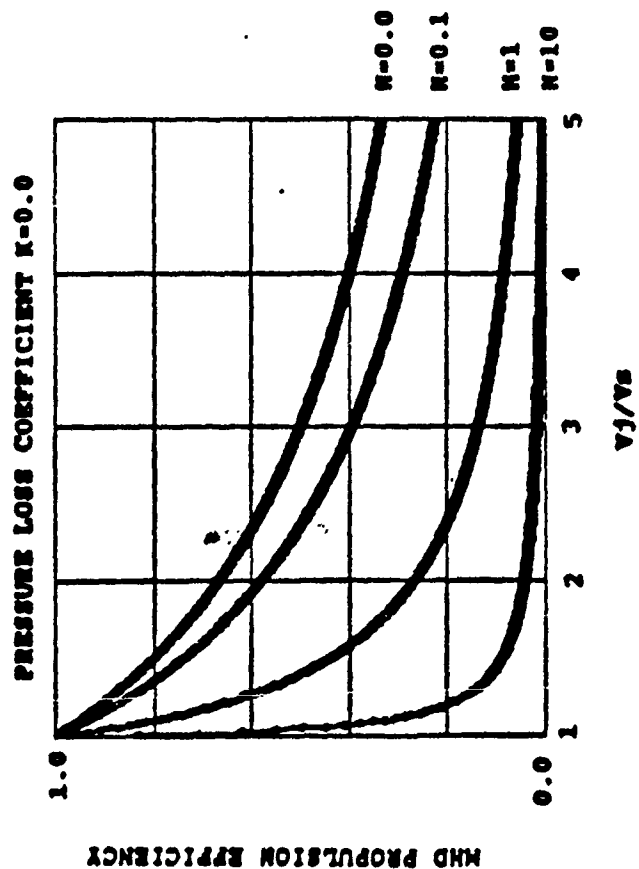
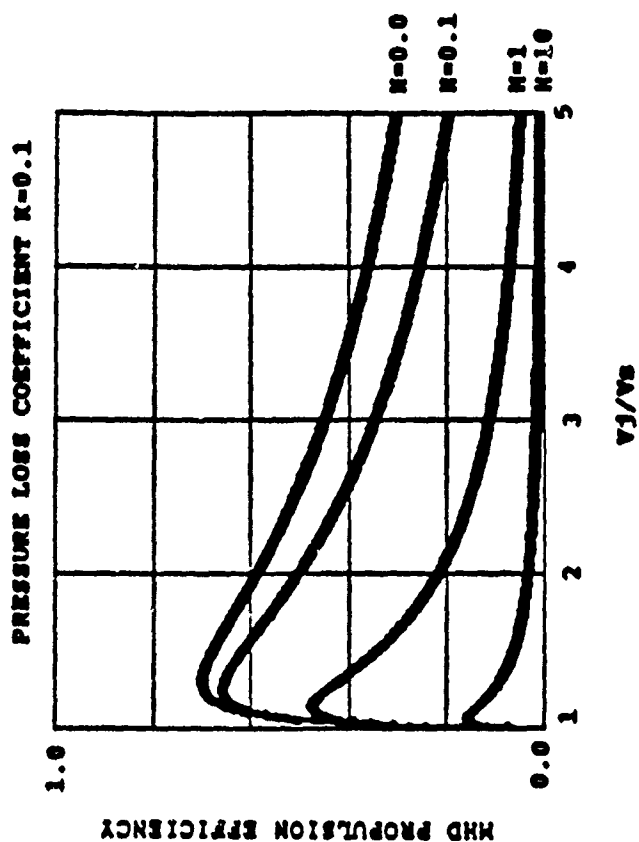
$$E = V_s B \{U + H [(1+k)U^2 - 1]\} = \text{Electric field}$$

$$D = \frac{2\sqrt{C_D} A_s}{\pi U(U-1)} = \text{Channel Diameter}$$

MHD Propulsion Efficiency

These two graphs indicate the efficiency as a function of the ratio of the jet and torpedo velocities and as a function of the factor H . The first graph is the lossless case and the second graph is a case where the loss term is assigned a value of 10%. Note that in both graphs as the value of H decreases the efficiency increases for a fixed ratio of velocities. This implies that an increase in conductivity causes an increase in efficiency.

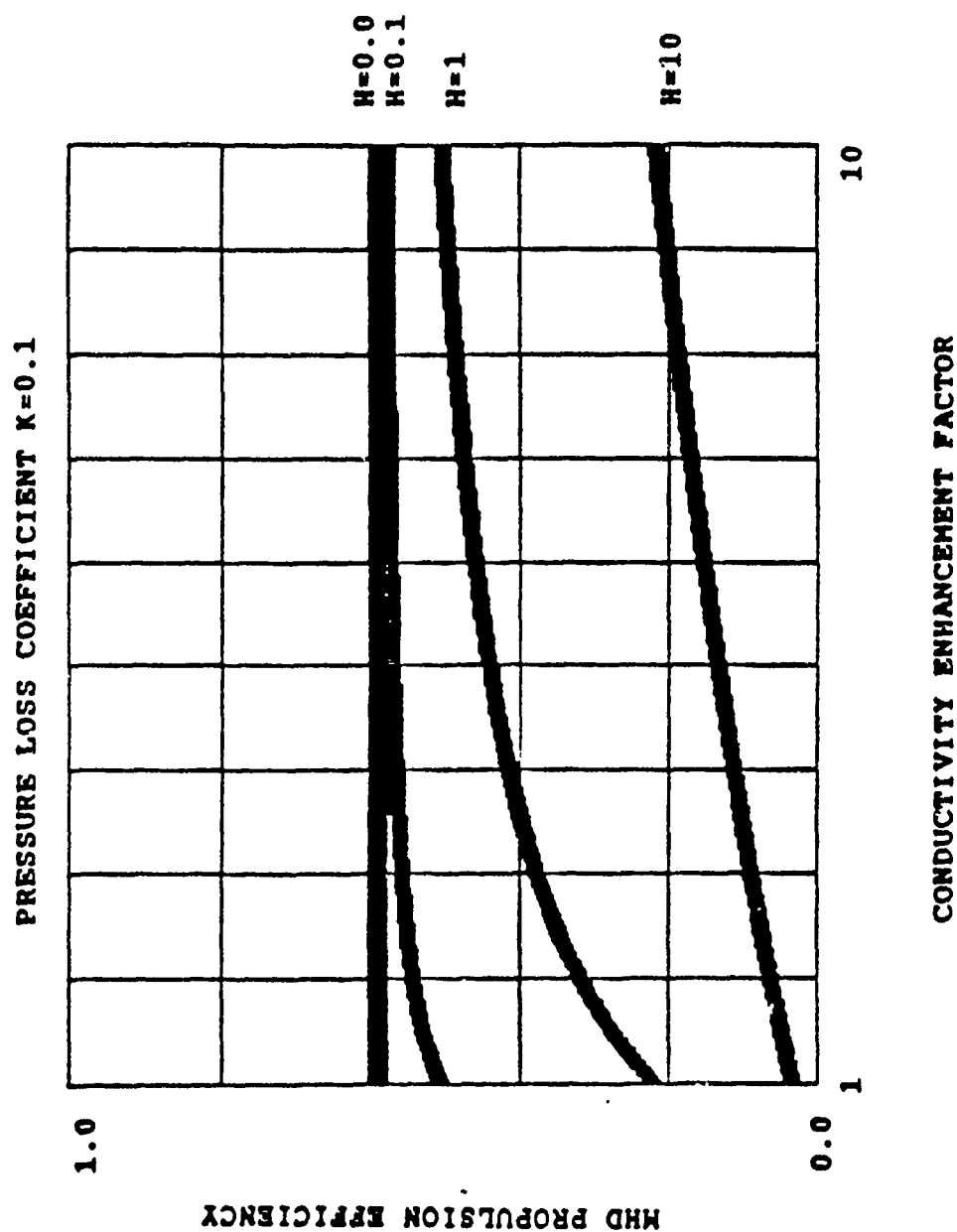
MHD PROPULSION EFFICIENCY



Efficiency vs. Enhancement Factor

If one were to plot the efficiency equation as a function of conductivity enhancement and hold the ratio of velocities constant at two, the resulting plot would look like this. For large values of H (originally) the efficiency increases the most for increasing conductivity. For small values of H the increase in conductivity may have no effect. In this case there is little need to worry about increasing the efficiency because it is already high. This plot was generated for the case in which the loss parameter was 10%. Note that for the value of H equal to one the efficiency doubles for a factor of three increase in conductivity.

EFFICIENCY VS ENHANCEMENT FACTOR



Electrical Conductivity In Seawater

To understand how to increase the conductivity one must realize two important facts. The first is that the reason for the poor electrical conductivity of water arises because electrical conduction occurs via ion transport and not electron transport as with gases. The mobility of ions is orders of magnitude lower than that of electrons. For ions in water the mobility is around 100 cm/sec per V/cm. The second important fact is related to the first fact in that this low mobility requires many ions to be present to carry any appreciable currents. The conduction ion density in seawater exceeds 10^{20} ion pairs per cm³. This leads us to the conclusion that we need to either increase the number of ions or increase the mobility of the charge carriers. The ion density may be increased using an auxiliary energy source in the form of a beam of electrons, photons, x-rays, etc. Another approach is to use some additive to increase the number of ions or introduce charge carriers with higher mobilities. Some possibilities include metallic flakes or chemical additives (electrolytes).

ELECTRICAL CONDUCTIVITY IN SEAWATER

- **Conductivity is Proportional to Charge Carrier Mobility and Density**
- **Current is Primarily Carried by Ions in Seawater**
 - Ion mobility is on the order of $100 \frac{\text{cm/sec}}{\text{V/cm}}$
 - Ion density is on the order of 10^{20} ion pairs/cm³
- **Use Auxiliary Energy to Increase Ion Density**
 - Laser, e-beam, x-ray, etc.
- **Use Additives to Increase Ion Density and/or Mobility**
 - Thermal
 - Metallic
 - Chemical (electrolytes)

Energy Requirements for Enhancement of Seawater Conductivity

Let us address the first suggestion of using an auxiliary energy source to increase the conductivity. The ion density for seawater is on the order of 2×10^{20} ion pairs per cm^3 . In order to double the conductivity, we need to produce the same number of ions assuming that the ions we generate have the same mobility as the intrinsic charge carriers in the seawater. To generate these ions it will require more than an electron volt to remove an electron from a neutral. This is a highly optimistic value and the number probably exceeds 10 eV but let's be optimistic. Assuming a torpedo duct volume of 1 cubic meter, an input power of 100 horsepower, and a voltage of 200 volts we arrive at some interesting numbers. The input power is 74 kW and the energy required to generate 10^{20} ion pairs is 32 joules per cubic centimeter. Finally, the required auxiliary power is calculated to be greater than 92 megawatts. This again is an optimistic number in that it assumes no recombination losses in the enhancement region. A realistic value (due to this effect) could easily be an order of magnitude greater. This indicates that using an auxiliary energy source to enhance the conductivity would result in decreasing the system efficiency by at least three orders of magnitude. Obviously this method is not recommended.

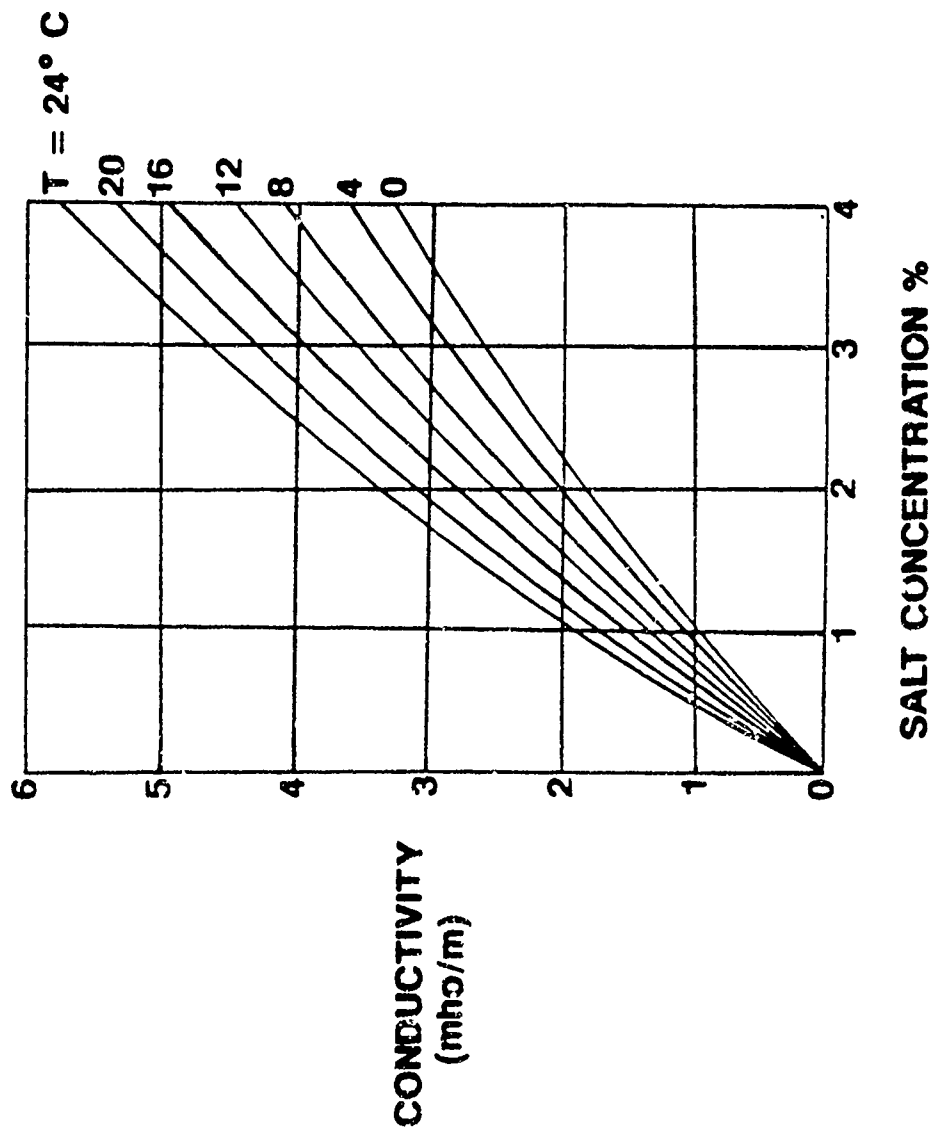
ENERGY REQUIREMENTS FOR ENHANCEMENT OF SEAWATER CONDUCTIVITY

- To Double the Conductivity We Need 2×10^{20} Ion Pairs per cm^3
 - Assume these ions have same mobility as NaCl ions
 - Energy to produce one ion pair $\geq 1 \text{ eV}$
- Calculate Required Enhancement Power for 1 m^3 , 100 HP MHD Power, 200 V
 - MHD power = 74 kW
 - Enhancement energy per shot $\geq 32 \text{ J/cm}^3$
 - Enhancement power $\geq 92 \text{ MW}$
- This Indicates That Doubling the MHD Efficiency in This Manner Reduces the System Efficiency by at Least 3 Orders of Magnitude

Thermal Conductivity Enhancement

Another possible means to enhance the conductivity of seawater is to raise the temperature of the water. This graph illustrates the effect of temperature on the conductivity of seawater. You can see that for the nominal case of 3.5% salt at 0 degrees C, the conductivity is 3 mho/m. If the temperature is increased to 24 degrees C, the conductivity increases to over 5 mho/m.

THERMAL CONDUCTIVITY ENHANCEMENT



Power Requirements for Thermal Conductivity Enhancement

This viewgraph illustrates that the amount of power required to change the temperature of water is very large. Assuming a channel diameter of 30 cm and a flow velocity of 20 knots, the power required to raise the water temperature one degree is on the order of 3 MW or 4000 HP. The amount of energy required to raise the temperature by 24 degrees in a one meter diameter duct with the same flow velocity requires more power than a ship can be expected to deliver.

POWER REQUIREMENTS FOR THERMAL CONDUCTIVITY

- **Begin With Specific Heat
4.2 J/cm³/°C**
- **Assume Water Velocity of 20 Knots (10 m/sec)**
- **Specific Heat x Velocity = Specific Power
4.2 kW/cm²/°C**
- **Consider Channel Diameter of 30 cm (12 in) and ΔT of 1 °C**

Thermal Power = 3 MW or 4000 HP

Metallic Additives

If we next consider additives to seawater, one may consider metallic additives in the form of flakes or pellets. Metallic materials seem to be of some advantage in that the conductivity of metals is some six orders of magnitude better than seawater. The metallic particles help the conductivity by providing a high conductivity path for conduction currents through some fraction of the MHD volume. If one assumes a worst case example where all of the metallic additive collects at one electrode, one may calculate a conductivity enhancement factor based on the relative volume of metallic material. Based on this worst case approach it is easy to see that this will have little effect on the conductivity until the ratio of volumes approaches unity.

METALLIC ADDITIVES

- Metals Have Conductivities 1 Million Times Greater Than Seawater
- Metallic Particles Provide High Conductivity Paths for Some Fraction of the Conducting Volume
- Define $\sigma_T = \sigma_o \epsilon$

where σ_o is the original seawater conductivity

and ϵ is the conductivity enhancement factor

$$\epsilon \approx \frac{1}{1 - \frac{\text{Vol metal}}{\text{Vol total}}}$$

Chemical Additives

Chemical additives may be used in the form of electrolytes to increase the number of ions used as charge carriers. If the right additive is used, the net mobility of the ions can be increased. Two possibilities include: NaCl because it is already in the water and HCl because it contributes an ion (H^+) which has the highest mobility (see chart). From a standpoint of conductivity enhancement, HCL appears to be the best.

CHEMICAL ADDITIVES

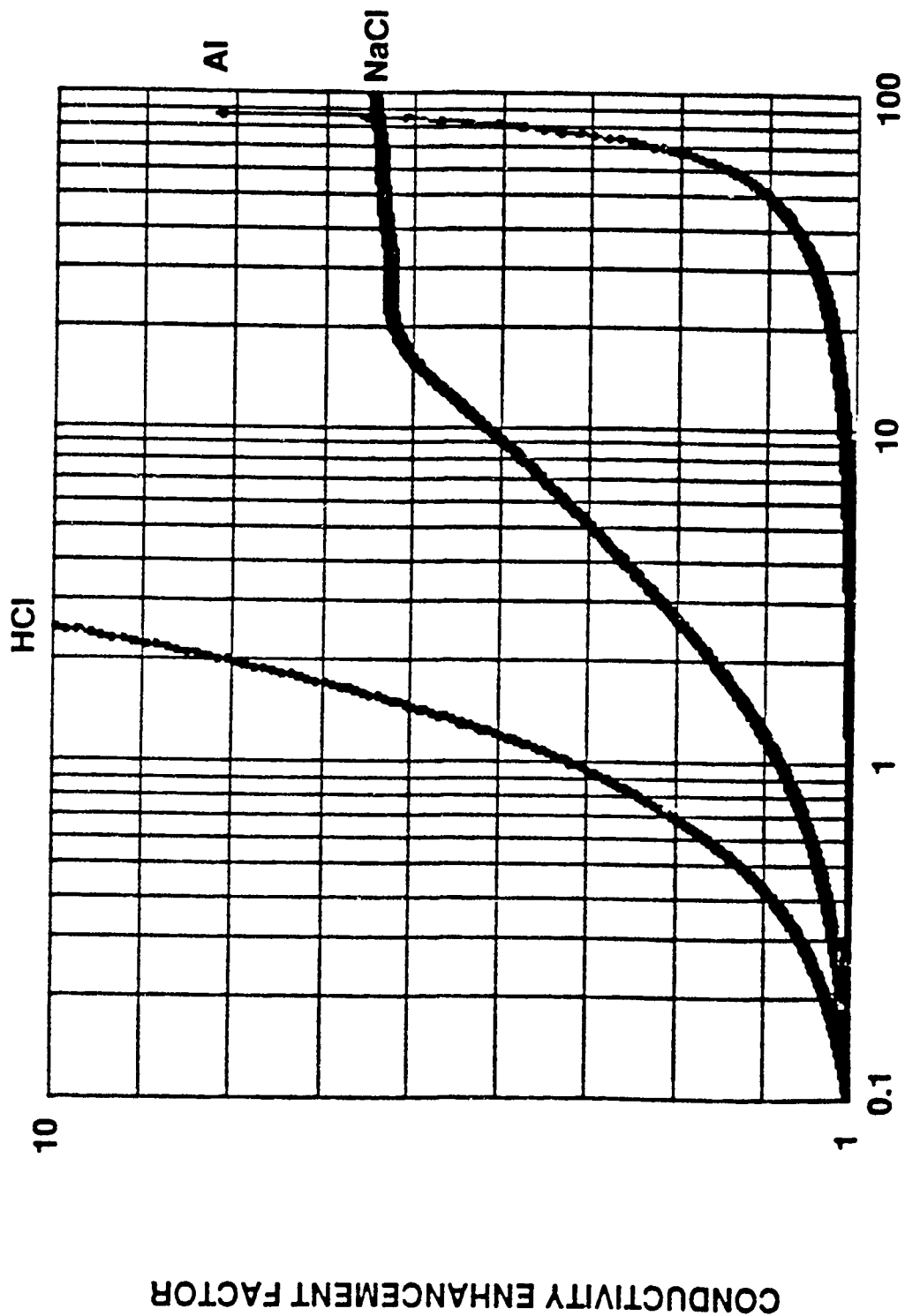
- Electrolyte Additives Increase Ion Density
- Ions can be Added Which Have Higher Mobilities
- Possible Additives Include:
 - NaCl - it is already in the water
 - HCl - appears to be the most effective

Li ⁺	0.51	Cl ⁻	(1)
Na ⁺	0.66	Br ⁻	1.03
K ⁺	0.97	I ⁻	0.99
Rb ⁺	1.02	OH ⁻	2.6
H ⁺	4.6	HCO ₃ ⁻	0.58
Ca ²⁺	0.78	NO ₃ ⁻	0.93
Sr ²⁺	0.78	SO ₄ ²⁻	1.05
Ba ²⁺	0.84		
Relative Ion Mobilities in Water at 2° C			

Enhancement vs. % Additive

This graph indicates the percent of additive needed to achieve a certain conductivity enhancement factor. It is clear that HCl is the most volume efficient additive. To increase the conductivity by a factor of four, one must add only one percent pure HCl. To achieve the same increase using NaCl or metal, one must use five percent or seventy five percent solutions.

ENHANCEMENT VS % ADDITIVE



PERCENT SOLUTE (by volume)

Spectra Technology

Enhancement Using HCl

An example of the use of HCl can be based on the one percent additive to achieve a factor of four increase in conductivity. Reasonable torpedo parameters are used to calculate an efficiency of ten percent using HCl as an additive. This requires an additive pump rate of 15 gallons per minute. The range of the torpedo (assuming it used HCl for the duration of the run) is limited to about 5 km or 500 seconds of operation. This appears to be somewhat limiting for some torpedo scenarios. An alternative is to use HCl for short bursts of high acceleration or final high speed pursuit.

ENHANCEMENT USING HCl

- 1% HCl by Volume Increases the Conductivity by a Factor of Three
 - Assume:
 - Torpedo size
 - Magnetic field
 - Torpedo speed
 - V_i/V_s
 - Calculate:
 - Duct diameter
 - Efficiency
 - Gallons/minute of HCl
 - Range
- | |
|-----------------------------|
| 0.5 m (dia.) x 5 m (length) |
| 5 Telsa |
| 10 m/s |
| 2 |
| 11 cm |
| 10% |
| 15 |
| 5 km (500 sec.) |

Chemical Additives

This viewgraph illustrates an assortment of potential chemical additives and the required amounts to increase the conductivity by a factor of 4. Whereas HCl appeared to be the best additive, it was found that HCl is not available with concentrations higher than 37%. The best candidate appears to be NaOH. Use of NaOH requires the least weight and the least relative volume of any other additive in the survey. A slight problem with NaOH is that it is a solid (powder) and must be mixed well in the water channel to effectively increase the conductivity.

CHEMICAL ADDITIVES

MATERIALS	mw	γ (mmho/cm) @ 1% wt	% OF MATERIAL IN CONC ACIDS	% BY WEIGHT FOR 4x cond	DENSITY gr/ml	RELATIVE VOLUME ml/% WEIGHT
Ammonium Chloride (NH_4Cl)	53.5	20.4	-	6.74	1.53	2.21
Hydrochloric Acid (HCl)	36.5	92.9	37	4.04	1.18	1.72
Lithium Chloride (LiCl)	42.4	19.0	-	7.34	2.07	1.78
Nitric Acid (HNO_3)	63.0	56.1	90	2.76	1.50	0.92
Potassium Chloride (KCl)	74.6	15.7	-	8.84	1.98	2.23
Potassium Hydroxide (KOH)	56.1	38.5	-	4.04	2.04	0.99
Sodium Chloride (NaCl)	58.4	16.0	-	8.72	2.16	2.01
Sodium Hydroxide (NaOH)	40.0	48.6	-	2.86	2.13	0.67
Sulfuric Acid (H_2SO_4)	98.1	47.8	96	3.02	1.84	0.82
Hydrogen Bromide (HBr)	80.9	69.6	48	4.16	1.5	1.29
Hydrogen Iodide (HI)	127.9	70.6	47	4.18	1.5	1.40

Mixing of Additives

In looking at the technology required for injection of additives, it became apparent that a problem which needs to be addressed is the problem of mixing of the additive with the seawater. If the additive is not mixed with the seawater, it will not effectively modify the conductivity. A quick survey of the literature found an amazing lack of information regarding injection and mixing of electrolytes in water. An estimation was made based upon scaling particle mixing in gas flows. The result of the estimation exercise indicated that a length of 40 times the injector nozzle diameter is needed mix the additive with the water. This translates into a mixing length of greater than 40 cm. For torpedo applications, this may be an unreasonable length.

MIXING OF ADDITIVES

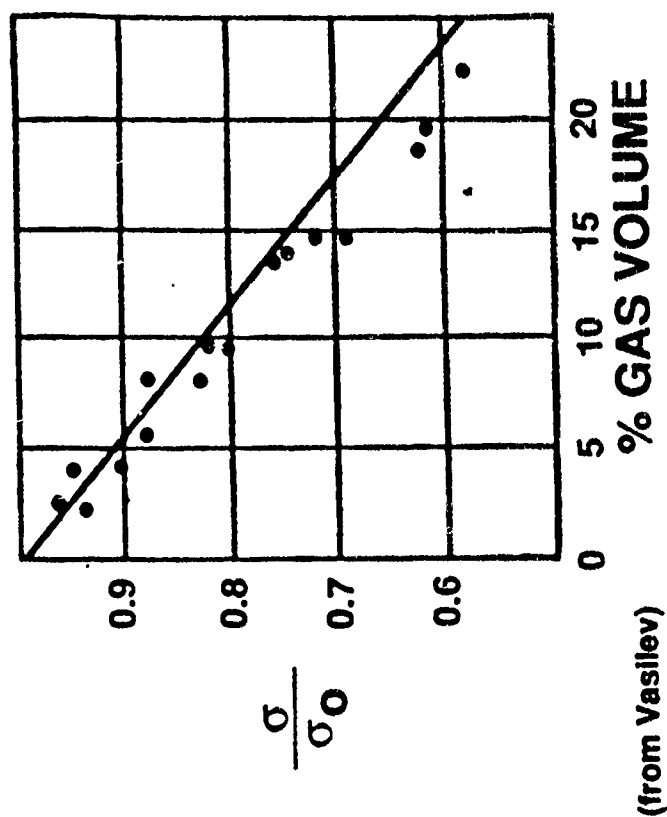
- **Insufficient Mixing Leads to Incomplete Conductivity Enhancement**
- **Diffusion Processes are too Slow to Ensure Uniform Mixing**
 - **Must rely on turbulent mixing**
- **Data is Nonexistent on Turbulent Mixing for Seawater Flows**
- **Scaling From Turbulent Mixing of Particles in Gas Flows Gives an Indication of the Scope of the Problem**
 - **Required mixing lengths are on the order of 40 nozzle diameters**

Conductivity Reduction Due to Bubbles

Here is a plot of the effective reduction of conductivity due to bubbles in the conduction channel. It is estimated that even under worst conditions the bubble gas volume will not exceed 5%. Therefore, the reduction of conductivity due to bubbles should not exceed 10%.

CONDUCTIVITY REDUCTION DUE TO BUBBLES

- Bubble Sources:
 - Gas produced by electrolysis
 - Cavitation (nozzles, screens, etc.)
- Soviets Have Studied the Problem in Terms of:
 - Theoretical models of two phase streams
 - Experimental measurements in saltwater



Operational Scenarios For Conductivity Enhancement

It does not seem reasonable to expect that a chemical additive would be used for continuous operation unless some procedure for recovery is used. Since such a recover process does not seem practical, one must think of scenarios under which chemical additives make sense. Propulsor start up is a very inefficient process. Chemical additives could be used to increase the start up efficiency. Since the scaling of efficiency indicates lower efficiency at higher speeds, chemical additives could be used to give bursts of high speed at higher efficiencies. High levels of acceleration are also characterized by low efficiency. Chemical additives could be used to give higher accelerations for the same expenditure of power. Finally, chemical additives can be used during very short missions such as crossing river deltas and some polar operations.

OPERATIONAL SCENARIOS FOR CONDUCTIVITY ENHANCEMENT

- **Propulsor Start Up**
 - Initial water velocity is zero
 - Efficiency at start up is very low
- **High Speed/High Efficiency**
 - Burst mode
- **High Acceleration**
 - Increased efficiency
- **VSM* Operations**

• **Very Short Missions**

Summary

Conductivity can be enhanced by a number of means. Many of these means appear to be impractical. Chemical additives appear to be the best candidates with NaOH leading the choices of chemical additives. Chemical additives do not appear practical for all applications but some short time operations can use chemical additives to increase efficiency. Several issues have been identified including: selection of chemical additives (Is NaOH really the best?), injection of additives (solid injection), mixing of additives in the flow stream, and bubble effects on conductivity, especially near the electrodes.

SUMMARY

- **Conductivity can be Enhanced**
- **Chemical Additives Appear to be the Best Candidates**
- **Conductivity Should be Enhanced for Some Operations**
- **Key Issues**
 - **Chemical additive selection**
 - **Additive injection**
 - **Turbulent mixing**
 - **Bubble effects on conductivity**

**SOME FUNDAMENTAL FLUID MECHANICS AND
ELECTROCHEMICAL ISSUES OF
MHD SEAWATER THRUSTER**

Presented by

Y.C.L. Susan Wu

DARPA/ONR Workshop On MHD Submarine Propulsion

November 16 and 17, 1989
San Diego, CA

Hosted by
The Naval Ocean System Center

Presentation by
Y. C. L. Susan Wu, Ph.D.

Engineering Research & Consulting, Inc.

UTSI Research Park, Bldg. 2
P. O. Box 417
Tullahoma, TN 37388
(615) 455-9915

Some Fundamental Fluid Mechanics and Electrochemical Issues of MHD Seawater Thruster

By

Y. C. L. Susan Wu
Engineering Research & Consulting, Inc.
Tullahoma, TN 37388

1.0 INTRODUCTION

Research of maritime magnetohydrodynamic (MHD) propulsion was carried out extensively during the sixties (Ref. 1-9). Subsequent to this period a decade of silence on the subject followed during which very little active research was conducted. However, once again MHD propulsion has begun to receive serious attention (Ref. 10-13). This resurgence of interest has been driven by advances in technologies related to MHD, in particular, superconducting magnet technology, and by the need for advanced propulsion systems for both industrial and military applications.

On the international scene, one of the more publicized and ambitious efforts for the development of maritime MHD is being pursued in Japan. The Japan Foundation for Shipbuilding Advancement has established a committee to research and develop a superconductive electromagnetic propelled vessel. This government subsidized research has a total budget of around \$40 million. The scope of the Japanese research is impressive. It includes the construction and testing of a prototype experimental ship. The schedule for this project calls for completion of the hull, fitting of the propulsion system and preliminary tests of the prototype ship by 1989. Sea trials to evaluate the ship performance

are scheduled for 1990. Characteristics for the experimental ship and its MHD thrusters are summarized in Table 1.

TABLE 1
PARAMETERS OF THE JAPANESE MHD EXPERIMENTAL SHIP

Displacement:	150 ton
Length:	22 m
Breadth:	10 m
Thrust:	8,000 N
Speed:	8 Knots
Propelling system:	
Type:	twin propelling units with 6 dipole coils
ID of duct:	0.26 m
Length of electrodes:	2.5 m
B:	4 T
I_{\max} :	4,000 amp/m ²
Lorentz force:	8,000 N x 2
Thrust:	4,000 N x 2
Capacity of main generator:	3,800 kw
Total weight of the system:	100 Tons

Information available in the open literature has indicated that an active program for development of MHD ship propulsion has been continuous in the Soviet Union for many years. General specifications

of physical features and performance estimates of contemporary Soviet naval vessels, in particular, submarines, suggest that there is a strong possibility that electromagnetic propulsion systems may currently be in use.

Recently the U.S. Navy has challenged the national scientific community to review the current state-of-the-art in MHD and to project the feasibility of applying this technology to meet their future needs. The two primary areas for utilizing MHD that have been cited are reduction of ship drag through MHD induced turbulence/wake suppression and MHD propulsion. Several features of MHD propulsion for application to both surface vessels and submersibles are most attractive to the Navy. Foremost among these are the high system efficiency and ship speed that can ideally be attainable with the seawater MHD thruster. In parallel to these gross advantages are other unique features which MHD offers, such as, design simplicity from both the operation and control viewpoints and the stealth characteristics that this type of system is capable of displaying. In combination these traits are especially desirable for advanced submarines and torpedoes. These latter two applications are those for which accelerated Naval research programs are beginning to emerge.

MHD shows definite promise of being the choice technology for future advanced submarine propulsion. However, its rapid deployment into use is contingent upon detailed clarification of several unknowns that are related to the seawater MHD process. These unknowns need to be quantified in carefully designed laboratory experiments.

2.0 IDEAL MHD THRUSTER OPERATION

The electric field intensity and current density are governed by the Ohm's law,

$$\vec{j} = \sigma (\vec{E} + \vec{u} \times \vec{B}) \quad (1)$$

where \vec{j} is current density, σ the electrical conductivity, \vec{u} the water velocity and \vec{B} the magnetic induction.

For a thruster the electromagnetic force (Lorentz force) per volume to accelerate the fluid is given by,

$$\vec{F} = \vec{j} \times \vec{B} \quad (2)$$

An electromagnetic efficiency η_e is defined as

$$\begin{aligned} \eta_e &= \frac{\text{Work done by Lorentz force/volume}}{\text{Electric Power Input/volume}} \\ &= \frac{(\vec{j} \times \vec{B}) \cdot \vec{u}}{\vec{j} \cdot \vec{E}} \end{aligned} \quad (3)$$

Utilizing Ohm's law, one obtains

$$\eta_e = \frac{(\vec{j} \times \vec{B}) \cdot \vec{u}}{(\vec{j} \times \vec{B}) \cdot \vec{u} + j^2/\sigma} \quad (4)$$

where j^2/σ is Joule dissipation, $(\vec{j} \times \vec{B}) \cdot \vec{u}$ is the work done by the Lorentz force and $\vec{j} \cdot \vec{E}$ is electric power input, all per unit volume. To obtain the total current, total power input, and so on, proper surface or volume integrations are required.

In one dimensional configuration, the above equations become

$$j = \sigma (E - uB) \quad (5)$$

$$F = jB \quad (6)$$

$$\eta_e = \frac{j u B}{j E} = \frac{u B}{E} \quad (7)$$

We can re-write the pertinent variables in terms of η_e ,

$$j = \sigma u B \frac{1 - \eta_e}{\eta_e} \quad (8)$$

$$E = \frac{u B}{\eta_e} \quad (9)$$

$$F = jB = \sigma u B^2 \frac{1 - \eta_e}{\eta_e} \quad (10)$$

$$jE = \sigma u^2 B^2 \frac{1 - \eta_e}{\eta_e^2} \quad (11)$$

The above equations represent the ideal thruster performance characteristics. Figure 1 is current density and electric field intensity as function of the electromagnetic efficiency for several values of uB and at a conductivity of 4.5 mhos/m. It can be seen for a given current density or electric field intensity, the efficiency increases with increasing uB . Therefore, the electromagnetic thruster favors high speed and high magnetic induction. For example, with $B = 10T$,

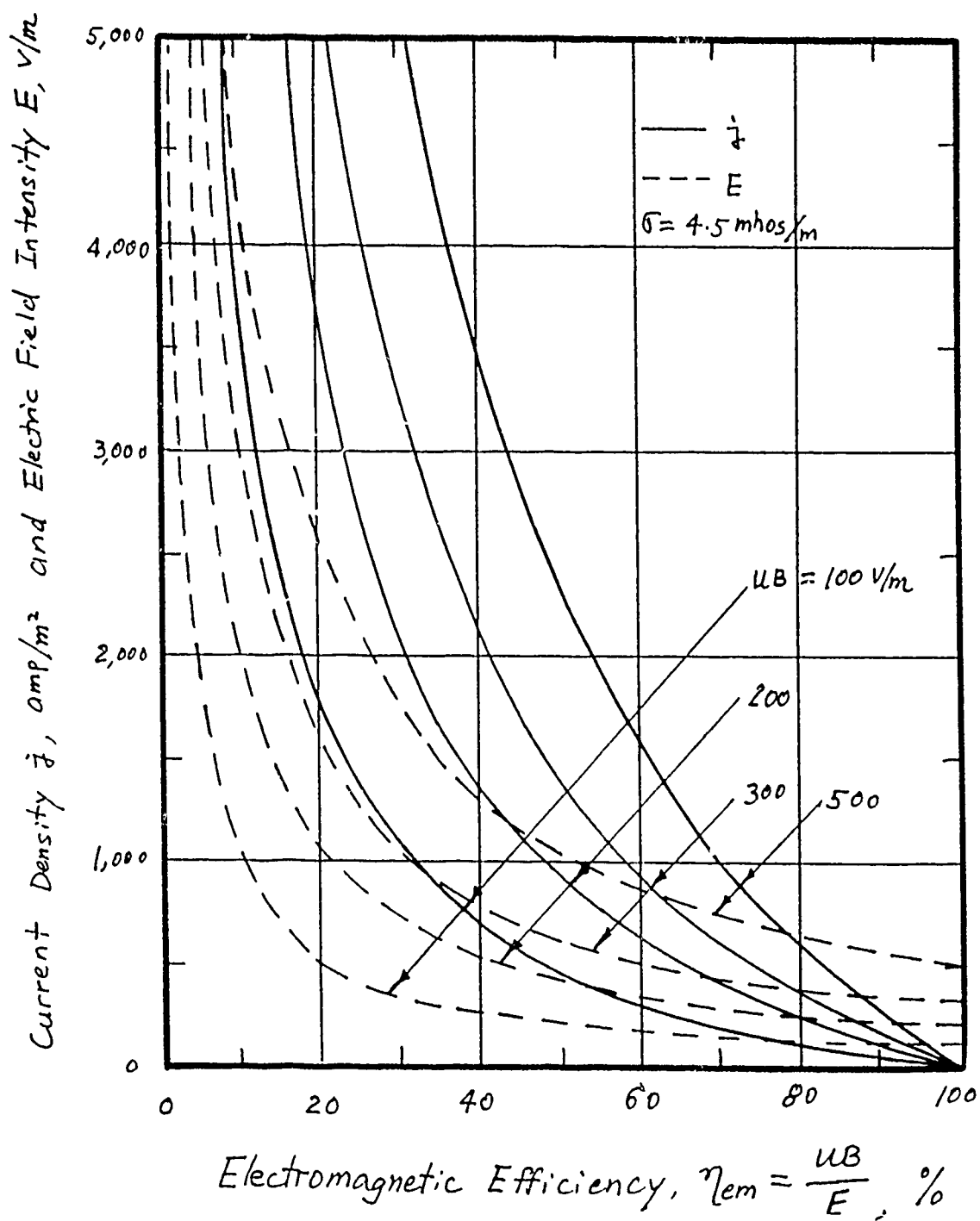


Figure 1. Current Density and Electric Field Intensity as Function of Electromagnetic Efficiency for an Ideal Electromagnetic Thruster

$u = 10 \text{ m/s}$ and an electric field intensity of 500 v/m , the corresponding efficiency is 20 percent. This gives the current density of $1,800 \text{ amp/m}^2$. However, if the velocity is increased to 20 m/s , then the corresponding efficiency is increased to 40 percent but the current density is decreased to $1,350 \text{ amp/m}^2$. This means that for a required thrust, larger thruster is required. This gives the designer the freedom to trade-off several parameters, for example, operating at a different electric field intensity. Similarly, one can keep a given current density and find the corresponding efficiency and electric field intensity. Once the values of η_e and uB are known, the electric power required per volume and work done by the Lorentz force and Joule dissipation per volume can be found from Figure 2. At $uB = 100$, the power required per volume is 0.9 MW/m^3 and the work done by the Lorentz force per volume is 0.18 MW/m^3 . The difference between the two values is the Joule dissipation (0.72 MW/m^3). On the other hand, when $uB = 200$, the power input per volume is 0.675 MW/m^3 and the work done by the Lorentz force is 0.27 MW/m^3 and the Joule dissipation per volume is 0.405 MW/m^3 .

3.0 LOSS MECHANISMS OF ELECTROMAGNETIC THRUSTER

Like all devices, the physical and chemical processes occurring are far more complex than the ideal one-dimensional picture. Figure 3 shows the inherent three-dimensional nature of an electromagnetic thruster and the various loss mechanisms. At the inlet of the thruster there are boundary layers and possible cross-flows or swirl depending on the inlet geometry. The electrolysis process will generate hydrogen gas at the cathode and chlorine gas at the anode. Due to buoyancy, gas bubbles

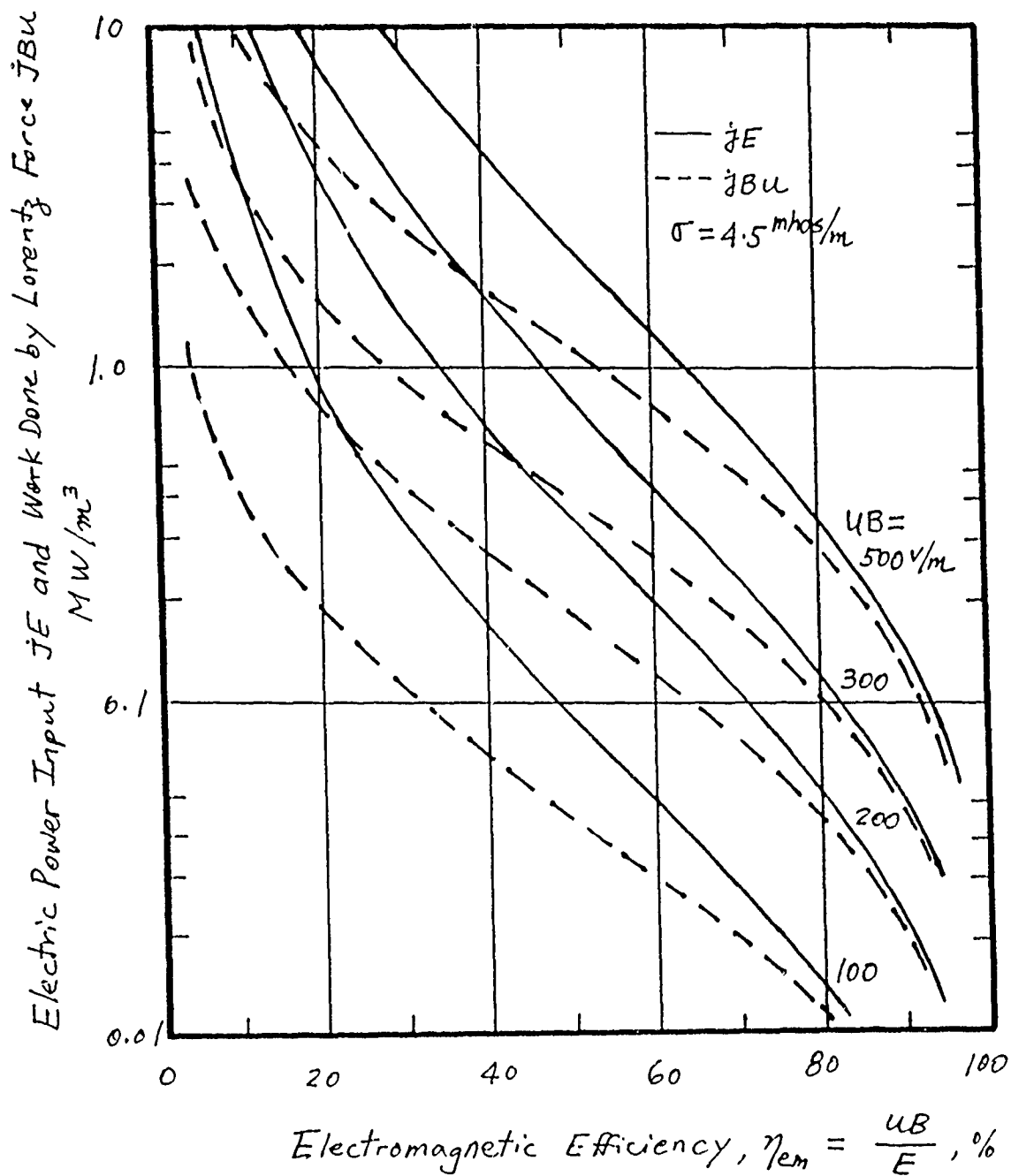


Figure 2. Electric Power and Work Done by Lorentz Force per Volume Versus Electromagnetic Efficiency for an Ideal Electromagnetic Thruster

Schematic Representation of Inherently Three-Dimensional Phenomena in Linear MHD Seawater Thruster

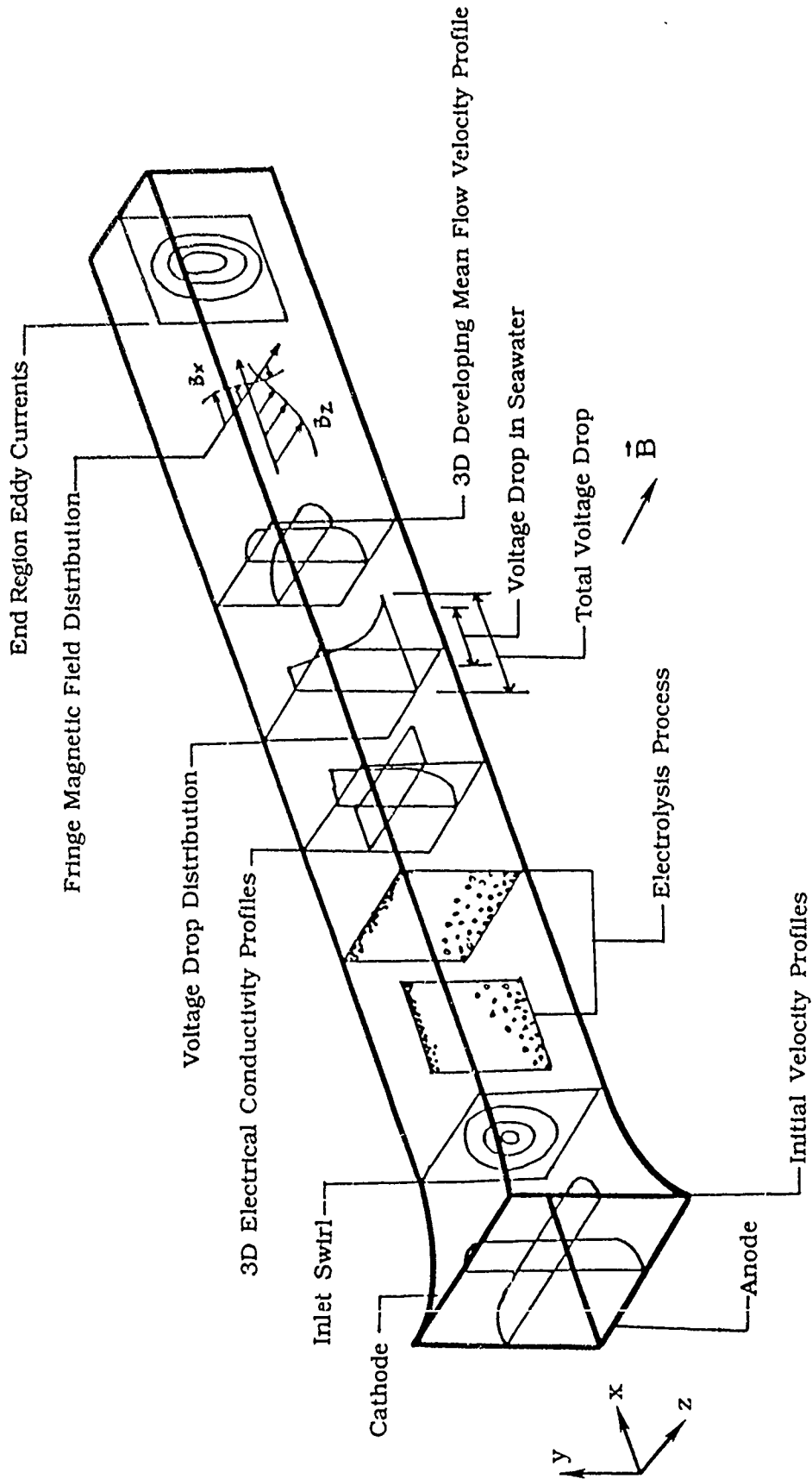


Figure 3.

will rise and interact with the seawater. However, the horizontal electrode located on the top of the thruster will experience a different situation. The gas bubbles will tend to stick on the electrode due to the buoyancy force. Consequently, the bubbles may break and form a gas pocket or film. The non-conducting gas may cause severe losses to limit electric current to flow (increased voltage drop), cavitation and electrode corrosion. Different electrode orientation and wall suction can reduce these losses. However, there are no data available to quantify these effects. In addition to the electrical conductivity degradation, bubble boundary layer may increase the friction loss.

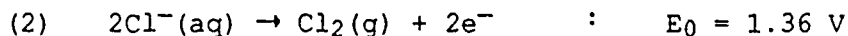
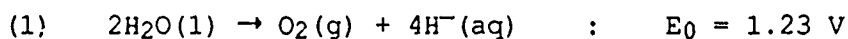
Additional factors also come into play in the electromagnetic thruster. Vehicle velocity plays an important role as bubbles will be swept away by the seawater. Chlorine generated at the anode will immediately undergo hydrolysis. Hydrogen bubbles will dissolve in the seawater within a fraction of a second. This means that for very long thruster, hydrogen generated upstream will be partially dissolved downstream. Consequently, the signatures caused by hydrogen bubbles will not be important for downstream. However, the effect of hydrogen gas on the local electrical conductivity and the bubble boundary layer will be important. The lack of quantitative data prevent the accurate prediction of thruster performance, configuration optimization and design.

4.0 ELECTROLYSIS

4.1 Sea Water Electrolysis Reactions

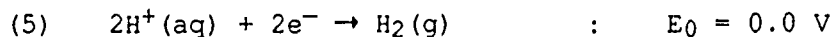
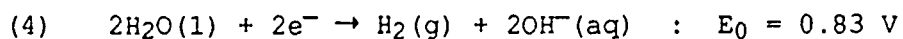
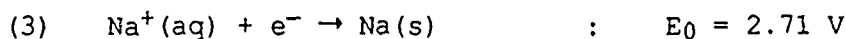
Although the dominant chemical species dissolved in seawater is salt (NaCl), seawater is known to contain several trace species which could

possibly electrolyze. A representative study of the affinity for electrolysis of many species is given in reference 14. Following the results of this study, it is noted that at the anode species will be oxidized whereas at the cathode a reduction reaction occurs. The dominant oxidization reactions which can occur at the anode are



where E_0 represents the standard reduction potential for each of these reactions. The lower reduction potential noted for H_2O suggests that water should be preferentially oxidized at the anode. However, static laboratory experiments have found that the dominant gas liberated at the anode is chlorine (Cl_2) rather than oxygen (O_2). The reason determined for this discrepancy is that it was found that the potential required to initiate the first reaction is considerable higher than that required to initiate the chlorine reaction.

Three dominant reduction reactions are possible at the cathode:



Due to the negligible reduction reaction potential, reaction (5) is most preferential over the others. However, free atomic hydrogen ions (H_2^+) concentrations are too low of a concentration in water with salinity comparable to that of seawater to make reaction (5) dominate. Rather it is the direct reduction of liquid water (H_2O) to hydrogen gas (H_2) and the hydroxide ion (OH^-) which dominates, reaction (4). For seawater with high salinity, or in the case where seeding is used in the MHD thruster,

this may not be the case. However, in all situations hydrogen gas is liberated at the cathode.

4.2 Effect of Bubbles on Seawater Electrical Conductivity

As has been cited in the above section, the electrolysis process will produce nonconducting gas bubbles which when mixed with the seawater will reduce its bulk conductivity. This effect will degrade the MHD thruster performance. To illustrate the degree to which thruster performance may be affected by electrolysis, the following discussions provide some detail as to the physics which governs the electrolysis and bubble generation processes.

To determine the bulk electrical conductivity of a bubble-water stream typical to the environment inside the MHD thruster requires knowledge of subtle characteristics of the bubble dynamics. Such criteria as gas generation rates, bubble size and distribution are required. These characteristics are difficult to define for the bubbling stream since the dynamic history of the bubbles is not necessarily a stochastic process. That is, the nature by which bubbles interact with the turbulent carrying phase is uncertain. Such definitions are further complicated by the fact that the individual gas bubbles will exhibit chaotic motion in the stream driven by a variety of body forces, i.e., assume arbitrary shapes, become deformed, pulsate, and periodically break-up and coagulate. Therefore, it is noted here that unverified assumptions are necessary to develop a phenomenological of the turbulent bubble dynamic process. The most confident means of achieving a knowledge of the effect of electrolysis on seawater conductivity remains through experiment and direct measurements.

Let ϕ be the average volumetric fraction of gas content in the stream. Assume that the bubbles are spherical with radius r . Let the thruster length be l , width be w and distance between electrodes be d . Then the densest packing of bubbles gives the value of ϕ_{\max} , where

$$\begin{aligned}\phi_{\max} &= \frac{(V_{\text{gas}})_{\max}}{V} = \frac{\frac{3}{4} \pi r^3}{dlw} \left(\frac{d}{2r} \right) \left(\frac{l}{2r} \right) \left(\frac{w}{2r} \right) \\ &= \frac{\pi}{6}\end{aligned}\quad (12)$$

The electrical conductivity reduction due to the presence of bubbles is given by (Ref. 15)

$$\frac{\sigma_{\text{ef}}}{\sigma} = \frac{1}{1 - \frac{3}{2} \frac{\phi}{1 - \left(\frac{9\pi}{16} \phi^2 \right)^{1/3}}}\quad (13)$$

where σ is the liquid conductivity, σ_{ef} is the effective electrical conductivity in the bubbling stream.

From ϕ_{\max} we can obtain σ_{ef}^* as

$$\frac{\sigma_{\text{ef}}^*}{\sigma} = \frac{1}{1 + \frac{\left(\frac{\pi}{4} \right)}{1 - \frac{\pi}{4}}} = 0.215$$

The above equation states that at $\phi_{\max} = \pi/6$, the minimum effective conductivity σ_{ef}^* is about 1/5 of the liquid conductivity σ . Figure 4 is a plot of Equation (13) when bubbles do not break up to form large pocket or film.

When the dynamics of bubbles are taken into consideration, Vasilév showed that the volumetric gas content ϕ can be determined by (Ref. 16)

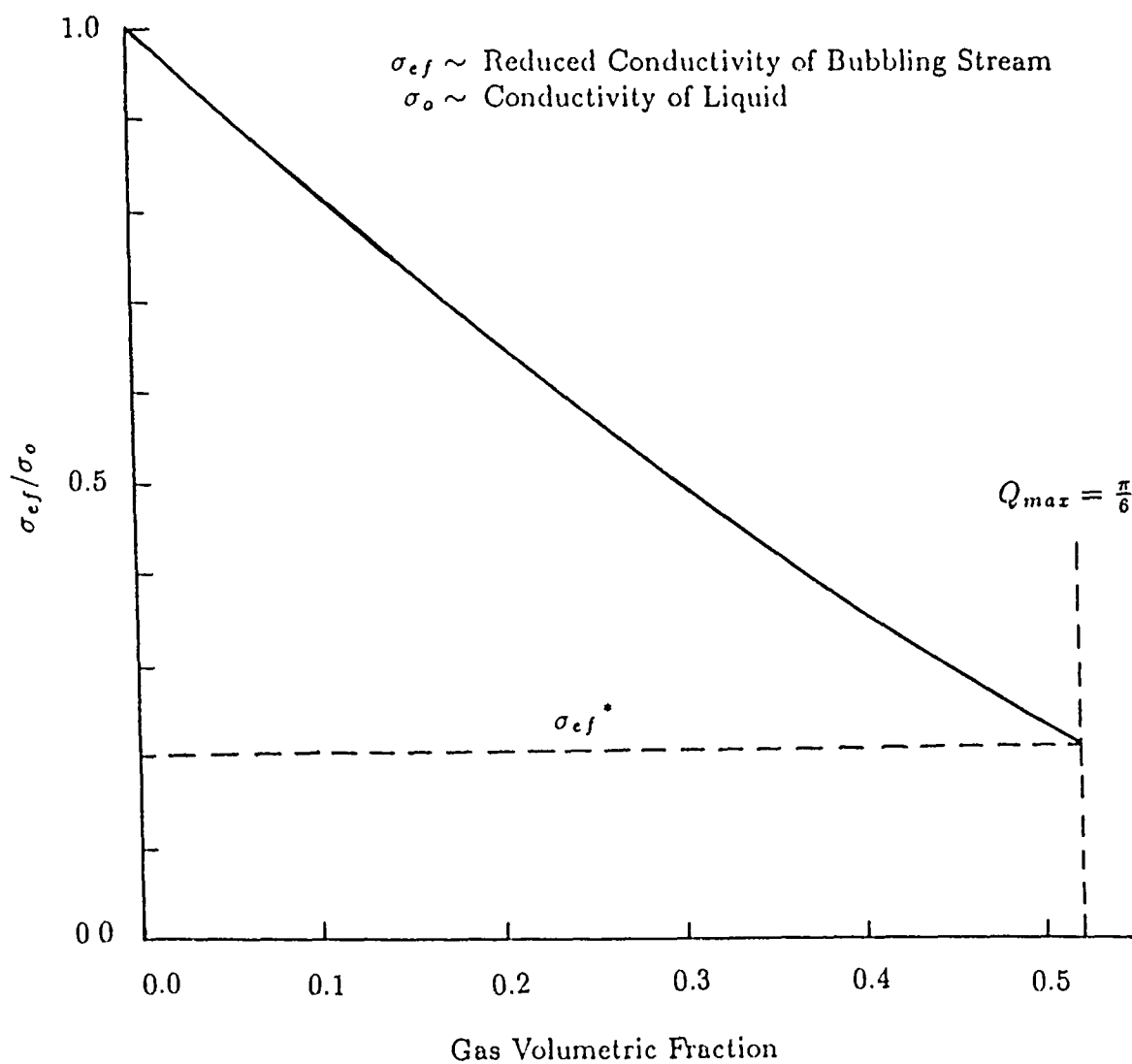


Figure 4. Reduction in Electrical Conductivity Due to Presence of Gas Bubbles

$$\phi = \frac{j}{2V_y F} \frac{RT}{p_0 + 2\Sigma/r_0} \quad (14)$$

where j is current density, F the Faraday number, $1F = 96,500$ C, R is universal gas constant, p_0 is the pressure at the duct entrance, Σ is the coefficient of surface tension at the interphase boundary, and r_0 the breakaway bubble radius.

Substituting $\phi_{\max} = \pi/6$ into Equation (14) allows us to determine the value of j_{\max} ,

$$j_{\max} = \frac{\pi}{3} V_y \left(p_0 + 2 \frac{\Sigma}{r_0} \right) \frac{F}{RT} \quad (15)$$

Equation (15) indicates that the thruster may not function (e.g., j_{\max} too low) if the buoying velocity of the bubbles is too low. This suggests that the electrode configuration is very important for optimum thruster performance.

5.0 FLUID MECHANICS

Fluid mechanics plays a very important role for both surface ships and submerged vehicles. Water is the environment where ships travel, consequently fluid mechanics to ships is equivalent as aerodynamics to flying vehicles. For a MHD seawater thruster, it, in many ways, resembles an air breathing engine. Consequently, fluid mechanics takes on an added dimension to the traditional role which fluid mechanics has played in ships. Furthermore, the interactions of seawater with electromagnetic fields further complicated the importance of fluid mechanics.

Due to the presence of the electrolysis process, the electrical conductivity of the seawater inside the thruster is no longer constant. In turn, the current density and Lorentz force will be non-uniform. The

conventional boundary layer also plays an important role regarding both acceleration and friction losses.

In addition to the thruster itself, both the inlet and the wake are also important to the overall performance and detections. The inlet must produce a uniform velocity profile with thin boundary layers. The wake drag and signature must be minimized for submarine and torpedo applications.

6.0 A RECOMMENDED EXPERIMENTAL PROGRAM

Much of the uncertainties of the seawater electromagnetic thrusters is due to the lack of fundamental data. It is recommended that a rigorous experimental program be established to quantify the various mechanisms which affect the performance of the thruster.

The University of Tennessee Space Institute has an existing cryogenic cooled 6 Tesla magnet. Figure 5 shows the 6T magnet layout, Figures 6 and 7 show the center line field strength distribution across the pole faces and the voltage-current pulse characteristics. Table 2 is the magnet design characteristics. The magnet is an excess property from the U.S. Air Force and now belongs to The University of Tennessee Space Institute (UTSI). UTSI plans to make space available for the installation of the magnet in the near future. Power supply, however, is not available for the magnet.

The test facility is shown schematically in Figure 8. The test section dimensions are selected to fit the inside of the magnet's opening and allow additional space for accessing the area for optical instrumentation. In order to obtain basic scientific data, a rectangular shaped cross section is preferred to a circular or any other

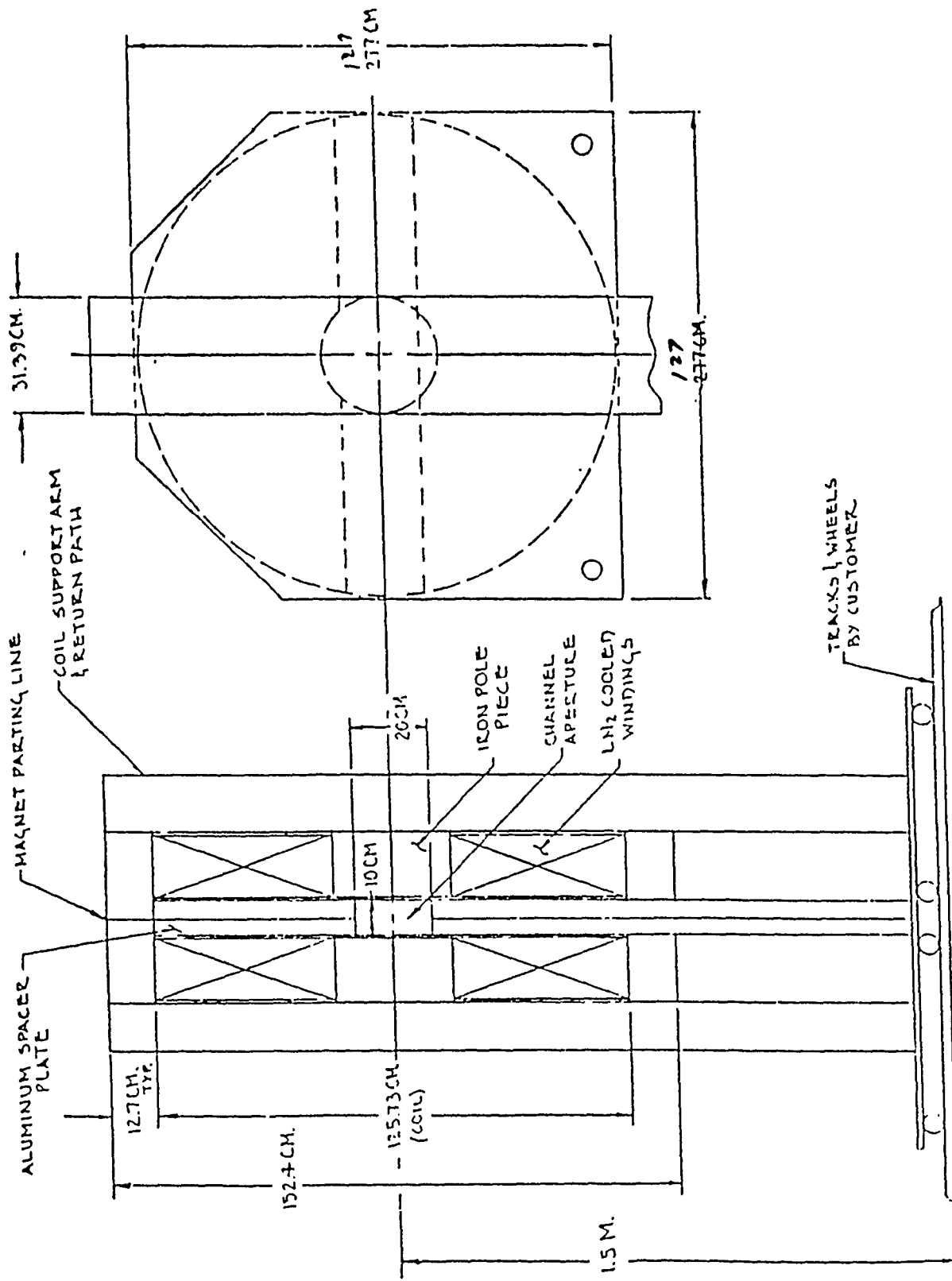


Figure 5. 6.0 Tesla Magnet Field - Mechanical Drawing

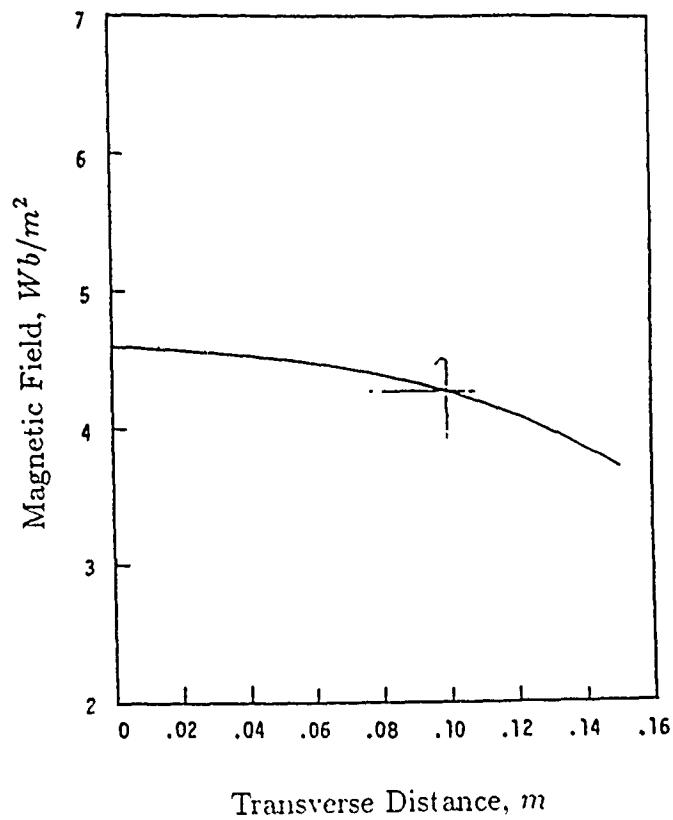
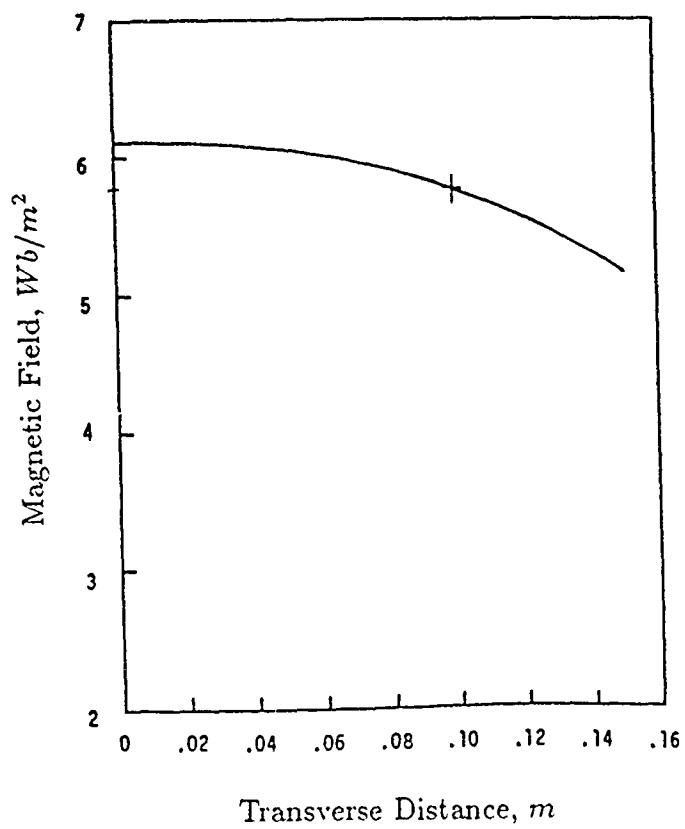


Figure 6. 6.0 Tesla Magnet Field Profile

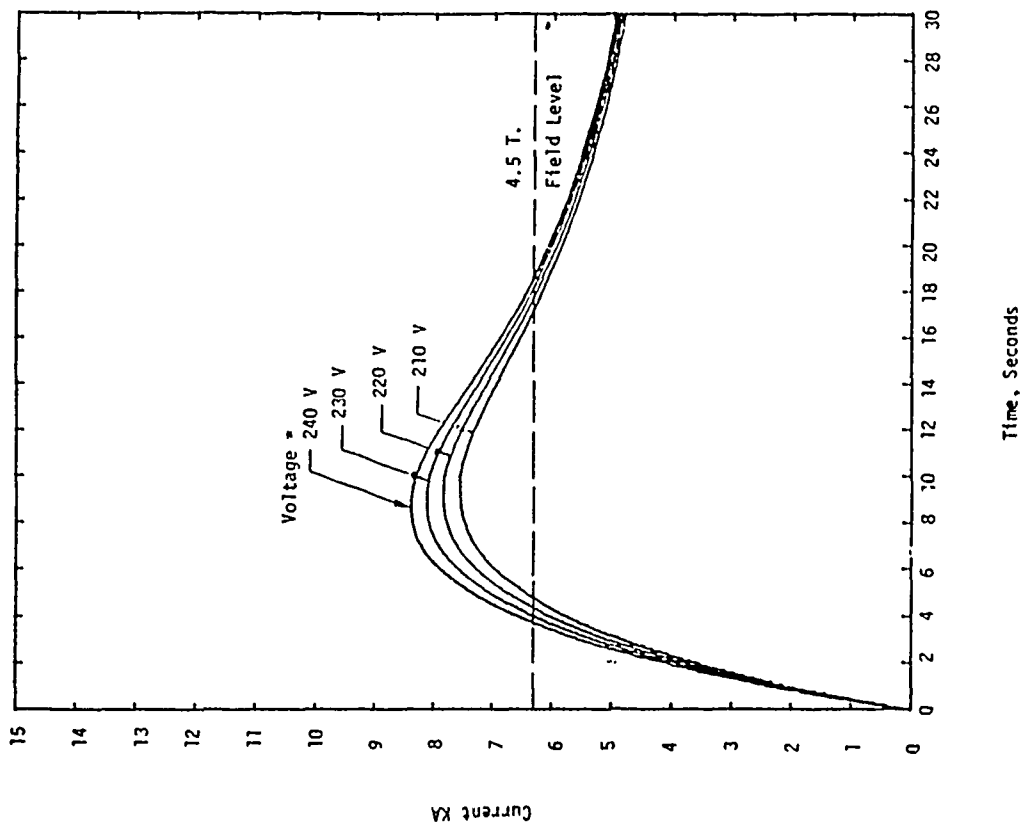
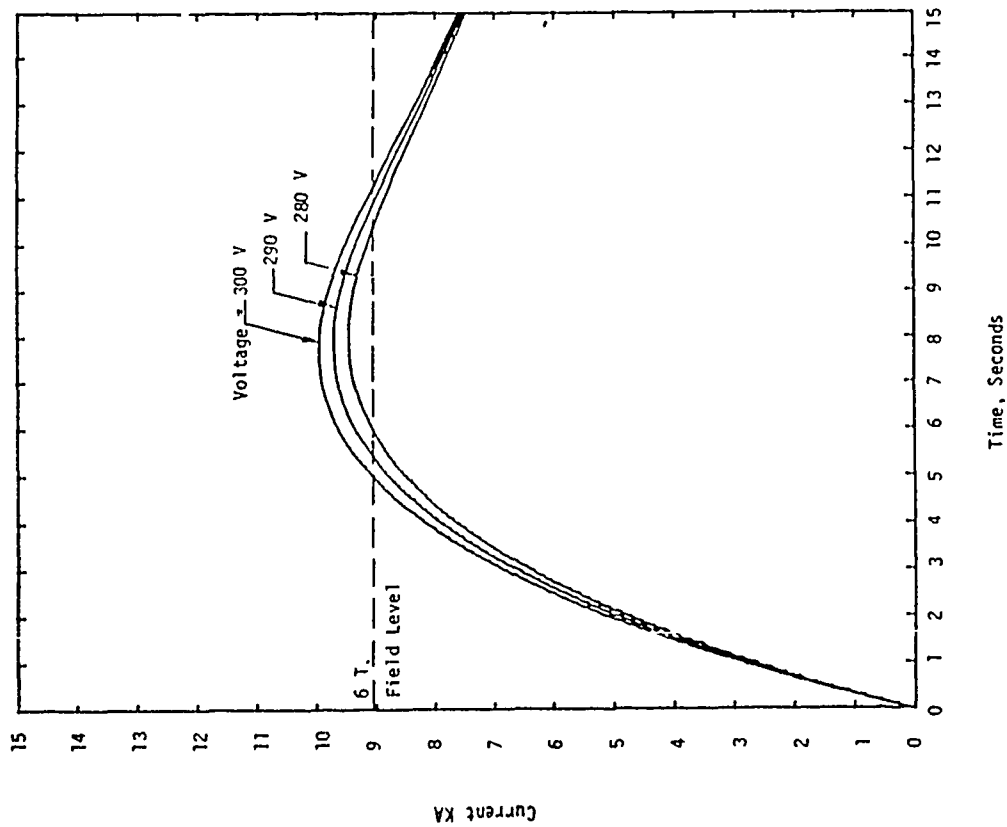


Figure 7. Transient Operational Characteristics of the Magnet

TABLE 2

6.0 Tesla Magnet Design Specifications

Physical Size

Conductor Size : 0.58 in x 0.58 in
 Cooling Passage : 0.323 in Diameter
 Conductor Length : 2,600 ft
 Conductor Weight : 2,600 lbs

Structure Weight : 1,800 lbs
 Total Weight : 4,400 lb

Magnet Bore

Width : 10 cm
 Length : 20 cm
 Volume : 2 cm x 2 cm x 20 cm (5% Field Homogeneity)

Cooldown Characteristics

Coolant : LN₂
 Coolant Requirement : 750 liters
 Coil Resistance @ 80 K : .0122 Ohms

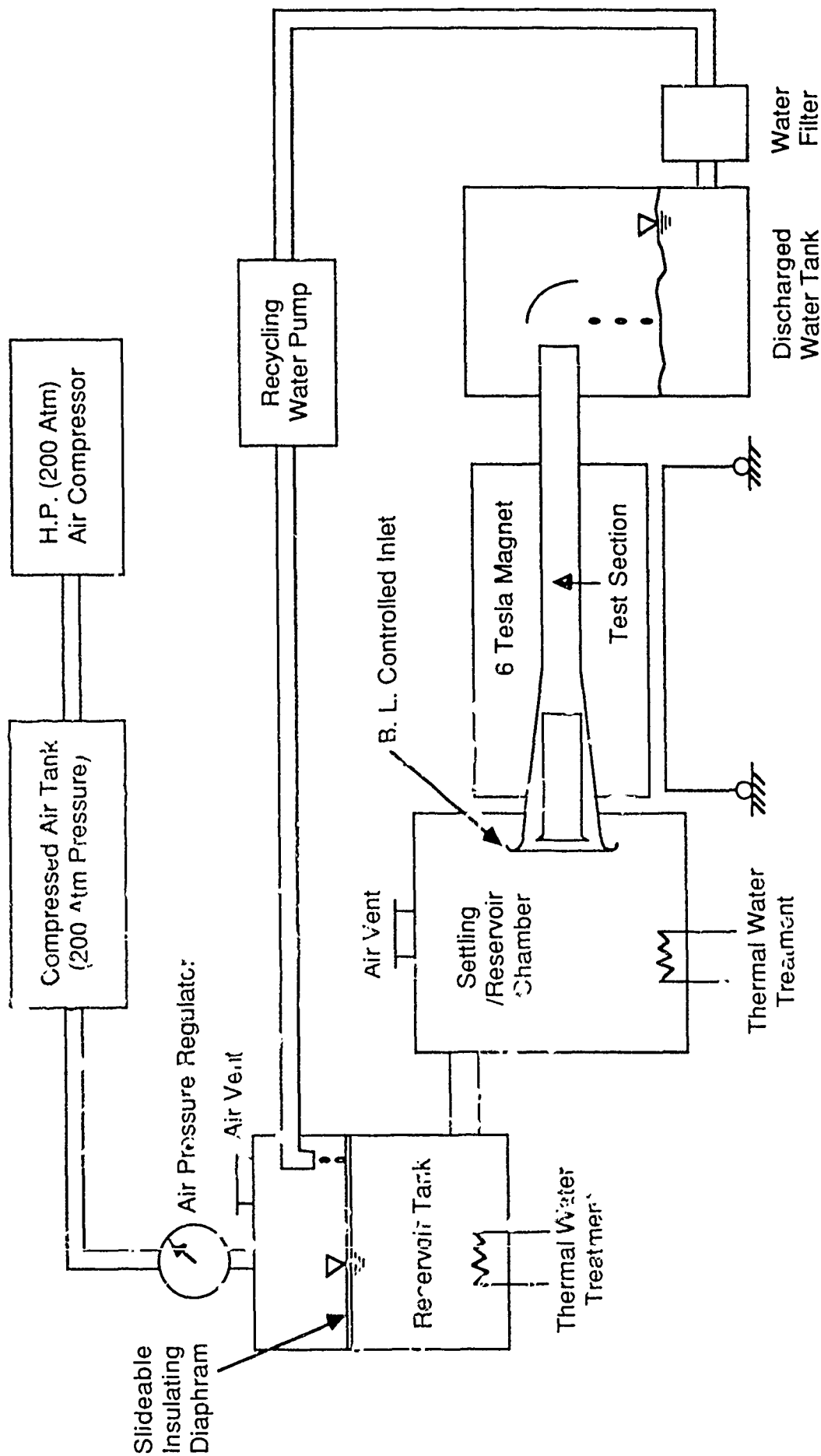
Operational Characteristics

6.0 Tesla Mode Operation

Current : 8,660 Amps
 Voltage : 350 Volts
 Power : 3.01 MW
 Amp Turns : 3.88×10^7
 Time : 5 seconds (@ Field > 6.0 T)

4.5 Tesla Mode Operation

Current : 6,000 Amps
 Voltage : 315 Volts
 Power : 1.89 MW
 Amp Turns : 2.69×10^7
 Time : 15 seconds (@ Field > 4.5 T)



Schematic Overall Facility Layout

Figure 8.

shape. With these considerations, the test section is determined as 5cm(W) x 5cm(H) x 120 cm(L) with a square cross section, horizontally mounted open circuit. The electrodes can be placed either horizontally or vertically depending on the magnet orientation. The side plates will be equipped with optical windows for a direct viewing of electrodes.

Other parameters are:

$$\rho = 1.02 \text{ kg/l}$$

$$u_{\max} = 30 \text{ m/sec}$$

$$\sigma = 4.5 \text{ mhos/m}$$

$$B = 6 \text{ T}$$

$$S_e = \text{electrode area} = lw = 120 \times 5 \text{ cm}^2$$

The maximum volume flow rate is $Q = uA = 75 \text{ l/s} = 1.189 \text{ GPM}$.

The amount of power required to operate the thruster can be calculated below. Using Ohm's law we have the power density as

$$jE = juB + \frac{j^2}{\sigma}$$

The total power to the thruster is

$$IV = IuBd + \frac{I^2}{L\sigma}$$

The power consumed for electrolysis IV_o ($V_o = 2.19$ volts for NaCl solution) can be added to the above equation and we obtain the total power required as

$$IV = IuBd + I^2 R + IV_o$$

where the first term represents the power used for acceleration, the second term is dissipation (Joule heat) and the last term is power

consumed by the electrolysis effects, which is much smaller than the other two terms.

Figure 9 shows the power requirement for current density up to 1 amp/cm², while Figure 10 shows the low current range, up to 0.1 amp/cm². Power required for electrolysis is also shown in these figures which can be added to obtain the total power requirement. Figure 10 also shows the dissipation loss curve, IR².

To estimate the amount of gases generated by the electrolysis process, let us assume

$$j = 0.5 \text{ amp/cm}^2, \text{ thus}$$

$$I = jS_e = 300 \text{ amperes}$$

From Faraday's law we obtain,

$$\text{Cl}_2 = 300 \times 0.3674 \times 10^{-3} \text{ g/sec} = 1.102 \times 10^{-1} \text{ g/sec}$$

$$\text{H}_2 = 300 \times 0.0104 \times 10^{-3} \text{ g/sec} = 3.12 \times 10^{-3} \text{ g/sec}$$

The volume of the gases under standard conditions are:

$$V_{\text{H}_2} = (3.12 \times 10^{-3} \text{ g/sec}) / (0.09 \text{ g/l}) = 3.46 \times 10^{-2} \text{ l/sec}$$

$$V_{\text{Cl}_2} = (1.102 \times 10^{-1} \text{ g/sec}) / (3.19 \text{ g/l}) = 3.46 \times 10^{-2} \text{ l/sec}$$

$$V_{\text{H}_2\text{O}} = 75 \text{ l/sec}$$

$$\frac{V_{\text{H}_2} + V_{\text{Cl}_2}}{V_{\text{H}_2\text{O}}} = .09\%$$

The volume of the gases is very small as compared to the total volume of the duct. The effects on electrical conductivity is insignificant if the bubbles are uniformly dispersed in the liquid. However, it is not known how the bubbles are distributed near the electrode surfaces, nor do we know whether a film of gas will form. The latter is detrimental to the electrical conductivity. Investigating

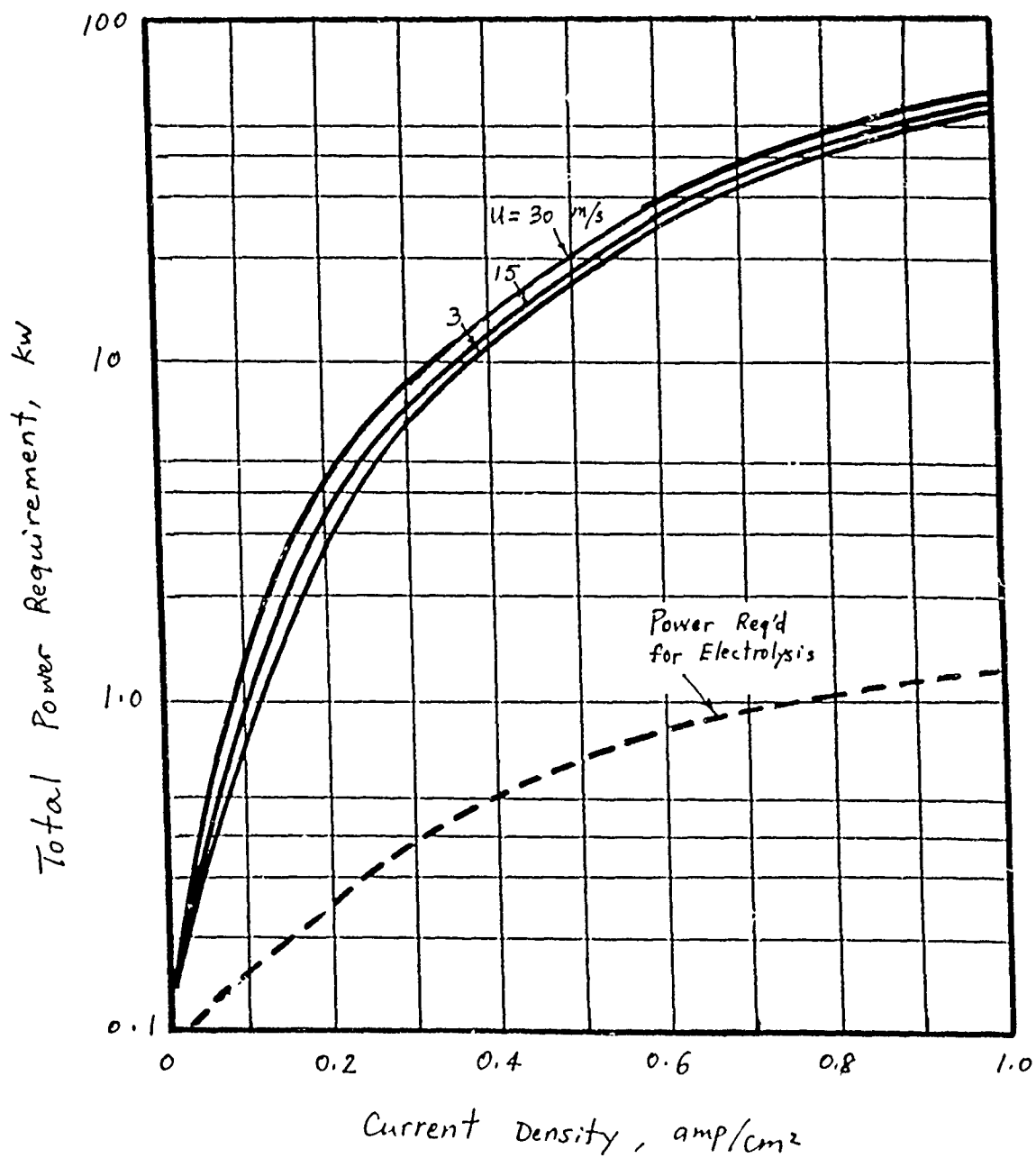


Figure 9. Power Requirement as Function of Current Density
(5 cm x 5 cm x 120 cm channel)

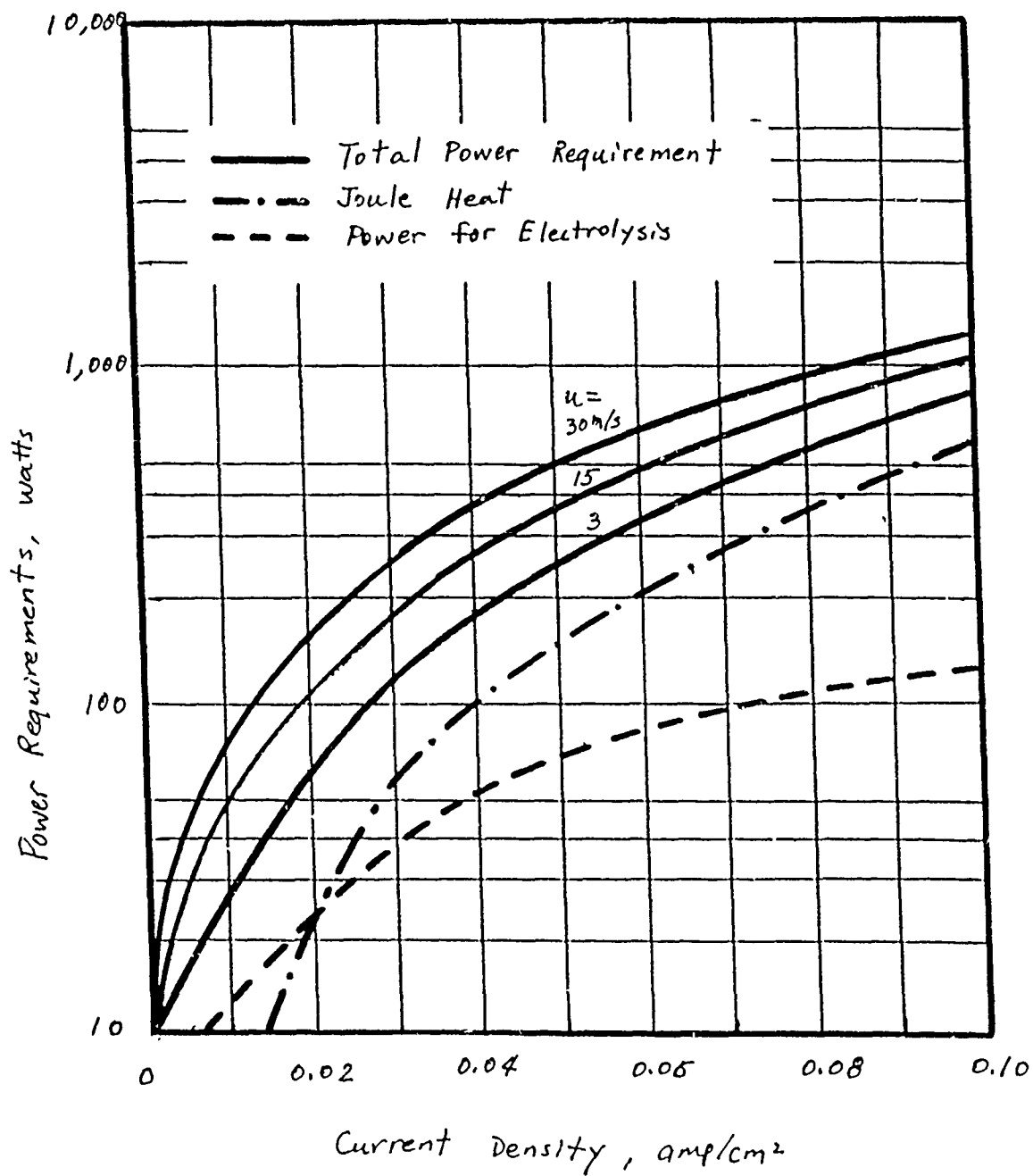


Figure 10. Power Requirement at Low Current Density of a 5 cm x 5 cm x 120 cm Test Section

bubble boundary layer and its effects on the electrical performance of the thruster is one of the key issues needed to be addressed.

7.0 CONCLUSIONS

Ideal thruster performance characteristics are presented and various loss mechanisms of seawater electromagnetic thrusters are discussed. The lack of quantitative experimental data seriously impact the ability to accurately predict the thruster performance, optimize thruster configuration and engineering data for design. It is recommended that a rigorous experimental program be initiated to investigate the fundamental issues of fluid mechanics, electrolysis and thruster performance characteristics.

REFERENCES

1. Rice, W. A., U.S. Patent 2997013, Aug. 1961.
2. Phillips, O. M., "The Prospects for Magnetohydrodynamic Ship Propulsion", Journal of Ship Research, pp. 43-51, March 1962.
3. Friauf, J. B., "Electromagnetic Ship Propulsion", Journal of American Society of Naval Engineers, pp. 139-142, Feb. 1961.
4. Doragh, P. A., "Magnetohydrodynamic Ship Propulsion Using Superconducting Magnets", Society of Naval Architects and Marine Engineers Annual Meeting, New York, Nov. 1963.
5. Way, S., "Propulsion of Submarines by Lorentz Forces in the Surrounding Sea", ASME WA/Ener 7, Nov. 1964.
6. Way, S. and Devlin, C., "Prospects for One Electromagnetic Submarine", AIAA paper 67-432, 1967.
7. Resler, E. L., Jr., "Magnetohydrodynamic Propulsion for Sea Vehicles".
8. Saji, Y., Kitano, M. and Iwata, A., "Basic Study of a Superconducting Electromagnetic Thrust Device for Propulsion in Seawater", Advanced Cryogenic Engineering, Vol. 23, pp. 159-169, 1967.
9. Way, S., "Electromagnetic Propulsion for Cargo Submarines", Journal of Hydronautics, Vol. 2, No. 2, pp. 49-57, 1968.

10. Yakovlev, V. I., "Theory of an Induction MHD Propellor with a Free Field", Zhurnal Prikladnoi Mekhaniki i Tekhuicheskoi Fiziki, No. 3, pp. 105-116, May-June, 1980.
11. Vasil'ev, A. P. and Kirko, I. M., "Optimization of a Marine MHD Propeller", Zhurnal Prikladnoi Mekhaniki i Tekhnicheskoi Fiziki, No. 3, pp. 86-94, May-June 1981.
12. Meng, J. C. S., Ed., "Proceedings of the NUSC/Industry Superconducting Electromagnetic Thruster (SCEMT) Workshop", NUSC Technical Document 6800, 1 June 1989.
13. Cott, D. W., Daniel, V. W. and Carrington, R. A., "Annular DC MHD Thrusters for Submarines", 27th Symposium on Engineering Aspects of Magnetohydrodynamics, Reno, ND, June 1989.
14. Chang, R., "Chemistry", Third Edition, pp. 790-791, Random House, 1987.
15. Vasil'ev, A. P., "Experimental Investigation of the Electrical Conductivity of a Two-Phase Stream", Inzhenerno-Fizicheskii Zhurnal, Vol. 39, No. 4, pp. 649-653, Oct. 1980.
16. Vasil'ev, A. P., "Experimental Study of Conduction-Type MHD-Channel Operating with Electrolyte", Magnitraya Gidrodinamika, No. 3, pp. 122-128, July-Sept. 1982.

THIS PAGE IS INTENTIONALLY BLANK

**BUBBLE PHENOMENA IN
SEAWATER MHD THRUSTERS**

Presented by

M. Brouillette

(Used with permission of STD Research Corporation, June 1990)

Bubble Phenomena in Seawater MHD Thrusters

M. Brouillette, G. S. Winckelmans
C. D. Maxwell, and S. T. Demetriades

STD Research Corporation
Arcadia, California

Abstract

The MHD submarine propulsion and pumping concepts offer the advantage of having no external moving parts, such as a propeller or turbine rotor, to produce acoustic noise. At first sight such a system would therefore appear to be much quieter. However, the passage of an electrical current in seawater may produce gas bubbles which can affect the performance and the acoustic signature of such thrusters.

This paper examines some of the scientific and technical issues to be resolved to ensure the attractiveness of the seawater MHD propulsion and pumping concepts. The emphasis is placed on the generation of bubbles on the surface of the electrodes and the possible sources of acoustic signature from them. Also reported are preliminary experiments performed in the STD Research Corporation Electrode Testing Rig (STD-ETR) on the formation of gas bubbles in seawater and saltwater.

1. INTRODUCTION

STD Research Corporation has supported work in saline water MHD since the company was founded in 1964. Early work was directed towards the realization of a practical MHD pump for conducting liquids including seawater, and a seawater MHD thruster. This field has been the subject of a low-level, long term effort at STD Research Corporation throughout the years, since it lies within an area of great interest to the company.

It should be noted that STD Research Corporation has built and used several types of saltwater MHD test facilities. One of these facilities was used in a prize-winning Science Fair project in 1986. Recently, STD Research Corporation has performed theoretical calculations on fluid dynamic aspects of bubble generation by hydrolysis and has put in operation a pressurized saltwater electrode testing rig.

We have found in our theoretical work that the two problems of bubbles and hydrodynamics are inextricably tied together for a large number of interesting conditions, and that the omission of the bubble problem from the incompressible flow problem often leads to trivial results. In our experimental work, we have found that there is no substitute for the study of the real working fluid (seawater), and that results obtained at atmospheric pressure conditions may be much different than results at depth.

2. BUBBLE DYNAMICS OF SEAWATER MHD THRUSTERS

2.1 Bernoulli analysis of MHD thrusters

The operation of ideal seawater MHD thrusters can be analyzed if it is assumed that the flow is incompressible and inviscid. The Bernoulli equation can easily be modified to take account of the Lorentz force. The Bernoulli equation then becomes

$$p_a + \frac{1}{2}\rho_w u_a^2 + \int_a^b J(x)B(x)dx = p_b + \frac{1}{2}\rho_w u_b^2, \quad (1)$$

where p is the static pressure, u is the flow velocity, $J(x)$ is the local current density, $B(x)$ is the local magnetic field, ρ_w is the density of water and the subscripts refer to each section a and b , respectively. Also used is the continuity equation, i.e., $u_a A_a = u_b A_b$.

For the general analysis of an MHD thruster, the following convention will be used for the flow in the frame of reference of the thruster (cf. Fig. 1): Station 0 refers to upstream infinity of a streamtube passing through the thruster, stations 1 and 2 refer to the thruster inlet and outlet, respectively, and station 3 refers to downstream infinity of the same thruster streamtube. In the frame of reference of the stationary water, the speed of the thruster is thus u_0 . At stations 0 and 3 the pressure matches that of the surroundings, and thus corresponds to the hydrostatic pressure p_∞ in the water at the depth of operation of the thruster. The pressure in the flow field near the exit of the thruster is probably not equal to the hydrostatic pressure in the water at the depth of operation of the thruster because of the external hydrodynamics of the outer shell of the thruster. Since p_2 matches the outside pressure at the exit, which is not necessarily p_0 , there is a pressure difference between the exit of the thruster and water at infinity. However, the assumption that $p_2 = p_0$ is usually made for simple Bernoulli-type analyses, as is shown in the figure.

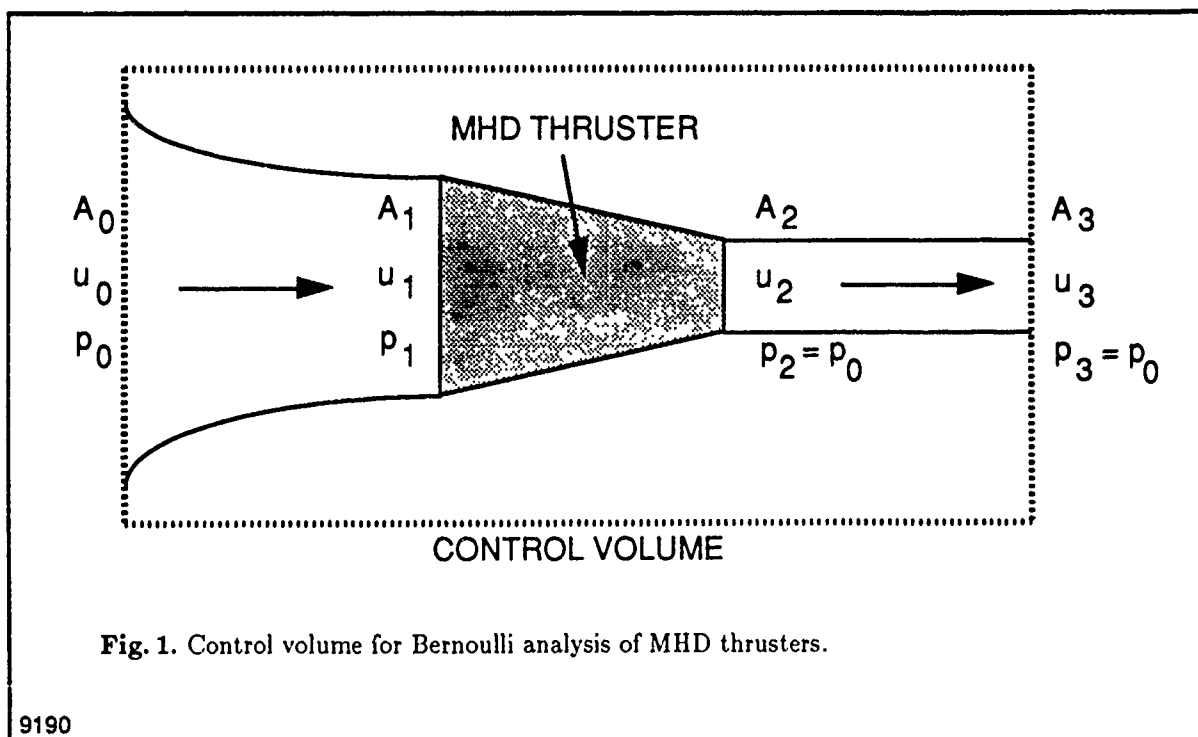


Fig. 1. Control volume for Bernoulli analysis of MHD thrusters.

Various geometries can be studied. The simplest is the constant area thruster without inlet diffuser and exhaust nozzle (Fig. 2). From continuity, the inlet and outlet velocities are equal, i.e., $u_1 = u_2$

In the limit that the thruster is short, the well-known actuator-disc propeller theory (e.g., cf. Ref. 1, p. 674) can be used to compute the MHD channel flow velocity u_1 and the exhaust pressure p_2 as a function of submarine speed and MHD parameters. These results are:

$$u_1 = u_2 = \frac{1}{2}u_0 + \frac{1}{2}\left(u_0^2 + \frac{2JBL}{\rho_w}\right)^{1/2} \quad (2)$$

and

$$p_2 = p_0 + \frac{1}{4}\rho_w u_0^2 + \frac{3}{4}JBL - \frac{1}{4}\rho_w u_0 \left(u_0^2 + \frac{2JBL}{\rho_w}\right)^{1/2} \quad (3)$$

Even though L is small for this particular case, JBL can be finite. It is seen that there can be a large pressure difference between the exit of the thruster and the far field in this case, and a vena contracta is necessary in the slipstream of the thruster to provide for the pressure adjustment.

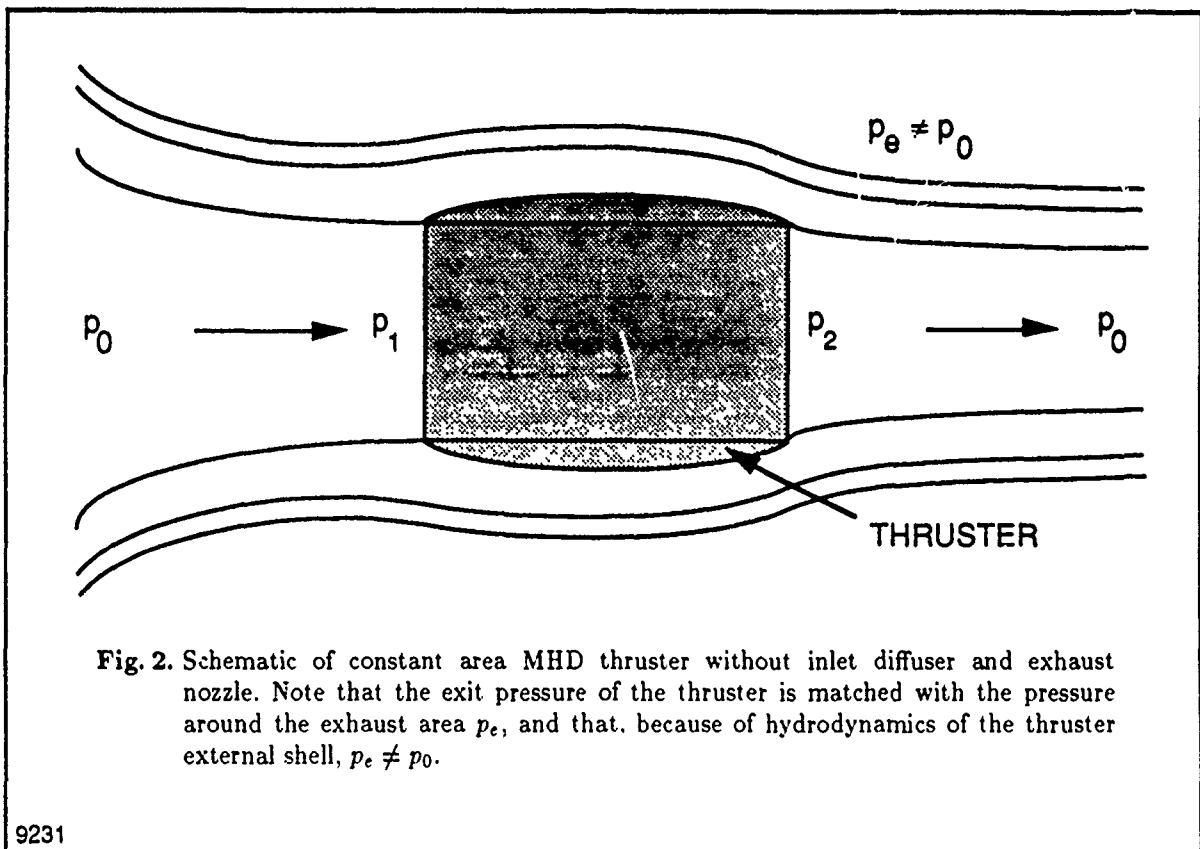


Fig. 2. Schematic of constant area MHD thruster without inlet diffuser and exhaust nozzle. Note that the exit pressure of the thruster is matched with the pressure around the exhaust area p_e , and that, because of hydrodynamics of the thruster external shell, $p_e \neq p_0$.

For larger aspect ratios (i.e., $L/D > 3$), the flow field for the constant area thruster without inlet diffuser and exhaust nozzle tends to a condition in which the exit pressure is ideally matched with that of the surroundings at infinity, and the slipstream is comprised of parallel streamlines. For this case, simple, ideal, 1-D Bernoulli analyses are not sufficient, mainly because of complex inlet phenomena.

Pressure matching between the exhaust jet coming out from the thruster and the flow field surrounding the back end of the device has at least two important implications. First, the drag penalty incurred if significant entrainment of fluid in the shear layer separating the streams issuing from inside and outside the thruster must be considered. This phenomenon is also present in propeller-driven devices. Second, if bubbles are present in the exhaust trail of the thruster, a pressure mismatch at some point

between the exit of the thruster (station 2) and downstream infinity (station 3) will lead to acoustic noise generation by bubble oscillation.

Although pressure matching along any exhaust streamline is not possible, the pressure mismatch can be made smaller by careful design of the internal geometry and electromagnetic parameters of the thruster. These problems can be addressed by the use of the incompressible versions of the STD/MHD computer codes to obtain more elaborate and realistic solutions that include boundary layer effects such as separation, vorticity, 2-phase (bubble) flows, etc.

2.2 Bubble Phenomena

The passage of an electric current through seawater can lead to effects with positive or negative implications for the performance and quietness of an MHD propulsion device. These include: chemical reactions taking place at the electrodes, modification of fluid mechanics of the flow over the electrodes by bubble generation and Ohmic heating. This section will look more closely at gas bubble creation and its subsequent effects on the electrical and fluid dynamical electrode phenomena.

2.2.1 Electrode Chemistry

Without taking into account the chemical reactions involving the electrode material itself, some very important chemistry takes place at both the cathode and anode when they are used to pass an electrical current through seawater. From a standpoint of activation energy, the chemical reactions in saltwater are possible only if the applied voltage is at least greater than the voltage required for each individual chemical reaction. For simplicity, only the sodium chloride component of seawater is considered here: At the anode, Cl^- ions combine to form chlorine gas (Cl_2) and water electrolyzes to form oxygen gas (O_2). At the cathode, H^+ ions combine and water electrolysis takes place to form hydrogen gas (H_2). If the applied voltage is greater than 1.36 Volts, then all those reactions are possible. If real seawater, which has a more complicated composition than the simple NaCl solution, is considered, then more complex chemical reactions would take place. Preliminary experimental observations in the STD-Electrode Testing Rig have shown a marked difference in the bubble dynamics between salt solutions and real seawater.

Chemical reactions involving the electrode material may be undesirable from at least two standpoints. First, the degradation of the electrodes would cause their surface to become non-uniform and lead to an increase in drag, and therefore degrade the performance of the thruster. Second, the products formed by these reactions can accumulate on the surface of the electrodes or on other underwater components as scale deposits, or could increase detectability by leaving an exhaust trace of different properties, such as color or pH, than that of the surrounding seawater. However, it should also be noted that chemical reactions involving the electrodes can be used advantageously to increase the conductivity of the MHD working fluid and to suppress bubble formation.

2.2.2 Bubble Formation

Possible adverse effects of the formation of gas on the surface of the electrodes include the increase of the effective resistance of the solution, which would prevent the desired electrical current density to be carried from one electrode to the other. Furthermore, the exhaust of a large amount of bubbles behind the thruster would cause a trail which might be observable. If the bubbles experience a pressure gradient at the exit of the thruster, an acoustic signature might be produced by bubble oscillation.

Assuming that all the gas produced at the electrodes forms into bubbles, and if surface tension is neglected, then the volumetric rate of gas formation can be obtained. At the cathode, where the arrival of two electrons causes the formation of one hydrogen gas molecule, the volumetric rate of production of hydrogen gas \dot{Q}_{H_2} (in m^3/s at 0°C) is given by:

$$\dot{Q}_{\text{H}_2} = \frac{\mathcal{K}I}{p_{\text{amb}}} \quad (4)$$

where I is the total current passing through the electrode (in Amperes). p_{amb} is the ambient absolute pressure (in atmospheres or Pascals) and $\mathcal{K} = 1.16 \times 10^{-2} \text{kg} \cdot \text{m}^2/\text{A} \cdot \text{s}^3 = 1.16 \times 10^{-7} \text{m}^3 \cdot \text{atm}/\text{A} \cdot \text{s}$.

The formation of gas at the anode can also be calculated, but because both oxygen and chlorine gases are formed there, it is necessary to know the chemical processes in more detail. However, the total volumetric gas formation at the cathode can never exceed that at the anode, and therefore, the value for hydrogen formation can be used as an upper bound for the combined formation of oxygen and chlorine gas bubbles.

Another important consideration about the formation of gas bubbles at the electrodes is their size. Many factors could influence the size of the bubbles forming on the electrodes. The ambient pressure p_{amb} is a primary factor, along with surface tension σ_T , since they are related to the bubble radius R by: $p_b = p_{amb} + \frac{2\sigma_T}{R}$ where p_b is the gas pressure inside the bubble. Other possible factors include: (i) the current density supplied to the electrodes, (ii) the electrode material and the number and size of possible nucleation sites, (iii) the electrode geometry, (iv) the water flow velocity, which influences the shearing forces under which the bubbles must form, (v) the water temperature, which affects both the solubility of the gas and the surface tension of the gas-water interface, and (vi) the actual composition of the seawater, which affects electrode chemistry.

After they are formed, the bubbles are entrained by the water flowing in the duct. The size of the bubbles affects the time taken by the bubbles to relax to the velocity of the water flow and also determines their vertical, buoyancy-induced velocity. Furthermore, the bubble size influences the time taken for the gas within a bubble to dissolve into the water surroundings and affects the acoustic energy when a bubble undergoes a volume change because of a pressure gradient. These issues are examined in more detail in the following sections.

2.2.3 Bubble velocity relaxation

The effect of the gas bubbles on the water flow inside the MHD channel depends primarily on the relative velocity between the bubbles and the water flow. If there is a large velocity difference, a boundary layer will form on the surface of the bubble itself, leading to an increase in mass, momentum and energy transfer by molecular diffusion, viscosity and conduction, respectively. If the relative velocity is very large, high strain rates may even shred the bubble to pieces. If there is no relative velocity between the bubbles and the water, then the analysis for the dissolution and cooling of the bubbles is also greatly simplified.

The time t_u taken by a stationary gas bubble to be accelerated by a water flow to the velocity u_w of water can be evaluated by considering the sum of the forces on a single accelerating bubble. If the Reynolds number ($\equiv \rho_w u_w R / \mu_w$, where μ_w is the dynamic viscosity of water) for the flow over the spherical bubble is small enough, the drag force D on the bubble is obtained by modifying Stokes' formula to account for the fact that the shear field on a bubble is different than that on a solid sphere (cf. e.g., Ref. 2). Then, the time taken by a bubble to be accelerated to 99 percent of the water velocity is given by:

$$t_u \approx \frac{R^2 \rho_u}{\mu_w} \quad (5)$$

It is seen that t_u is independent of the bubble gas density and of the velocity of the water flow. For typical values of bubble size of $R = 10 \mu\text{m}$, then $t_u \approx 0.1 \text{ ms}$ and for $R = 100 \mu\text{m}$, then $t_u \approx 10 \text{ ms}$. Since the residence time $t_L \equiv L/\bar{u}$ of the flow inside the MHD channel is usually much larger than this, then it can be assumed that most of the bubbles are at rest with respect to the water flow throughout the MHD channel. However, one should keep in mind that this simple analysis neglects the mutual interaction of the bubbles. Therefore, the time taken by the bubbles to come to rest with respect to the water flow might be longer because the bubbles might be coalescing in bunches.

2.2.4 Buoyancy-Induced Vertical Velocity of Bubbles

By the same type of analysis presented in the previous section, the terminal velocity induced by buoyancy forces on the bubbles can be computed as:

$$u_B = \frac{R^2 g}{\nu_w} \quad (6)$$

For example, for $R = 10 \mu\text{m}$, then $u_B \approx 0.3 \text{ mm/s}$ and for $R = 100 \mu\text{m}$, then $u_B \approx 3 \text{ cm/s}$. For typical bubble residence times inside the MHD thruster, the vertical displacements associated with buoyancy-induced motions are not large.

2.2.3 Gas Solubility

Because seawater is not saturated with any of the possible gas species produced by electrochemistry at the electrode, the bubble's size will decrease with time by dissolution of the gas into water. Of interest is the determination of the time t_D taken to dissolve a bubble of a known size. If this time is shorter than the residence time of a bubble inside the MHD channel, then no bubbles will be present at the exit of the generator.

The process by which the gas is dissolved is simple molecular diffusion, and the analysis can be performed by using results obtained from Fick's law, since, as seen in the previous section, the bubbles can be assumed to be at rest with respect to the water flow. It is assumed that the gas composition is known, that the bubble remains spherical, the gas concentration in the water is negligible and, as the bubble dissolves and shrinks, that its temperature remains in equilibrium with the surroundings. The time t_D required to dissolve a bubble completely, i.e., to reduce its radius from an initial value R_0 to zero is given by:

$$t_D = \frac{1}{3D} \left[\frac{3}{2} R_0^2 - \frac{4\sigma_T^2}{p_{amb}^2} \ln \left(\frac{2\sigma_T}{R_0 p_{amb} + 2\sigma_T} \right) - \frac{2\sigma_T}{p_{amb}} R_0 \right] \quad (7)$$

where D is the molecular diffusion coefficient, p_{amb} is the pressure outside the bubble and σ_T is the surface tension coefficient. If surface tension is neglected, the time required to dissolve a bubble of size R_0 is given by: $t_D = (R_0^2/2D)$.

For example, for a hydrogen gas bubble having an initial radius of $10 \mu\text{m}$ at $p_{amb} = 1 \text{ bar}$ and $T_{amb} = 25^\circ\text{C}$, the time taken to dissolve it completely is calculated to be $t_D = 15 \text{ ms}$. For $R_0 = 100 \mu\text{m}$ then $t_D = 1.5 \text{ s}$. As the ambient pressure is increased with submarine depth, the size of the bubbles decreases and thus their dissolution time is reduced. From Eq. (7), one also sees that the effect of surface tension becomes smaller with depth, i.e., with increased p_{amb} .

Values of molecular diffusion coefficients for the gases of interest for the present problem are shown in Table 1 (from Ref. 3, p. 534).

Table 1. Molecular diffusivities of gases in water.

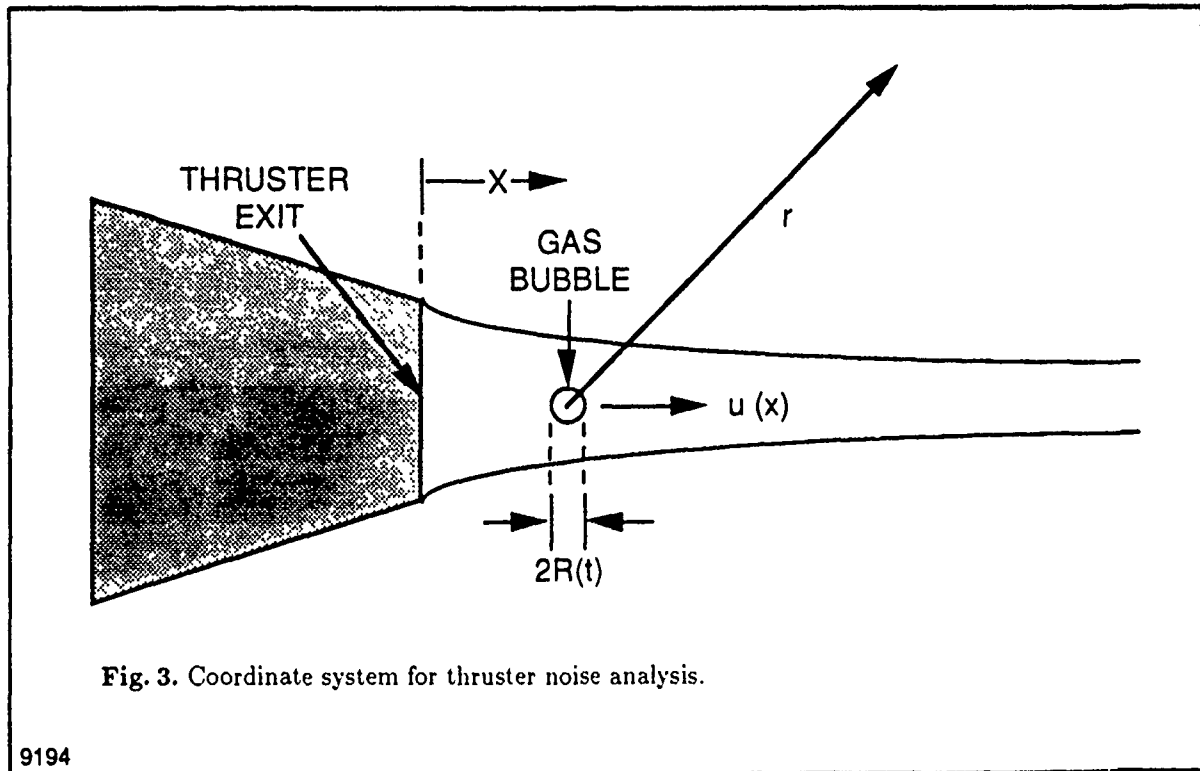
Gas	Molecular diffusion coefficient D ($\times 10^{-9} \text{ m}^2/\text{s}$)
Hydrogen at 25°C	3.36
Oxygen at 25°C	2.60
Chlorine at 12°C	1.40

Preliminary experimental observations of bubble formation by seawater electrolysis (cf Section 3) has shown that dissolution times are much larger than the values predicted by the theory presented above. One reason to explain this disagreement could be that bubbles formed in real seawater are of a different nature than those formed in pure or salt water, such that the diffusion coefficient and the surface tension can be different than the assumed values. These effects need to be investigated.

2.2.6 Noise Generation by Bubbles

If the dissolution time t_D of gas bubbles is larger than their residence time inside the MHD channel, then bubbles will be present in the exhaust trail of the thruster. If the exit pressure of the thruster is not matched with the hydrostatic pressure of the surrounding water or if there is any other pressure gradient in the slipstream, each bubble will have to adjust its volume to this change in pressure. In doing so, the bubbles also send out acoustic waves which must be evaluated. If surface tension is neglected and the gas temperature is assumed to remain in equilibrium with the water temperature, the ratio of the size R_2 of a bubble at the exit of a constant area MHD thruster to its size R_3 after it has adjusted to the hydrostatic pressure $p_3 = p_\infty = p_0$ can be obtained from: $R_3/R_2 = (p_2/p_0)^{1/3}$.

If the change in radius of the bubble is small compared to its radius, then a simple 3-D acoustic theory can be used to determine the intensity of the acoustic radiation. The geometry of interest is shown in Fig. 3, where r is the radial distance from the center of the bubble. The equation for the change in bubble size as a function of surrounding pressure was first derived by Rayleigh (Ref. 4), and subsequently modified to include the effects of viscosity and surface tension (cf., Ref. 5). If it is assumed that the gas bubble motion follows a polytropic law of compression/expansion with a polytropic exponent κ , then its natural frequency of oscillation is given by: $\omega_0^2 = (3\kappa p_b - (2\sigma_T/R_0))/(\rho_w R_0^2)$. If the change in volume of the bubble is isothermal then $\kappa = 1$ and if it is isentropic $\kappa = \gamma$, the specific heat ratio. With this assumption, energy dissipation arises only from liquid viscosity and compressibility. A more accurate, but more tedious, analysis would involve the solution of the complete set of linearized conservation equations of mass, momentum and energy both in the gas and the water (cf. Refs. 6 and 7).



It is also supposed that, to first order, the bubbles experience a constant pressure gradient, so that the ambient pressure varies linearly with time, i.e.,

$$p_{amb} = p_2 \left(1 + \frac{u_2}{p_2} \frac{dp}{dx} t \right) \quad \text{where} \quad \frac{dp}{dx} \approx \frac{p_2 - p_0}{\ell_p} \quad (8)$$

The pressure relaxation length ℓ_p has to be determined from the fluid mechanics of the flow in the region of the pressure nonuniformity.

If $\kappa \approx 1$ then $\omega_0^2 \approx (p_2/\rho_w R_0^2)$, and the expression for the radiated energy Φ can be expressed as:

$$\Phi(r) = \left(\frac{1}{r^2}\right) \left(\frac{dp}{dx}\right)^2 \frac{u_2^2 R_0^4}{8a_w p_2} \quad (9)$$

where a_w is the sound speed in water.

The energy radiated by a single bubble can be used to estimate the total noise of the entire collection of bubbles in the slipstream. Since there is a large number of bubbles all oscillating with a different phase, an observer at a large distance from the device would not feel a variation in mass or momentum flux. Then the group of emitting bubbles can be represented as a quadrupole noise source, similar to the sources causing the noise at the exhaust of jet engines (cf. Refs. 8 and 9). The quadrupole solution can be directly obtained from the single bubble relation as:

$$\Phi^{\text{quadrupole}} = \Phi_{\text{bubble}}^{\text{single}} \left(\frac{2\pi\ell}{\lambda}\right)^4 \quad (10)$$

where $\Phi_{\text{bubble}}^{\text{single}}$ is the average acoustic energy radiated by one bubble, as obtained from Eq. (9), ℓ is the average spacing between the bubbles and λ is the wavelength of the sound emitted by the bubbles, obtained from $\lambda = 2\pi a_w/\omega$. The total acoustic energy flux emitted by all the bubbles can then be obtained by multiplying the contribution of one quadrupole (i.e., Eq. (10)) by the total number of quadrupoles N_q . Since the bubble oscillations decay rapidly due to damping, we only consider as noise sources the bubbles present in a slab of thickness $(u_2 \rho_w R_0^2)/\mu_w$ in the exhaust trail of the thruster.

For the short constant area thruster without inlet diffuser and exhaust nozzle, i.e., the actuator disc thruster of Section 2.1, if gas solubility is ignored, the total average acoustic energy flux becomes:

$$\Phi^{\text{total}} = 0.050 \frac{p_2 A_1^{4/3} R_0^3 u_2^{10/3}}{a_w^5 \rho_w \mu_w \dot{Q}_{H_2}^{1/3}} \left(\frac{dp}{dx}\right)^2 \left(\frac{1}{r^2}\right) \quad (11)$$

All these parameters are easily obtained from the operating conditions of the MHD thruster, except for R_0 and ℓ_p that need to be evaluated separately.

It can be seen from this formula that the noise output: (i) increases with bubble size, (ii) increases with thruster size, (iii) increases with submarine speed, (iv) increases with submarine depth. The dependence of the total acoustic energy flux on applied current density J and magnetic field B can also be obtained from Eq. (20) by substituting the expressions for u_2 , p_2 and \dot{Q}_{H_2} given by Eq. (2), Eq. (3) and Eq. (4), respectively. It is found that the noise level increases with both applied current density and magnetic field.

It is seen that, in the study of the noise problem, efforts should be focused on the study of the two unknown parameters in this equation: bubble size and the time taken for the exhaust flow to be pressure matched with the hydrostatic water pressure (i.e., the determination of the value of the pressure relaxation length ℓ_p from Eq. (13) or the characteristic length of any other pressure disturbance in the slipstream). As with the solubility analysis, the size of the bubbles is thus critical to the evaluation of noise generation by MHD thrusters. Not only will the noise produced by a seawater MHD device decrease with bubble size, but as it will be seen below, the acoustic waves emitted by smaller bubbles will be attenuated more as they propagate into seawater because of their higher oscillation frequency.

To evaluate an upper bound to the source level (SL) of constant area MHD thrusters, consider bubbles in the slipstream of the actuator disc thruster. The decibel (dB) level of underwater acoustic sources is defined as (cf. Ref. 10):

$$\text{SL (dB)} = 10 \log_{10} \frac{\Phi(\text{at } r = 1 \text{ yard})}{0.67 \times 10^{-18} \text{ W/m}^2} \quad (12)$$

For example, consider a thruster with $J = 5000 \text{ A/m}^2$ and $BL = 100 \text{ T} \cdot \text{m}$ and a thruster area of $A_1 = 1 \text{ m}^2$. Assume operation of the submarine at depths of 0 and 100 m, at speeds from 5 to 20 m/s. For illustration, two possible bubble sizes are considered: $R_0 = 10 \text{ } \mu\text{m}$ and $R_0 = 100 \text{ } \mu\text{m}$. Also, the constant ℓ_p can be estimated from Eq.(13), from thruster internal and external hydrodynamics. Calculations were performed with ℓ_p either 1 m or 10 m, both reasonable values. The results are shown in Table 2. It is found that a maximum noise level of 121 dB is produced at a submarine depth of 100 m and the maximum speed of $u_0 = 20 \text{ m/s}$, with a bubble size $R_0 = 100 \text{ } \mu\text{m}$. The minimum noise level, 60 dB, is produced at sea level at 5 m/s, with $R_0 = 10 \text{ } \mu\text{m}$. This can be compared to typical values of broadband acoustic level data given in Ref. 10. They range from around 130-140 dB for electric submarines used in the Second World War, to 90-110 dB for SSBN-726 class submarines. Considering that the present calculation effectively places an upper bound to the noise level of seawater MHD thrusters, it appears that this type of propulsion could achieve a reduction in noise level over today's most sophisticated devices. Furthermore, various noise abatement approaches could be used to reduce the noise generated even more. For example, this could be achieved by changing the geometry of the thruster and its exhaust trail, by acoustically treating the outlet region of the device, by preventing the escape of bubbles and finally by ensuring that the bubbles remain small or nonexistent.

This discussion points out the need for integrating noise analysis to the design of MHD submarine thruster, since noise performance is probably as important as efficiency.

The noise attenuation in the seawater surrounding the thruster can be evaluated from simple acoustic theory (cf. Ref. 11). In one dimension, the acoustic flux at a location x is related to that at $x = 0$ by:

$$\Phi(x) = \Phi(0) \exp \left(-\frac{\omega^2 \delta}{a_w^2} \right) \quad (13)$$

where the diffusivity δ is defined as:

$$\delta = \frac{\mu_w}{\rho_w} \left(\frac{4}{3} + \frac{\mu_{vw}}{\mu_w} + f(Pr) \right) \quad (14)$$

In this case, noise attenuation is due to both viscous dissipation, through μ_w and μ_{vw} , the latter being the bulk viscosity of water, and heat diffusion, through a function f of the Prandtl number Pr . For pure water, $\delta = 4.4 \cdot 10^{-6} \text{ m}^2/\text{s}$. For seawater, δ is somewhat larger and depends on frequency. A plot of attenuation vs. frequency in seawater is given on page 245 of Ref. 10.

Noise attenuation also takes place at the source of submarine noise, i.e., inside the exhaust trail of the thruster, because of noise absorption by the bubbles themselves. For this case, the attenuation can be evaluated by modeling the bubble-water mixture as a fluid having the same properties of water, except for a higher bulk viscosity. The bulk viscosity of a bubble-water mixture has been evaluated analytically by Taylor (Ref. 12) as:

$$\mu_v = \frac{4}{3} \frac{\mu}{X_v} + \frac{2}{3} \mu \quad (15)$$

where X_v is the volume fraction of gas in mixture. This formula is valid for $X_v > 10^{-4}$; the compressibility of water has to be taken into account for smaller values of X_v . The high bulk viscosity of the bubble-water mixture is such that the diffusion coefficient δ is about four orders of magnitude larger than that of water alone, leading to a much higher attenuation coefficient.

In view of the large attenuation coefficient for noise of high frequency, it is seen that, if the bubbles can be kept small, the seawater MHD propulsion concept could fulfill its promise of difficult acoustic detection.

Table 2. Noise produced by a constant area MHD thruster, i.e., actuator disc thruster with $J = 5000 \text{ A/m}^2$, $BL = 100\text{T} \cdot \text{m}$ and $A_1 = 1 \text{ m}^2$.

p_0 (bars)	u_0 (m/s)	R_0 (μm)	ℓ_p (m)	SL (dB)
1	5	10	1	80
			10	60
			100	110
		10	1	90
			10	81
			100	61
	10	10	1	111
			10	91
			100	82
		10	1	62
			10	112
			100	92
	15	10	1	84
			10	64
			100	114
		10	1	94
			10	87
			100	67
10	5	10	1	117
			10	97
			100	88
		10	1	68
			10	118
			100	98
	10	10	1	90
			10	70
			100	120
		10	1	100
			10	91
			100	71
	15	10	1	121
			10	101
			100	
		10	1	
			10	
			100	

2.2.7 Ohmic Losses

In addition to the bubble formation problem, the passage of large currents into the water electrolyte causes a temperature increase by electrical losses. If the temperature increase is large a significant thermal signature could be observed at the exit of the thruster. The temperature increase ΔT for the constant area thruster having a constant current density is given by:

$$\Delta T = \frac{J^2 L}{\sigma \rho_w C u_1} \quad (16)$$

where σ is the electrical conductivity and C is the heat capacity of seawater. For the case discussed in the previous section, with $u_1 = 10$ m/s, the temperature increase is about 1.2°C . This may or may not pose a problem, depending on depth, sea-state and enemy detection capabilities.

This discussion on temperature signature, as well as considerations about electrical losses, point out the need for thrusters operating with the largest possible magnetic field and the lowest possible applied current density.

2.2.8 Boundary Layer Modification and Drag Reduction by Bubble Injection

The performance of the seawater MHD thruster will depend strongly on the influence of the bubble formation on the flow over the electrodes and the sidewalls. Numerical models are needed to predict and optimize the performance of the device. Computer models for both laminar and turbulent boundary layer and channel flows have proven their effectiveness. However, the modification of these models or the creation of new ones to take bubble phenomena into account cannot be expected to be successful before a good data base is available for these particular flows.

For turbulent boundary layer flows with bubble injection, these models may be modified by assuming that the characteristics of the turbulence are unchanged by the addition of gas bubbles (e.g., Ref. 13). This assumption is valid if the rate of bubble injection is small, but it has been found that, at higher injection values, the basic nature of the turbulence is indeed modified (cf. Ref. 14). Furthermore, because of the presence of coherent structures in these turbulent flows, an analysis based on a turbulence model adapted from bubble-less flow might not be adequate, since the average electrical properties of the flow would be very sensitive to the structures developing in the actual flow with bubbles. For a more realistic analysis and efficient optimization of MHD seawater propulsion devices, it is necessary that new computer codes be developed and that experiments be initiated to provide input and validation data.

The experimental study of Ref. 14 also reported a dramatic reduction in skin friction by bubble injection for flat plate, turbulent boundary layer flows in water. Miniature flush-mounted hot film probe measurements of the shear stresses downstream of a gas bubble ejection section have shown that a fivefold reduction in skin friction is achievable for this flow. Therefore, bubble generation at the electrodes could be used advantageously to improve the performance of a seawater MHD thruster.

3. OBSERVATIONS OF BUBBLE FORMATION IN HIGH PRESSURE SEAWATER

To define critical issues on the performance of electrodes in seawater, as well as to perform preliminary measurements on bubble size and gaseous film evolution as a function of electrode material, surface treatment, current density and ambient pressure, we have performed tests with a small electrode testing rig (ETR).

The testing device, shown in Fig. 4, comprises a 260 cm^3 volume that can be pressurized up to 100 bars, which corresponds to a submarine depth of 1000 m. Two electrodes, each having a surface area of 19.3 cm^2 are facing each other, 5.1 cm apart. The test rig is made out of clear acrylic so that visualization of the electrode phenomena can be accomplished.

We have performed preliminary experiments on the suitability of various electrode materials and on the structure of free convection flows of bubbles over vertical electrodes with some very interesting results.

3.1 Electrode Material

Preliminary experiments with both copper and graphite electrodes have shown that, because of chemical reactions, copper does not seem to be a suitable choice. Graphite, on the other hand, was observed to tolerate large values of current densities without suffering any surface damage on either electrode.

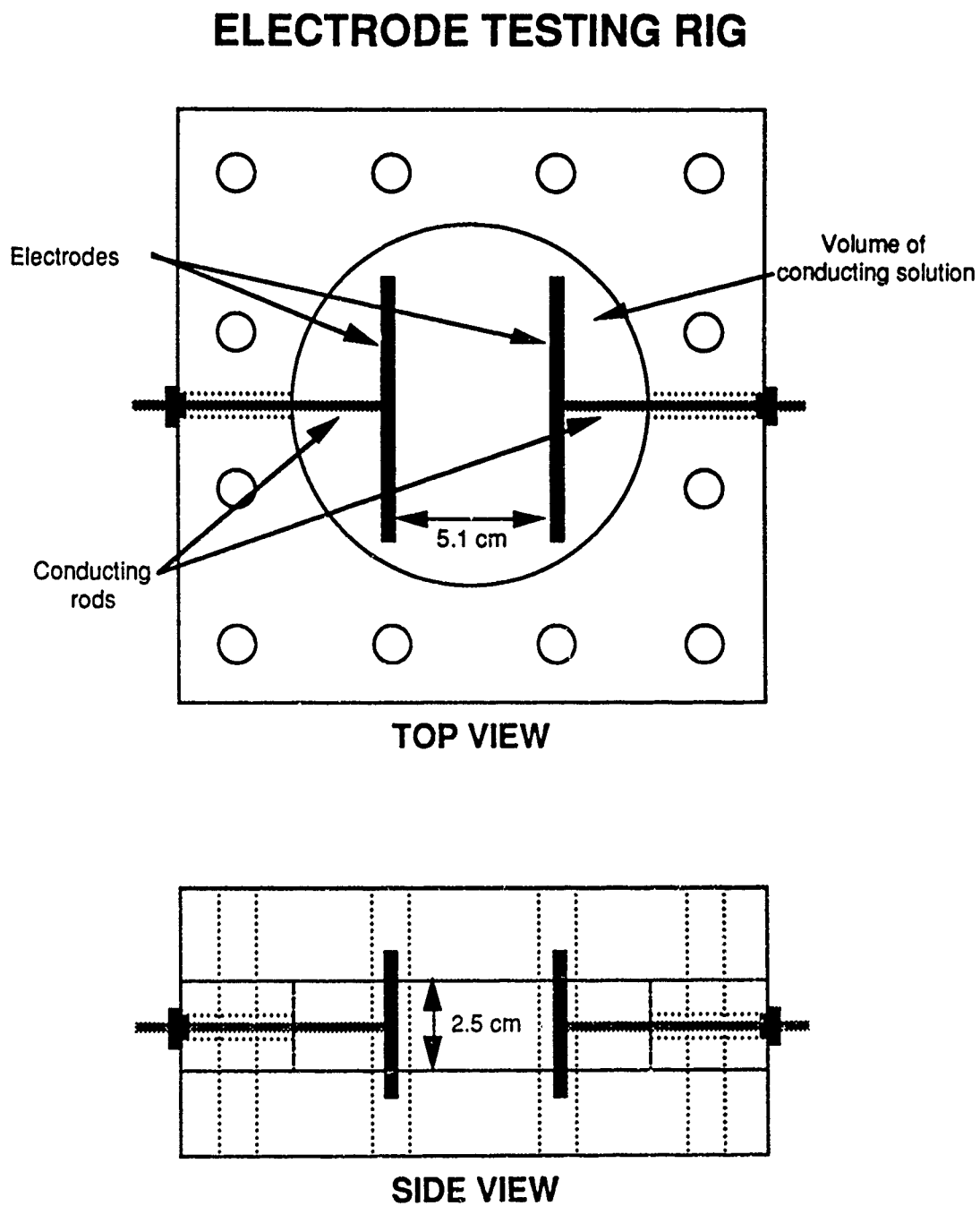


Fig. 4. Schematic of STD Research Corporation Electrode Testing Rig (ETR).

9201P

3.2 Free Convection of Bubbles over Vertical Electrodes

Experiments were performed with vertical electrodes, to examine the buoyancy-induced (i.e., free convection) flow of bubbles over the electrodes. Preliminary observations show that this flow of bubbles over the electrodes is similar to single-phase, single-fluid (i.e., ordinary) forced convection turbulent boundary layer flow over a flat plate. It was observed that the flow over the lower part of the electrode is laminar. At some distance from the lower end of the electrode (which corresponds to the leading edge of the flat plate) transition is observed to occur to what seems to be a turbulent flow. It has been found that the hydrogen gas flow over the cathode and the oxygen and chlorine gas flow over the anode have very distinguishable features.

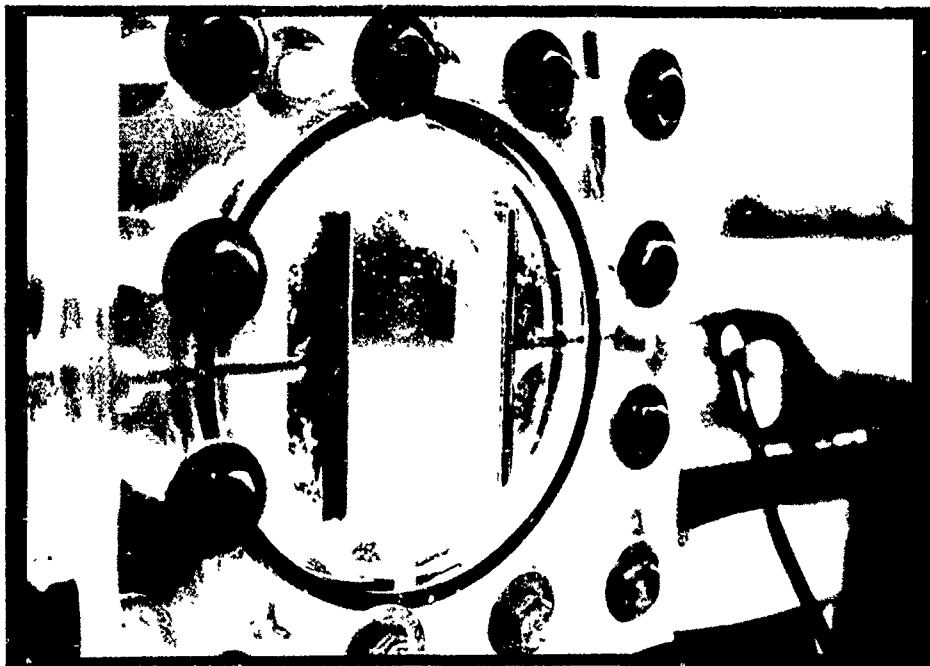
The influence of electrolyte composition and ambient pressure on the transition point location and the observable characteristics of the subsequent turbulent flow has also been investigated. It has been found that saltwater, a 3.5 percent by mass solution of rock salt into tap water, exhibits different characteristics than real seawater collected at Topanga Beach, California. The turbulent flow in the seawater has features than are analogous to the oblique Tollmien-Schlichting waves and the turbulent spots common to ordinary turbulent boundary layers (Ref. 15). The appearance of lifting turbulent spots is also accentuated as the pressure is increased. These electrode phenomena are shown in Fig. 5 and Fig. 6 for a current density of 9000 A/m^2 in real seawater at a pressure of 34 bars. The oblique instability waves are clearly visible in the close-up of Fig. 6. These waves were not observed at atmospheric pressure and the rock salt solution did not exhibit those turbulent structures. This difference in behavior between seawater and saltwater could be attributable to different values of viscosity for these two solutions, which could affect the effective Reynolds number for this flow. Furthermore, since the seawater has a larger number of dissolved salts than the simple saltwater solution, the nature of the products at the electrodes could be different.

4. CONCLUSIONS

Passage of an electric current in seawater can lead to gas bubble generation by chemical reactions. The formation, evolution, trajectories, and history of these bubbles and the magnetohydrodynamics of the flow are intimately connected. Since the bubbles are likely to be small, they will reach a terminal velocity with respect to the surrounding water very rapidly, unless bunching up slows down this process. The size of the bubbles is a critical parameter because. (i) it determines the time taken by the bubbles to dissolve, and therefore whether or not bubbles are present in the slipstream of the thruster and (ii) it influences the level of acoustic noise emitted by bubbles when exposed to pressure gradients of sufficient magnitude. Other issues possibly depending on bubble size include the increased resistivity of the bubble-water mixture and the skin friction drag reduction by bubble formation on the electrodes. A number of the STD/MHD codes can give elaborate and realistic solutions of the combined bubble/magnetohydrodynamic problem.

Work on a small test rig at STD Research Corporation has shown that there exists a marked difference between phenomena observed in real seawater and simple saltwater and between operation at surface pressure and operation at depth. Observations of bubble lifetime suggest that the usual bubble properties may be different for seawater, owing to the complex chemical composition of the latter.

(A)



(B)

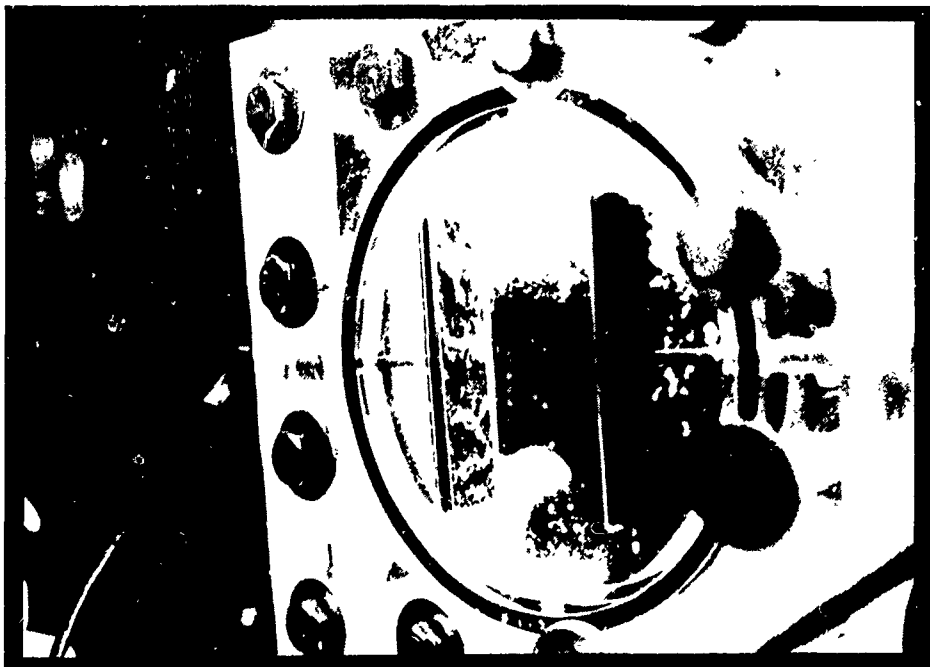


Fig. 5. Free convection bubble flow pattern in ETR with graphite electrodes. $J = 9000 \text{ A/m}^2$, $p = 34 \text{ atm}$. (a) Hydrogen bubble flow over cathode, (b) Chlorine and oxygen flow over anode.

9197P

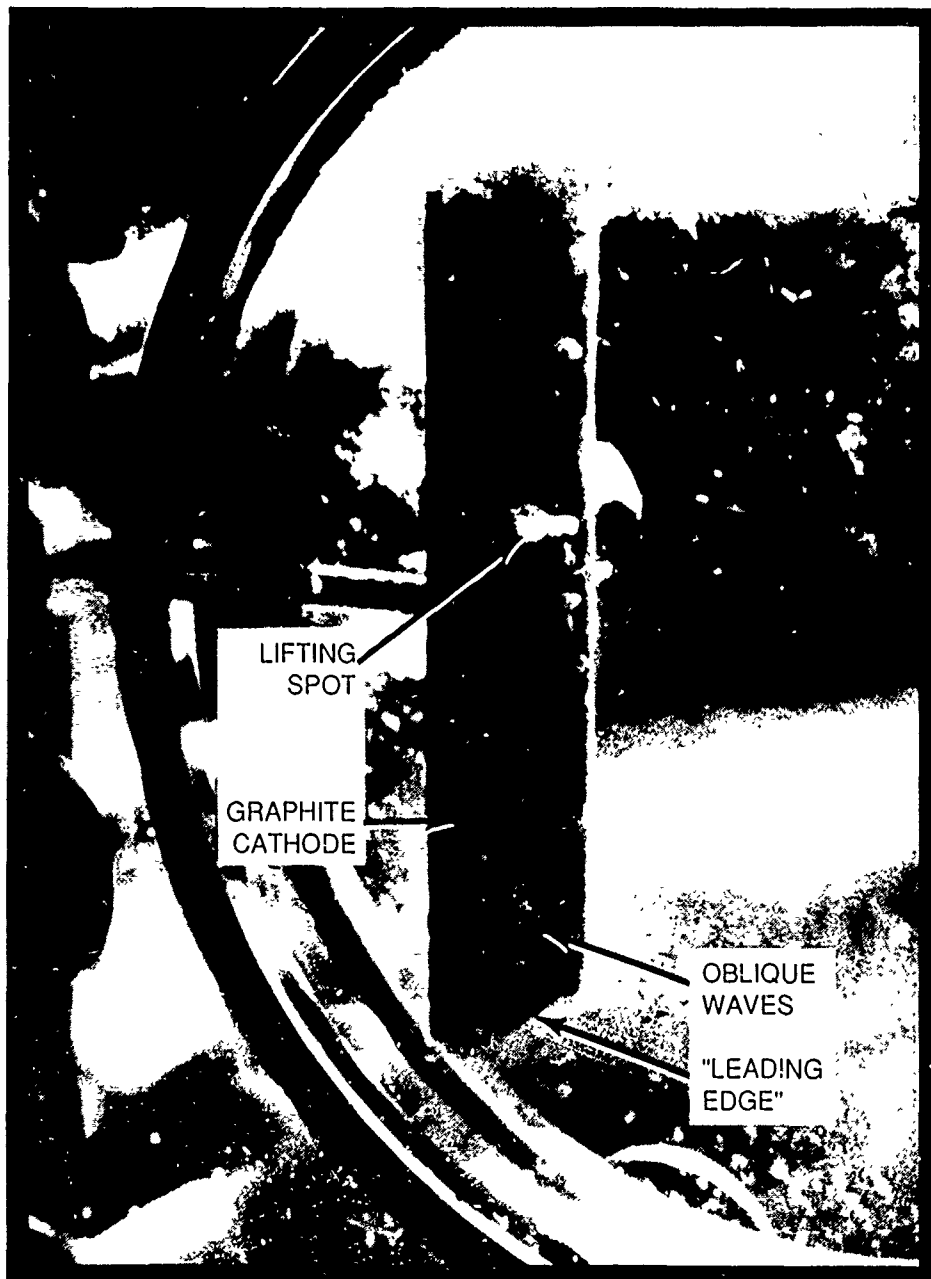


Fig. 6. Free convection pattern in ETR with graphite electrodes. $J = 9000 \text{ A/m}^2$, $p = 34$ atm. Close-up of chlorine and oxygen flow over anode.

9199P

References

1. Duncan, W.J., Thom, A.S. and Young, A.D., *Mechanics of Fluids*, Edward Arnold, London, 1970, p. 674-677.
2. Batchelor, G.K., *An Introduction to Fluid Dynamics*, Cambridge University Press, Cambridge, 1967, p. 229-240.
3. Kreith, F. and Black, W.Z., *Basic Heat Transfer*, Harper and Row, New York, 1980, p. 480-486.
4. Rayleigh, Lord, *Philos. Mag.*, Vol. 34, 1917, p. 94-98.
5. Plesset, M.S. and Prosperetti, A., "Bubble Dynamics and Cavitation," *Ann. Rev. Fluid Mech.*, Vol. 9, 1977, p. 145-185.
6. Pfriem, H., *Akust. Zh.*, Vol. 5, 1940, p. 202-212.
7. Plesset, M.S. and Hsieh, D.Y., *Phys. Fluids*, Vol. 3, 1960, p.882-892.
8. Lighthill, M.J., "On Sound Generated Aerodynamically," *Proc. Roy. Soc.*, Vol. A 211, 1952, p. 566.
9. Ffowcs Williams, J.E., "Flow Noise," *Annual Review of Fluid Mechanics*, Annual Reviews, 1969.
10. Stefanick, T., *Strategic Antisubmarine Warfare and Naval Strategy*, Lexington Books, Lexington, 1987, p. 241-291.
11. Thompson, P.A., *Compressible-fluid Dynamics*, Maple Press Company, 1984, p. 225-233.
12. Taylor, G.I., "The Two Coefficients of Viscosity for an Incompressible Fluid Containing Air Bubbles," *Proc. Roy. Soc.*, Vol. A 226, 1953, p. 34-39.
13. Vasil'ev, A.P., "Empirical Method for Calculating a Bubble Boundary Layer on the Electrode of a Conduction MHD Channel," *Magnitnaya Gidrodinamika*, No. 3, July-September 1986, p. 104-109.
14. Pal, S. Deutsch, S. and Merkle, C.L., "A Comparison of Shear Stress Fluctuation Statistics Between Microbubble Modified and Polymer Modified Turbulent Boundary Layers," *Phys. Fluids A*, Vol. 1, No. 8, August 1989, p. 1360-1362.
15. Tritton, D.J., *Physical Fluid Dynamics*, Van Nostrand Reinhold (UK), Wokingham, 1977, p. 222-228.

THIS PAGE IS INTENTIONALLY BLANK

**LOW NOISE ELECTRODE SYSTEMS FOR
MHD PROPULSION**

Presented by

J. K. Koester

LOW NOISE ELECTRODE SYSTEMS FOR MHD PROPULSION

J.K. Koester
MHD Instruments Company
Palo Alto, CA

INTRODUCTION

The promise of MHD propulsion for submarines is governed by the development of powerful superconducting magnets. With sufficient magnetic field, the inherent electrical conductivity of sea water allows efficient MHD propulsion at high speeds. However, the use of superconducting magnets restricts the MHD propulsion device to DC crossed fields. Since sea water is an electrolytic conductor, electrolysis occurs at the electrodes under DC operation and gases are evolved. The resulting formation of large numbers of bubbles greatly enhances the acoustic noise signature of the submarine. Furthermore, these gases and reaction products are left in the wake and may eventually rise to the surface.

Fundamental phenomena of electrode operation for MHD propulsion are briefly described here. Governing electrode parameters are identified and their characteristic values for MHD submarine propulsion are delineated. An electrode test stand for investigating electrode systems is described and some preliminary test results are presented. Potential electrode concepts for eliminating the formation of bubbles are described. Finally, recommendations for promising low noise electrode systems are given.

MHD Propulsion Parameters. MHD propulsion may be based on either external or internal electrode configurations.[1] In either case, limiting ideal performance is defined by momentum change considerations and the governing equations may readily be derived for either configuration in terms of effective duct area, A . The ideal equations for thrust, T , and propulsion efficiency, η , are summarized by Figure 1. Ideal efficiency is governed by two parameters: the velocity ratio, z , and the MHD interaction parameter, S . The minimum electrode current density required for MHD propulsion is given by:

$$J = (\rho u^2 / 2BL) * (z^2 - 1) \quad (E1)$$

where B is magnetic field strength, L is magnet length, ρ is sea water density, u is submarine velocity, and z is the jet pump velocity ratio.

For large thrust at a reasonable duct area, the velocity ratio must be around 1.2 which implies an ideal jet efficiency of 91%. For good MHD efficiency (>80%), the interaction parameter, S , should be near unity. This sets a criteria on conductivity and

Fig. 1. MHD JET PUMP PERFORMANCE EQUATIONS

$$\begin{aligned}
 T &= \rho A u^2 z (z-1) & \text{where } z &\equiv u_j / u \\
 p_E &= T u / \eta & \eta &= \eta_j * \eta_M \\
 \eta_j &= \frac{2}{1+z} \\
 \eta_M &= \frac{1}{\left[1 + \frac{(z^2-1)}{2zS} \right]} & \text{where } S &\equiv \frac{\sigma B^2 L}{\rho u} \\
 J &= \frac{\rho u^2}{2 B L} (z^2-1)
 \end{aligned}$$

magnet design as shown by Figure 2. At a speed of 30 m/sec and $S = 0.7$, this criteria is:

$$\sigma B^2 L > 22,000 \quad (E2)$$

For example, with a sea water conductivity of 4 S/m, we require a magnet of 14 Tesla field strength over a length of 30 meters. This high efficiency thruster configuration requires an electrode current density of only 0.05 A/sq cm. A magnet with the parameters, $B = 4$ T and $L = 10$ m, results in a current density of 0.5 A/sq cm. For comparable efficiency with this small magnet, sea water conductivity must be enhanced to a value over 100 S/m. Conversely, thrust performance can be maintained by operating at high current density and low efficiency. Over a wide range of operational scenarios, the required electrode current density ranges from less than a tenth of an ampere per sq cm to a value near 1 A/sq cm.

Sea water contains about 33-37 g/kg of dissolved chloride salts (mostly sodium with significant concentrations of magnesium, calcium, and potassium). The sodium and chlorine species form positive and negative ions respectively which respond to electric fields. Although their mobility is low (about $6 \times 10^{-8} \text{ m}^2/\text{V-s}$), the ion number density is high so that a conductivity of around 4 S/m results. This low mobility results in a low Hall parameter (around 10^{-6}) even at a field strength of 20 Tesla. Thus, as shown by Figure 2, the Hall parameter effects which are significant in gaseous MHD systems may be neglected here.

FUNDAMENTAL ELECTRODE BEHAVIOR

The electrolysis behavior between inert electrodes of a moderate solution of NaCl in water is well known.[2] The electrode reactions for inert electrodes are shown by Figure 3. Negative chlorine ions are attracted to the anode where they give up their electron and form chlorine gas. The positive sodium ions are attracted to the cathode, but do not plate out as metallic sodium. Instead, they react at the cathode to form sodium hydroxide and hydrogen gas. Since the gas molecules released at each electrode involve two electrons, the volumetric flux is the same and is proportional to electrode current density:

$$\dot{V} = 0.12 * J / (1 + h/10.1) \quad [\text{cc/sec-sq cm}] \quad (E3)$$

where J has units of A/sq cm, h is depth in meters and standard temperature is assumed.

This simplified picture of sea water electrolysis results in defined volumetric fluxes of hydrogen and chlorine gases while the solution becomes more alkaline (as shown by the overall reaction equation in Figure 3). In reality, the fundamental phenomena which control the electrode electrochemistry and bubble dynamics is exceedingly complex. Factors which control bubble

Fig. 2. ELECTRODE PARAMETER RANGE

For Good Efficiency: $z \leq \sim 1.2, S \geq \sim 0.7$

\Rightarrow at $u = 30 \text{ m/sec}$

$$\sigma(B^2 L) \geq 22,000 \quad J \leq \frac{20}{BL} \quad (\text{A/cm}^2)$$

for $4\text{T} \times 10 \text{ m Magnet}$: $J = 0.5 \text{ A/cm}^2$

for $14\text{T} \times 30 \text{ m Magnet}$: $J = 0.05 \text{ A/cm}^2$

Sea Water: $\sigma \sim 4 \text{ S/m}$

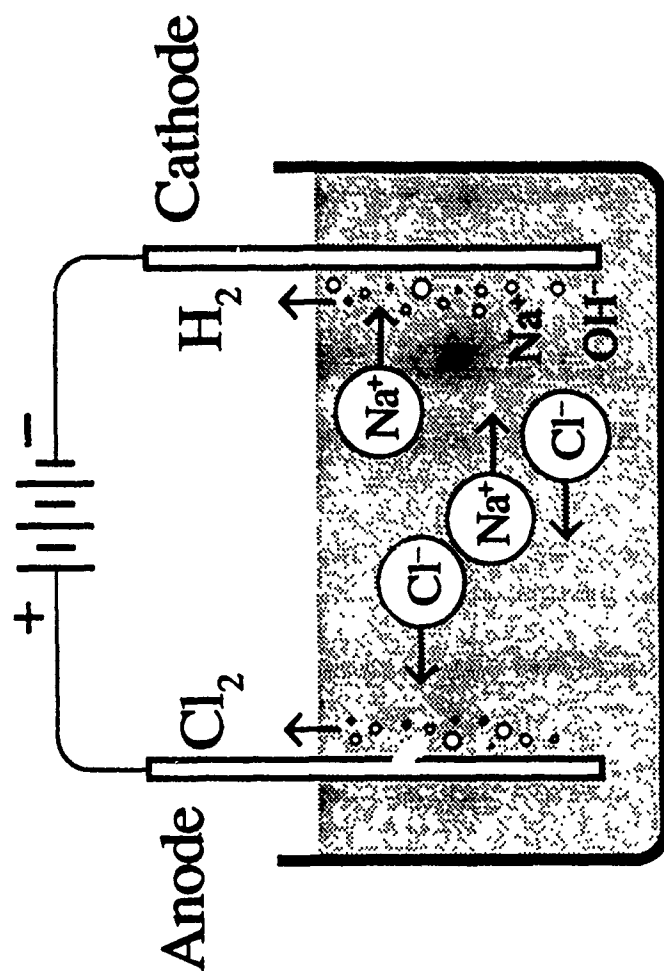
$$\omega\tau = \mu B \sim 6 \times 10^{-8} \left(\frac{\text{m}^2}{\text{V-s}} \right) \times 20 (\text{T})$$

$$\Rightarrow \omega\tau \sim 10^{-6} \ll 1$$

Conclude: Neglect Hall Effects

Current Density Range = $0.05 - 0.5 \text{ A/cm}^2$

Fig. 3. BASIC ELECTROLYSIS BEHAVIOR



Cathode Reaction: $2\text{H}_2\text{O} + 2\text{e}^- \rightarrow \text{H}_2 + 2\text{OH}^-$

Anode Reaction: $2\text{Cl}^- - 2\text{e}^- \rightarrow \text{Cl}_2$

Net Reaction: $2\text{H}_2\text{O} + 2\text{Cl}^- \rightarrow \text{H}_2(\text{g}) + \text{Cl}_2(\text{g}) + 2\text{OH}^-$

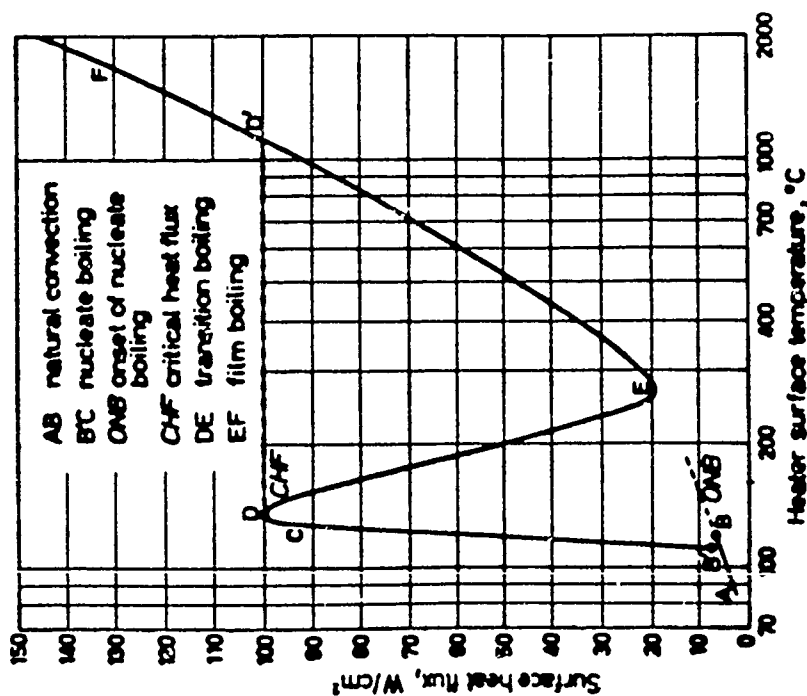
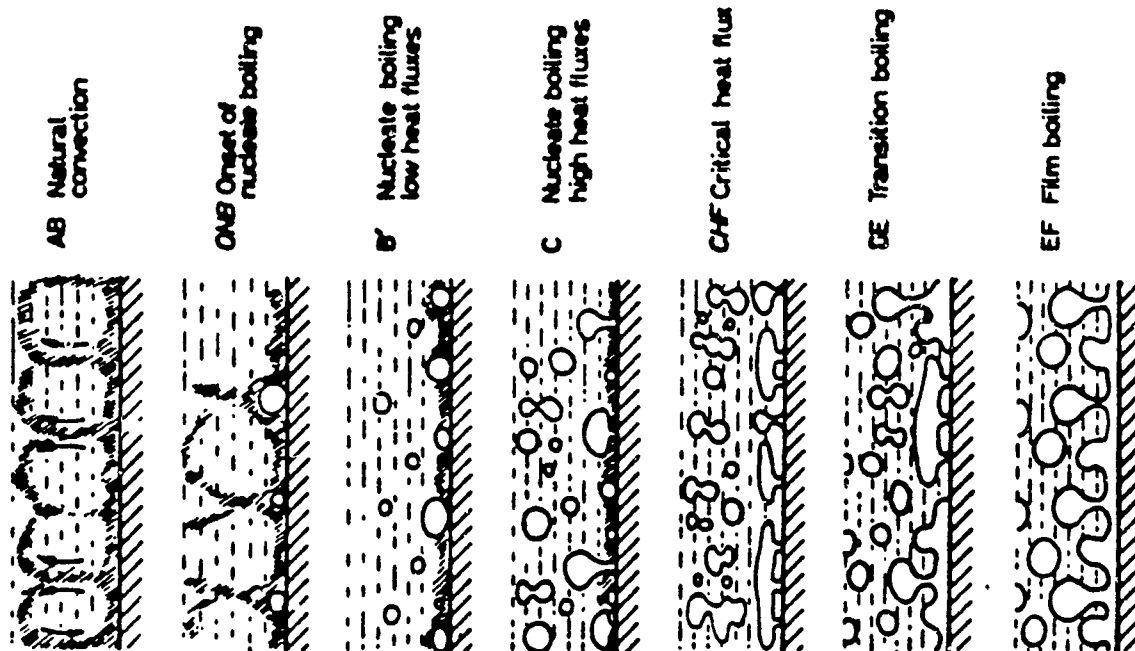
nucleation, growth, and size evolution include mechanical forces, electrochemical reactions, hydrolysis, solution mass transport by diffusion and convection, and the electrode surface properties.[3] Understanding of these governing processes is necessary for the development of low noise electrodes for the MHD propulsion application.

Extensive experience on bubble evolution and dynamics is available from studies of two-phase heat transfer and from work on electrolysis cells. The behavior of vapor bubbles generated in the boiling process is summarized in Figure 4.[4] For liquid at the boiling point, small bubbles form at nucleation sites on the heated surface and grow until mechanical forces overcome the surface tension forces holding them. As the heat flux rate is increased, the generation rate of vapor increases until the entire surface becomes enveloped in vapor (film boiling). Before film boiling occurs, a maximum in the heat flux (critical heat flux) is reached (point D in Figure 4). An analogy between boiling and electrolysis may be developed in terms of the volumetric rate of gas generation. These relations are shown by Figure 5. For electrolysis, the gas generation rate is proportional to current density, while in the case of boiling, the vapor rate is proportional to heat flux. At the critical heat flux value of 100 W/sq cm, vapor is generated at the rate of 74 cc/sec per sq cm. For pool boiling of water at one atmosphere, the departure diameter of the vapor bubbles is in the 1 to 2.5 mm range. These results will be compared with a corresponding electrolysis experiment in the next section.

Studies of sea water electrolysis cells for chlorine production are especially instructive.[5,6] Chlorine gas is readily dissolved and undergoes hydrolysis to form hypochlorite. A host of complex hydrolysis, electrochemical, and solution chemical reactions take place which result in the formation of hypochlorous acid, chlorate, and the generation of oxygen gas (depending on the anode material). Solution near the anode becomes very acidic with a pH value of 1 to 2 while the cathode becomes highly basic with a pH factor of 11 to 14. Since sea water contains dissolved magnesium and calcium, this basic cathode region results in deposits of magnesium and calcium hydroxides. These deposits are a major design problem for electrolysis cells with various techniques used for alleviation.

Bubble Induced Noise. Small voids of gas or vapor induce a dramatic effect on the acoustic behavior of a liquid. The essence of this effect may be understood by considering a spherical bubble surrounded by liquid as indicated by Figure 6. For variations in bubble radius, a , the gas within the bubble acts as a spring while the inertia of the surrounding water acts as a mass. This leads to the classic equation for undamped oscillation with the bubble radius varying sinusoidally in time. The natural (or resonant) frequency of oscillation depends on gas gamma, pressure, and liquid density and bubble size as shown on Figure 6. For sea water, the resonant frequency varies as 3.25 kHz

Fig. 4. ELECTROLYSIS BUBBLE ANALOG
With SATURATED BOILING OF WATER



Pool Boiling

Fig. 5. VOLUMETRIC RATE OF GAS GENERATION

Electrolysis: at Cathode or Anode

$$\dot{V} = \frac{0.12}{\left[1 + \frac{h}{10.1} \right]} * J \left(\frac{\text{cc}}{\text{sec} - \text{cm}^2} \right)$$

where J in (A / cm²), depth h in (m), at STD Temperature.

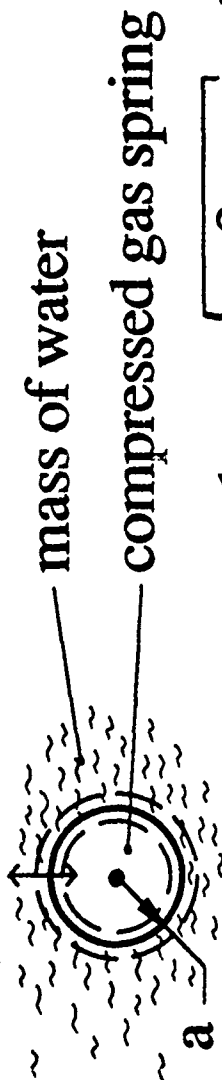
Saturated Boiling: at p = 1 atm

$$\dot{V} = 0.74 * \dot{q}_w \left(\frac{\text{cc}}{\text{sec} - \text{cm}^2} \right)$$

where Heat Flux \dot{q}_w in (W / cm²)

Fig. 6. BUBBLE INDUCED NOISE

Bubbles are spherical oscillators:



$$\text{Resonant Frequency: } f_o = \frac{1}{2\pi} \sqrt{\frac{3\gamma p}{\rho}} \frac{1}{a}$$

$$\text{at } p = 1 \text{ atm} \quad f_o = \frac{3.25}{a \text{ (mm)}} \quad (\text{kHz})$$

Excited bubbles act as spherical radiators:

$$\text{quadrupole response} \sim \frac{1}{\left[\left(\frac{\omega a}{c} \right)^2 - \left(\frac{\omega_o a}{c} \right)^2 \right]^2 \left(1 + \frac{j \omega a}{c} \right)^2}$$

At resonance, amplification factor = 10^{11}

divided by bubble radius in mm. Surface tension increases this frequency somewhat for bubbles less than 10 microns in radius.

These lightly damped bubbles are easily excited by pressure variations within the liquid and radiate spherical acoustic waves. The response to a turbulent quadripole excitation source is shown on Figure 6.[7] At resonant frequencies, this equation indicates that the bubbles will amplify the quadripole noise by a factor of 11 orders of magnitude. This resonant response falls off at other frequencies, but even at very low frequencies, the amplification factor is over 7 orders of magnitude. This resonant characteristic give turbulent liquid flows a distinctive acoustic signature depending on the size of entrained bubbles.

Conversely, bubbles in a quiescent region are strong absorbers and tend to shield an incoming noise source. However, for the MHD propulsion application, bubbles entrained in the thruster boundary layers will likely encounter strong shear forces in the thruster wake and become highly excited. The resulting noise field will depend on bubble size and number density as well as on the details of the thruster exhaust and interaction with the submarine wake.

PRELIMINARY ELECTRODE TEST RESULTS

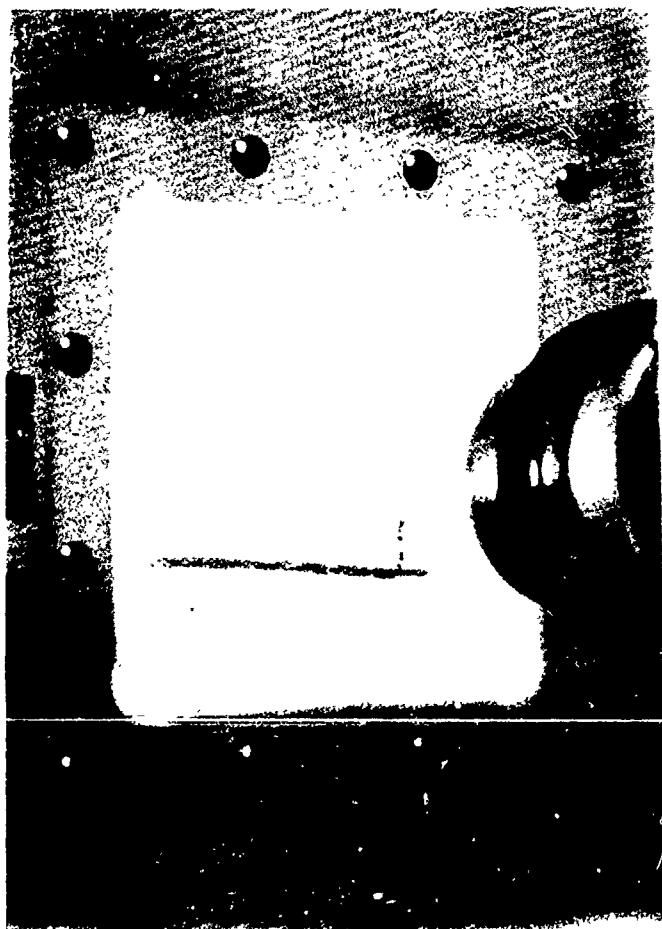
A basic electrode experiment was set up to delineate and clarify fundamental behavior. This experimental setup is shown by the photographs in Figure 7. By analogy with pool boiling experiments with heated rods, a copper rod electrode with a diameter of 1.27 mm was tested using San Francisco Bay sea water. This cathode was driven by a 2.5 kW DC power supply over a wide range of current densities. The evolved bubbles are side illuminated with a flood lamp and observed through an optical port. A rising column of fine hydrogen bubbles are visible in the right hand photograph in the color plate. A voltage probe is visible above the rod cathode.

A unique feature of this preliminary experiment was the use of a prototype gated, intensified video camera. This camera is based on a microprocessor controlled microchannel plate intensifier tube. The intensifier tube image is focused on a standard CCD video camera so that the object can be viewed on a conventional monochrome monitor and recorded with standard frame grabber equipment. The onboard microprocessor and timing circuits allow shutter speeds down to only 40 nanoseconds which are synchronized with the 60 Hz video camera. Thus, the motion of very small bubbles can be captured even at relatively high flow speeds and recorded for computer analysis.

Several electrode materials were tested for experimental suitability: copper, stainless steel, and titanium cathodes, and copper, stainless steel, tantalum, molybdenum, platinum, and graphite anodes. All of the cathode materials resulted in a clean and well behaved evolution of fine hydrogen bubbles. The

MHD INSTRUMENTS

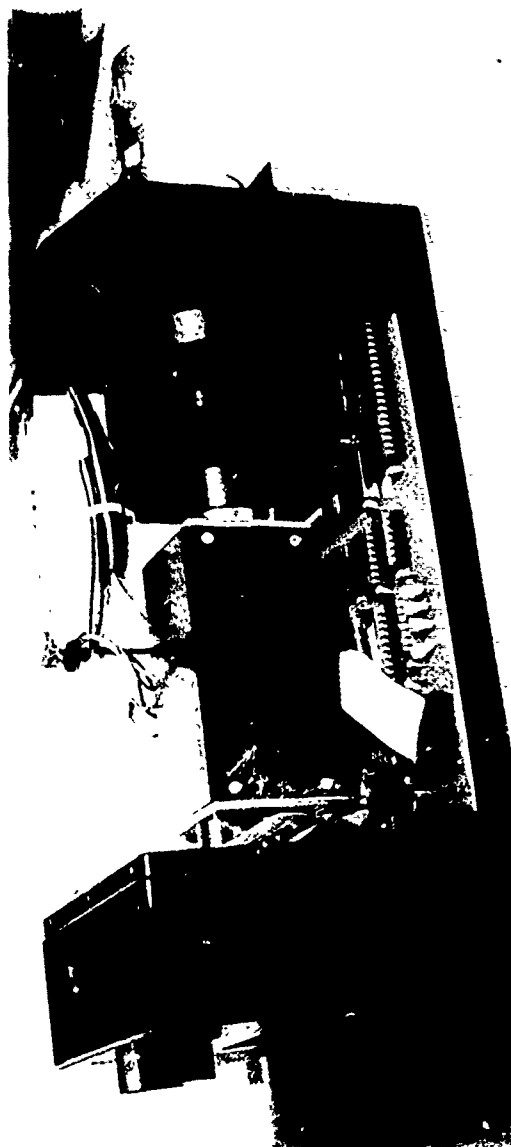
Fig. 7. ELECTRODE TEST SETUP



Viewing Port



Hydrogen Bubbles



Gated, Intensified
Video Camera

stainless steel anode contaminated the solution with a black inky substance; the copper anode turned the solution yellow, then blue-green. The tantalum anode quickly become anodized with a nonconducting purple film. Both the solid platinum and the graphite anodes performed well. Bubble activity was noted for each of these anodes, although not as vigorously as at the cathode. Experiments were conducted with the copper rod cathode and with the platinum anode. Deposits rapidly formed and were observed beneath each of the electrodes after short tests.

The electrical characteristics of the rod cathode is shown in Figure 8. At low current densities, a nearly linear characteristic is observed with a voltage threshold of around 1 volt. At high current densities, the characteristic flattens out and a limiting value near 12 A/sq cm was observed; here, the rod electrode was enveloped in gas. Surprisingly, the discharge continued at this high current density by an arcing phenomena through the hydrogen gas barrier. This arc discharge resulted in concentrated glowing discharges which moved erratically over the rod electrode surface. However, for MHD propulsion at current densities below 1 A/sq cm, nearly linear operation with low voltage drops is indicated.

The vertical axis of the J-V characteristic may be associated with gas generation which is proportional to current density. Here, electrode voltage provides the driving force for gas generation. This situation is analogous to boiling in which vapor production is proportional to heat flux which is driven by surface temperature. The J-V characteristic of Figure 8 is qualitatively similar to the heat flux curve of Figure 4. However, the maximum gas generation for the electrolysis experiment is 1.4 cc/sec per sq cm versus a value of 74 for the boiling case. Thus, the boiling situation generates 54 times more vapor at the critical point than for the corresponding electrolysis case.

Preliminary images of the magnified, stop-action bubble behavior were obtained by the direct photographing of the monitor with a still camera. Some examples of bubble behavior are shown by Figure 9. For this "pool" experiment, in which bubbles rise by buoyancy, a shutter speed of 1 millisecond is sufficient to "freeze" the bubble motion. Note the obvious increase in bubble size with increase in current density. This effect is shown quantitatively by the preliminary data presented by Figure 10. Here, the average bubble diameter is in the 100 to 200 micron range (considerably smaller than the 1-2 mm size observed in pool boiling experiments). The last photograph in Figure 9 illustrates the use of a longer time exposure to produce a "streak" display of bubble motion. These streaks indicate both the bubble speed as well as their direction. Measured bubble speeds are in the range of 5 to 8 cm/sec.

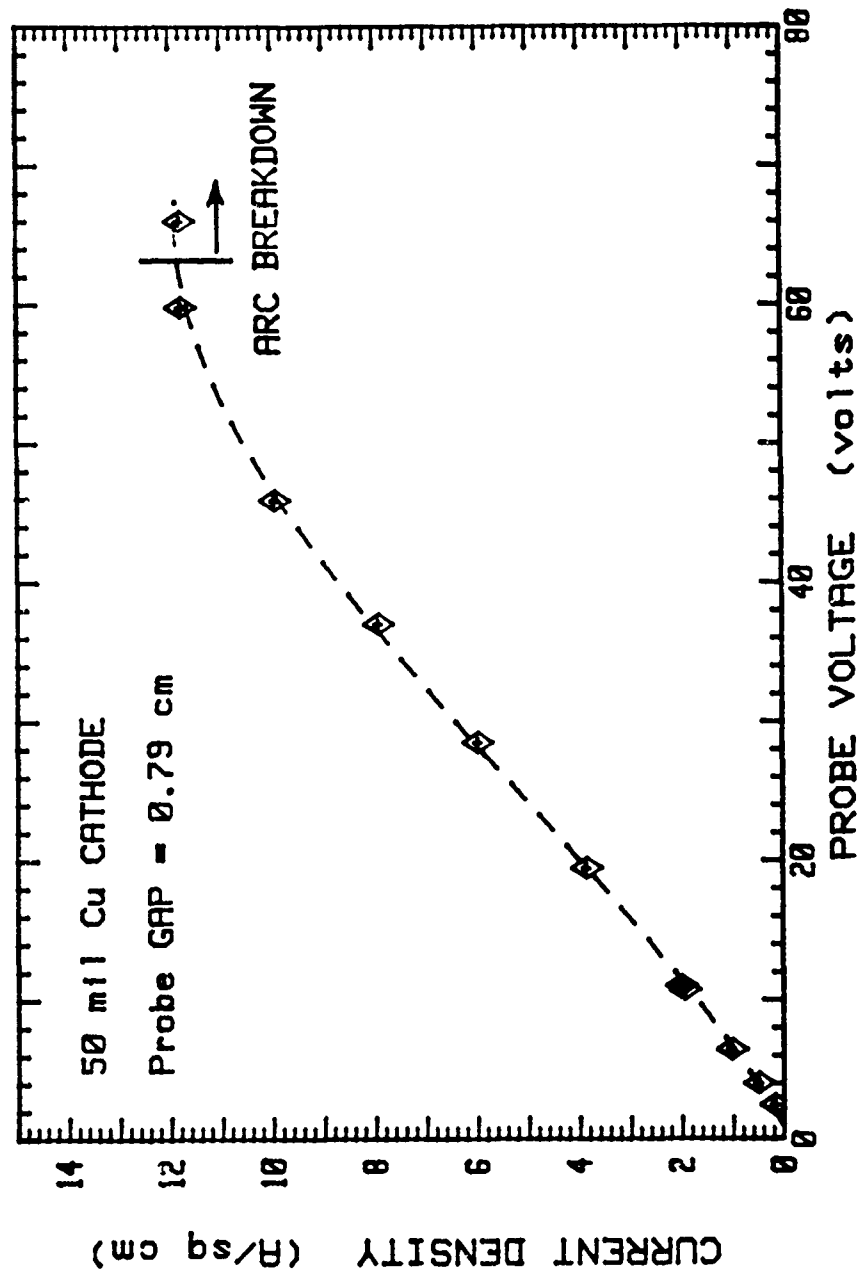
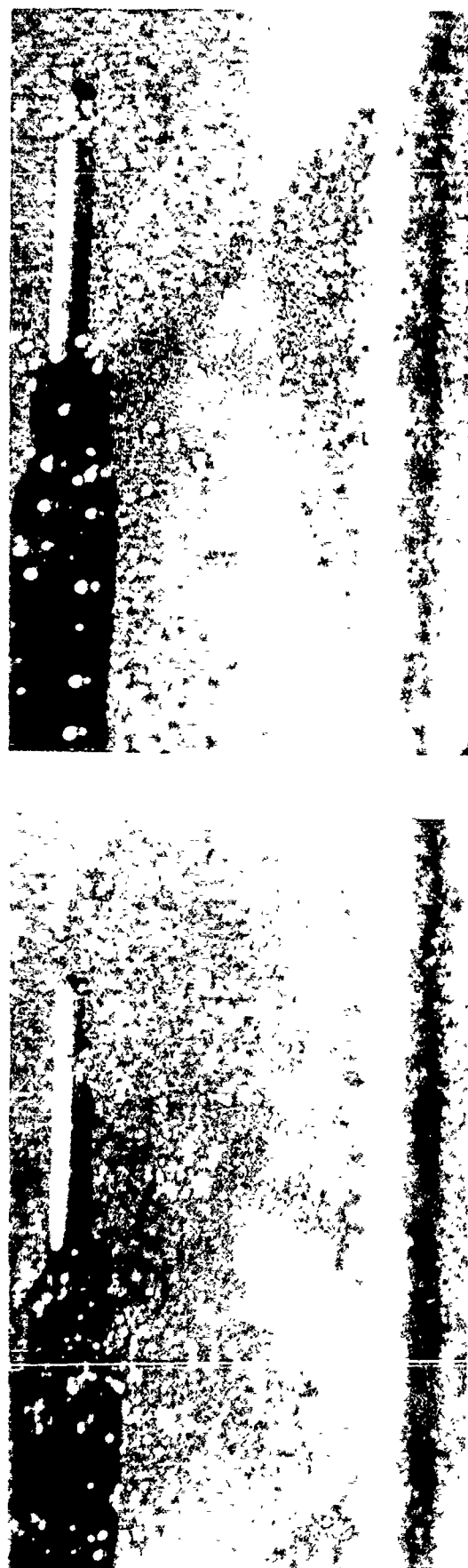


Fig. 8. Current Density vs Cathode Voltage Drop

MHD INSTRUMENTS INTENSIFIED VIDEO IMAGES OF CATHODE



$J = 2.0 \text{ A/sq cm, 1 ms}$



$J = 1.0 \text{ A/sq cm, 10 ms}$

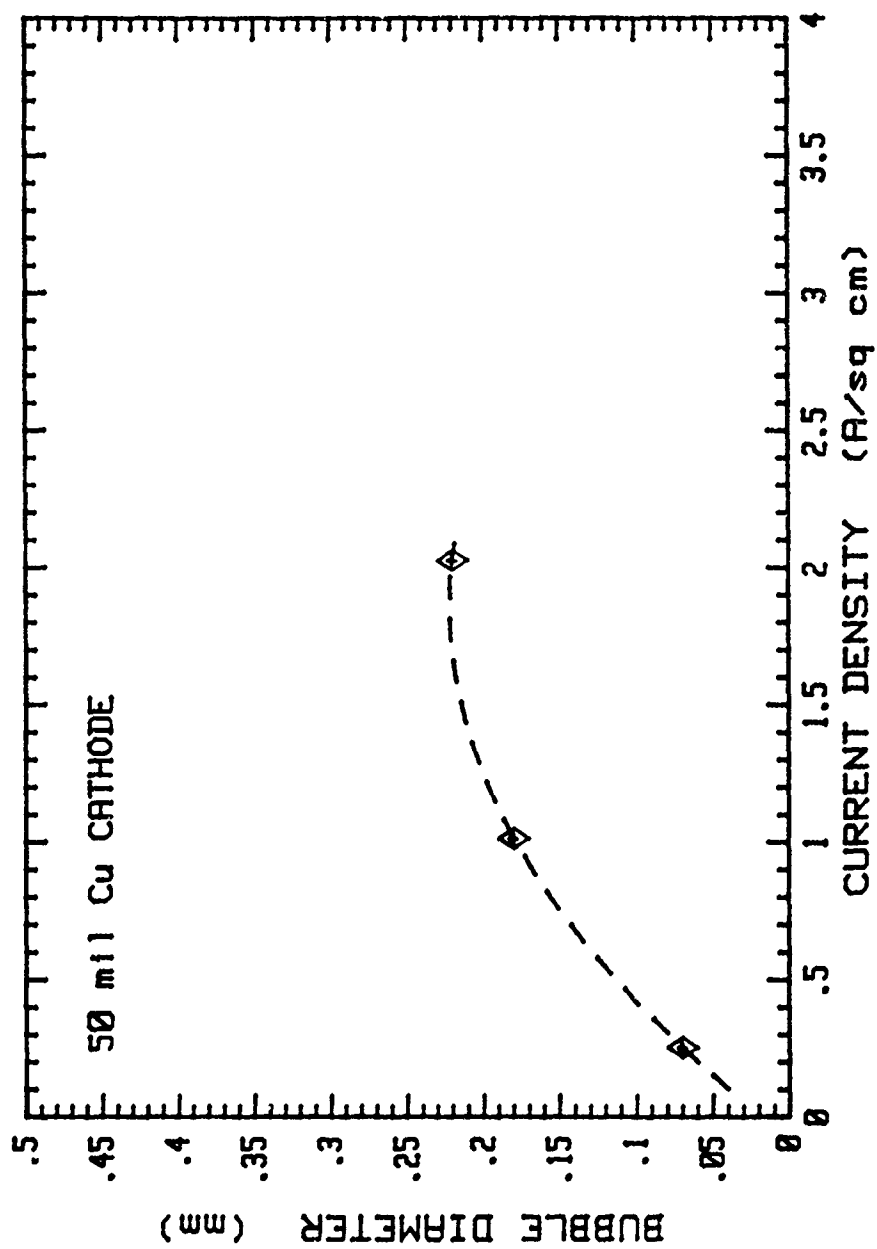
MHD INSTRUMENTS

Fig. 10. Bubble Diameter vs Current Density

LOW NOISE CONCEPTS

Concepts for developing a low noise propulsion system depend on the control of bubble size and distribution. The ideal goal of gasless electrodes would eliminate the bubble problem at its source. Eliminating bubbles by the thruster exit would greatly reduce the impact of bubble generation. Potential concepts for "gasless" electrodes are listed below (not in order of feasibility):

1. Modify sea water for electronic conductivity.
2. Mechanical separation of bubbles from boundary layer.
3. Dissolve gas by surface nucleation and bubble dynamics.
4. Sacrificial anodes and/or cathodes.
5. Hydrogen absorbing cathode.
6. Fluid reactant supplied at anode.

Of these six potential concepts, the first is judged very difficult and is not considered further. The second approach is considered feasible, at some reduction in thruster efficiency, but would introduce additional mechanical equipment and necessitate a device to eliminate collected gases. Approach three is highly desirable if an appropriate surface could be developed. Sacrificial electrodes are not consistent with the requirement for long life electrodes. Method five would require a technique for removing hydrogen from the cathode material as well as absorbing it. Recovered hydrogen could have value as a reactant either for energy or for the production of a conductivity enhancing material (e.g. HCl). Finally, chlorine and oxygen gases produced at the anode might be eliminated by introducing a suitable reactant.

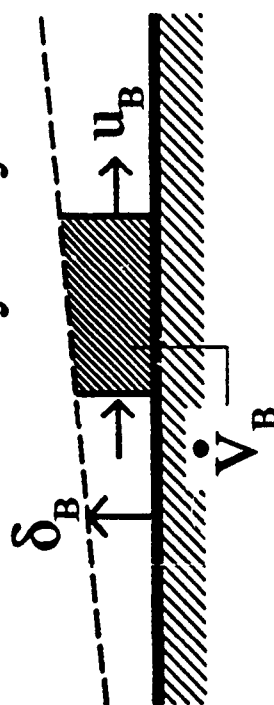
The feasibility of dissolving generated gases is assessed by considering the bubble "boundary" layer which will develop over the flat plate electrodes in the MHD thruster. As depicted in Figure 11, conservation of bubble mass requires a balance between generated gases and convection of bubbles within the boundary layer. By assuming a constant bubble convective velocity based on some fraction, f_B , of the mean flow velocity, u , a first order differential equation for the effective thickness of gases within the boundary layer results. The solution of this equation is shown in the table of Figure 11 for the worse case conditions of relatively high current density and a pressure of one atmosphere. The thickness of the corresponding electrode convective boundary layer is shown for comparison. Note that the gas volume to water volume ratio is less than 2 percent even for a 50 meter long electrode. Thus, considerable water volume is available for dissolving electrode gases if their solubility permits.

Gas solubility is governed by Henry's Law at moderate pressures as shown on Figure 11. At standard conditions, chlorine gas is readily absorbed while hydrogen has a volume solubility of only 1.9 percent. Even for the case presented, sufficiently small and

ESTIMATES ON DISSOLVING GAS

FIG. 11.

Bubble "Boundary" Layer:



$$\frac{d\delta_B}{dx} = \frac{\dot{V}_B}{u_B} \approx \frac{0.12J}{f_B * u}$$

	x (m)	δ_B (mm)	δ_{BL} (mm)	δ_B / δ_{BL} (%)
at u = 30 m / sec	1	0.10	12	0.8
J = 0.5 A / cm ²	2	0.19	21	0.9
	10	0.96	76	1.3
$f_B \sim 0.2$	50	4.81	275	1.7

Gas Solubility: Henry's Law $w = k * p$

Volume Solubility at 1 atm / 25C

H₂ : 1.9%

Cl₂ : 210%

Conclude: Chlorine gas readily absorbed: Hydrogen could be absorbed. Effect improves with depth.

well distributed hydrogen bubbles could be dissolved within the boundary layer. Since the bubble "boundary" layer becomes proportionately smaller with higher pressure at depth, the possibility of dissolving the gases improves.

CONCLUSIONS AND RECOMMENDATIONS

Overall features of electrode operation have been investigated in preliminary experiments. Bubble generation and motion was directly observed with a gated, intensified video camera. At prototypic values of current density, linear cathode operation was noted with the evolution of small gas bubbles. These bubbles were about a factor of ten smaller than water vapor bubbles observed in pool boiling. Clean operation with reduced bubbling was observed at platinum anodes. Deposits developed quickly in the vicinity of both electrodes. Observed operation at current densities below 1 A/sq cm were similar to results reported in sea water electrolysis cells.

Unlike sea water electrolysis cells, MHD thruster electrodes will be separated by a large gap so that they will operate in chemically decoupled boundary layers. Furthermore, the MHD electrodes will likely operate at higher current densities and in the presence of faster flows. Instead of electrochemical conversion efficiency, MHD electrode design is driven by control of gas evolution. A separate program of applied research is needed for the development of suitable electrodes for MHD propulsion.

The development of low noise electrodes by controlling their gas evolution characteristics appears promising. The understanding of the kinetic and chemical factors which affect bubble behavior is required for this development. A small, flexible, well instrumented electrode test facility is recommended for this effort. Critical environmental factors required for such a test stand include pressure and shear stress. Other important test parameters include current density, temperature, and sea water mixture. The dynamics of very small bubbles should be directly observed with high speed video equipment, such as described above. Additional instrumentation for measuring the chemical behavior near the test electrodes is needed. The dynamic, chemical, and surface characteristics which favor small bubble evolution should be sought in these experiments.

REFERENCES

1. S. Way, "Electromagnetic Propulsion for Cargo Submarines", J. Hydronautics, Vol.2, No. 2, April 1968, pp. 49-57.
2. J.V. Quagliano, Chemistry, Prentice-Hall, Inc., Englewood Cliffs, NJ, 1958, pp. 396-401.
3. P.J. Sides, "Phenomena and Effects of Electrolytic Gas Evolution", Modern Aspects of Electrochemistry, No. 18, edited by R.E. White, J.O'M. Bockris, and B.E. Conway, Plenum Press, New York, NY, 1986, pp. 303-354.
4. J.G. Collier, Convective Boiling and Condensation, McGraw-Hill, Inc., New York, NY, 1981, pp. 121-133.
5. L. Hammar and G. Wranglen, "Cathodic and Anodic Efficiency Losses in Chlorate Electrolysis", Electrochimica Acta, Vol. 9, No. 1, 1964, pp. 1-16.
6. J.E. Bennett, "Seawater Electrolysis", Symposium on Electrochemical Reaction Engineering, University of Southampton, April, 1979.
7. A.P. Dowling and J.E.Ffowcs Williams, Sound and Sources of Sound, Ellis Horwood Limited, Chichester, England, 1983, pp. 179-181.

SUMMARIES OF WORK GROUP FINDINGS

REPORT ON MHD PROPULSION MAGNET

Presented by

B. Wang

O N R / D A R P A W O R K S H O P

ON M H D P R O P U L S I O N

R E P O R T O N

M H D P R O P U L S I O N M A G N E T

SUBMIT BY : MHD MAGNET GROUP

CHAIRMAN : BERT WANG, (PRESIDENT OF WANG NMR INC.)

Bert Wang

PAYOFF

The important payoff of demonstrating feasibility of superconducting MHD propulsion system is obvious. A superconducting MHD propulsion system requires no mechanical moving parts and thus has negligible acoustic signature. As high temperature superconductor technology becomes available in the near future, there is great potential that superconducting MHD propulsion system will become a superior propulsion system for submarine, torpedo or even commercial ocean-bound vessel. In the pursue of a quiet sea vessel, are must take superconducting MHD propulsion magnet technology into serious consideration. This technology deserve a development program.

SUMMARY

Our group identified three key issues in the area of magnet technology. In each of three issues, we identify the requirements, possible approach or solutions. However, we believe that MHD propulsion magnet requirements pose serious challenging problems which will require very experienced superconducting magnet engineers / scientists to go beyond the existing design approach, develop reduced force and fringing field magnet, develop advanced conductor, advance light weight support structures, and employ innovative cryogenic technique.

INTRODUCTION

Three important MHD propulsion magnet system issues are : light weight, survivability and the magnetic signature. All of these three issues must be addressed simultaneously and must involve system efficiency optimization of MHD propulsion system.

ISSUES NO. 1 - LIGHT WEIGHT MAGNET DESIGN

MHD propulsion magnet requires a very high field magnet system that is light weight, survivable and bears little or no magnetic signature. It was generally concluded that 8 to 12 T is a reasonable maximum field goal. Toroidal configuration coupled with clever design of light weight conductor and advanced composite force support are possible solutions. The viable design call for some radical departure from the past classical magnet design experiences. Therefore we identify following key tasks that magnet design must address :

In the near term, We should conduct a systematic parametric study coupled with a detailed magnet design analysis. This study should investigate the following tasks :

(A). Consider aluminum or other stabilizers as conductor stabilizer so that magnet weight will be minimized.

(B). Consider supercritical cooled or force-cooled helium as an alternative for pool boiling.

(C). Design a superconductor so that it has higher critical current density.

(D). Clever design and selection of advanced composite materials are needed to lower the magnet weight.

(E). A viable MHD propulsion magnet design must take into consideration of the minimization of stray field.

(F). Must consider other innovations of MHD configurations to reduce force and system weight requirements.

ISSUE NO. 2 - MAGNETIC SIGNATURE

We agreed that minimization of detectable magnetic signature is one of important requirement for MHD propulsion magnet design.

In the MHD magnetic working group, we have considerable discussion as to the issue of minimum detectable stray field or detectable field gradient. We must obtain such information, or establish such data as one of the MHD propulsion magnet design requirement.

Finally, even if a MHD magnet has acceptably low magnetic signature, the magnet designer should find out that a significant electromagnetic signature when magnet quenches.

ISSUES No. 3 - SURVIVABILITY

The survivability question on superconducting MHD magnet are as follows :

(A). Can the superconducting MHD magnet withstand vibration, shock, etc. mechanical disturbance.

(B). We must minimize magnet quenches if MHD magnet could not be made totally stable.

Because of the necessity of minimization of weight. it may be necessary to design MHD propulsion magnet employing intrinsic magnet stabilization criteria. Some intrinsic stable magnet can quench during charging or discharging processes. Magnetic resonance imaging (MRI) magnet is designed with such criteria. However, experience of MRI magnet shows that such magnet seldom quenches if it is made persistent. That is, power leads and power supply are removed after energization. Furthermore, Since there is no power leads, the helium boil off could be reduced by a factor of 10 to 100. This enhance the survivability of the vessel because it decrease the dependency of cryogens.

(C). Fast Recovery From Quench

Even quench is an unlikely event, a MHD propulsion magnet must design to quickly recover from quench. Permissible recovery time must be established as one of the important design creteria.

KEY ISSUES IN SUPERCONDUCTING MAGNETS

• MAGNET DESIGN

Should conduct a systematic parametric study coupled with a detailed magnet design analysis to obtain a system design that satisfy the DARPA goals. This study should investigate the following considerations:

- Al or other stabilizers
- Supercritical He or other forced coolants/conductors
- Higher J_{\max} superconductors
- Composite materials and design to increase maximum allowable stress levels
- Other innovative MHD configurations to reduce force and system weight requirements
- Minimization of stray field

Then R&D tasks should be defined to either satisfy the stated goals or to reestablish realistic goals

KEY ISSUES IN SUPERCONDUCTING MAGNETS, CONTD

- MAGNETIC SIGNATURE

- A clearly defined detectable stray field and its gradient should be obtained as a magnet design requirement
- Should understand the electromagnetic signature when a magnet module fails
- Magnet design should include consideration of minimization of detectable signature

KEY ISSUES IN SUPERCONDUCTING MAGNETS, CONTD

- SURVIVABILITY

- Must be able to survive and Navy shock resistance
- Should look into retractable persistent leads to minimize quench and helium boil off
- Magnet design should include fast recovery from quench

REPORT ON ELECTROLYSIS/ELECTRODE WORK GROUP

Presented by

K. E. Tempelmeyer

Discussion Summary:
Electrolysis/Electrode Work Group

by

Dr. K. E. Tempelmeyer
U.S. Naval Academy
Southern Illinois University

One process which is of particular importance to the MHD thruster performance is the current flow through the seawater. The current in a MHD thruster produces electrolysis of the seawater and the formation of H_2 bubbles (a phenomena absent in other MHD devices). The bubbles in turn produce noise and interfere with the passage of the current across the channel. This process is fundamental to any seawater MHD device. Because seawater electrolysis had not been investigated extensively at MHD thruster conditions, and because it is a central issue in the development of MHD thrusters the Group's general conclusion was that various aspects of the electrolysis should be investigated in much more detail. The discussed focused on three principle areas:

1. Electrode Performance
2. Electrode Surface Chemistry
3. Bubble Generation and Bubble Effects

Some of the experimental data on seawater electrolysis presented at the workshop was discussed further. It was concluded that this work was a good beginning. However, while these data begin to provide the engineering base to support the larger DARPA funded programs on MHD propulsion, many questions still remain which can be answered by small-scale tests. While there are significant advantages to jumping to prototype scale testing such as the program at ANL, these tests are expensive and inflexible. As a result, the strong sentiment of the Group was that additional small-scale and inexpensive

tests will provide a considerable risk reduction for the DARPA program and the means to examine many problems and screen materials and configurations to an extent which is not economically possible in the larger facilities. The Group recommended that small-scale supporting tests are needed to support the DARPA program and at modest costs, they will enhance the chances of success of the DARPA program.

OVERVIEW

1. Reliability of Testing in Simulated Seawater

The use of Instant Ocean is planned for the ANL and NUSC tests. While Instant Ocean reproduces over 25 constituents of ocean water including some of the organic material, it does not reproduce the living biota of the ocean. Ocean waters may form biological films over gas bubbles entrained in the water. This film can delay the gas bubbles from dissipating and can alter their dynamics. It is not known to what extent this will be important in seawater MHD thrusters and if biological films will effect the electrolysis process and increase the acoustic and chemical signatures in the wake. However, hydrogen bubbles effect the current flow in the MHD channel, the acoustic signature and the chemical signature in the wake. The systematic test program such as the one conducted at the Naval Academy could and should be expanded to make comparisons of the electrolysis process in real ocean waters with the results already obtained using Instant Ocean.

2. Measurement of Void Fraction and Bubble Size

The void fraction, β , (i.e. the volume rate of gas in the flow to the volume flow rate of the seawater) will be small in a submarine thruster, but it will influence:

- (a) The size of the bubbles
- (b) The speed of sound in the water and hence the acoustic signature

- (c) The electrical conductivity of the water (at high currents)
- (d) The skin friction coefficient at the electrode surfaces
- (e) The current carrying capability of the electrodes

The void fraction may develop as a master parameter in seawater MHD thrusters. An understanding of the effect of the void fraction on the performance of seawater thrusters is a problem requiring investigation. In particular, measurement of the overall void fraction and the means to measure the void fraction along the length of the channel would both provide useful information. Several techniques which are available to measure β were discussed (use of γ -rays, acoustic methods and optical techniques). Some commercially available instruments are available. In addition, the void fraction may be determined as a part of the bubble noise measurements. An "active" acoustic method can be used to obtain information concerning the bubble size distribution. This technique involves introducing sound at frequencies greatly different from those that naturally occur in the flow and measuring the attenuation of these signals at different operational conditions. Cross-correlations of different microphone outputs can be carried out to aid in the analysis of the noise signature of the electrolysis process. At the same time, this technique can provide an independent measure of the overall void fraction in the flow.

3. Chemical Signatures - The electrolysis process in an MHD seawater thruster produces chemical products at the electrodes which depend upon the electrode materials. Previous tests (some of which were reported during the Workshop) have demonstrated that corrosion resistant anodes produce hypochloride and at the cathode various hydroxides are formed (principally $Mg(OH)_2$ and $Ca(OH)_2$). In addition, hydrogen is produced at the cathode and can be produced at the anode. The test media used in MHD thruster experiments should be analyzed for

these and other compounds in a manner to indicate the formation rate of new chemical species which may produce a signature trail in real ocean waters.

4. Noise Measurements

Noise is critical for submarine application of MHD thrusters.

Preliminary noise measurements reported during the Workshop employed a hydrophone which protruded into the flow and moved from point to point. It is highly desirable to refine these measurements using an array of microphones which are flush mounted in the walls. Small-scale testing of noise measurement techniques would aid in developing and refining noise measurement in the ANL program and elsewhere. Some of the narrow-band peaks may be associated with the resonant frequency of bubbles, other peaks may be due to a variety of other factors associated with the channel size and velocity. A continuation of acoustic measurements with actual ocean water and in simulated seawater will contribute to our understanding of bubble noise and expedite the understanding of noise data which will be obtained in the other DARPA sponsored programs.

SPECIFIC ISSUES AND PROBLEMS

Issues and problems specific to the areas of (a) electrode performance, (b) electrode surface chemistry and (c) bubble generation and bubble effects are summarized in the attached lists. These topics cover the range of the discussion of the Electrolysis/Electrode Work Group. In almost every instance, there is insufficient experimental information to assess the feasibility of an MHD seawater thruster or for that matter, to confidently design test channels and facilities for large-scale experiments. As a result, this working group made several specific suggestions.

SUGGESTIONS

- * Continue small-scale experiments. They are necessary to the success of the currently planned large scale tests.
- * Expand the understanding of chemical scaling on the electrodes and the understanding of its consequences. This is not only important to the performance of the channel and its wake signature, it is important to the operation of closed-loop test facilities.
- * Since hydrogen bubble generation is unavoidable, learn how to make small H_2 bubbles. Electrode configurations at the onset of MHD seawater thruster development should be kept simple.
- * Generate an engineering data base of electrolysis effects at MHD operating conditions. This is not only important to successful thruster design but it is crucial to the operation of large-scale test facilities.
- * Measure the void fraction (i.e. mass of gas to the mass of the water). It may be a master parameter influencing the thruster performance.
- * Investigate the mechanisms of how bubbles break away from the electrode surface.
- * Study current losses due to bubbles and the formation of gas pockets. Successful MHD seawater thrusters will have to provide the means to get the gas away from the electrodes.
- * Consider the establishment of a small-scale electrode development program focused on the development of long lifetime electrodes which can operate with periodic current reversal.

DARPA has established a propulsive efficiency goal and the need to minimize and eliminate acoustic and chemical signatures. The objective of these

suggestions (if implemented) will provide basic information focused on these two DARPA requirements.

Finally, the need for and benefit of small-scale experiments to complement the larger scale test programs at ANL and NUSC cannot be overstated. Small-scale testing in a flexible facility allows an enormous amount of useful and timely data to be obtained in a short time. Such information would provide a significant risk reduction for the larger more expensive DARPA-supported programs. Moreover, this research will answer the important questions related to:

- (1) The effects of biological films on H_2 bubbles and the accuracy of simulating seawater in MHD facilities by salts such as Instant Ocean
- (2) The role of void fraction in the performance of and MHD thruster and its acoustic signature
- (3) The understanding of acoustic and chemical signatures from MHD thrusters
- (4) Provide a test bed for long-duration and screening tests to support the larger scale programs.

TRANSPARENCIES SUMMARIZING

DISCUSSION OF THE ELECTROLYSIS/

ELECTRODE WORK GROUP

K. E. Tempelmeyer, Work Group Chairman

**PRINCIPAL AREAS OF CONCERN FOR
ELECTRODES/ELECTROLYSIS**

A. ELECTRODE PERFORMANCE

- (a) ELECTRICAL CHARACTERISTICS**
- (b) DURABILITY**
- (c) OPERATING MODES**

B. ELECTRODE SURFACE CHEMISTRY

- (a) CHEMICAL SIGNATURE**
- (b) MATERIALS WHICH DEPOSIT**

C. BUBBLE GENERATION

- (a) BUBBLE DYNAMICS**
- (b) BUBBLE NOISE**
- (c) H₂ CAPTURE**
- (d) EFFECT ON DRAG**

A. ELECTRODE PERFORMANCE

1. REPEAT SMALL-SCALE EXPERIMENTS

- * COMPARE RESULTS FROM SEAWATER
TO THOSE FROM INSTANT OCEAN**
- * USE DIFFERENT REAL OCEAN WATERS**
- * DOCUMENT SEAWATER COMPOSITION**

2. FURTHER STUDY OF CURRENT DEGRADATION

- * LOSS DUE TO CHEMICAL SCALING >
LOSS DUE TO VOID FRACTION**
- * EVALUATE (VOID FRACTION)
VARIATION WITH X**

3. OPEN CIRCUIT TESTING WITH SEAWATER

- * FATE OF BIOLOGICAL MATTER**
- * IMPACT OF BIOLOGICAL MATTER**

4. DURABILITY/LIFETIME 40,000 --> 50,000

HRS

*** AVAILABLE ELECTRODES -**

ELECTROLYSIS INDUSTRY

*** QUESTION OF EROSION AT HIGH
VELOCITY**

**5. DEVELOP A SMALL-SCALE ELECTRODE
TEST PROGRAM**

6. LONG-RANGE ELECTRODE ISSUES:

*** POSSIBLE EROSION**

*** CATHODE --> RESIST OXIDATION &
SCALE DEPOSITS**

*** ANODES --> NO BUBBLE PRODUCTION**

*** MINIMIZE BUBBLE SIZE**

*** SURFACE EROSION**

7. POROUS ELECTRODES

***GAS DIFFUSION ELECTRODES**

***EXOTIC POSSIBILITIES**

***"KEEP IT SIMPLE"**

B. ELECTRODE SURFACE CHEMISTRY

1. CHEMISTRY OF MATERIALS WHICH WILL DEPOSIT ON ELECTRODES:

- * REAL OCEAN**
- * VARIATION WITH VARIOUS SALT
WATERS**

2. STUDY OF THE FATE OF Cl_2

3. CHEMICAL SIGNATURES

- * H_2**
- * HYPOCHLORIDE**
- * $\text{Mg}(\text{OH})_2/\text{Ca}(\text{OH})_2$, ETC.**

C. BUBBLE GENERATION

1. STUDY FACTORS WHICH IMPACT BUBBLE SIZE

- * TURBULENT SHEAR STRESS (V)**
- * CURRENT DENSITY & GAS
GENERATION RATE**
- * WALL SURFACE TENSION**
- * PRESSURE**
- * $j \times B$ IN BOUNDARY LAYER**
- * OCEAN COMPOSITION (FILM
COATING)**

2. NEED FOR DATA BASE - EXPERIMENTAL

- * SIZE DISTRIBUTION**

3. ANALYTICAL STUDY OF BUBBLE "BREAKAWAY" (DIFFICULT!!)

4. NEED TO MEASURE VOID FRACTION,

- * METHODS AVAILABLE**
-RAY
OPTICAL
- * IMPACTS UNDERSTANDING OF
SEVERAL FACTORS**

5. FURTHER STUDY OF THE FATE OF H₂
6. DON'T "CAPTURE" THE EVOLVED H₂
--> HANDLE IN THE THRUSTER
CHANNEL
7. LEARN HOW TO GENERATE SMALL
BUBBLES:
 - * NOISE
 - * SOLUBILITY
 - * UNDERSTAND BUBBLE
AGGLOMERATION WITH X
8. BUBBLE "FILM" AT DEPTH:
WILL IT EXIST?
9. COMPARE RESULTS BETWEEN
 - * REAL OCEAN
 - * INSTANT OCEAN

SUGGESTIONS

- * CONTINUE SMALL-SCALE EXPERIMENTS:
THEY ARE NECESSARY TO THE SUCCESS
OF THE PLANNED LARGER SCALE TESTS**
- * EXPAND UNDERSTANDING OF CHEMICAL
SCALING ON THE ELECTRODES**
- * LEARN HOW TO MAKE SMALL H₂
BUBBLES**
- * CONSIDER ELECTRODE EROSION
EXPERIMENT**
- * GENERATE DATA BASE OF
ELECTROLYSIS BUBBLES AT MHD
CONDITIONS**
- * MEASURE VOID FRACTION AT VARIOUS
OPERATING CONDITIONS**
- * INVESTIGATE BUBBLE BREAKAWAY**
- * MORE STUDY OF CURRENT LOSSES
DUE TO BUBBLES AND GAS POCKET
FORMATION**
- * CONSIDER SMALL-SCALE ELECTRODE
PROGRAM**

THIS PAGE IS INTENTIONALLY BLANK

REPORT ON CONDUCTIVITY ENHANCEMENT

Presented by

C. Young

ONR/DARPA Workshop on MHD Propulsion

Report on
Conductivity Enhancement

Group Members:

Chris Young (Spectra Technology)
Don Cott (MSEI/INEL)
John Lineberry (Univ. of Tenn.)
Lynn Parnell (NOSC)
George Winkelmanns (STD Research)

15 December, 1989

Conductivity Enhancement

Introduction:

The objective of this working group was to determine the critical issues associated with conductivity enhancement and to determine what approaches were appropriate to address each of these issues. Conductivity enhancement is envisioned by some as a means of increasing the efficiency of the MHD propulsion process. There are a number of basic science issues, technology issues, and mission or system related issues associated with conductivity enhancement. This report will present the basic science issues, technology related issues, mission specific issues, approaches to address these issues, and potential payoffs for conductivity enhancement. An introduction to the subject of conductivity enhancement was presented at the workshop. The presentation materials are attached to this report as appendix A.

Basic Science:

There are several basic science related issues associated with the topic of conductivity enhancement. These issues are issues which must be addressed before serious consideration can be given to technology issues. These basic science issues will open the door to a better understanding of conductivity enhancement and possibly indicate directions for new enhancement mechanisms which will have a tremendous impact on the technology associated with conductivity enhancement.

One of the first basic science issues which needs to be addressed is the issue of understanding the conduction physics in seawater. Seawater is a very complicated combination of salts, minerals, basic elements, and organic matter. This "junk" may have a significant impact on the higher order contributions to conductivity. Understanding the conduction physics in the presence of this "junk" and in the presence of high magnetic fields is very important. Magnetic fields operate on the charge carriers (ions) and cause these carriers to take paths which are not straight but curved as defined by basic charge kinetic theory. The combination of junk and high magnetic and electric fields may introduce the possibility of using some nonlinear effects to modify the conductivity.

An approach to understanding the basic conduction physics would begin with a search of the relevant seawater electrolysis literature. There is no need to reinvent the wheel. Since electrolysis is not usually performed in the presence of a strong magnetic field, this literature search can only be of limited help. Addressing this basic issue requires a

multidisciplined approach with the appropriate small scale experiments (with high magnetic fields and "real" seawater) and theoretical analysis.

Conductivity in seawater is defined by charge concentration and carrier mobility. A basic science issue is the need to understand ionic mobility (ability of the charge carriers to move in the presence of an electric field). The limits of ionic mobility need to be well understood. What specifically limits the mobility to some value? Is there a way to alter the medium to effect this limit one way or another? These are questions which must be answered. These questions may readily be answered through the proper theoretical studies and small scale experiments.

A third area of basic science issues concerns the basic fluid dynamics involved in the conduction channel in the presence of high magnetic fields, high electric fields, and conductivity enhancement mechanisms. The basic issues include mixing effects, medium disturbances and propagation of those disturbances, and fluid interactions (field induced or nozzle induced counterflows, etc.). Analytic as well as computational studies may be performed to develop scaling relations and maps for determining regimes of interest or regimes of problems. Laboratory measurements will be important for verifying the scaling. Laboratory measurements should include such things as flow field mapping and conductivity maps.

Finally, a general understanding of the basic energy requirements for conductivity enhancement must be addressed. Energy related issues include: energy requirements for ionization in the presence of complex E and H fields, energy requirements for solubility modification, and energy requirements for mobility enhancement. These basic energy requirement questions can be addressed by small scale experiments and theoretical studies with particular consideration given to the presence of strong fields.

Technology Issues:

The Conductivity Enhancement working group determined that there were a number of issues associated with the technology aspects of conductivity enhancement. The committee identified these issues and suggested a number of approaches to address these issues.

There are a host of specific issues associated with the general issue of enhancement material delivery or enhancement method. In other words, what form of materials or what method of delivery do we use to achieve the optimum conductivity enhancement? What is better, a particle delivery system or a system to deliver a solution? The approach to addressing this issue should include definition and optimization of each system to the extent that a comparison can be made, in other words, a system trade study should be developed.

Injection of chemical additives is an important issue. Several questions arise with respect to the injector performance (power required to inject

the chemicals), additional drag due to nozzle profile, and acoustic noise introduced by the injector and pressure gradients introduced by the chemical additives in the flow stream. Small scale experiments can be used to adequately address these particular issues.

The general area of material handling raises a number of important questions. Material handling apparatus can generate large levels of acoustic noise (mechanical pumps, valve noise, etc.). The materials which are to be handled have significant corrosive properties which will limit the kinds of materials which can be transported or limit the material choices for construction of the material handling system, conduction channel, etc. Due to the large number of moving parts in the material handling system, reliability should be a key concern. Most of these issues can be resolved through accurate systems studies which may rely on the extensive industrial experience in related material handling industries.

Associated with material handling of corrosive materials are the issues related to safety. These safety issues mainly involve containment of the chemicals and chemical vapors. The impact of these issues can be greatly reduced if safety is addressed early in the systems definition process. This attention to safety should involve, obviously, the people responsible and familiar with safety aboard submarines.

Finally, there are a number of issues associated with various signatures which may be generated by a conductivity enhancement system. Possible signatures include: acoustic (mechanical equipment), chemical (additives), radiation (possible ionization sources), and optical (chemical reactions, photoplankton). Approaches to these issues should include: defining the upper limits of acceptance of these signatures and the attenuation rates for propagation of these signatures.

Mission / System Issues:

A number of issues were brought forth which concern the mission or systems related aspects of conductivity enhancement. The mission related issues are those issues which are mission specific and would have significant impact on the configuration of the conductivity enhancement system. The systems related issues are those issues related to the systems configuration of the platform (submarine, torpedo, etc.) which may limit or otherwise impact the conductivity enhancement system.

A critical issue which must be addressed is the issue of mission definition. This issue would include aspects such as: range, acceleration, speed, depth of operation, and operational environment (temperature, salinity, etc.). This issue can be satisfied by the release of such information from the Navy or by a consensus agreement by all parties involved. The consensus would define a common mission scenario for all designers to use as a baseline case. The Navy could release real numbers for most mission related questions in a classified document and/or release the reasonable limits in an unclassified document.

The important system related issues involve optimization of the conductivity enhancement system with respect to all other systems. In other words, does a conductivity enhancement system actually reduce the overall system size or weight sufficiently to justify its use? This particular issue can be addressed by a complete systems trade which would require input from the other systems impacted by a conductivity enhancement system.

Payoff:

The final area that the Conductivity Enhancement Group addressed was the potential payoff for a conductivity enhancement system. It was determined that the system could offer increased efficiency leading to an overall platform size and weight reduction. Conductivity enhancement can also offer the potential to obtain an increase in acceleration over a platform which does not use conductivity enhancement. The addition of an enhancement system would allow operation, for short times, in fresh water areas such as lakes, rivers, polar regions, and high rainfall ocean areas. Furthermore, conductivity enhancement can offer the ability to fine tune the flow in the conduction channel to reduce drag and noise or to actually achieve steering of the output of the conduction channel.

Summary:

The Conductivity Enhancement working group identified key issues in the areas of basic science, technology, and missions/systems. The group identified possible approaches for addressing many of these issues and identified possible payoffs for application of this technology.

REPORT DOCUMENTATION PAGEForm Approved
OMB No. 0704-0188

Public reporting burden for this collection of information is estimated to average 1 hour per response, including the time for reviewing instructions, searching existing data sources, gathering and maintaining the data needed, and completing and reviewing the collection of information. Send comments regarding this burden estimate or any other aspect of this collection of information, including suggestions for reducing this burden, to Washington Headquarters Services, Directorate for Information Operations and Reports, 1215 Jefferson Davis Highway, Suite 1204, Arlington, VA 22202-4302, and to the Office of Management and Budget, Paperwork Reduction Project (0704-0188), Washington, DC 20503.

1. AGENCY USE ONLY (Leave blank)		2. REPORT DATE July 1990		3. REPORT TYPE AND DATES COVERED Final	
4. TITLE AND SUBTITLE SECOND ONR WORKSHOP ON MAGNETOHYDRODYNAMIC SUBMARINE PROPULSION				5. FUNDING NUMBERS	
6. AUTHOR(S)					
7. PERFORMING ORGANIZATION NAME(S) AND ADDRESS(ES) Naval Ocean Systems Center San Diego, CA 92152-5000				8. PERFORMING ORGANIZATION REPORT NUMBER NOSC TD 1869	
9. SPONSORING/MONITORING AGENCY NAME(S) AND ADDRESS(ES) Office of Naval Research 800 N. Quincy St. Arlington, VA 22217-5000				10. SPONSORING/MONITORING AGENCY REPORT NUMBER Defense Advanced Research Projects Agency 1515 Wilson Blvd., Suite 705 Arlington, VA 22209	
11. SUPPLEMENTARY NOTES					
12a. DISTRIBUTION/AVAILABILITY STATEMENT Approved for public release; distribution is unlimited.				12b. DISTRIBUTION CODE	
13. ABSTRACT (Maximum 200 words) This document provides the presentations made at the Second ONR Workshop on Magnetohydrodynamic Submarine Propulsion held on 16-17 November 1989 in San Diego, CA.					
14. SUBJECT TERMS magnetohydrodynamic submarine propulsion				15. NUMBER OF PAGES 436	
				16. PRICE CODE	
17. SECURITY CLASSIFICATION OF REPORT UNCLASSIFIED		18. SECURITY CLASSIFICATION OF THIS PAGE UNCLASSIFIED		19. SECURITY CLASSIFICATION OF ABSTRACT UNCLASSIFIED	
					20. LIMITATION OF ABSTRACT SAME AS REPORT